High dielectric permittivity materials in the development of resonators suitable for metamaterial and passive filter devices at microwave frequencies

Bahareh Moradi

Universitat Autònoma de Barcelona

High dielectric permittivity materials in the development of resonators suitable for metamaterial and passive filter devices at microwave frequencies

Ph.D. Thesis written by

Bahareh Moradi

Under the supervision of

Dr. Juan Jose Garcia Garcia

GAEMI Grupo de Aplicaciones ElectroMangéticas Industriales

Bellaterra (Cerdanyola del Vallès), February 2016

Universitat Autònoma
de Barcelona

The undersigned, Prof **Juan Jose Garcia Garcia** Professor of the Electronic Engineering Department of the Universitat Autònoma de Barcelona (UAB).

CERTIFY:

That the thesis entitled "*High dielectric permittivity materials in the development of resonators suitable for metamaterial and passive filter devices at microwave frequencies*" has been written by Bahareh Moradi under his supervision.

And hereby to acknowledge the above, sign the present.

Signature: Juan Jose Garcia Garcia

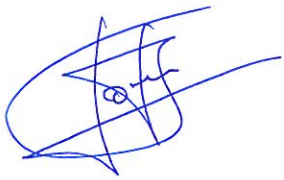

Bellaterra, February 2th 2016.

Abstract

Metamaterials (MTMs) represent an exciting emerging research area that promises to bring about important technological and scientific advancement in various areas such as telecommunication, radar, microelectronic, and medical imaging. The amount of research on this MTMs area has grown extremely quickly in this time. MTM structure are able to sustain strong sub-wavelength electromagnetic resonance and thus potentially applicable for component miniaturization.

Miniaturization, optimization of device performance through elimination of spurious frequencies, and possibility to control filter bandwidth over wide margins are challenges of present and future communication devices.

This thesis is focused on the study of both interesting subject (MTMs and miniaturization) which is new miniaturization strategies for MTMs component.

Since, the dielectric resonators (DR) are new type of MTMs distinguished by small dissipative losses as well as convenient conjugation with external structures; they are suitable choice for development process. The primary advantage in using a high dielectric constant as a DR is to miniaturize the filter size. The size of DR filter is considerably smaller than the dimension of waveguide filters operate at the same frequency. For a given dielectric constant, both resonant frequency and Q-factor are defined according to the dielectric resonator dimensions. That, the higher the dielectric constant, the smaller the space within which the fields are concentrated, the lower the dimension at a defined frequency.

To obtain the required compact sizes new stop-band filter is proposed in this work based on number of thick film high dielectric constant epoxy paste (TFDR) as DRs which excited with a microstrip line.

In addition, a band-pass filter is proposed based on embedded dielectric resonators (EDR) constitutes a new approach to the miniaturized resonators suitable for

metamaterials design without the Q degradation inherent to the coupling coefficient based on sub-wavelength particles.

Also this thesis is proposed a new band-pass filter based on split ring resonators (SRRs), which is a one of the popular MTMs building blocks today. The band-pass filters based on this concept can be very promising for the applications where miniaturization and compatibility with planar millimeter wave technology are the important issues. Also, for further miniaturization, embedded DR technology is reported.

Another approach for size reduction is modifying the traditional resonator to generate additional modes, which make the resonator to behave as a multimode resonator. Finally a compact ultra-wide band-pass (UWB) band-pass filter using grounded open ring resonator as a multimode resonator (MMR) is proposed. The approach allows using five resonances to produce a 128% fractional bandwidth into the ultra-wide band. A general theoretic framework has been established using transmission matrix description of the filter constituent components.

To demonstrate and validate designs functionality, all the proposed devices are implemented and fabricated, which a good agreement between simulations and measurement are obtained. Through these methods it is demonstrated that their equivalent circuit models provide an accurate description of the considered structures. Indeed, a clear relationship between their equivalents circuit model and the layout physical dimensions were found.

Resumen

Los metamateriales (MTMs) representan una interesante área de investigación emergente que promete lograr un importante progreso tecnológico y científico en diversas áreas como las telecomunicaciones, la microelectrónica, radar, e imágenes médicas. La cantidad de artículos dedicados a la investigación en esta área (MTMs) se mantiene en pleno crecimiento en la actualidad. Las estructuras MTMs pueden sostener una fuerte resonancia electromagnética con longitudes de onda electricamente pequeñas y por lo tanto son potencialmente aplicables para la miniaturización de los componentes.

La miniaturización, optimización del rendimiento del dispositivo mediante la eliminación de frecuencias espurias, y la posibilidad de controlar el ancho de banda del filtro para amplios márgenes de frecuencias es un reto para los presentes y futuros dispositivos de comunicación.

Esta tesis se focaliza en el estudio de ambos temas (MTMs y miniaturización) centrándose en las nuevas estrategias para la miniaturización de componentes basados en MTMs.

Desde la aparición de estos, los resonadores dieléctricos (DR) son un nuevo tipo de MTMs distinguidos por sus pequeñas pérdidas, así como su fácil combinación con estructuras externas; son la elección adecuada para todo proceso de desarrollo. La principal ventaja de utilizar una alta constante dieléctrica como DR es miniaturizar el tamaño del filtro. El tamaño del filtro de DR es considerablemente menor que la dimensión de la guía de ondas de otros filtros que operan a la misma frecuencia. Dada una constante dieléctrica, tanto la frecuencia de resonancia como el factor de calidad Q se definen a partir de las dimensiones del resonador dieléctrico. Cuanto mayor es la constante dieléctrica, menor es el espacio en el que se concentran los campos, y por lo tanto las dimensiones necesarias para trabajar a una frecuencia de operación definida quedan reducidas.

Con el objetivo de miniaturizar las dimensiones del dispositivo, en este trabajo se propone un nuevo diseño para un filtro rechaza banda basado en la alta constante dieléctrica que proporciona una fina capa de pasta epoxy (TFDR) como material DRs excitado a través de una línea microstrip.

Además, se propone un filtro pasa banda diseñado en base a los resonadores dieléctricos incrustados (EDR), esto constituye un nuevo enfoque en el campo de los resonadores miniaturizados adaptado a los metamateriales, logrando evitar la degradación del factor Q inherente al coeficiente de acoplamiento basado en partículas eléctricamente pequeñas.

En esta tesis se propone también un nuevo filtro pasa de banda basado en resonadores de anillo dividido (SRRs), que es uno de los bloques de construcción MTMs más popular hoy en día. Los filtros de paso de banda basados en este concepto resultan prometedores para las aplicaciones donde la miniaturización y la compatibilidad con la tecnología de ondas planares milimétricas son los requisitos críticos del diseño. Además, para mayor miniaturización, tecnología DR de incrustado es reportada.

Otro enfoque para la reducción de tamaño se basa en modificar el resonador tradicional para generar modos adicionales, los cuales hacen que el resonador se comporte como un resonador multimodal. Por último, se propone un filtro compacto paso banda de banda ultra ancha (UWB) utilizando un resonador de anillo abierto conectado a tierra empleado como un resonador multimodal (MMR). Esta propuesta permite utilizar cinco resonancias para producir un ancho de banda fraccional del 128% dentro de la banda ultra ancha.

Para demostrar y validar la funcionalidad de los diseños, todos los dispositivos propuestos se han implementado y fabricado, con una excelente concordancia entre las simulaciones y las medidas experimentales. A través de estos métodos ha quedado demostrado que los modelos de sus circuitos equivalentes proporcionan una descripción precisa del comportamiento de las estructuras. En este trabajo se ha conseguido relacionar una relación directa entre las dimensiones físicas del dispositivo y su modelo equivalente eléctrico en forma de circuito.

Acknowledgments

I would like to express my deep and sincere gratitude to my supervisor Prof. Juan Jose Garcia Garcia. I appreciate all his contributions of time, ideas and encouragements during my PhD study. It has been an honor for me to be his PhD student. I am thankful of his patience and support at every stage of this PhD work.

I am very grateful for the opportunity that was given to me by Grupo de Aplicaciones Electro mangeticas Industrials (GAEMI) to carry out this work as well as for sponsoring, and the use of facilities. I thank everybody in the GAEMI group for their continuous encouragements.

It is a pleasure to convey my gratitude to prof, Núria Barniol Beumala and prof, Arantxa Uranga.

I would like to express my thanks to my parents for their discrete but ever so precious moral support, my sister Homa, my brother Hamidreza and also my dears Kimiya and Farhak for their great love to me and for aiding me a lot to accept and enjoy my new life conditions in Spain.

Finally, I would like to special thank Meysam, my husband, for all his help and moral support.

Contents

Contents

CHAPTER 1

1 Introduction

The term microwave is typically used for frequencies between 3 and 300 GHz, with a corresponding electrical wavelength between $\lambda=c/f=10$ cm and $\lambda=1$mm, respectively. While any frequency within the electromagnetic spectrum associated with radio wave propagation is referred as Radio Frequency (RF) which the RF range is from very high frequency (VHF) (30–300 MHz) to ultra-high frequency (UHF) (300–3000 MHz).

The development of filter theory began in the years preceding World War II by pioneers such as Mason, Sykes, Darlington, Fano, Lawson, and Richards. In the early 1950s a group at Stanford Research Institute, consisting of G. Matthaei, L. Young, E. Jones and S. Cohn, became very active in microwave filter and coupler development.

The microwave filters are components which provide frequency selectivity in mobile, satellite communications, radar, army applications, and remote sensing systems operating at microwave frequencies. With the rapid advance in wireless communications, wireless devices, especially filters, are facing new challenges including high performance, small size, light weight and low cost.

Microwave circuits components include lumped passive elements [1] (such as resistors, capacitors, and inductors), distributed elements [2] (such as micro-strip, coplanar waveguide, or rectangular waveguide), and active elements [3] (such as field-effect transistors (FETs) or bipolar transistors).

Since the lumped circuit element may not be valid at high RF and microwave frequencies, microwave components often needs to be described as distributed elements. However, in this case the phase of the voltage or current changes over the physical

extent of the device because the device dimensions are on the order of the electrical wavelength.

At much lower frequencies the wavelength is large enough that there is insignificant phase variation cross the dimensions of a component. However, many authors uses lumped elements equivalent circuit models to describe the behavior of modern devices based on metamaterial concepts with the consequent derived drawbacks.

Lumped circuit elements such as inductors and capacitors are commonly employed as resonant circuits at lower frequencies. Resonators are used in a variety of applications, including filters, oscillators, frequency meters, and tuned amplifiers, open-end resonators, stub resonators, dielectric resonators and split ring resonators [4].

Fields inside the resonator store energy at the resonant frequency where equal storage of electric and magnetic energies occurs. Quality factor (Q) is used for measure of energy loss or dissipation per cycle as compared to the energy stored in the fields inside the resonator. Q factor is known as a parameter for assessing the performance of a resonator.

Resonators can be excited by either capacitive (E field) or inductive (H field), and in general there is a mix between both, being one of them dominant.

The situation in which two or more resonators are interchanging energy trough the electric or magnetic field is defined as coupled resonators. Coupled resonator filters have been extensively presented in literature for many applications [5-6-7]. There is a general technique for designing coupled resonator filters in the sense that it can be applied to any type of resonator despite its physical structure [16]. It has been applied to the design of waveguide filters [8], dielectric resonator filters [9], ceramic comb-line filters [10], micro-strip filters [11], superconducting filters [12], and micro-machined filters [13]. This design method is based on coupling coefficients of inter-coupled resonators and the external quality factors of the input and output resonators.

The general coupling matrix [14-15] is of importance for representing of coupled-resonator filter topologies. Modeling the circuit in matrix form is useful because matrix operations can be applied, such as inversion, similarity transformation, and partitioning.

Such operations simplify the synthesis, reconfiguration of the topology, and performance simulation of complex circuits.

In recent years new concepts in synthesis and fabrication techniques have allowed the construction of structures and composite materials. The first attempt to explore the concept of “artificial” materials appears to trace back to the late part of the nineteenth century when in 1898 Jagadis Chunder Bose conducted the first microwave experiment on twisted structures geometries that were essentially artificial chiral elements by today´s terminology [16]. Since then, artificial complex materials have been the subject of research for many investigators worldwide. Media with negative permeability does not exist in nature due to the weak magnetic interactions in most solid-state materials [17].

Wave propagation in media with simultaneously negative permittivity (ε) and permeability (μ) would propagate in a direction opposite to that of the flow of energy was discussed and analyzed by Veselago [18] in 1967. He concluded that plane-waves propagation in such media allowed by Maxwell′s equations could be described by an electric field intensity vector E, magnetic field intensity vector H and direction propagate vector k. If both ε and μ are positive then E, H and k form right hand material (RHM), but if $\varepsilon<0$ and $\mu<0$, then E, H and k form left-handed material (LHM).

The negative sign of the refractive index naturally arises in the theoretical description of the electromagnetic properties of materials with $\varepsilon<0$ and $\mu<0$. A negative refractive index means that the phase velocity (v_p) of a propagating wave, which describes the propagation of individual wave fronts in a wave group, is opposite to the movement of the energy flux of the wave, represented by the Poynting vector (S). A wave with the phase velocity opposite to the direction of energy flow is also sometimes referred to as a ‘backwards wave’.

Research in LHM was standing by for more than 30 years due to the lack of experimental verification. The first important advance on LHM occurred in 1996, when Pendry [19] realized the artificially electric plasma using the wire medium whose permittivity is negative.

The first artificial LHM was made by Smith [20] in 2001 using the combination of wires and split-ring resonators (SRRs). In this famous experiment, the negative refraction phenomenon was verified.

The second important advance on LHM came in 2005 when the gradient refractive index medium was realized to bend electromagnetic waves [21], and in 2006 when the optical transformation was proposed to make invisible cloaks and to control the propagation of electromagnetic waves by using Metamaterials (MTMs) [22].

MTMs, also known as LHM or negative refractive index material (NIM), which have interested in the scientific communities over the past 15 years.

MTMs are widely [23-24] used in the design of sub-wavelength sized resonators and microwave filters with enhanced bandwidth and performance. Realization of metamaterials can be divided into the resonant and transmission line approach. In the resonant approach the electric or magnetic polarizability of a host medium is modified through embedding sub-wavelength sized resonant. The transmission line [25] approach, on the other hand, consists of loading host transmission line networks with lumped elements such as capacitors, inductors and resistors.

Current implementations of metamaterials rely on infinite rods and split-ring resonators (SRRs) to achieve a negative permittivity and a negative permeability, simultaneously.

Actually, the term “split-ring resonator” was proposed long before Pendry’s work [19]. In the early 1980s, Hardy used a similar structure and this exact term to describe a hollow metallic cylinder with a linear cut that exhibited a magnetic resonance at about 1 GHz [26]. Pendry and coworkers reinvented the structure in its modern form.

The size of SRR should be much smaller than the free space wavelength at the frequency range of interest. From the equivalent circuit point of view, each SRR essentially behaves as a resonator circuit in response to the external field. These resonators can be modelled in a very rough description as parallel LC tanks. An estimation of the equivalent inductance L and capacitance C can gives an estimation of the resonance frequency in an SRR acting as a magnetic meta-atom. The double ring [27], which is a special case of the SRR [28], was used for the fabrication of a MTM. It consists of two conductive rings placed back to back on a thin dielectric substrate with

their slots oriented in opposite directions. Recently, the developments of electromagnetic band-gap (EBG) structures, single-negative (SNG) and double-negative (DNG) materials as subsets of MTMs are attracted by scientist.

Generally, EBG structures are defined as artificial periodic (or sometimes non-periodic) objects that prevent/assist the propagation of electromagnetic waves in a specified band of frequency for all incident angles and all polarization states.
The fundamental understanding of EBG structures can be derived from Brillouin's work in 1940s [29]. He demonstrated that a periodic lattice imposes restrictions on the k vectors of waves than may propagate within it.
From a simplistic viewpoint, periodic structures impose periodic boundary conditions to the propagation generating modes. Electromagnetic waves which do not satisfy these boundary conditions cannot propagate.
Due to their unique band gap features, EBG structures can be regarded as specific type of MTMs.

1.1 Motivation

Nowadays, microwave materials are being used in a variety of applications [30-31] ranging from communication to sensing devices. The emersion of MTMs with engineered and controllable electromagnetic properties enabled opportunities in the realization of enhanced microwave devices, such as antennas, filters, couplers, imaging systems and cloaking devices.

Permittivity ε and permeability μ are used to characterize the electric and magnetic properties of materials. In microwave engineering it is difficult to find a naturally material with arbitrary values of ε and μ. MTMs comprise artificially structured composite with controllable ε and μ that are difficult to obtain with naturally materials.

As an ordinary material is made of atoms or molecules, a MTM is an effective media composed by lattices of "artificial" molecules consisting of sub-wavelength sized metallo dielectric scatterers or inclusions (inclusions create by controlling the reactivity of atoms and molecules likewise nanostructured MTMs can be realized by controlling the positioning of these nano-inclusions.). If the size and periodicity of the inclusions is

smaller than the wavelength, the MTM can be regarded as homogeneous and its properties can be represented by macroscopic effective material parameters ε_r^{eff} and μ_r^{eff}.

Almost all bulk MTMs used at the present are based on only two structures: a dense array of thin wires combined with an array of split-ring resonators (SRRs) [32].

The wires are used to provide negative dielectric permittivity, while SRRs give negative magnetic permeability. The dynamic control over MTMs properties is nontrivial since they possess left-handed properties only in some finite frequency range, which is basically determined by the geometry of the structure. The possibility to control the effective parameters of the MTM using nonlinearity has recently been suggested in [33-34].

Conducting wires are polarized by the electric field, generating the desired relative permittivity, ε_r for all frequencies below a certain cut-off frequency. Below a special frequency (a cutoff frequency of the array) there is no propagation and an electromagnetic wave experience total reflection [32].

Therefore, to guarantee the effective media behavior of a periodic structure at a certain frequency, it is required that lattice constant (a) be lower than the wavelength ($a \ll \lambda$).

Although, the average lattice constant (p) in current MTMs is electromagnetically too large for high-quality refraction. Current MTMs are typically characterized by p/λ_g 1/5…1/15, so that, although refraction is dominating, diffraction/scattering effects tend to alter the purity of refractive effects and increase the transmission losses. Refractive effects are relatively diffuse, and consequently difficult to exploit in practical applications. To obtain very pure refractive phenomena, it is necessary to homogenize the MTM, that is, to decrease the structural feature p/λ_g by one order of magnitude or more. If this challenge can be met, MTMs behave as “real-artificial” materials that mean the unit cells of the MTM would be so small that they would really behave as atoms in natural materials so as to produce a perfectly homogeneous macroscopic response.

In natural media, the atomic lattice constant is of the order of the angstrom ($p \approx 10^{-10}$ m); therefore, we have in the microwave range an atomic lattice constant of the order of one thousands of millions smaller than wavelength ($p/\lambda_g = 10^{-9}$), which ensures a

perfectly homogeneous response to electromagnetic waves. Such a huge ratio between λ_g and p is not necessary to obtain good refraction; a decrease of p/λ_g in MTMs from ~ 1/10 to 1/100 would be perfectly sufficient, since scattering would have then become completely negligible.

As shown in Fig1.1, a MTM appears to be homogeneous for electromagnetic waves if the unit cells are electrically small.

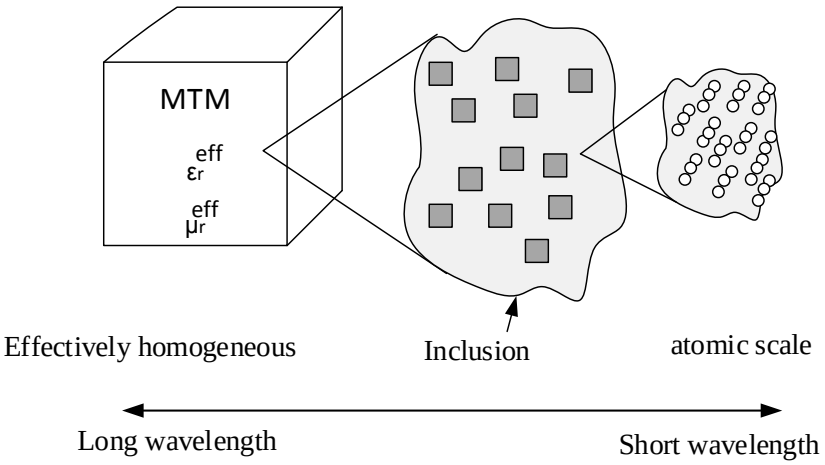

Fig.1. 1 Characteristic size of a MTM with sub-wavelength inclusions embedded in a host.

Recently, some authors have revisited the topic of artificial dielectrics on MTMs and, based on the works of Lewin [35] on the macroscopic properties array of particles embedded in a background matrix, have proposed theoretical solutions for LH MTM [36,37]. These solutions are very interesting because they represent the first specific suggestions for the realization of isotropic LH MTMs.

It is well known that dielectric properties can be modeled using distributed L-C networks. For a conventional dielectric, the per-unit-length capacitance and inductance can be directly related to the free-space permittivity and permeability, respectively, implying the use of a low-pass topology.

Electromagnetic bandgap (EBG) structure is a subgroup of MTMs, which exhibit stop bands for electromagnetic waves irrespective of polarization or angle of incidence.

The innovation of EBGs is the application of an array of periodic patches or apertures, i.e. lumped circuit elements, to produce a thin two–dimensional structure that must generally be described by band structure concepts, even though the thickness and periodicity are both much smaller than the operating wavelength. The EBG inhibits propagation of electromagnetic wave in certain range of frequency called bandgap which depend on its geometrical and material parameters

One of the main potential of MTMs is to synthesis and design of new microwave devices which can improve performance and new functionalities, due to the unique and controllable electromagnetic properties of these structures, as well as device miniaturization. .

Miniaturization, optimization of device performance through elimination of spurious frequencies, and possibility to control filter bandwidth over wide margins, are main issues for wireless communications.

The size reduction of microwave components is based on two features: (1) the small dimensions of the constitutive unit cells of MTMs and (2) the control of the electrical length, which covers a wide margin with a single-unit cell.

As MTMs are frequency-selective structures by nature, their application to the design of compact microwave filters seems to be straightforward.

To date, MTMs have commonly been formed from resonant conducting circuits that dimensions and spacing are much less than the wavelength of operation. By engineering the dipolar response of these resonant elements, an unprecedented range of effective material responses can be realized, including artificial magnetism and large positive and negative values of the effective ε and μ. There is an alternative approach to obtain artificial magnetism that relies instead on the resonances in sub-wavelength dielectric resonators. Sub-wavelength particles with very high positive dielectric permittivity support strong resonances with a large displacement current, which may give rise to strong magnetic field induced by contra-directional displacement currents. Moreover, the large dielectric constant implies a small wavelength inside the high-permittivity region; therefore the physical size of the resonator can be many times smaller than the free-space wavelength. This situation justifies the treatment of the system as a

macroscopically homogenous medium, and the use of effective constitutive parameters to describe its interaction with external waves is applicable.

The relative dielectric constant of the materials for constructing dielectric resonator in microwave filters generally was chosen from a higher value compared to the base substrate. The primary advantage in using a high dielectric constant is to miniaturize the filter size. The size of dielectric resonator filter is considerably smaller than the dimension of waveguide filters operate at the same frequency.

1.2 Aims and objectives

In spite of MTMs are conceptually interesting, suffers some major drawbacks that limit its utilization in practical applications. In this thesis is tried to give some proposal to overcome some of these drawbacks.

A major drawback in most MTMs realized to date is the losses that they exhibit. To overcome this suffering, high dielectric resonators, which can have spherical, cylindrical or cubic shape, are proposed.

From a loss reduction and fabrication tolerance point of view, in this work is tried to prove that dielectric resonators provide suitable performance for the MTMs designers. The dielectric resonators are based on different resonance modes. For dielectric resonators, their first resonance frequencies are so high (e.g. $10\sim20\ GHz$) that the long-wavelength condition cannot be met, so effective medium theory cannot be used to characterize them. As a result, it is desirable to design dielectric resonator whose resonance modes can be tuned to lower frequencies (e.g. $1\sim5\ GHz$). High-dielectric resonator with good temperature stability and low dielectric loss are required to guarantee the effective media effect. By depositing or embedding Epoxy paste as a high dielectric constant resonator on top and bottom of the wavelength, the first resonance can be tuned significantly to lower frequency (e.g. $1\sim5\ GHz$).range so as to meet the long-wavelength condition. The proposed high dielectric resonator in this dissertation is based on coupled of sub-wavelength high dielectric constant resonators

Another obstacle in MTMs practical applications is capable of blocking the surface electromagnetic wave propagation within a particular frequency band. This issue can be resolved by the implementation of EBG structures which possess periodic metal patches on a dielectric substrate. EBG structures have a property of preventing the surface waves at a specific frequency and also reflect back any incoming wave without any phase shift. In this thesis EBG was considered for which the periodicity is much smaller than the wavelength of the incident electromagnetic wave. Therefore, effective material parameters such as ε, μ and a refractive index can be defined. This definition establishes a direct relationship with artificial dielectrics which are deposited or/and embedded in the micro-strip line. One suitable host transmission line is the microstrip, which is a class of electromagnetic waveguide consisting of a strip conductor and a backplane, separated by a thin dielectric. Micro-strip lines are easily integrated with discrete or printed passive components, as well as active components, and the equipment required to design, construct, and test a micro-strip circuit is inexpensive and readily accessible.

The specific objectives of the thesis are as follows:

- Investigate a band-stop filtering with EBG structure by depositing thick film high dielectric constant resonators (TFDR) which Epoxy paste is used as a high DR constant.
  - ✓ Simulate the frequency response of the filters using electromagnetic simulator software.
  - ✓ Fabricate and measure the frequency response of the filter
- Explore a band-pass filtering with EBG structure by embedded high dielectric resonators (EDR) which epoxy paste is used as a high DR constant.
  - ✓ Simulate, fabricate and measure the frequency response of the filter.
- Propose a band-pass filtering with SRR and miniaturization filter with EDR which epoxy paste is used as a high DR constant.
  - ✓ Simulate, fabricate and measure the frequency response of the filter
- Develop new configuration of multi-mode resonators (MMR) to achieve an ultra-wideband (UWB) filter.
  - ✓ Calculate filter parameters and the matrix concept, based on the transmission line theory
  - ✓ Simulate, fabricate and measure the frequency response of the filter.

1.3 Scope and Organization

After the introduction, Chapter 2 is devoted to review the theoretical concept used in the thesis. Fundamental theories of microwave filters based on passive components are reviewed in Chapter 2. The passive technology can be understood as the combination of two different kinds of elements: transmission lines and resonators. In some cases, the transmission lines acts as resonators and eventually lumped elements can be introduced into the circuits to load the lines or act as resonators. The associated loses to the lumped elements makes them not recommendable to their utilization in complex structures. From loses point of view it seems to be wanted the utilization of resonators.

Dielectric resonators are used to replace waveguide filters in such demanding applications as satellite communications where microstrip and strip-line resonators cannot be used because of their inherently high losses. The typical utilization of DRs is in microwave stable fixed-frequency oscillators, narrow band filters. The advantages of DRs are high efficiency and high temperature stability. For the applications of DRs in microwave filters, it is necessary to study the coupling between two dielectric resonators which is studied in chapter. The relative dielectric constant of the materials for constructing DR in microwave filters generally was chosen from a higher value compared to the base substrate. The primary advantage in using a high dielectric constant is to miniaturize the filter size. The size of DR filter is considerably smaller than the dimension of waveguide filters operate at the same frequency.

The lumped-element sufficient enough at low frequencies, but two problems arise at higher RF and microwave frequencies. First, lumped-element inductors and capacitors are generally available only for a limited range of values, and can be difficult to implement at microwave frequencies. Distributed elements such as open-circuited or short-circuited transmission line stubs, are often used to approximate ideal lumped elements. In addition, at microwave frequencies the distances between filter components is not negligible. The first problem is treated with Richards' transformation, which can be used to convert lumped elements to transmission line sections. Kuroda's identities can then be used to physically separate filter elements by using transmission line sections. Because such additional transmission line sections do not affect the filter

response, this type of design is called redundant filter synthesis. These drawbacks are explained in the following of chapter 2.

In microwave resonators circuit, exchanging stored energy is the same way in lumped element circuit resonator which stored energy transferred between an inductor and a capacitor and back again in every period. Spatially resonators with stored electric energy and they may be described in terms of their quality factor (Q).

Then chapter 2 is continued to fundamental problems of filter design which that the pass-band loss is inversely proportional to the filter bandwidth. Thus for very narrow band applications it is often the case that very high resonator Q factors must be used in order to achieve low pass-band loss. Further increases in Q, may be achieved by using dielectric resonators as the resonant elements within filters. The electromagnetic properties of these devices and the design theories for waveguide and dielectric resonator filters are described in this chapter.

Chapter 3 is devoted to the dielectric resonators descriptions and different ways to deal with these elements in the design process. The DRs are used to replace waveguide filters in such demanding applications as satellite communications where micro-strip and strip-line resonators cannot be used because of their inherently high losses. A recent advance in miniaturization of microwave circuits has been the appearance of the low-loss temperature-stable dielectric resonators. There are some characteristic for DRs. First, the concentration of the electric fields within any material is directly related to its complex permittivity. While the real part of the permittivity is most directly related to the propagation velocity of waves in a material, and the imaginary part is directly linked to the losses incurred as electromagnetic waves travel through a medium. Second, for a given dielectric constant, both resonant frequency and Q-factor are defined according to the dielectric resonator dimensions. That, the higher the dielectric constant, the smaller the space within which the fields are concentrated, the lower the dimension at a defined frequency. These characteristic are explained in chapter 3. Materials with high dielectric constants are required in order to provide miniaturization at the frequencies typically used for wireless applications. Materials that are commonly used in dielectric resonator filters are ceramics, such as barium tetratitanate compounds. The advantage of using an epoxy/$BaTiO_3$ composite is that it combines the low temperature process ability of epoxy along with the high dielectric constant of $BaTiO_3$. The experimental and fabrication process for epoxy/$BaTiO_3$ composite is investigated in this chapter.

Since, the DRs are novel type of MTMs distinguished by small dissipative losses as well as convenient conjugation with external structures, brief history of MTMs is studied in the first part of chapter 4. The theory, design, and experiments involving planar transmission-line based MTMs, SSR and EBG are described in this part.

The aim of chapter 4 is the development of the scattering theory of electro-magnetic waves on the DRs, located in the various transmission lines, as well as an investigation of the band-pass and band-stop filters.

In chapter 4 a novel stop-band filter consists of three cylindrical dielectric resonators were excited with a microstrip line is investigated. In the following a new approach of designing a band-pass filter by applying a combination of microstrip ring and embedded dielectric resonators is presented. DRs' interaction leads to considerable spectrum and provide efficient coupling when are closely placed to each other. To analyze the coupling, first field analysis of single resonator based on epoxy paste commercial dielectric constant is investigated and then relation between the coupling coefficient, k, and the spacing between the two resonators are studied.

Since, the sub-wavelength property of the Split Ring Resonator (SRR) has been successfully applied to the miniaturization of passive microwaves devices, a band-pass filter by utilization of SRR technology is reported in this part. Further miniaturize design could be done by including high dielectric constant in the center of the SRR.

Another approach to reduction size of filter is to modify the traditional resonator to generate additional modes, which make the resonator to behave as a multimode resonator. Thus one physical resonator can be treated as multiple electrical resonators. Last part of this chapter is proposed a novel multimode resonator (MMR) ultra-wide band-pass (UWB) filter design using a grounded open ring resonator.

1.4 References

[1] C. A. Desoer and E. S. Kuh, "Basic Circuit Theory," McGraw-Hill, New York, 1969.

[2] H. J. De Los Santos, "Introduction to Micro electro mechanical (MEM) Microwave Systems", Norwood, MA: Artech House, 1999.

[3] R. Carso, "High frequency amplifiers," John Wiley& Sons, New York, 1975.

[4] J. G. Garcia, F. Martin, F. Falconc, J. Bonache J.D. Baena I. Gil, E. Amat, T. Lopetegi, M. A. G. Laso, J. A. M. ltunnendi, M. Sorolla and R. Marques, "Microwave filters with improved stopband based on sub-wavelength resonators," IEEE Trans. Microwave Theory Tech., Vol 53, No 6, pp 1997-2004, 2005.

[5] M. B. King, L. W. Heep and J. C. Andle, "1500 MHz Coupled Resonator Filter," Proceedings IEEE Ultra sonics Symposium, pp 127-130, 1987.

[6] P. V. Wright, "Low-cost High-Performance Resonator and Coupled-Resonator Design: NSPUDT and Other Innovative Structures," Proceedings 43rd Annual Symposium on Frequency Control, pp 574-587, 1989.

[7] D. Ash, "Coupled Resonator Phase Shift Oscillator," U. S. Patent No. 4,760,352, 1988.

[8] A. E. Atia and A. E. Williams, "Narrow-band-pass waveguide filters," IEEE Trans.,MTT-20, pp 258–265, 1972.

[9] C. Wang, H. W. Yao, K. A. Zaki and R. R. Mansour, "Mixed modes cylindrical planar dielectric resonator filters with rectangular enclosure," IEEE Trans., MTT-43, pp 2817–2823, 1995.

[10] H. W. Yao, C. Wang and K. A. Zaki, "Quarter wavelength ceramic comb-line filters," IEEE Trans., MTT-44, pp 2673–2679, 1996.

[11] J. S. Hong and M. J. Lancaster, "Couplings of micro-strip square open-loop resonators for cross coupled planar microwave filters." IEEE Trans, MTT-44, pp 2099–2109,1996

[12] J. S. Hong, M. J. Lancaster, D. Jedamzikand and R. B. Greed, "On the development of super conducting microstrip filters for mobile communications applications," IEEE Trans, MTT-47, pp1656-1663, 1999.

[13] P. Blondy, A. R. Brown, D. Cros and G. M. Rebeiz, "Low loss micro machined filters for millimeter wave telecommunication systems," IEEE MTT-S, Digest, pp 1181-1184, 1998.

[14] R. J. Cameron, "General coupling matrix synthesis methods for Chebyshev filtering functions," EEE Trans. Microwave Theory Tech., vol. 47, pp. 433–442, 1999.

[15] R. J. Cameron "Advanced Coupling Matrix Synthesis Techniques for Microwave Filters" IEEE Transaction on Microwave Theory and Techniques, Vol 51, No 1, 2003.

[16] J. C. Bose, "On the rotation of plane of polarization of electric waves by a twisted structure," Proc Roy Soc, Vol 63, pp 146-152, 1898.

[17] L. D. Landau, E. M. Lifshitz and L. P. Pitaevskii "Electrodynamics of Continuous Media," Pergamon, New York, 1984.

[18] V. G. Veselago, "The electrodynamics of substances with simultaneously negative values of and μ," Soviet Physics Uspekhi, Vol 10, No 4, pp 509-514, 1968.

[19] J.B. Pendry, A. J. Holden, W. J. Stewart, and I. Youngs, "Extremely low frequency plasmons in metallic microstructures," Physical Review Letters, Vol 76, pp 4773- 4776, 1996.

[20] R. A. Shelby, D. R. Smith and S. Schultz, "Experimental verification of a negative index of refraction," Science 292, pp 77-79, 2001.

[21] D. R. Smith, J. J. Mock, A. F. Starr and D. Schurig, "Gradient index metamaterials," Phys. Rev. E 71, 036609, 2005.

[22] U. Leonhardt, "Optical conformal mapping," Science 312, pp 1777-1780, 2006.

[23] F. Aznar, J. G. Garcia, M. Gil, J. Bonache and F. Martin. "Strategies for the miniaturization of metamaterial resonators," Microwave and Optical Technology Letters, Vol 50, pp 1263-1270, ISSN 1098-2760, 2008.

[24] P.A. Belov, Y. Hao, S. Sudhakaran, "Subwavelength microwave imaging using an array of parallel conducting wires as a lens", Physical Review B, vol. 73, 033108 (1-4), 2006.

[25] G. V. Eleftheriades and K. G. Balmain, "Negative Refraction Metamaterials." Fundamental Principles and Applications, Wiley IEEE Press, pp 53-91, 2005.

[26] W.N. Hardy and L. A. Whitehead, "Split-ring resonator for use in magnetic resonance from 200 - 2000 MHz," Rev Sci Instrum, 52, pp 213–216, 1981.

[27] R. Marques, F. Medina and R. Rafii-El-Idrissi, "Role of anisotropy in negative permeability and left-handed metamaterials," Phys Rev B, Vol 65, pp 1-6, 2002.

[28] J. B. Pendry, A. Holden, J. D. Robbins and J.W. Stewart, "Magnetism from conductors and enhanced nonlinear phenomena," IEEE Trans MTT, Vol 47, No 11, pp. 2075-2084, 1999.
[29] L. Brillouin, "Wave Propagation in Periodic Structures: Electric Filters and Crystal Lattices", McGraw-Hill, New York, 1946.
[30] C. Caloz and T. Itoh. "Electromagnetic Metamaterials," Transmission Line Theory and microwave Applications, John Wiley& Sons, pp 1-25, 2004.
[31] R. Marques, F. Martin and M. Sorolla. "Metamaterials with Negative Parameters: Theory, Design and Microwave Applications, John Wiley& Sons, pp 1-48, 2008.
[32] N. Engheta, and R. W. Ziolkowski, "Electromagnetic Metamaterials: Physics and Engineering Explorations," Wiley-IEEE Press, USA, 2006.
[33] A. A. Zharov, I. V. Shadrivov and Yu. S. Kivshar, "Nonlinear properties of left-handed metamaterials," Phys Rev. Lett. 91, pp 037401-4, 2003.
[34] M. Lapine, M. Gorkunov, and K. H. Ringhofer. "Nonlinearity of a metamaterial arising from diode insertions in to resonant conductive elements," Phys Rev, E 67, pp 065601-4, 2003.
[35] L. Lewin "The electrical constants of a material loaded with spherical particles," Proc. Inst. Elec. Eng., Vol 94, pp 65-68, 1947.
[36] C. L. Holloway, E. F. Kuester, J. Baker-Jarvis, and P. Kabos,"A double negative (DNG) composite medium composed of magnetodielectric spherical particles embedded in a matrix," IEEE Trans. Antennas Propagat., Vol 51, No 10, pp 2596-2603, 2003.
[37] O. G. Vendik and M. S. Gashinova "Artificial double negative (DNG) media composed by two different dielectric sphere lattices embedded in a dielectric matrix," Proc. European Microwave Conference, Netherlands, pp 1209-1212, 2004.

CHAPTER 2

2 Passive technology

The passive technology can be understood as the combination of two different kinds of elements: transmission lines and resonators. In some cases, the transmission lines acts as resonators and eventually lumped elements can be introduced into the circuits to load the lines or act as resonators. The associated loses to the lumped elements makes them not recommendable to their utilization in complex structures. From loses point of view it seems to be wanted the utilization of distributed resonators. Different possibilities to include resonators which are the DRs; however, the excitation structures constitute an important drawback for their utilization.

As was pointed out in the previous section, the utilization of DR could help to increase the device performance and they could be modeled as a combination of L, C and R lumped elements.

The fundamental characteristic that distinguishes RF engineering from microwave engineering is directly related to the frequency (and thus the wavelength, λ). This distinction arises fundamentally from the finite speed of propagation of electromagnetic waves (and thus, by extension, currents and voltages). In free space, $\lambda = c/f$, where "*f*" is the frequency of the signal and "c" is the speed of light. For low-frequency and RF circuits, the signal wavelength is much larger than the size of the electronic system and circuit components. In contrast, for a microwave system the sizes of typical electronic

components are often comparable to the signal wavelength. As illustrated in Figure 2.1, for components smaller than the wavelength (i.e., $l < \lambda/10$), the finite velocity of the electromagnetic signal as it propagates through the component leads to a modest difference in phase at opposite ends of the component. For components comparable to or larger than the wavelength, however, this end-to-end phase difference becomes increasingly significant.

By increasing frequency into the microwave spectrum it is easy to see that lumped element theories could not suffice, e.g. the wavelength at 10 GHz is only 3 cm and circuit elements may easily have dimensions in excess of a quarter wavelength.

For this reason circuit components commonly used at lower frequencies, such as resistors, capacitors, and inductors, are not readily available. The relationships between the wavelength and physical dimensions enables new classes of distributed components to be constructed that have no analogy at lower frequencies It is thus necessary to have design theories which are pertinent to distributed circuits.

Networks consisting of arbitrary connections of distributed circuit elements do not have a unified design theory. Although analysis of such circuits may be accomplished by solving Maxwell's equations using, for example, finite element analysis, this is not the same as having a design theory. As an example a circuit consisting of an interconnection of transmission lines of different lengths would require a theoretical approach using more than one complex variable. Since, a lumped element is circuit could be completely described in terms of one complex frequency variable.

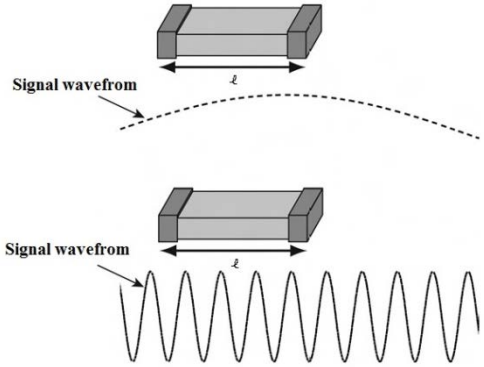

Fig. 2. 1 Schematic representation of component dimensions relative to signal wavelengths. Conventional lumped-element analysis techniques are typically applicable for components for which $l<\lambda/10$ (a) since the phase change due to electromagnetic propagation across the component is small, while for component with $l>\lambda/10$ (b) the phase change is significant and a distributed circuit description is more appropriate[1].

This chapter a brief review of the definitions and fundamental concepts used in the study of passive circuit.

Section 2.1 is focused on the passive equivalent circuit elements and this is followed by a brief discussion on the elements of linear circuit analysis. The circuit is composed of resistors, capacitors, inductors, and voltage and/or current sources, and each of these circuit elements is given a symbol together with a mathematical expression (i.e., the voltage-current or simply *v-i* relation) relating its terminal voltage and current at every instant of time. Once the network and the *v-i* relation for each element is specified, Kirchhoff's voltage and current laws can be applied, possibly together with the physical principles to be introduced in this section. Also this section is included the limitation of lumped equivalent circuit models utilization.

Since, a mathematical model describes the behavior of a physical system or device in terms of a set of equations, together with a schematic diagram of the device containing the symbols of its elements, their connections, and numerical values. Then a physical electrical system can be represented graphically by a network (which includes resistors, inductors, and capacitors as its components). Passive network analysis described in section 2.1.1. And this is continued with classification of electrical circuits into various categories. Four of the more familiar classifications are (a) linear and nonlinear circuits, (b) time-invariant and time-varying circuits, (c) passive and active circuits, and (d) The bounded real condition.

A linear circuit can be described by a set of linear equations; otherwise it is a nonlinear circuit. A time-invariant circuit or system implies that none of the components of the circuit have parameters that vary with time; otherwise it is a time-variant system. If the total energy delivered to a given circuit is nonnegative at any instant of time, the circuit is said to be passive; otherwise it is active. In reality all real microwave filters contain resistive elements but it is useful in the initial design process to simplify things by working with lossless networks. The concept of the input impedance of a network in terms of the complex frequency variable has led to the properties of positive real and bounded real functions. These four concepts are reviewed section 2.1.1. Also transfer functions, frequency response, and stability analysis are discussed.

Another method of classify is based on circuit configurations (topology), which gives rise to such terms as ladders. Circuit and system analyses that conduce an understanding of meaningful topological structures could be Foster´s theorem which explained in detail in section 2.1.2.

Circuits can use of inductors and capacitors in different ways to achieve their functionality. RLC circuits are simple enough to allow full analysis, and rich enough to form the basis for most of the circuits. Section 2.1.3 is presented the exploration of the frequency response of RLC circuits by investigating the parallel and series RLC circuit.
Resonators can be coupled to create frequency selective structures which are used in microwave devices.
Coupled microwave resonators are required components in modern communication systems in particular for design of RF/microwave filters (narrow band pass filter).
There are some techniques based on coupling matrix for coupled resonators arranged in a two-port network. Coupling matrix can be formulated either from a set of loop equations or from a set of node equations. This leads to a very useful formula for analysis and synthesis of coupled-resonator filter circuits in terms of coupling coefficients and external quality factors which are explained in detail in section 2.1.4.
There are two drawbacks in using lumped element at RF and microwave frequencies. First, lumped-element inductors and capacitors are available only for a limited range of values, and can be difficult to implement at microwave frequencies. Distributed elements such as transmission line, are often used to approximate ideal lumped elements which are explained in section 2.2. This is followed by transmission line ABCD parameters for two ports. Second drawback is, at microwave frequencies the distances between filter components is not negligible. The first problem is covered with Richards' transformation, which can be used to convert lumped elements to transmission line sections. The second problem is covered by Kuroda's identities. It can be used to physically separate filter elements by using transmission line sections. Because such additional transmission line sections do not affect the filter response.
The concept of Richards' transformation and Kuroda identities are explained in section 2.2.3. And also the coupled transmission line equivalent circuit is included in this section.
At microwave frequencies, "parasitic" effects limit the performance of passive elements. The effects of dissipation, due to leakage currents, are measured by the quality factor Q of the capacitor and inductor. The losses in an inductor and capacitor equation are calculated in section 2.3.1.
Determination of dissipation factor in function of frequency is based on measuring a loaded quality factor Q_L of the micro-strip ring resonator structure at each resonance frequency. The loaded quality factor includes losses, which are due to external load and

the micro-strip ring resonator itself. This is continued by the unloaded quality factor Q_u which includes the total losses of the micro-strip ring resonator.

2.1 Lumped-element equivalent circuit model

Lumped element such as resistors, capacitors, and inductors in microwave circuits is defined as a passive component whose size across any dimension is much smaller than the operating wavelength.

Lumped elements are widely used in couplers, filters, power dividers/combiners, impedance transformers, baluns, control circuits, mixers, multipliers, oscillators, and amplifiers.

For sufficiently small component dimensions, there are no variations in resistance, capacitance, and inductance except as associated with any frequency dependence of material resistivity, permittivity, and permeability

Since in ordinary RF design, the circuit components are small compared to a wavelength, they can be modelled as lumped elements for which Kirchhoff's voltage and current laws apply at every instant in time. Parasitic inductances and capacitances are incorporated to accurately model the frequency dependencies and the phase shifts, but these quantities can be related with an appropriate lumped-element equivalent circuit. In practice, for the applicability of a lumped-element equivalent circuit is that the component size should be less than $\lambda/10$ at the frequency of operation. For microwave frequencies for which component size exceeds approximately $\lambda/10$, the finite propagation velocity of electromagnetic waves can no longer be as easily absorbed into simple lumped-element equivalent circuits.

When the signal frequencies imposed on a passive network are small so that their associated wavelengths are large, the classic lumped circuit approximation applies to all circuit level analyses conducted on the network. This lumped circuit presumption is convenient from several perspectives. For example, it allows branch elements of the circuit undergoing study to be identified, and it permits a straightforward analytical definition of the volt-ampere properties of these elements. Due to this branch identification attribute, the lumped circuit approximation supports the Kirchhoff laws to determine circuit equilibrium.

In this case, the current flowing into one terminal of a two-terminal branch element is, at any instant of time, precisely the same as the current that resultantly flows out of the

branch. And voltages with respect to any reference node along any length of interconnect are, at any instant of time, identical and independent of the actual line length.

Analytical complexities occurred when the signal frequencies of interest increases to RF and microwave frequency that their wavelengths are comparable to, or even smaller than, the feature sizes of the elements embedded in a circuit. In this case, branch elements and their connective junctions and nodes are blurred because of distributed resistances.

An ideal lumped element is not realizable even at lower microwave frequencies because of the associated parasitic reactance due to fringing fields. At RF and microwave frequencies, each component has associated electric and magnetic fields and finite dissipative loss. Thus, such components store or release electric and magnetic energies across them and their resistance accounts for the dissipated power.

Lumped element equivalent circuit model simplifies the description of the behavior of circuit which consists of basic circuit elements (L, C, or R) with the associated parasitic. These comprehensive descriptions are including the effect of ground plane, fringing fields, proximity effects, substrate material and thickness and conductor thickness. Thus, an equivalent circuit representation of a lumped element with its parasitic and their frequency-dependent characteristics is essential for accurate element modelling. An equivalent circuit model consists of the circuit elements necessary to fully describe its response, including resonances, if any. Models can be developed using analytical, electromagnetic simulation, and measurement based methods.

There are two main drawbacks for the utilization of lumped equivalent circuit models. First, a low-loss narrowband filter having bandwidth cannot be designed using a lumped-element approach due to its low Q values. Second, there is not a clear relation between the circuit elements and the physical dimensions.

At higher microwave frequencies, and particularly at millimeter-wave frequencies, lumped elements are very difficult, or even impossible, to achieve because of dimensional limitations in fabrication technologies. For these frequencies, the time delay associated with signal propagation from one end of a component to the other is an appreciable fraction of the signal period, and thus lumped-element descriptions are no longer adequate to describe the electrical behaviour. A distributed-element model is required to accurately capture the electrical behaviour.

In applications where it is possible to utilize lumped elements, the advantages are usually small dimensions, wideband characteristics, and low production cost. Their

drawbacks are lower Q and lower power-handling capability as compared with distributed circuits.

2.1.1 Network Analysis

At microwave frequencies, the use of voltmeters and ammeters for the direct measurement of voltages and currents do not exist. For this reason, voltage and current, as a measure of the level of electrical excitation of a network, could not be useful at microwave frequencies. On the other hand, it is beneficial to be able to describe the operation of a microwave network, such as a filter, in terms of voltages, currents, and impedances in order to make optimum use of low-frequency network concepts.

It is the purpose of this part to describe passive network concepts and provide equations that are useful in the rest of the thesis.Passive networks are manufactured using a variety of technologies, e.g. coaxial resonators, micro-strip, waveguide. However, they are normally designed using low-pass prototype networks as a starting point, regardless of the eventual physical realisation. Low-pass prototype networks are two-port lumped element networks with an angular cut-off frequency of ω=1, operating from a 1 Ω generator into a 1 Ω load. A typical low-pass prototype network is shown in Fig 2.2.

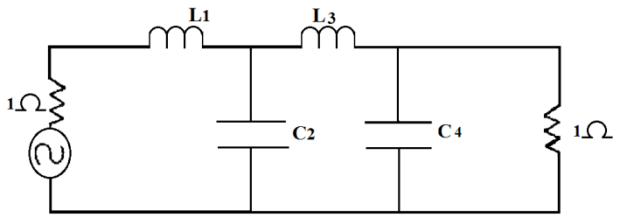

Fig. 2. 2 A typical low pass prototype network.

These network methods assume a basic understanding of Laplace transform theory and of the operation of inductors, capacitors and resistors. One port network was considered as presented in Fig 2.3.

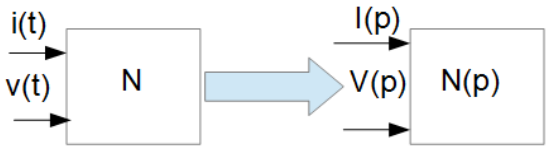

Fig. 2. 3 A one-port network and its Laplace transform equivalent.

This one-port network is excited by a voltage v(t) producing a current flow i(t). The Laplace transform of the voltage is V(p) and the resultant current is I(p).

This is the ratio of the Laplace transforms of its output and input signals. The voltage transfer function H(s) of a filter can be written as:

$$\mathbf{H(s)} = \frac{\mathbf{Vout(s)}}{\mathbf{Vin(s)}} \tag{2. 1}$$

Where Vin(s) and Vout(s) is the input and output signal voltages and s is the complex frequency variable.

Frequency response can be extracted from the transfer function which is an important aspect of classical control systems.

In the case of passive filters, high-pass, band-pass, or stop-band filters can be obtained by applying the frequency transformations to the impedances of normalized low-pass filter with 1-Ω input–output impedance and a 1-rad cutoff frequency.

Consider the fundamental limits on achievable selectivity by examining an “ideal” low-pass filter. This is defined as a two-port device with infinite selectivity as in Fig 2.4. The ideal low-pass transfer function is characterized by a magnitude function that is a constant in the pass-band and zero in the stop-band.

The corresponding phase is linear in the pass-band and the phase delay is a constant there. Such a low-pass filter cannot be represented by a quotient of finite-degree rational polynomials, it is necessary to seek some approximation to it. This may be done by having amplitude; phase and delay stay within prescribed tolerances.

The magnitude of the gain of the low-pass filter is unity in the pass-band and immediately drops to zero in the stop-band with no transition region. Hence [2]

$$|\mathbf{H(j\omega)}| = \mathbf{1} \quad |\boldsymbol{\omega}| < \boldsymbol{\omega_c} \tag{2. 2}$$

$$|\mathbf{H(j\omega)}| = \mathbf{0} \quad |\boldsymbol{\omega}| > \boldsymbol{\omega_c} \tag{2. 3}$$

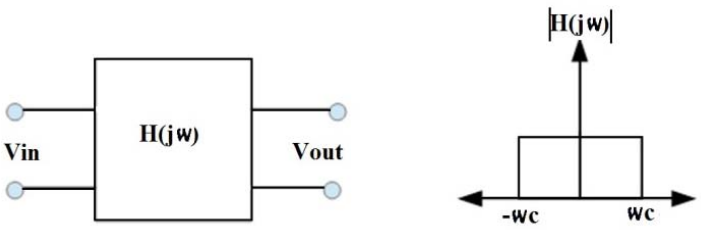

Fig. 2. 4 Ideal low pass filter and its frequency response.

The phase response of the filter is assumed to be linear in the pass-band.

Hence

$$\varphi(\omega) - k\omega \tag{2. 4}$$

That φ (ω) is characteristic of a phase.

The group delay is the derivative of the transmission phase with respect to the angular frequency. It is a measure of the distortion in the signal introduced, by phase differences for different frequencies and is defined as

$$T_g = -\frac{d\varphi(\omega)}{d\omega} \tag{2. 5}$$

Here φ is the transmission phase in radians and ω is the angular frequency in radians per second. From this definition, a linear phase (in respect to frequency) is represented by a constant group delay. The group delay is the slope of the graph of S_{21} (phase) as a function of frequency.

Consider a lumped element filter with the transfer function:

$$\mathbf{S_{21}(\rho)} = \frac{\mathbf{N(p)}}{\mathbf{P(p)}} \tag{2. 6}$$

Which p is the complex frequency variable. This is defined as a minimum phase network if there are no poles or zero in the right half p plane,

N (p)≠ 0 P (p) ≠ 0 Re p> 0

This defines N (p) and D (p) as Hurwitz polynomials.

A ladder network with N circuit elements has N transmission zero at infinity. Since all the transmission zero is at infinity the gain response must be a rational function with constant numerator. The zero of transmission is the zero of the numerator or the infinities of the denominator.

Hence the power gain is given by:

$$|\mathrm{H(j\omega)}|^2 = \frac{1}{\mathrm{A_N(\omega^2)}} \tag{2. 7}$$

That $\mathrm{A_N}(\omega^2)$ is a polynomial of degree N in ω^2 .

There are fundamental limits on the achievable performance of electrical filters, regardless of the physical construction. No finite device can produce an “ideal” or infinitely selective amplitude response. Furthermore, there are relationships between the phase and amplitude characteristics of minimum phase networks.

A lossless network is simply one that cannot absorb power. This does not mean that the delivered power at every port is zero; rather, it means the total power flowing into the device must equal the total power exiting the device.

In this part useful techniques for the analysis and synthesis of low-pass networks are developed. These network methods are basic understanding of Laplace transform theory and of the operation of inductors, capacitors and resistors. This part is developed by some imposed constraints when they are applied and H(s) has been designed that meet these constraints, and then a physical implementation is assured.
Some of these restrictions, which should be considered for filter design, are selected in order to provide theoretical concepts that are useful in the rest of the thesis.

2.1.1 Imposed constraint

This part is developed by some imposed constraints when they are applied and H(s) has been designed that meet these constraints, and then a physical implementation is assured. Some of these restrictions, which should be considered for filter design, are selected in order to provide theoretical concepts that are useful in the rest of the thesis.
These imposed constraints contain time invariant, linearity, passivity and the bounded real conditions which are explained as followed.

2.1.2 Linearity

The filter is considered here to be linear;
If a voltage $v_1(t)$across the terminals of *N* produces a current $i_1(t)$then

$$v_1(t) \rightarrow i_1(t)$$

$$v_2(t) \rightarrow i_2(t)$$

Now if the network is linear then the principle of superposition holds.

$$\alpha v_1(t) + \beta v_2(t) \rightarrow \alpha i_1(t) + \beta i_2(t) \quad (2.8)$$

That α and β are constants [2].

2.1.3 Passivity

If the network is also passive then the amount of energy which may be extracted from the network up to any point in time may not exceed the energy supplied to the network up to that point in time. Combining this property with property that all physical networks gives rise to real responses to real stimuli yield that Z(p) is a “positive real function”.

Z (p) is real for p real (2. 9)

$$\text{Re } Z(p)>0 \text{ for } p>0 \quad (2.\ 10)$$

Relation (2.9) implies that the coefficients of N (p) and D (p) are all real. Relation (2.10) implies that Z (p) has no poles or zero in the right half plane, i.e. both N(p) and D(p) are Hurwitz polynomials [2].

2.1.4 Time invariant

Since it is assumed that the designed analog filter will be implemented with fixed-value resistors, capacitors and inductors then the implementation could be time invariant, therefore;

If

$$v(t) \rightarrow i(t)$$

Then

$$v(t-\tau) \rightarrow i(t-\tau)$$

That (τ) is an arbitrary time delay. A time-invariant filter is built up from elements whose values do not change with time during the operation of the filter.

If a linear time-invariant network is excited by a voltage v(t) where:

$$v(t)=0 \text{ for } t<0$$

Then the relationship between voltage and current may be expressed as follows:

$$v(p) = Z(p)I(p) \quad (2.\ 11)$$

While v(p) is the Laplace transform of v(t) and I(p) is the Laplace transform of i(t). Here *p* is the complex frequency variable; Z(p) is the input impedance of the network, which is independent of v(t) and for a finite lumped network is a rational function of (p).

$$Z(p) = \frac{N(p)}{D(P)} \quad (2.\ 12)$$

In this case Z(p) may be expressed as the ratio of two polynomials [2].

2.1.5 The bounded real condition

The input impedance of passive linear time-invariant networks is a positive real function. In microwave filter design it is often desirable to work with reflection coefficients rather than input impedances.

The reflection coefficient Γ(p) of a network with an input impedance Z(p) is related to Z(p) by

$$\Gamma(p) = \mp \frac{Z(p)-1}{Z(p)+1} \quad (2.13)$$

Γ(p) is real for *(p)* real.

$0 \leq \Gamma(p) \leq 1$ for real $p > 0$

2.1.6 Lossless networks

In reality all real microwave filters contain resistive elements but it is useful in the initial design process to simplify things by working with lossless networks.

For positive real Z (p)

$$Z(p)|_{p-j\omega} = Z(j\omega) = R(\omega) + jX(\omega) \quad (2.14)$$

Where

$$R(\omega) = \text{Re } Z(j\omega) \quad (2.15)$$

$$X(\omega) = \text{Im } Z(j\omega) \quad (2.16)$$

By definition for a lossless network

$$R(\omega) = 0$$

If the input impedance of an one port network written in the form of

$$Z(p) = \frac{m_1+n_1}{m_2+n_2} \quad (2.17)$$

While m_1 and n_1 are the even and odd parts of N(p) and $m_2$and n_2 are the even and odd parts of D(p).

Z(p) may be split into an even polynomial plus an odd polynomial such as,

$$Z(p) = EV\ Z(p) + Odd\ Z(p)$$

Now even polynomials contain only even powers of *p* and odd polynomials contain only odd powers of "p". Hence Even Z(jω) is purely real and Odd Z (jω) is purely imaginary.

After calculation, Z(p) is the ratio of an even polynomial to an odd polynomial or an odd polynomial to an even polynomial. Z(p) is then known as a "reactance function". Now since Z(p) is positive real it cannot have any right half-plane poles or zero and Z(-p) cannot have any left half-plane poles or zero. However

$$Z(p) = -Z(-p) \quad (2.18)$$

Thus Z(p) can have neither right half-plane nor left half-plane zero. The poles and zero of a reactance function must thus lie on the imaginary axis. Furthermore, the poles of Z(p) may be shown to have positive real residues, yielding a general solution for a reactance function of the form

$$Z(p) = A_\infty p + \frac{A_0}{p} + \sum_{i=1}^{m} \frac{2A_i p}{p^2+\omega_i{}^2} \tag{2. 19}$$

Where the residues A_∞, A_0 and A_i is all real and positive.

Furthermore, for p=jω,

$$Z(j\omega) = jX(\omega) \tag{2. 20}$$

Where

$$X(\omega) = A_\infty \omega - \frac{A_0}{\omega} + \sum_{i=1}^{m} \frac{2A_i \omega}{\omega_i^2-\omega^2} \tag{2. 21}$$

And

$$\frac{dX(\omega)}{d\omega} = A_\infty \omega + \frac{A_0}{\omega^2} + \sum_{i=1}^{m} 2A_i \frac{\omega_i^2+\omega^2}{\omega_i^2-\omega^2} \tag{2. 22}$$

Therefore

$$\frac{dX(\omega)}{d\omega} > 0 \tag{2. 23}$$

The fact that the differential of X (ω) is always positive implies that the poles and zero of X(ω) must be crossed. If parallel L and C tuned circuit is considered therefore impedance of this circuit is

$$Z(p) = \frac{1}{CP+(\frac{1}{LP})} = \frac{P/C}{P^2+(1/LC)} \tag{2. 24}$$

From (2.19) and (2.24) we can see that the general equivalent circuit for a reactance function is the network shown in Fig 2.5. This process of working backward from an impedance function to the actual physical circuit is known as “synthesis”. The particular method shown here is known as Foster synthesis [3], where the circuit is derived by a partial fraction expansion of the impedance function. Therefore concept of the input impedance of a network in terms of the complex frequency variable has led to the properties of positive real and bounded real functions.

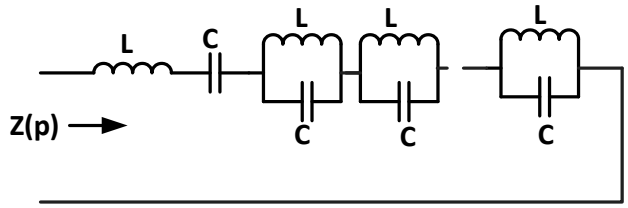

Fig. 2. 5 Foster realization of Z(p).

Foster´s theorem is an important theorem in the fields of electrical network analysis and synthesis. The theorem states that the reactance of a passive, lossless two-terminal (one-port) network always strictly monotonically increases with frequency. It is easily seen that the reactance of inductors and capacitors individually increase with frequency and from that basis a proof for passive lossless networks generally can be constructed. A Foster network must be passive, so an active network, containing a power source, not obey Foster´s theorem.

2.1.2 Foster equivalent circuit model

As has been shown in previous part, it has been shown that linear reciprocal lossless electromagnetic structures can be represented by canonical Foster equivalent circuits.

There are two simple canonical forms for the realization of one-port reactance functions are the first and second Foster forms.

The first Foster form realization of a one-port immittance function is obtained by expanding Z(s) by partial fractions and identifying terms in the summation with impedances of simple networks

$$Z(s) = Z_1(s) + Z_2(s) + Z_3(s) + \cdots . Z_n(s) \tag{2. 25}$$

The general form for Eq. (2.25) is obtained

$$Z(s) = \frac{K_0}{s} + \sum_{i=1}^{n} \frac{2K_i s}{s^2 + {\omega_i}^2} + K_\infty s \tag{2. 26}$$

If the function in Eq. (2.26) has a pole at s=0 and at s=jω its order is reduced by one if either of these poles is extracted from Z(s). If the function Z(s) has a pair of conjugate poles at $s=\pm j\omega_i$ the order is reduced by two if these poles are extracted in the form of a tank circuit.

Figure 2.6 gives the schematic diagram of the first Foster form realization of an impedance function.

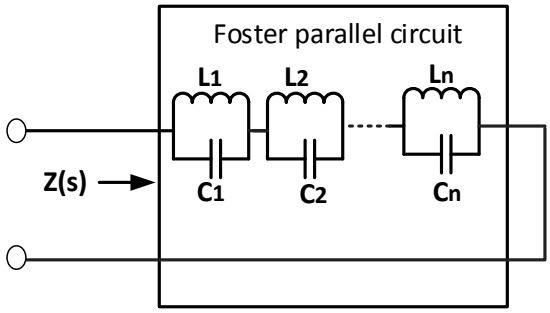

Fig. 2. 6 Foster parallel LC equivalent circuit.

The second Foster form realization of a one-port immittance function is the dual of the first one except that it involves a partial fraction expansion of an admittance function instead of an impedance one:

$$\mathrm{Y(s)} = \mathrm{Y_1(s)} + \mathrm{Y_1(s)} + \mathrm{Y_3(s)} + \cdots . \mathrm{Y_n(s)} \tag{2. 27}$$

The general form for the above equation is deduced by duality from Eq. (2.26)

$$\mathrm{Y}(s) = \frac{K_0}{s} + \sum_{i=1}^{n} \frac{2K_i s}{s^2 + {\omega_i}^2} + \cdots K_\infty s \tag{2. 28}$$

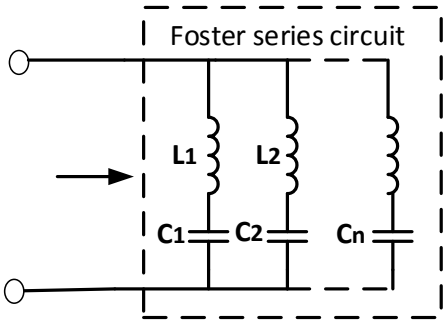

Fig. 2. 7 Foster series LC equivalent circuit.

The order of the function in Eq. (2.28) is reduced by one if it has a pole at s=0 or s=j∞ removed in the form of shunt inductance or capacitance. It is reduced by two if it has a pair of conjugate poles at $s=\pm j\omega_i$ extracted in the form of a shunt tank circuit in shunt with the input terminals.

The second Foster realization of a one-port immittance function has the form depicted in Fig. 2.7.

2.1.3 Resonator Circuits

Resonators could be considered as important components since they typically form filter networks. They are also used in controlling or stabilizing the frequency for oscillators, wave meters for frequency measurements, frequency discriminators, and measurement systems. At frequencies near resonance, a microwave resonator can be modeled by either a series or parallel RLC lumped-element equivalent circuit as illustrated in Fig 2.8 [4].

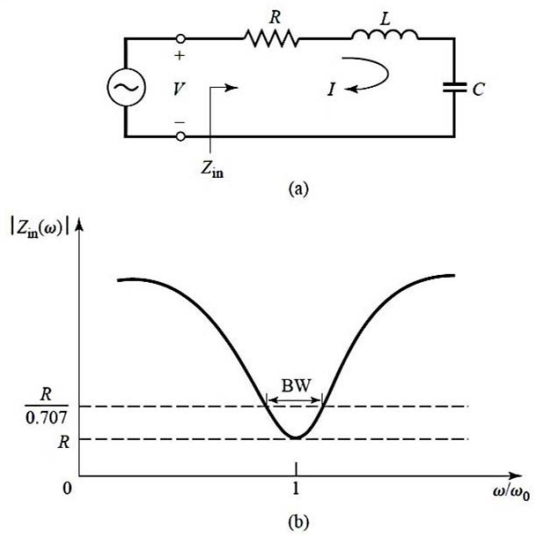

Fig. 2. 8 A series *RLC* resonator and its response. (a) A series *RLC* resonator circuit. (b) Input impedance magnitude versus frequency [4].

The input impedance can then be rewritten from

$$Z_{in} = R + j\omega L\left(1 - \frac{1}{\omega^2 LC}\right) \tag{2. 29}$$
$$= R + j\left(\omega L - \frac{1}{\omega C}\right)$$

The frequency $\omega = \omega_0 = \frac{1}{\sqrt{LC}}$ is called the resonance frequency of the RLC network.

The bandwidth is the difference between the half power frequencies

$$BW = \omega_2 - \omega_1 = \frac{R}{L} \tag{2. 30}$$

That ω_0 is the geometric mean of ω_1 and ω_2.

$$\boldsymbol{\omega_0 = \sqrt{\omega_1 \omega_2}} \tag{2. 31}$$

The Q factor is

$$Q = \frac{\omega_0}{BW} = \frac{\omega_0 L}{R} = \frac{1}{\omega_0 RC} \tag{2. 32}$$

Therefore at the resonant frequency the impedance seen by the source is purely resistive. This implies that at resonance frequency the inductor/capacitor combination acts as a short circuit

The parallel RLC resonant circuit, shown in Fig 2.9a, is the dual of the series RLC circuit.

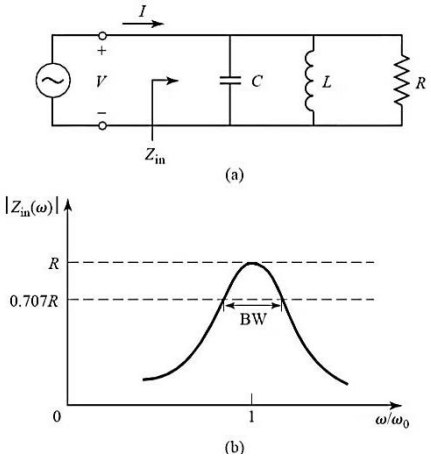

Fig. 2. 9 A parallel RLC resonator and its response. (a) A parallel RLC circuit. (b) Input impedance magnitude versus frequency [4].

The input impedance is

$$Z_{in} = (\frac{1}{R} + \frac{1}{j\omega L} + j\omega C)^{-1} \tag{2. 33}$$

At the resonance1-ω^2LC=0 frequency and the impedance seen by the source is purely resistive. And the bandwidth for the parallel RLC circuit is

$$BW = \omega_2 - \omega_1 = \frac{1}{RC} \tag{2. 34}$$

The Q factor is

$$Q = \frac{\omega_0}{BW} = \omega_0 RC = \frac{R}{\omega_0 L} \tag{2. 35}$$

The parallel combination of the capacitor and the inductor acts as an open circuit. Therefore at the resonance the total current flows through the resistor.

2.1.4 Coupled resonator circuit

The situation in which two or more resonators are interchanging energy trough the electric or magnetic field is defined as coupled resonators. Coupled microwave resonators are essential components in modern communication systems in particular for design of RF/microwave filters (narrow band pass filter). A general theory of cross-coupled resonator band-pass filters was developed in the 1970s by Atia and Williams [5]–[6]. There is a general technique for designing coupled resonator filters in the sense that it can be applied to any type of resonator despite its physical structure. It has been applied to the design of waveguide filters [7], dielectric resonator filters [8], ceramic comb-line filters [9], micro-strip filters [10], superconducting filters [11], and micro-machined filters [12]. Such a technique is based on coupling matrix for coupled resonators arranged in a two-port network. Coupling matrix can be formulated either from a set of loop equations or from a set of node equations. This leads to a very useful formula for analysis and synthesis of coupled-resonator filter circuits in terms of coupling coefficients and external quality factors.

It is worthwhile introducing some fundamental concepts in coupled-resonator filter theory that relate to the current work as following.

2.1.4.1 General coupled matrix for coupled resonator filter

Shown in Fig 2.10(a) is an equivalent circuit of n-coupled resonators, where L, C, and R denote the inductance, capacitance, and resistance, respectively; (i) represent the loop current; and (e_s) the voltage source. Using the voltage law, which is one of Kirchhoff's two circuit laws and states that the algebraic sum of the voltage drops around any closed path in a network is zero, we can write down the loop equations for the circuit of Fig 2.10(a)

$$\left(R1 + j\omega L_1 + \frac{1}{j\omega C_1}\right) i_1 - j\omega L_{12} i_2 \dots\dots\dots - j\omega L_{1n} i_n = e_s$$

$$-j\omega L_{21} i_1 + \left(j\omega L_2 + \frac{1}{j\omega C_2}\right) i_2 \dots\dots\dots - j\omega L_{2n} i_n = 0 \qquad (2.\ 36)$$

$$-j\omega L_{n1} i_1 - j\omega L_{n2} i_2 \dots\dots + \left(R_n + j\omega L_n + \frac{1}{j\omega C_n}\right) i_n = 0$$

In which $L_{ij}=L_{ji}$ represents the mutual inductance between resonators i and j, and the all loop currents are supposed to have the same direction as shown in Fig 2.10(a), so that the voltage drops due to the mutual inductance have a negative sign.

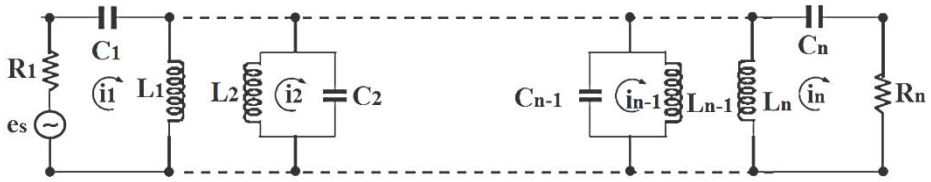

(a)

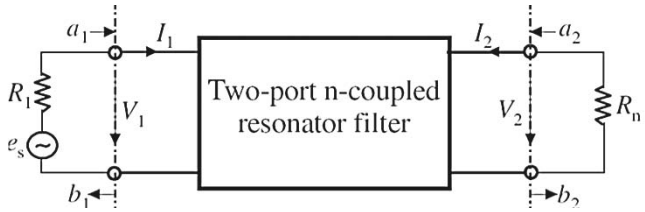

(b)

Fig. 2. 10 (a) Equivalent circuit of *n*-coupled resonators for loop-equation formulation. (b) Its network representation.

This set of equations can be represented in matrix form where [Z] is an n × n impedance matrix.

$$\begin{bmatrix} \boldsymbol{R_1 + j\omega L_1 + \frac{1}{j\omega C_1}} & \boldsymbol{-j\omega L_{12}} & \dots & \boldsymbol{-j\omega L_{1n}} \\ \boldsymbol{-j\omega L_{21}} & \boldsymbol{-j\omega L_2 + \frac{1}{j\omega C_2}} & \dots & \boldsymbol{-j\omega L_{2n}} \\ \vdots & \vdots & \vdots & \vdots \\ \boldsymbol{-j\omega L_{n1}} & \boldsymbol{-j\omega L_{n2}} & \dots & \boldsymbol{R_n + j\omega L_n + \frac{1}{j\omega C_n}} \end{bmatrix} \begin{bmatrix} \boldsymbol{i_1} \\ \boldsymbol{i_2} \\ \vdots \\ \boldsymbol{i_n} \end{bmatrix} = \begin{bmatrix} \boldsymbol{e_s} \\ \boldsymbol{0} \\ \vdots \\ \boldsymbol{0} \end{bmatrix} \qquad (2.\ 37)$$

Or

$$[Z].[i]=[e]$$

For simplicity, let us first consider a synchronously tuned filter. In this case, the all resonators resonate at the same frequency, namely the mid-band frequency of filter $\omega_0 = 1/\sqrt{LC}$, where $L=L_1=L_2=\ldots L_n$ and $C=C_1=C_2=\ldots C_n$. The impedance matrix in (2.37) may be expressed by

$$[Z]=\omega_0.L.FBW.[\hat{Z}] \quad (2.\ 38)$$

Where $FBW=\Delta\omega/\omega_0$ is the fractional bandwidth of filter, and $[\hat{Z}]$is the normalized impedance matrix.

2.1.4.2 General theory of couplings

After determining the required coupling matrix for the desired filtering characteristic, the next important step for the filter design is to establish the relationship between the value of every required coupling coefficient and the physical structure of coupled resonators so as to find the physical dimensions of the filter for fabrication. In general, the coupling coefficient of coupled RF/microwave resonators, which can be different in structure and can have different self-resonant frequencies (see Fig 2.11), may be defined on the basis of the ratio of coupled energy to stored energy.

$$\boldsymbol{k} = \frac{\iiint \varepsilon \underline{\boldsymbol{E}}_1.\underline{\boldsymbol{E}}_2 dv}{\sqrt{\iiint \varepsilon|\underline{\boldsymbol{E}}_1|^2 dv \times \iiint \varepsilon|\underline{\boldsymbol{E}}_2|^2 dv}} + \frac{\iiint \mu \underline{\boldsymbol{H}}_1.\underline{\boldsymbol{H}}_2 dv}{\sqrt{\iiint |\underline{\boldsymbol{H}}_1|^2 dv \times \iiint \varepsilon|\underline{\boldsymbol{H}}_2|^2 dv}} \quad (2.\ 39)$$

Where E and H represent the electric and magnetic field vectors, respectively, and we now use the more traditional notation k instead of M for the coupling coefficient.

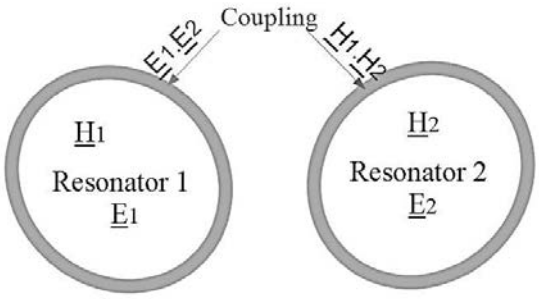

Fig. 2. 11 General coupled RF/microwave resonators where resonators 1 and 2 can be different in structure and have different resonant frequencies.

In general, the coupling coefficient k of coupled microwave resonators which can be different in structure and can have different self-resonant frequencies as referred to Fig. 2.11 may be defined on the basis of a ratio of coupled energy to stored energy. Note that all fields are determined at resonance, and the volume integrals are over all effected regions with permittivity of ε and permeability of μ. The first term on the right-hand side represents the electric coupling and the second term the magnetic coupling. It should be remarked that the interaction of the coupled resonators is mathematically described by the dot operation of their space vector fields, which allows the coupling to have either positive or negative sign. A positive sign would imply that the coupling enhances the stored energy of uncoupled resonators, whereas a negative sign would indicate a reduction. Therefore, the electric and magnetic couplings could either have the same effect if they have the same sign, or have the opposite effect if their signs are opposite. Obviously, the direct evaluation of the coupling coefficient from Eq (2.39) requires knowledge of the field distributions and performance of the space integrals. This is not an easy task unless analytical solutions of the fields exist. On the other hand, it may be much easier by using full-wave EM simulation or experiment to find some characteristic frequencies that are associated with the coupling of coupled RF/microwave resonators. The coupling coefficient can then be determined against the physical structure of coupled resonators if the relationship between the coupling coefficient and the characteristic frequencies is established. In what follows, we derive the formulation of such relationships. Before proceeding further, it might be worth pointing out that although the following derivations are based on lumped-element circuit models, the outcomes are also valid for distributed Element coupled structures on a narrow-band basis.

2.1.4.3 Electric Coupling

An equivalent lumped-element circuit model for electrically coupled RF/microwave resonators is given in Fig 2.12(a), where L and C are the self-inductance and self-capacitance, so that $(LC)^{-1/2}$ equals the angular resonant frequency of uncoupled resonators, and C_m represents the mutual capacitance. If the coupled structure is a distributed element, the lumped-element circuit equivalence is valid on a narrow-band basis, namely, near its resonance. Now, if we look into reference planes T_1–T'_1 and T_2–

T'$_2$, a two-port network that may be described by the following set of equations can be obtained:

$$\boldsymbol{I_1 = j\omega C V_1 - j\omega C_m V_2} \quad \text{(2. 40a)}$$

$$I_2 = j\omega C V_2 - j\omega C_m V_1 \quad \text{(2.40b)}$$

In which a sinusoidal waveform is assumed. It might be well to mention that (2.40) implies that the self-capacitance C is the capacitance seen in one resonant loop of Figure 2.12(a) when the capacitance in the adjacent loop is shorted out.

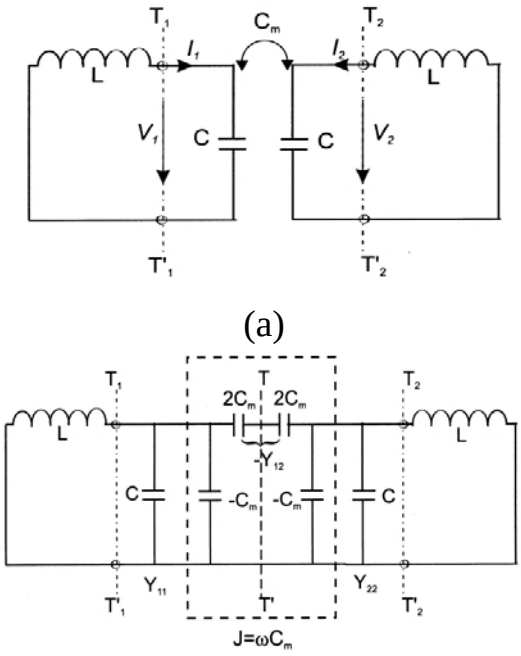

Fig. 2. 12 (a) Synchronously tuned coupled resonator circuit with electric coupling. (b) An alternative form of the equivalent circuit with an admittance inverter J =ωC_m to represent the coupling [10].

Thus, the second terms on the R.H.S. of Eq 2.40 are the induced currents resulting from the increasing voltage in resonant loop 2 and loop 1, respectively. From Eq 2.40 four Y parameters can easily be found from definitions

$$Y_{11}=Y_{22}=j\omega C \quad \text{(2. 41)}$$

$$Y_{12}=Y_{21}=-j\omega C_m$$

According to the network theory [13] an alternative form of the equivalent circuit in Fig 2.12(a) can be obtained and is shown in Fig 2.12(b). This form yields the same two-port parameters as those of the circuit of Fig 2.12(a), but it is more convenient for our discussions. Actually, it can be shown that the electric coupling between the two

resonant loops is represented by an admittance inverter J=ωC_m. If the symmetry plane T–T' in Figure 2.12(b) is replaced by an electric wall (or a short circuit), the resultant circuit has a resonant frequency.

$$f_e = \frac{1}{2\pi\sqrt{L(C+C_m)}} \quad (2.\ 42)$$

This resonant frequency is lower than that of an uncoupled single resonator. A physical explanation is that the coupling effect enhances the capability to store charge of the single resonator when the electric wall is inserted in the symmetrical plane of the coupled structure. Similarly, replacing the symmetry plane in Fig 2.12(b) by a magnetic wall (or an open circuit) results in a single resonant circuit having a resonant frequency.

$$f_m = \frac{1}{2\pi\sqrt{L(C-C_m)}} \quad (2.\ 43)$$

In this case, the coupling effect reduces the capability to store charge so that the resonant frequency is increased. Equations (2.42) and (2.43) can be used to find the electric coupling coefficient k_E.

$$k_E = \frac{{f_m}^2-{f_e}^2}{{f_m}^2+{f_e}^2} = \frac{C_m}{C} \quad (2.\ 44)$$

That is not only identical to the definition of ratio of the coupled electric energy to the stored energy of uncoupled single resonator, but also consistent with the coupling coefficient for coupled-resonator filter.

2.1.4.4 Magnetic Coupling

Shown in Fig 2.13(a) is an equivalent lumped-element circuit model for magnetically coupled resonator structures, where L and C are the self-inductance and self-capacitance, and Lm represents the mutual inductance. In this case, the coupling equations describing the two-port network at reference planes T_1–T'_1 and T_2–T'_2 are

$$V_1 = j\omega L I_1 - j\omega L_m I_2 \quad (2.\ 45a)$$

$$V_1 = j\omega L I_1 - j\omega L_m I_2 \quad (2.45b)$$

The equations 2.45 also imply that the self-inductance L is the inductance seen in one resonant loop of Fig 2.13(a) when the adjacent loop is open-circuited. Thus, the second terms on the R.H.S. of (2.45) are the induced voltages resulting from the increasing current in loops 2 and 1, respectively.

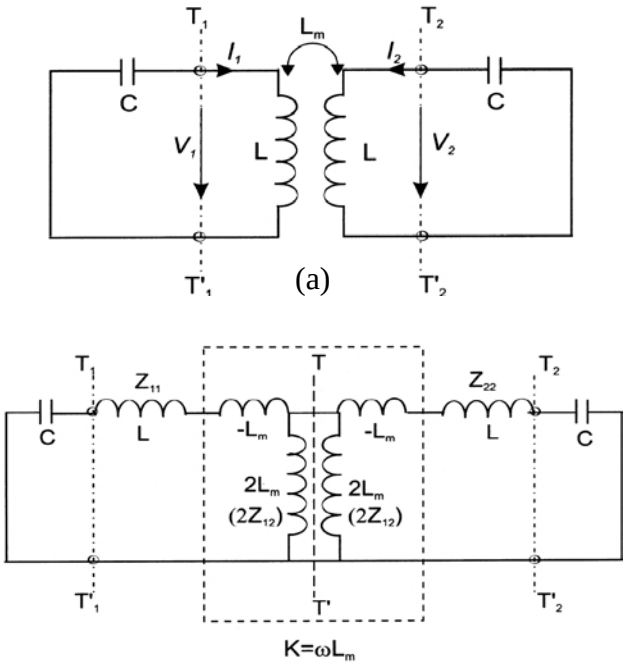

Fig. 2. 13 (a) Synchronously tuned coupled resonator circuit with magnetic coupling. (b) An alternative form of the equivalent circuit with an impedance inverter $K = \omega L_m$ to represent the coupling.

It should be noticed that the two loop currents in Fig 2.13(a) flow in the opposite directions, so that the voltage drops due to the mutual inductance have a positive sign. From Eq 2.45 four Z parameters can be found

$$Z_{11}=Z_{22}=j\omega L \qquad (2.\ 46)$$

$$Z_{12}=Z_{21}= -j\omega L_m$$

Shown in Fig 2.13(b) is an alternative form of equivalent circuit having the same network parameters as those of Fig 2.13(a).It can be shown that the magnetic coupling between the two resonant loops is represented by an impedance inverter $K= \omega L_m$. If the symmetry plane T–T' in Fig 2.13(b) is replaced by an electric wall (or a short circuit), the resultant single resonant circuit has a resonant frequency.

$$f_e = \frac{1}{2\pi\sqrt{L(C+C_m)}} \qquad (2.\ 47)$$

It can be shown that the increase in resonant frequency is due to the coupling effect reducing the stored flux in the single resonator circuit when the electric wall is inserted in the symmetric plane. If a magnetic wall (or an open circuit) replaces the symmetry plane in Fig 2.13(b), the resultant single resonant circuit has a resonant frequency.

$$f_m = \frac{1}{2\pi\sqrt{L(C-C_m)}} \qquad (2.\ 48)$$

In this case, it turns out that the coupling effect increases the stored flux, so that the resonant frequency is shifted down.
Similarly, (2.47) and (2.48) can be used to find the magnetic coupling coefficient k_m

$$k_m = \frac{f_e^{\,2} - f_m^{\,2}}{f_e^{\,2} + f_m^{\,2}} = \frac{L_m}{L} \tag{2. 49}$$

It should be emphasized that the magnetic coupling coefficient defined by (2.49) corresponds to the definition of the ratio of the coupled magnetic energy to the stored energy of an uncoupled single resonator.

2.1.4.5 Mixed Coupling

For coupled-resonator structures, with both the electric and magnetic couplings, a network representation is given in Fig 2.14(a). Notice that the Y parameters are the parameters of a two-port network located on the left side of reference plane T_1–T'_1 and the right side of reference plane T_2–T'_2, while the Z parameters are the parameters of the other two-port network located on the right side of reference plane T_1–T'_1 and the left side of reference plane T_2–T'_2. The Y and Z parameters are defined by

$$Y_{11}=Y_{22}=\boldsymbol{j\omega C} \tag{2. 50a}$$

$$Y_{12}=Y_{21}= -j\,\omega C_m{}' \tag{2.50b}$$

That C, L, C_m', and L_m' are the self-capacitance, the self-inductance, the mutual capacitance, and the mutual inductance of an associated equivalent lumped-element circuit shown in Fig 2.14(b). One can also identify an impedance inverter $K=\omega Lm'$.

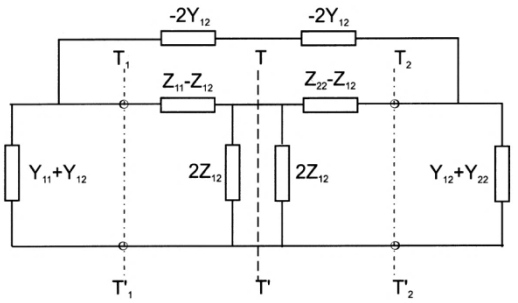

(a)

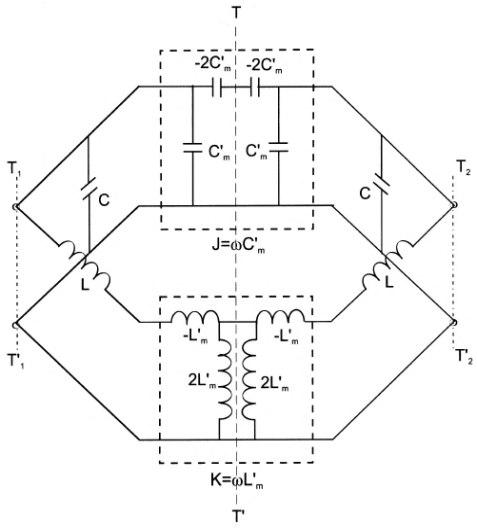

(b)

Fig. 2. 14 (*a*) Network representation of synchronously tuned coupled resonator circuit with mixed coupling. (*b*) An associated equivalent circuit with an impedance inverter $K = \omega L_m$ and an admittance inverter $J = \omega C_m$ to represent the magnetic coupling and electric coupling, respectively.

And an admittance inverter $J=\omega C_m{}'$, which represent the magnetic coupling and the electric coupling, respectively. By inserting an electric wall and a magnetic wall, respectively, into the symmetry plane of the equivalent circuit in Fig 2.14(b) we obtain.

$$f_e = \frac{1}{2\pi\sqrt{(L-L_m{}')(C-C_m{}')}} \tag{2. 51}$$

$$f_m = \frac{1}{2\pi\sqrt{(L+L_m{}')(C+C_m{}')}} \tag{2. 52}$$

Both the magnetic and electric couplings have the same effect on the resonant frequency shifting, as can be seen that in this case

From (2.51) and (2.52), the mixed coupling coefficient $k_x$can be found to be

$$k_x = \frac{{f_e}^2-{f_m}^2}{{f_e}^2+{f_m}^2} = \frac{CL_m{}'+LC_m{}'}{LC+L_m{}'C_m{}'} \tag{2. 53}$$

It is reasonable to assume that $L'_m C'_m \ll LC$, and thus equation (2.53) becomes

$$k_x = \frac{L_m'}{L} + \frac{C_m'}{C} = k_M' + k_E' \quad (2.54)$$

This clearly indicates that the mixed coupling results from the superposition of the magnetic and electric couplings. Care should be taken for the mixed coupling because the superposition of both the magnetic and electric couplings can result in two opposite effects, either enhancing or canceling each other as mentioned before.

If we allow either the mutual inductance or the mutual capacitance in Fig 2.14(b) to change sign, we will find that both couplings tend to cancel each other out. It should be remarked that for numerical computations, depending on the particular EM simulator used, as well as the coupling structure analyzed, it may sometimes be difficult to implement the electric wall, the magnetic wall, or even both in the simulation. This difficulty is more obvious for experiments. The difficulty can be removed easily by analyzing or measuring the whole coupling structure instead of the half, and finding the natural resonant frequencies of two resonant peaks, observable from the resonant frequency response. It has been proved that the two natural resonant frequencies obtained in this way are *fe* and *fm* . this can also be seen in the next section when we consider a more general case, namely the asynchronously tuned coupled-resonator circuits.

2.2 Distributed element equivalent circuit model

As was pointed out in first section, ideal lumped circuit elements are often unattainable at microwave frequencies, so distributed elements are frequently use.

Distributed-element circuits are those where the physical dimensions of one or more of the components affect the circuit performance. In many important circuits the distributed components can be represented in terms of transmission line models.

The analysis of transmission line circuits is a natural extension of lumped-element circuit analysis. Kirchoff's current law continues valid at any node and Kirchoff's voltage law must hold around any loop. Voltage and current relations for lumped element resistances (Ohm's Law), inductive reactance, and capacitive reactance are augmented with those for transmission lines. Circuits are solved by using the current and voltage relationships to create a system of equations which can then be solved for

branch currents and node voltages. Transmission line nodes exist at the input and the output and they may be combined with other elements in series and in parallel.

The theory of distributed circuits bridges circuit theory and Maxwell's equations.

The central difference between lumped and distributed circuit theories is time delay t_d when signal (v, i) travels from one point to another. The signal travels with velocity v=c/n, where "c" is the light velocity in vacuum, "n" is the refractive index of the medium where EM fields exist. Distributed circuit theory matters when t_d is comparable or longer than the "signal time scale".

The behaviour of distributed circuits with respect to parameter changes is usually very important. There are two parameters which variation is of most interest to determine performance of distributed circuit. First one is physical dimension (e.g. length) which due to tolerance considerations in fabricating. Second one is frequency bandwidth due to circuits require more than a single frequency to operate or communicate.

In many circuits the distributed components can be represented in terms of transmission line models. Transmission line theory bridges the gap between field analysis and basic circuit theory and therefore is of importance in the analysis of microwave circuits and devices. There is a difference between circuit theory and transmission line theory which is electrical size.

Circuit analysis assumes that the physical dimensions of the network are much smaller than the electrical wavelength, while transmission lines may be a considerable fraction of a wavelength, or many wavelengths, in size. Thus a transmission line is a distributed-parameter network, where voltages and currents can vary in magnitude and phase over its length, while ordinary circuit analysis deals with lumped elements, where voltage and current do not vary appreciably over the physical dimension of the elements.

As shown in Fig 2.15a, a transmission line is often schematically represented as a two-wire line since transmission lines have at least two conductors.

Transmission line is used to carry information and described by a series inductor and a shunt capacitance. Inductors and capacitors are referred to as lumped elements, and transmission lines as distributed elements.

The piece of line of incremental length Δz of Fig 2.15a can be modelled as a lumped-element circuit, as shown in Fig 2.15b, where R, L, G, and C are per-unit-length quantities defined as follows:

R = series resistance per unit length, for both conductors, in Ω/m.

L = series inductance per unit length, for both conductors, in H/m.

G = shunt conductance per unit length, in S/m.

C = shunt capacitance per unit length, in F/m.

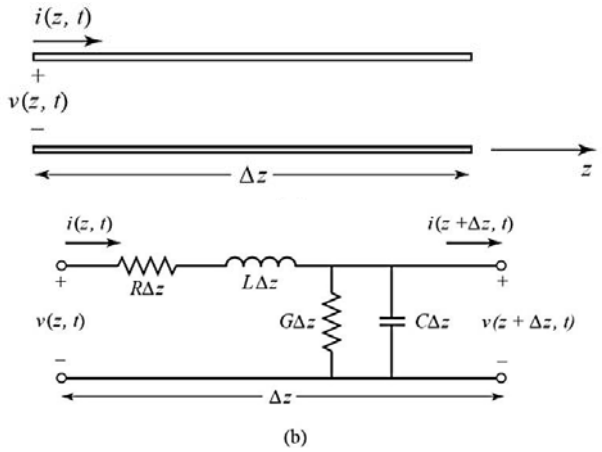

Fig. 2. 15 Voltage and current definitions and equivalent circuit for an incremental length of transmission line. (a) Voltage and current definitions. (b) Lumped-element equivalent circuit.

The series inductance L represents the total self-inductance of the two conductors, and the shunt capacitance C is due to the close proximity of the two conductors. The series resistance R represents the resistance due to the finite conductivity of the individual conductors, and the shunt conductance G is due to dielectric loss in the material between the conductors. R and G, therefore, represent loss. A finite length of transmission line can be viewed as a cascade of sections of the form shown in Fig 2.15b.

Transmission line is lossless in the absence of R and G. By using the equivalent circuit, analysis of electric and magnetic vector fields is substituted by that of scalar voltage between and current along the line, greatly simplifying the math. And values of R, L, G and C depend on geometry and material characteristics of transmission line.

2.2.1 Transmission line models

At microwave frequencies the use of distributed circuit elements is widespread. These differ from zero-dimensional lumped circuits by the fact that one or more dimensions are a significant fraction of the operating wavelength. As shown in Fig 2.16 for one dimensional line, the transfer matrix is given by [14]

$$\begin{bmatrix} V_1 \\ I_1 \end{bmatrix} = \begin{bmatrix} \cosh(\gamma l) & Z_0 \sinh(\gamma l) \\ Y_0 \sinh(\gamma l) & \cosh(\gamma l) \end{bmatrix} \begin{bmatrix} V_2 \\ I_2 \end{bmatrix} \quad (2.55)$$

That Z_o is the characteristic impedance of the line. The value of Z_o depends on the physical construction of the line and is the ratio of voltage to current at any point p along the line. γ is the propagation constant of the line and

$$\gamma = \alpha + j\beta \quad (2.56)$$

Where α is the attenuation constant and β is the phase constant. For a lossless line

$$\gamma = j\beta \quad (2.57)$$

And the transfer matrix reduces to

$$[T] = \begin{bmatrix} \cos(\beta l) & jZ_0 \sin(\beta l) \\ j\frac{\sin(\beta l)}{Z_0} & \cos(\beta l) \end{bmatrix} \quad (2.58)$$

Now

$$\boldsymbol{\beta = \frac{2\pi}{\lambda}} \quad (2.59)$$

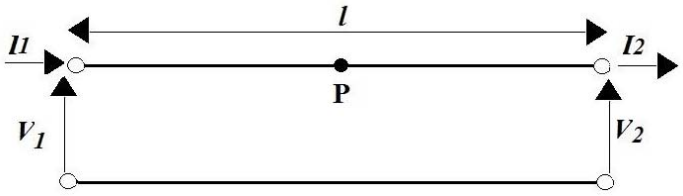

Fig. 2. 16 One dimensional transmission line.

For any wave propagating at velocity *v* with wavelength λ

$$v = f\lambda \quad (2.60)$$

Hence

$$\beta = \frac{\omega}{v} \quad (2.61)$$

$$\beta l = \frac{\omega l}{v} = \alpha\omega \quad (2.62)$$

Where

$$\alpha = \frac{\omega}{v} \quad (2.63)$$

Thus the section of lossless transmission line has a transfer matrix which is a function of frequency as follows.

$$[T] = \begin{bmatrix} \cos(\alpha l) & jZ_0 \sin(\alpha l) \\ j\frac{\sin(\alpha l)}{Z_0} & \cos(\alpha l) \end{bmatrix} \quad (2.64)$$

Where

$$Y_0 = \frac{1}{Z_0} \tag{2. 65}$$

If a transmission line is terminated in a short circuit then the input impedance is

$$Z_{in}(j\omega) = jZ_0 \tan(\alpha\omega) \tag{2. 66}$$

And if a transmission line is terminated in an open circuit then the input impedance is

$$Z_{in}(j\omega) = -jZ_0 / \tan(\alpha\omega) \tag{2. 67}$$

2.2.2 Equivalent circuit models based on transfer (ABCD) matrix

The Z, Y, and S parameter representations can be used to characterize a microwave network with an arbitrary number of ports, but in practice many microwave networks consist of a cascade connection of two or more two-port networks. In this case it is convenient to define a 2×2 transmission, or ABCD, matrix, for each two-port network. The ABCD matrix of the cascade connection of two or more two-port networks can be easily found by multiplying the ABCD matrices of the individual two-ports. The ABCD matrix is defined for a two-port network in terms of the total voltages and currents as shown in Figure 2.17a and the following

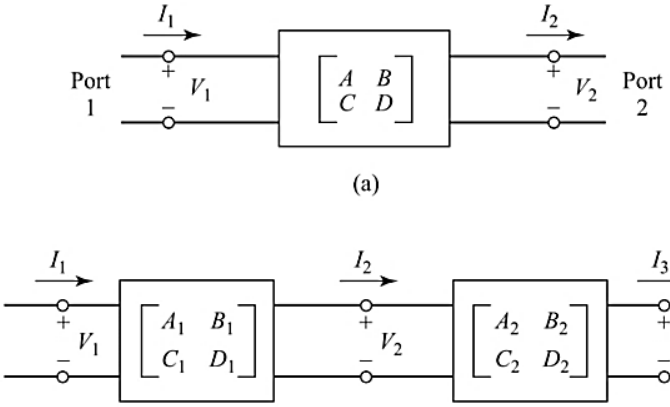

Fig. 2. 17 (a) A two-port network; (b) a cascade connection of two-port networks.

$$V_1 = AV_2 + BI_2$$
$$I_1 = CV_2 + DI_2$$

or in matrix form as

$$\begin{bmatrix} V_1 \\ I_1 \end{bmatrix} = \begin{bmatrix} A & B \\ C & D \end{bmatrix} \begin{bmatrix} V_2 \\ I_2 \end{bmatrix} \tag{2.68a,b}$$

$$\begin{bmatrix} V_2 \\ I_2 \end{bmatrix} = \begin{bmatrix} A & B \\ C & D \end{bmatrix} \begin{bmatrix} V_3 \\ I_3 \end{bmatrix}$$

Substituting (2.68b) into (2.68a) gives

$$\begin{bmatrix} V_1 \\ I_1 \end{bmatrix} = \begin{bmatrix} A_1 & B_1 \\ C_1 & D_1 \end{bmatrix} \begin{bmatrix} A_2 & B_2 \\ C_2 & D_2 \end{bmatrix} \begin{bmatrix} V_3 \\ I_3 \end{bmatrix} \quad (2.\ 69)$$

This shows that the ABCD matrix of the cascade connection of the two networks is equal to the product of the ABCD matrices representing the individual two-ports. Note that the order of multiplication of the matrix must be the same as the order in which the networks are arranged since matrix multiplication is not, in general, commutative. The usefulness of the ABCD matrix representation lies in the fact that a library of ABCD matrices for elementary two-port networks can be built up, and applied in building-block method to more complicated microwave networks that consist of cascades of these simpler two-ports.

2.2.2.1 Network parameter formulation of simple ring resonator

A micro-strip ring resonator is a simple transmission line resonator Fig 2.18 shows one possible circuit arrangement. The ring resonator is only a transmission line formed in a closed loop. The basic circuit consists of the feed lines, coupling gaps, and the resonator.

The dielectric material (substrate) used in planar transmission lines is characterized by the loss tangent (which accounts for dielectric losses) and by the dielectric constant (which determines the phase velocity). Although these parameters are supplied by the manufacturer with the corresponding tolerances, there are sometimes substantial variations that make necessary the characterization of the material (i.e., the measurement of the dielectric constant and the loss tangent) for an accurate design. The dielectric constant and the loss tangent of a substrate material can be experimentally inferred by means of a micro-strip ring resonator configuration (Fig. 2.18) [15-16-17].

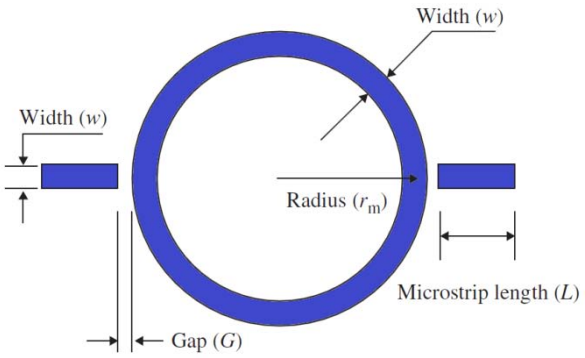

Fig. 2. 18 The micro-strip ring resonator**.**

Power is coupled into and out of the resonator through feed lines and coupling gaps. If the distance between the feed lines and the resonator is large, then the coupling gaps do not affect the resonant frequencies of the ring. This type of coupling is referred to in the literature as “loose coupling”. Loose coupling is a manifestation of the negligibly small capacitance of the coupling gap. If the feed lines are moved closer to the resonator, however, the coupling becomes tight and the gap capacitances become appreciable. This causes the resonant frequencies of the circuit to deviate from the intrinsic resonant frequencies of the ring. Hence, to accurately model the ring resonator, the capacitances of the coupling gaps should be considered. For a ring resonator, resonances occur at those frequencies where the ring circumference is a multiple of the wavelength, λ_g. The resonance condition can thus be expressed as follows:

$$\boldsymbol{\lambda_g = \frac{2\pi r_m}{n} = \frac{v_p}{\sqrt{\varepsilon_{re}}}\frac{1}{f_n}} \tag{2. 70}$$

Where n refers to the nth-order resonance and r_m is the mean ring radius. The effective dielectric constant is thus

$$\boldsymbol{\varepsilon_{re} = \left(\frac{nc}{2\pi r_m f_n}\right)^2} \tag{2. 71}$$

The Eq (2.71) relation is valid for the loose coupling case, as it does not take into account the coupling gap effects. From this equation, the resonant frequencies for different modes can be calculated since λ_g are frequency dependent. For the first mode, the maximum of the field occur at the coupling gap locations, and nulls occur 90° from the coupling gap locations.

There exists in a non-dispersive medium a linear relationship between the frequency and the phase constant or wavenumber, β, where $\beta=2\pi/\lambda_g$. If the frequency doubles, then

likewise the wavenumber doubles. In a dispersive medium this is not true. The microstrip line is a dispersive medium. The dispersion in a microstrip line can be explained by examining the effective permittivity, ε_{eff}. In microstrip the effective permittivity is a measure of the fields confined in the region beneath the strip. In the case of very narrow lines or a very low frequency the field is almost equally shared by the air (ε_r=1) and the substrate so that, at this extreme, $\varepsilon_{eff} \approx \frac{1}{2}(\varepsilon_r + 1)\ as\ f \to 0$. Where ε_r is the relative dielectric of the substrate. For very wide lines or a very high frequency nearly all of the field is confined to the substrate dielectric, and therefore at this extreme, $\varepsilon_{eff} \approx \varepsilon_r\ as\ f \to \infty$.

It is therefore obvious that the effective permittivity is frequency dependent, increasing as the frequency increases. The effective permittivity is defined as the square of the ratio of the velocity in free space, c, to the phase velocity, υ_p, in microstrip, or

$$\varepsilon_{eff} = \left(\frac{c}{\vartheta_p}\right)^2 \tag{2. 72}$$

For any propagating wave, the velocity is given by the appropriate frequency wavelength product. In the microstrip line, the velocity is $\upsilon_p = f\lambda_g$. Substituting for υ_p in Equation (2.72) results in the equation

$$\varepsilon_{eff} = \left(\frac{c}{f\lambda_g}\right)^2 \tag{2. 73}$$

The device shown in Fig 2.19 is represented as a network circuit as shown in Fig 2.18 Each shaded box in Fig 2.19 is a separately modeled in the ABCD parameter formulation of the network parameters. The feed lines, which are approximately lossless and matched to 50 Ω, are not considered in this model because it is possible to determine the permittivity of the substrate using only the magnitude of the S_{21} parameter.

Fig. 2. 19 Network circuit of planar ring resonator.

The gap slightly affects the resonant frequencies of the ring resonator but greatly affects the peak amplitudes of the S_{21} parameter of the device. In order to take these effects into account, an equivalent circuit for the gap must be included in the description of the device. In Fig 2.19, the boxes labeled “Left Gap” and “Right Gap” is modeled as a pair of capacitors as shown in Fig 2.20.

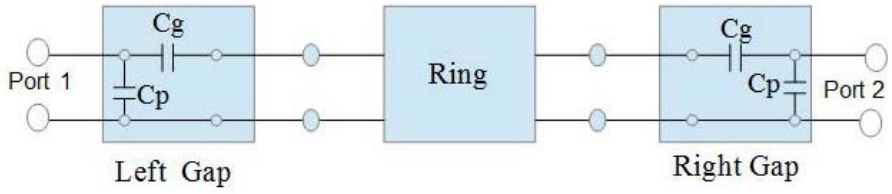

Fig. 2. 20 Network circuit of ring resonator with gap model detail.

Each gap is modeled by a parasitic capacitor C_p and a gap capacitance C_g following the work of Yu and Chang in [18]. The response of a system can be simply calculated as the product of the ABCD parameter matrices of cascaded elements. The development of the ABCD matrices for particular elements is described such as:

$$[ABCD]_{Cp} = \begin{bmatrix} 1 & 0 \\ j\omega C_p & 1 \end{bmatrix} \tag{2. 74}$$

$$[ABCD]_{Cg} = \begin{bmatrix} 1 & \frac{1}{j\omega C_g} \\ 0 & 1 \end{bmatrix} \tag{2. 75}$$

$$[ABCD]_{left} = [ABCD]_{Cp}[ABCD]_{Cg} = \begin{bmatrix} 1 & \frac{1}{j\omega C_g} \\ j\omega C_p & 1 \end{bmatrix} \tag{2. 76}$$

$$[ABCD]_{right} = [ABCD]_{Cg}[ABCD]_{Cp} = \begin{bmatrix} 1+\frac{C_p}{C_g} & \frac{1}{j\omega C_g} \\ j\omega C_p & 1 \end{bmatrix} \tag{2. 77}$$

Since the electrical length of the ring is λ/2 at resonance, it follows that its diameter is λ/2π at this frequency, i.e., relatively small compared to the wavelength [19].

In this section, the basic network input-output parameter relations and ABCD-parameters are reviewed. Rules of connecting networks are pretend to show how more complicated circuits can be constructed by series and parallel cascading of individual network blocks.

2.2.3 The problems from the distributed equivalent circuit

The lumped-element which was discussed in the sections 2.1 sufficient enough at low frequencies, but two problems arise at higher RF and microwave frequencies. First, lumped-element inductors and capacitors are generally available only for a limited range of values, and can be difficult to implement at microwave frequencies. Distributed elements such as open-circuited or short-circuited transmission line stubs, are often used to approximate ideal lumped elements. In addition, at microwave frequencies the distances between filter components is not negligible. The first problem is treated with Richards' transformation, which can be used to convert lumped elements to transmission line sections. Kuroda's identities can then be used to physically separate filter elements by using transmission line sections. Because such additional transmission line sections do not affect the filter response, this type of design is called redundant filter synthesis. It is possible to design microwave filters that take advantage of these sections to improve the filter response [20]; such non redundant synthesis does not have a lumped-element counterpart.

2.2.3.1 Richard's transformation and Kuroda's identities

Richard's Transformation and Kuroda's Identities focus on uses of λ/8 lines, for which $X=jZ_o$. Richard's idea [21] is to use variable Z_o (width of micro-strip, for example) to create lumped elements from transmission lines. A lumped low-pass prototype filter can be implemented using λ/8 lines of appropriate Z_o to replace lumped L and C elements. So if we need an inductance of L for a prototype filter normalized to cut-off frequency $\omega_c=1$ and admittance $g_o=1$, then a λ/8 transmission line stub can be substituted that has $Z_o=L$ as shown in Fig 2.21.

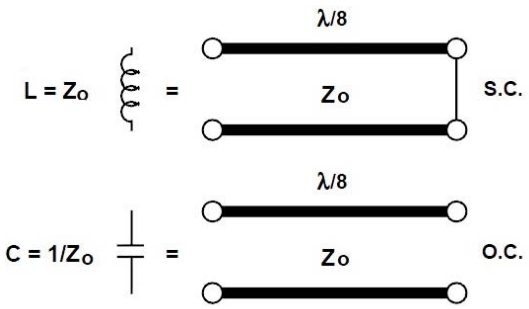

Fig. 2. 21 The λ/8 transmission line sections are called commensurate lines, since they are all the same length in a given filter.

Kuroda's idea [22] is use the λ/8 line of appropriate Z_o to transform awkward or unrealizable elements to those with more tractable values and geometry. As an example, the series inductive stub in the diagram here can be replaced by a shunt capacitive stub on the other end of the λ/8 line, with different values of characteristic impedance determined by

$$k = n^2 = 1 + \frac{Z_1}{Z_2} \tag{2. 78}$$

As an example, a prototype network with the values is considered

L=Z_1=0.5 and Z_2=1 $k = n^2 = 1 + \frac{Z_1}{Z_2}$=1.5

So for the equivalent network, the series transmission line element has Z=1.5Z_1=0.75 and the shunt capacitive stub has Z=1.5Z_2=1.5. Kuroda's four identities are a means of eliminating series stubs that arise from series L or C in prototype networks.

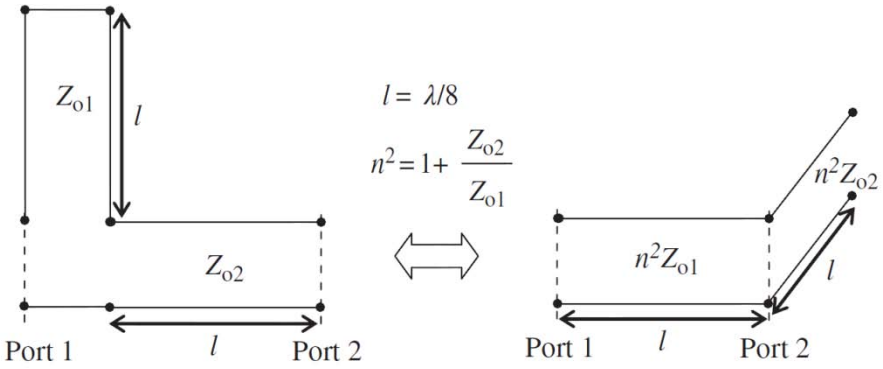

Fig. 2. 22 The equivalence for the most commonly used identity, which removes a series stub by transforming it to a shunt stub along with adjustment of characteristic impedances of the λ/8 lines.

The inductors and capacitors represent short-circuit and open-circuit stubs, respectively. The ABCD matrix of a length of transmission line with characteristic impedance Z_1 is

$$\begin{bmatrix} A & B \\ C & D \end{bmatrix} = \begin{bmatrix} cos\beta l & jZ_1 sin\beta l \\ \frac{j}{Z_1} sin\beta l & cos\beta l \end{bmatrix} = \frac{1}{\sqrt{1+\Omega^2}} \begin{bmatrix} 1 & j\Omega Z_1 \\ \frac{j\Omega}{Z_1} & 1 \end{bmatrix}$$

where Ω = tan βl.

2.2.3.2 Coupled-transmission line equivalent circuits

Fabrication of band-pass or band-stop coupled line filters is particularly easy in micro-strip or strip-line form for bandwidths less than about 20%. Wider bandwidth filters require very tightly coupled lines, which are difficult to fabricate. The filter

characteristics of a single quarter-wave coupled line section are studied. Other filter designs using coupled lines can be found in reference [14].

A pair of coupled transmission lines with the imposed terminal conditions, such as open-circuited or short-circuited at any two of its four ports, is an important type of two-port network in filter designs. The equivalent circuits may be derived from the general coupled-line network in Fig 2.23 by utilizing its general four-port voltage–current relationships:

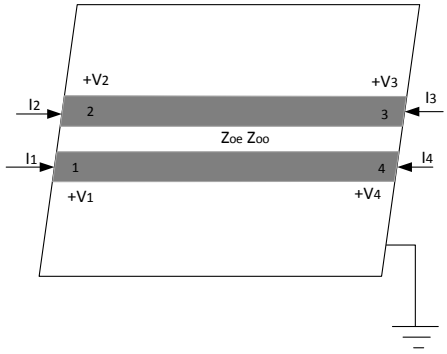

Fig. 2. 23 A parallel coupled line section with port voltage and current definitions.

The coupled transmission lines are characterized trough the even and odd characteristic impedance and electric length (Z_{oe}, θ_e, and Z_{oo}, θ_o respectively). This implies the coexistence of two different modes with different phase velocity and propagating with different effective relative permittivity. The distributed equivalent circuit model can be described by a single ABCD matrix between the input and output ports.

$$Z_{11} = Z_{22} = Z_{33} = Z_{44} = \frac{-j}{2}(Z_{oe} + Z_{oo})cot\theta \quad (2.\ 79)$$

$$Z_{12} = Z_{21} = Z_{34} = Z_{43} = \frac{-j}{2}(Z_{oe} - Z_{oo})cot\theta \quad (2.\ 80)$$

$$Z_{13} = Z_{31} = Z_{24} = Z_{42} = \frac{-j}{2}(Z_{oe} - Z_{oo})csc\theta \quad (2.\ 81)$$

$$Z_{14} = Z_{41} = Z_{23} = Z_{32} = \frac{-j}{2}(Z_{oe} + Z_{oo})csc\theta \quad (2.\ 82)$$

Although expressions are complicated, the Z_{oe} and Z_{oo} impedances can be analytically evaluated from the substrate thickness (h), and the width (W) and separation (S) of the coupled lines.

2.3 Quality Factors

So far, filters have considered comprised of lossless elements, except for resistive terminations. However, in reality, any practical microwave filter have loss elements with finite unloaded quality factors in association with power dissipation in these elements. Such parasitic dissipation may frequently lead to substantial differences between the response of the filter actually realized and that of the ideal one designed with lossless elements. It is thus desirable to estimate the effects of dissipation on insertion loss characteristics.

2.3.1 Loss Considerations for resonators

When a resonant circuit or cavity is used as a load in a microwave circuit, several different Q factors can be defined. The first Q factor accounts for internal losses. It is the unloaded Q factor, Q_u. Second, the external Q factor, Q_D, accounts for external losses. Next, Q factor of conductor loss Q_c. Lastly, the loaded Q factor, Q_L, is the overall Q factor, and includes both internal and external losses. The unloaded quality factor is defined as

$$Q_u = \omega \frac{\text{average energy stored in resonator}}{\text{power dissipated in resonator}} \tag{2. 83}$$

The unloaded quality factor Q_u which includes the total losses of the resonator can be calculated from the measured value of the loaded quality factor [4].

$$Q_u = \frac{Q_L}{(1-10^{-\frac{L}{20}})} \tag{2. 84}$$

However, Q_u is depends on total insertion loss (L) of the system. The total loss of the resonator is inversely proportional to loaded quality factor. The loaded quality factor includes losses, which are due to external load and the resonator itself. Source of the external load is the feed lines, connector interfaces and measurement cables. The loaded quality factor Q_L can be obtained from –3dB bandwidth of a resonance peak [23],

$$Q_L = \frac{F_0}{BW_{-3dB}} \tag{2. 85}$$

Where, F_0 is resonance frequency and BW_{-3dB} is the -3dB band-with (in hertz).

The total unloaded quality factor can be found by adding these losses together, resulting in

$$\frac{1}{Q_L} = \frac{1}{Q_D} + \frac{1}{Q_u} + \frac{1}{Q_C} \tag{2. 86}$$

Minimum transmission loss, or equivalently maximum Q_L, is achieved at the resonance frequency F_0 by minimizing the bandwidth (BW), according to Eq. (2.81), because in this case very little power is dissipated in the cavity since its bandwidth is extremely narrow. So, in this case, benefit transmission characteristics can be obtained. But bandwidth is so restricted that a modulated signal, even with a modest bandwidth, cannot be transmitted without distortion through the resonating structure. In conclusion, a modulated signal cannot be transmitted efficiently through a resonating propagation medium.

The loss in a dielectric substrate may be attributed

$$\frac{1}{Q_D} = tan\delta(subatrate) = \frac{\varepsilon''}{\varepsilon'} \tag{2. 87}$$

Where, tanδ is the dielectric loss tangent. The design of high-speed circuits requires knowledge of the dielectric constant (ε_r) and loss parameter (tanδ) of the substrate. It is desirable to develop a method allowing the design engineer to personally determine the ε_r and tanδ of a substrate material.

Conductor loss Q_C can be determined from only the computation of resonant frequencies

$$Q_c = \sqrt{2\omega\mu_0\sigma}\ \ H \tag{2. 88}$$

Where σ is the conductivity and the other variables have the usual meaning.

2.3.2 Unloaded Quality Factors of Lossy Reactive Elements

The losses in an inductor are conventionally represented by a resistance R connected in series with a pure inductance L, as indicated in Fig 2.24a. The unloaded quality factor Q_u of the loss inductor is defined by

$$Q_u = \frac{\omega L}{R} \tag{2. 89}$$

In a similar, a loss capacitor may have an equivalent circuit, as shown in Fig 2.24b, where G is a conductance connected in parallel with a pure capacitance C. The Q_u of the loss capacitor is defined by

$$Q_u = \frac{\omega C}{G} \tag{2. 90}$$

Note that in the above definitions, ω denotes some particular frequency at which the Q_u is measured. For a low-pass or a high-pass filter, ω is usually the cut-off frequency; while for a band-pass or band-stop filter, ω is the centres frequency.

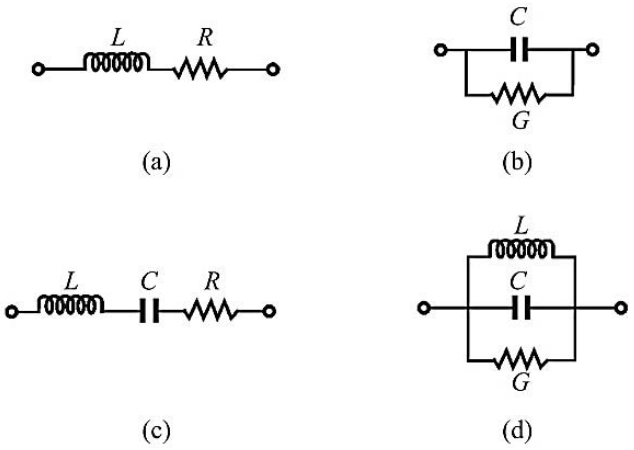

Fig. 2. 24 Circuit representation of loss reactive elements and resonators.

For loss resonators, they are most conveniently represented by the equivalent circuits shown in Fig 2.24c and d. The unloaded quality factors of these two equivalent resonant circuits have the same forms as those defined in Eq. (2.87) and (2.88), respectively, but in this case ω is normally the resonant frequency, namely $\omega = 1/\sqrt{LC}$. As can be seen for lossless reactive elements, R→0 and G→0 so that $Q_u \rightarrow \infty$. However, in practice, the Q_u can be finite because the inherent losses of the microwave components.

Summary

This chapter covered passive components for the implementation of RF/microwave circuits and, in particular, those exploiting passive filters. Passive filters introduce less noise, consume less power, and have wide bandwidth and linear operating range. The losses are small for low frequencies but at higher frequencies, the losses become the important consideration and unfortunately, they are limited to lower electrical performances.

Miniaturization of passive components often increases the frequencies at which lumped-element circuit models are sufficiently accurate. By reducing component dimensions the time delay for propagation through a component is proportionally reduced. The realization of lumped elements (L, C, and R) at microwave frequencies is possible by keeping the component size smaller than the operating wavelength. However, when the component size becomes greater than $\lambda/10$, these components have undesirable associated parasitic such as resistance, capacitance, and inductance. At RF and higher frequencies, the reactance of the parasitic becomes notable, with increasing frequency resulting in higher loss and spurious resonances. Thus, empirical expressions are not accurate enough to predict lumped element performance accurately. Therefore, at microwave frequencies the use of distributed circuit elements in implementing passive microwave devices is widespread.

Distributed L‑C network topologies have been used to describe the electromagnetic properties of homogeneous media, particularly in the lumped-element modeling of transmission lines.

Given the wide range of lengths of signal interconnections, models are relevant; the lumped RC model suitable for short interconnections, the distributed RC model for low-to-moderate speed signals on longer-length interconnections and the distributed RLC model for high-speed signals on longer interconnections. Accurate modeling of signals propagating on an interconnection requires detailed knowledge of the capacitance C' and inductance L' per unit length along the length of the line.

2.4 References

[1] M. Golio, "RF and microwave passive and active technologies" Arizona, U.S.A. ISBN 978-0-8493-7220-9, 2008

[2] Ian. C. Hunter "Theory and Design of Microwave Filter", ser. Electromagnetic Wave 48, London, U.K. IEE Press, 2001.

[3] Foster, R.M "A reactance theorem", Bell System Technical Journal, (3), pp. 259-67, 1924

[4] D. M. Pozar, "Microwave Engineering," New York. Wiley, 1998.

[5] A. Atia and Williams, "New type of waveguide bandpass filters for satellite transponders," COMSAT Tech. Rev., vol. 1, no. 1, pp. 21-43, 1971.

[6] A. E. Atia, A. E. Williams, and R. W. Newcomb, "Narrow-band multiple-coupled cavity synthesis," IEEE Trans. Circuit Syst., vol. CAS-21, pp. 649–655, 1974.

[7] A. E. Atia and A. E. Williams, "Narrow-bandpass waveguide filters," IEEE Trans., MTT-20, pp 258–265, 1972.

[8] C. Wang, H.-W. Yao, K. A. Zaki, and R. R. Mansour, "Mixed modes cylindrical planar dielectric resonator filters with rectangular enclosure," IEEE Trans., MTT-43, pp 2817–2823, 1995.

[9] H.-W. Yao, C. Wang, and K. A. Zaki, "Quarter wavelength ceramic combline filters," IEEE Trans., MTT-44, pp 2673–2679, 1996

[10] J.-S. Hong and M. J. Lancaster, "Couplings of microstrip square open-loop resonators for cross-coupled planar microwave filters," IEEE Trans., MTT-44, pp 2099-2109, 1996.

[11] J.-S. Hong, M. J. Lancaster, D. Jedamzik, and R B. Greed, "On the development of superconducting microstrip filters for mobile communications applications," IEEE Trans., MTT-47, pp 1656-1663, 1999

[12] P. Blondy, A. R. Brown, D. Cros, and G. M. Rebeiz, "Low loss micromachined filters for millimeter-wave telecommunication systems," IEEE MTT-S, Digest, 1181–1184, 1998.

[13] C. G. Montgomery, R. H. Dicke, and E. M. Purcell, Principle of Microwave Circuits, McGraw-Hill, New York, 1948.

[14] K.F. Sander and G.A.L. Reed. "Transmission and propagation of electromagnetic waves," Cambridge University Press, Cambridge, pp.170-71, 1986.

[15] G. Zou, H. Gronqvist, P. Starski, and J. Liu, "Characterization of liquid crystal polymer for high frequency system-in-a-package applications," IEEE Trans. Adv. Packag., vol. 25, pp. 503-508, 2002.

[16] K. Chang, "Microwave Ring Circuits and Antennas," John Wiley, New York, 1994.

[17] L. Yang, A. Rida, and R. Vyas, M. M. Tentzeris "RFID tag and RF structures on a paper substrate using inkjet-printing technology," IEEE Trans. Microw. Theory Technol., vol. 55, pp. 2894-2901, 2007.

[18] C. C. Yu and K. Chang, "Transmission-line analysis of a capacitively coupled microstrip-ring resonator," IEEE Trans. Microwave Theory and Techniques, vol. 45, no. 11, pp. 2018-2024, 1997.

[19] R. Ludwig and P. Bretchko, "Single- and multiport networks in RF Circuit Design: Theory and Applications," Upper Saddle River, NJ: Prentice Hall, 2000.

[20] W. A. Davis, "Microwave Semiconductor Circuit Design," Van Nostrand Reinhold, New York, 1984.

[21] P. I. Richards, "Resistor-Transmission Line Circuits," Proceedings of the IRE, vol. 36, pp. 217-220, 1948.

[22] H. Ozaki and J. Ishii, "Synthesis of a class of strip-line filters," IRE Trans. Circuit Theory, CT-5, pp 104–109, 1958.

[23] Kai. Chang, "Microwave Ring Circuits and Antennas," John Wiley & Sons, Inc. United States of America, ISBN 0-47-13109-1. 1996.

CHAPTER 3

3 Analysis and modeling of Dielectric Resonator

The concept of the “dielectric resonator” first appeared in 1939 when R.D. Richtmyer [1] from Stanford University showed that metalized dielectric objects (sphere and toroid) can function as microwave resonators. However, his theoretical work failed to generate significant interest, and practically nothing happened in this area for more than 25 years. In1953, a paper by Schlicke [2] reported on super high dielectric constant materials (~1,000 or more) and their applications at relatively low RF frequencies. In the early 1960s, researchers from Columbia University, Okaya and Barash [3], have rediscovered dielectric resonators during their work on high dielectric materials, paramagnetic resonance. Their papers provided the first analysis of modes and resonator design. Nevertheless, the dielectric resonator was still far from practical applications. High dielectric constant materials such as rutile exhibited poor temperature stability causing correspondingly large resonant frequency changes. For this reason, in spite of high Q factor and small size, dielectric resonators were not considered for use in microwave devices. In the mid-1960s, S. Cohn [4] and his co-workers at Rantec Corporation performed the first extensive theoretical and experimental evaluation of the dielectric resonator. Rutile ceramics were used for experiments that had an isotropic dielectric constant in the order of 100. Again, poor temperature stability prevented development of practical components. The next major breakthrough came from Japan

when Murata Mfg. Co. produced (Zr-Sn) TiO_4 ceramics [5]. They offered adjustable compositions so that the temperature coefficient could be varied between+10 and –12 ppm/degree C. These devices became commercially available at reasonable prices. Afterward, the theoretical work and use of dielectric resonators expanded rapidly.

In natural dielectrics, local electromagnetic interactions at the atomic or molecular level produced by an applied field result in a macroscopic response that may be described by an electric permittivity and magnetic permeability. These constitutive parameters acquire meaning only when the lattice exhibits some degree of spatial order and the wavelength of the impressed field is longer than the lattice spacing.

It would seem that any attempt to synthesize particular material parameters requires access to the scatter itself that makes it difficult to achieve. However, it is apparent that the long-wavelength condition can be met at scales far more accessible than those of atoms and molecules, indeed, for sufficiently long wavelengths. For instance, those corresponding to RF/microwave frequencies-electromagnetic scatter may be fabricated with entirely practicable dimensions, and would react to applied fields much similar to the atoms and molecules of a crystal lattice. Furthermore, at wavelengths substantially longer than the obstacle spacing, ordered arrays of these inclusions would behave like effective media and exhibit dielectric properties [6].

There are two reasons that this chapter is devoted to dielectric resonator concept. First, the wavelength inside the DR, λ_g is inversely proportional to the square root of the dielectric constant $\lambda_0/\sqrt{\varepsilon_r}$ (where λ_0 is the free space wavelength at the resonant frequency and ε_r is dielectric constant.). And the dielectric constant is proportional to DR size therefore, when their first resonance frequencies are so high that the long-wavelength condition cannot be met, so effective medium theory cannot be used to characterize them. As a result, it is suitable to design dielectric resonator which resonance modes can be tuned to lower frequencies. High-dielectric resonator with good temperature stability and low dielectric loss are required to guarantee the effective media effect. By using an artificial dielectric such as a high dielectric constant resonator, the first resonance can be tuned significantly to lower frequency range so as to meet the long-wavelength condition.

Second, a recent advance in miniaturization of microwave circuits has been the appearance of the low-loss temperature-stable dielectric resonators. These dielectric

resonators are used to replace waveguide filters in such demanding applications as satellite communications where microstrip and strip-line resonators cannot be used because of their inherently high losses. The typical applications of DRs are in microwave stable fixed-frequency oscillators, narrow band filters. The advantages of DRs are high efficiency and high temperature stability.

The characterization of dielectric materials has long been an area of intensive research interest. The permittivity, permeability, and conductivity of a given material are all of main interest in decisions of how a given material could be utilized. There are some characteristic for DRs. First, the concentration of the electric fields within any material is directly related to its complex permittivity. While the real part of the permittivity is most directly related to the propagation velocity of waves in a material, and the imaginary part is directly linked to the losses incurred as electromagnetic waves travel through a medium. Second, for a given dielectric constant, both resonant frequency and Q-factor are defined according to the dielectric resonator dimensions. That, the higher the dielectric constant, the smaller the space within which the fields are concentrated, the lower the dimension at a defined frequency. Section 3.1 is reviewed these characterization and is explained the possible geometry DR shapes, radiating modes yielding typical resonant frequencies. DRs have a limited bandwidth of operation due to their resonant nature, but this can be improved by reducing the inherent Q-factor of the resonant One simple approach for reducing the Q-factor is to decrease the dielectric constant [7]. Materials with high dielectric constants are required in order to provide miniaturization at the frequencies typically used for wireless applications. Most materials that are commonly used in dielectric resonator filters are ceramics, such as barium tetratitanate compounds. The advantage of using an epoxy/$BaTiO_3$ composite is, that it combines the low temperature process ability of epoxy along with the high dielectric constant of $BaTiO_3$ [8]. The experimental and fabrication process for epoxy/$BaTiO_3$ composite is investigated in section 3.2.

Even though many different approaches have been devised to electrically characterize material properties, they all rely on the same underlying technique. By applying an excitation to a material and observing the resulting phase and magnitude response of the reflected and transmitted signals, the electrical material properties of a sample can be determined. A common method for excitation is, coupled dielectric resonators in microwave circuits by proximity to micro-strip lines. Micro-strip coupling could excite

the magnetic fields in the DR to produce the short horizontal magnetic dipole mode. The level of coupling can be adjusted by the lateral position of the DR with respect to the micro-strip line and on the relative permittivity of the DR. Section 3.3 is presented different resonator coupled techniques.

3.1 Characteristics of a DR

A small disc or cube (or other shape) of dielectric material can also be used as a microwave resonator. The operation of such a dielectric resonator is similar in principle to the rectangular or cylindrical cavity resonators previously discussed. Dielectric resonators typically use materials with low loss and a high dielectric constant, ensuring that most of the fields will be contained within the dielectric. Unlike metallic cavities, however, there is some field fringing or leakage from the sides and ends of a dielectric resonator (which are not metalized), leading to a small radiation loss and consequent lowering of Q. A dielectric resonator is generally smaller in size, cost, and weight than an equivalent metallic cavity, and it can easily be incorporated into microwave integrated circuits and coupled to planar transmission lines. Materials with dielectric constants in the range of 10–100 are generally used, with barium tetratitanate and titanium dioxide being typical examples. Conductor losses are absent, but dielectric loss usually increases with dielectric constant; Q_s of up to several thousand can sometimes be achieved, however. By using an adjustable metal plate above the resonator, the resonant frequency can be mechanically tuned.

DRs offer advantages in increasing the performance of RF and microwave devices which make it an ideal candidate for wireless application; low design profile and wide bandwidth [9]. The DR has a high flexibility to adopt a shape over a wide frequency range. A small disc or cube (or other shape) of dielectric material can also be used as a microwave resonator. The operation of such a DR is similar in principle to the rectangular or cylindrical cavity resonators and it can increases the Q-factor in a microwave circuit. The size, location and shape of the DRs including the height and size area are influence the matching of the circuit. The match combination of dielectric resonators and microwave circuit capable to generate additional coupling effect that can

be merged together to produce a wideband device as well as increasing the transmitting power and reduce the insertion loss.

The design of a DR in any geometry must satisfy various specifications including: the resonant frequency, the field distribution inside the resonator, the radiated field and also the bandwidth. Similar to common metal wall cavities, an infinite number of operating modes exist and may be excited in DRs satisfying boundary conditions. Resonator modes can be classified into two categories, Transverse Electric (TE) and Transverse Magnetic (TM). TE and TM must refer to a coordinate axis. In general, TE to an axis implies the Electric field component in that axis vanishes, or equivalently two electric components Transverse (perpendicular) to that axis exist. Similarly for TM, Magnetic is replaced with Electric in the above statement. Mode indices e.g., TE_{113} (rectangular cavity analyzed in Cartesian coordinates) indicate how many of the electromagnetic field variations along each coordinate have (in this case 1 along x and y, and 3 along z).The case of a dielectric resonator situation is more complicated.

The field distribution and resonant frequencies for a resonator can be calculated analytically. To modify, it should be taken into consideration that in actuality some of the electromagnetic field leaks out of the resonator and eventually decays exponentially in its vicinity. This leaking field portion is described by a mode subscript δ. Mode subscript δ is always smaller than one and varies with the field confinement in a resonator. If the dielectric constant of the resonator increases, more of the electromagnetic field is confined in the resonator and the mode subscript δ starts approaching one.

The $TE_{01\delta}$ mode is the most popular and is used in single mode filters and oscillators. $HE_{11\delta}$ (HE indicates a hybrid mode) is used in high performance, dual mode filters [10], directional filters and oscillators.

The dielectric resonator is considered as a short length “L”, of dielectric waveguide opens at both ends. The lowest order TE mode of this guide is the TE_{01} mode, and is the dual of the TM_{01} mode of a circular metallic waveguide. The fields for different modes are sketched in Fig 3.1b, c. Because of the high permittivity of the resonator, propagation along the z-axis can occur inside the dielectric at the resonant frequency, but the fields could be cutoff in the air regions around the dielectric.

The main dimension of a DR is proportional to $\lambda_0\sqrt{\varepsilon_r}$ where λ_0 is the wavelength in free space and ε_r is the relative dielectric constant; the resonator dimensions become smaller when compared to λ as ε_r increases. Since the dimensions of an air-filled cavity are of the order of λ, a DR has much smaller dimensions than the cavity resonator. One of the importance characteristic of DR is, for a given dielectric constant, both resonant frequency and Q-factor are defined according to the resonator dimensions.

The H_z field (Fig 3.1d) is; higher order resonant modes have more variations in the z direction inside the resonator. Because the resonant length for the $TE_{01\delta}$ mode is less than $\lambda_g/2$ (where λ_g is the guide wavelength of the TE_{01} dielectric waveguide mode), the symbol $\delta=2L/\lambda_g<1$ is used to denote the z variation of the resonant mode. The equivalent circuit of the resonator looks like a length of transmission line terminated in purely reactive loads at both ends.

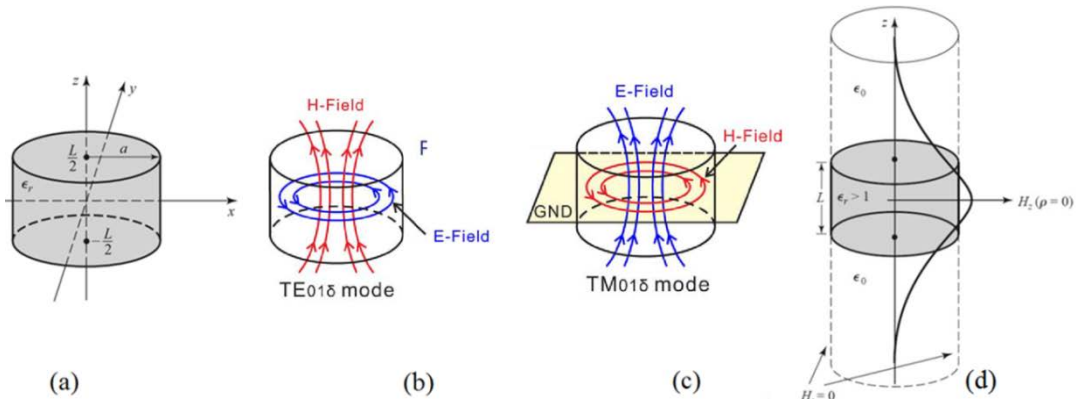

Fig. 3. 1 a) Geometry of a , b) Sketch of the cylindrical DR field configurations TE_{01} mode, c) $TM_{01\delta}$ mode, d) Magnetic wall boundary condition approximation and distribution of H_Z versus z for $\rho=0$ of the first mode of a cylindrical dielectric resonator.

In the analysis of resonator characteristics, one of the most essential properties is the resonant frequency which is determined by the value of relative permittivity.

The dielectric constant of a material is a parameter that reflects the capability of a material to confine a microwave. The higher this parameter means better in term of microwave signals confinement in the substrate.

The dielectric constant identify, ratio of the stored electrical energy in the material to that stored in vacuum and that is commonly expressed as $\varepsilon_r=\varepsilon/\varepsilon_0$ where ε_0 is called permittivity of free space, i.e., the dielectric constant values are referenced with respect to the air ($\varepsilon_r=1$).

From the electromagnetic theory point of view, the definition of electric displacement (electric flux density) D_f is:

$$D_f = \varepsilon E \tag{3. 1}$$

Where $\varepsilon=\varepsilon_0\varepsilon_r$ is the absolute permittivity (or permittivity), ε_r is the relative permittivity, $\varepsilon_0 \approx \frac{1}{36\pi} \times 10^{-9}\ F/m$ is the free space permittivity and E is the electric field. Permittivity describes the interaction of a material with an electric field E and is a complex quantity.

$$k = \frac{\varepsilon}{\varepsilon_0} = \varepsilon_r = \varepsilon_r' - j\,\varepsilon_r'' \tag{3. 2}$$

Dielectric constant (k) is equivalent to relative permittivity (ε_r) or the absolute permittivity (ε) relative to the permittivity of free space (ε_0). The real part of permittivity (ε_r') is a measure of how much energy from an external electric field is stored in a material. The imaginary part of permittivity (ε_r'') is called the loss factor and is a measure of how dissipative or lossy a material is to an external electric field. The imaginary part of permittivity (ε_r) is always greater than zero and is usually much smaller than (ε_r'). The loss factor includes the effects of both dielectric loss and conductivity. When complex permittivity is drawn as a simple vector diagram (Fig 3.2), the real and imaginary components are 90° out of phase. The vector sum forms an angle d with the real axis (ε_r'). The relative "lossiness" of a material is the ratio of the energy lost to the energy stored.

$$tan\delta = \frac{\varepsilon_r''}{\varepsilon_r'} = D = \frac{1}{Q} = \frac{Energy\ lost\ per\ cycle}{Energy\ stored\ per\ cycle} \tag{3. 3}$$

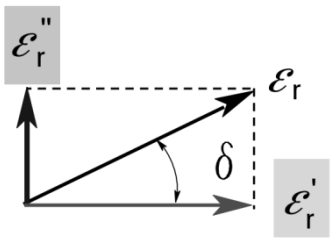

Fig. 3. 2 Loss tangent vector diagram

The loss tangent or tanδ is defined as the ratio of the imaginary part of the dielectric constant to the real part. D denotes dissipation factor and unloaded Q that accounts for the energy loss which is especially important for a narrow bandwidth and multistage band-pass filter. The loss tangent tanδ is called tan delta, tangent loss or dissipation factor. It is important to note that permittivity is not constant. It can change with

frequency, temperature, orientation, mixture, pressure, and molecular structure of the material.

3.1.1 Cavities and waveguides

The electromagnetic waves are reflected almost completely from the surfaces of good conductors. This suggests that metal tubes can used to guide electromagnetic waves from one place to another; and metal boxes to store electromagnetic energy in the form of standing waves.

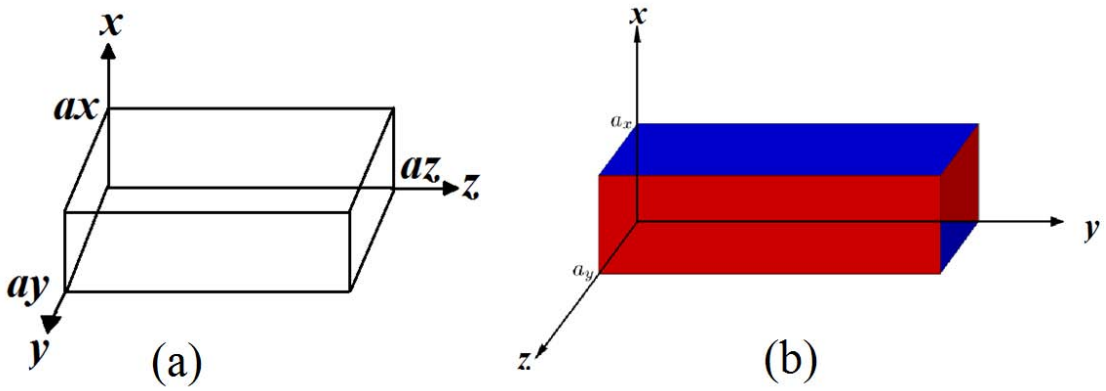

Fig. 3. 3 a) Rectangular cavity with perfect conducting walls b) Conducting tube with rectangular cross-section, of height and width a_x and a_y.

In free space, the wave equation for the electric field had the solution:

$$\vec{E}(\vec{r},t) = \overrightarrow{E_0} e^{j(\omega t - \vec{k}.\vec{r})} \tag{3. 4}$$

To satisfy the boundary conditions inside a conducting cavity, we write a solution of the form:

$$E_x = E_{x0}\, cosk_x x\, sink_y y\, sink_z z\, e^{j\omega t} \tag{3. 5}$$

$$E_y = E_{y0}\, sink_x x\, cosk_y y\, sink_z z\, e^{j\omega t} \tag{3. 6}$$

$$E_z = E_{z0}\, sink_x x\, sink_y y\, cosk_z z\, e^{j\omega t} \tag{3. 7}$$

Notice that a cosine dependence on the coordinate corresponding to the component of the field; and a sine dependence on the other coordinates.

The condition that the tangential component of the electric or magnetic field vanishes at all the conducting walls imposes the constraints on the components of the wave vector:

$$k_x = \frac{\pi n_x}{a_x} \qquad k_y = \frac{\pi n_y}{a_y} \qquad k_z = \frac{\pi n_z}{a_z} \tag{3. 8}$$

For any integers n_x, n_y and n_z.

n_x, n_y and n_z are called mode numbers: they specify the dependence of the electric field on the coordinates. At least two of the mode numbers must be non-zero, otherwise the field vanishes everywhere.

The wave vector and the frequency must be related:

$$\vec{k}^2 = k_x^2 + k_y^2 + k_z^2 = \frac{\omega^2}{c^2} \tag{3. 9}$$

Since the components of the wave vector are constrained to discrete values (since the mode numbers must be integers), the frequency is only allowed to take certain values:

$$\omega = \pi c \sqrt{\frac{n_x^2}{a_x^2} + \frac{n_y^2}{a_y^2} + \frac{n_z^2}{a_z^2}} \tag{3. 10}$$

c is the speed of light in the cavity and the possible values of ω are called the resonant frequencies.

Given an electric field in a particular mode, the associated magnetic field may be found from Maxwell's equation:

$$\nabla \times \vec{E} = -\dot{\vec{B}} \tag{3. 11}$$

To satisfy Maxwell's equations at all times, the time dependence of the magnetic field must be the same (to within a constant phase angle) as the time dependence of the electric field. Therefore, Eq (3.11) becomes:

$$\nabla \times \vec{E} = -j\omega\vec{B} \tag{3. 12}$$

The (0, 1, 1) mode is the mode with the lowest frequency in a cube-shaped cavity. The wave numbers are given by:

k_x=0 and k_y=k_z=$\frac{\pi}{a}$

where a is the length of the side of the cavity. The electric field is given by:

$$E_x = E_0 \ \sin(k_y y) sin(k_z z)\ e^{j\omega t}$$

$$E_y = 0$$

$$E_z = 0$$

By solving Maxwell´s equation gives for the magnetic field

$$B_x = 0$$

$$B_y = j\frac{k_z}{\omega}E_0 \ \sin(k_y y)cos(k_z z)\ e^{j\omega t}$$

$$B_z = -j\frac{k_y}{\omega}E_0 \cos(k_y y)sin(k_z z)\ e^{j\omega t}$$

Consider a perfectly conducting tube with rectangular cross-section, of height and width a_x and a_y. This is essentially a cavity resonator with length $a_z \rightarrow \infty$. By comparison with the rectangular cavity case, expect to find standing waves in x and y, with plane wave solution in z. Therefore a solution of the form:

$$E_x = E_{x0}\ cosk_x x\ sink_y y\ e^{j(\omega t - k_z z)} \quad (3.\ 13)$$

$$E_y = E_{y0}\ sink_x x\ cosk_y y\ \ e^{j(\omega t - k_z z)} \quad (3.\ 14)$$

$$E_z = -jE_{z0}\ sink_x x\ sink_y y\ \ e^{j(\omega t - k_z z)} \quad (3.\ 15)$$

The minimum frequency for a propagating wave is called the cut-off frequency, ω_{co}:

$$\boldsymbol{\omega_{co} = \pi c\sqrt{\frac{n_x^2}{a_x^2} + \frac{n_y^2}{a_y^2}}} \quad (3.\ 16)$$

It is possible for fields to oscillate in a waveguide at frequencies below the cut-off frequency. However, such fields do not constitute travelling waves.

If $\omega < \omega_{co}$ then $k_z^2 < 0$ so k_z must be imaginary ($k_z = jB$).

The horizontal field component (for example) in this case would be:

$$E_x = E_{x0}\ cosk_x x\ sink_y y\ e^{-\beta z}e^{j\omega t}$$

Note that there is an exponential decay of the field amplitude in the z direction, rather than an oscillation. The fields in this case constitute an "evanescent" wave.

For waves above the cut-off frequency, the variation of E_x with longitudinal position and time is:

$$E_x \sim e^{j(\omega t - k_z z)} \tag{3. 17}$$

And this equation would be similarly for all other field components. The phase velocity, v_p is the speed at which a particle would have to move along the waveguide to stay at constant phase with respect to the fields, i.e: ωt-$k_z z$=constant. Hence the phase velocity is:

$$\boldsymbol{v_p = \frac{dz}{dt} = \frac{\omega}{k_z}} \tag{3. 18}$$

Using the dispersion relation (3.9) we can write the phase velocity:

$$\boldsymbol{v_p = \frac{\omega}{k_z} = c\frac{\sqrt{k_x^2+k_y^2+k_z^2}}{k_z}} \tag{3. 19}$$

Therefore v_p>c

The phase velocity in the waveguide is greater than the speed of light.

3.1.2 Resonant Frequencies of TE01δ

The geometry of a cylindrical dielectric resonator is shown in Figure 3.1a. The basic operation of the $TE_{01\delta}$ mode can be explained as follows. The dielectric resonator is considered as a short length, L, of dielectric waveguide open at both ends. The lowest order TE mode of this guide is the TE_{01} mode, and is the dual of the TM_{01} mode of a circular metallic waveguide. Because of the high permittivity of the resonator, propagation along the z-axis can occur inside the dielectric at the resonant frequency, but the fields will be cut off (evanescent) in the air regions around the dielectric. Thus the Hz field will look like that sketched in Figure 3.1d; higher order resonant modes will have more variations in the z direction inside the resonator. Because the resonant length for the $TE_{01\delta}$ mode is less than λg/2 (where λ_g is the guide wavelength of the TE_{01} dielectric waveguide mode), the symbol $\delta=2L/\lambda_g<1$ is used to denote the z variation of the resonant mode. The equivalent circuit of the resonator looks like a length of transmission line terminated in purely reactive loads at both ends.

At the surface of regions of high permittivity, the boundary behaves like a perfect electric conductor, PEC, or short-circuit boundary when observed from the air to

dielectric regions. The boundary, when observed from dielectric to air, can be approximated by a hypothetical perfect magnetic conductor, PMC, on which the normal components of the electric field and tangential components of the magnetic field vanish at the boundary. This causes total internal reflections resulting in the confinement of energy in the high permittivity object. To a first approximation, a DR can be explained as a hypothetical perfect magnetic conductor, PMC, waveguide cavity, therefore, the field distribution and resonant frequencies for such a resonator can be calculated analytically. The magnetic wall waveguide below cutoff with a dielectric resonator situated in the middle is as shown in Fig 3.1d.

It is assumed that a magnetic wall boundary condition can be imposed at $\rho=a$. This approximation is based on the fact that the reflection coefficient of a wave in a high dielectric constant region incident on an air-filled region approaches +1:

$$\Gamma = \frac{\eta_0-\eta}{\eta_0+\eta} = \frac{\sqrt{\varepsilon_r}-1}{\sqrt{\varepsilon_r}+1} \to 1 \qquad as\ \varepsilon \to \infty \tag{3. 20}$$

This reflection coefficient is the same as that obtained at an ideal magnetic wall boundary condition, or a perfect open circuit. That η_0 and η denote the wave impedance of the air and the dielectric respectively.

The geometry of a cylindrical cavity is shown in Fig 3.4. As in the case of the rectangular cavity, the solution is simplified by beginning with the circular waveguide modes, which already satisfy the necessary boundary conditions on the wall of the circular waveguide.

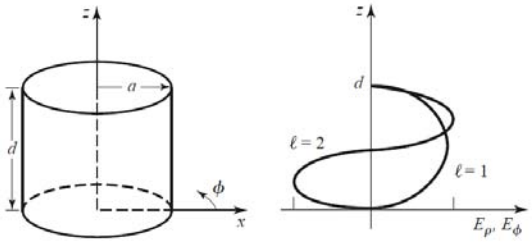

Fig. 3. 4 A cylindrical resonant cavity, and the electric field distribution for resonant modes with *l*=1 or *l*=2.

The transverse electric fields (E_ρ, E_φ) of the TE_{nm} or TM_{nm} circular waveguide mode can be written as

$$\bar{E}_t(\rho,\varphi,z) = \bar{e}(\rho,\varphi)(A^+e^{-jB_{nm}z} + A^-e^{jB_{nm}z}) \tag{3. 21}$$

Where $.e(\rho, \varphi)$ represents the transverse variation of the mode, and A^+ and A^- are arbitrary amplitudes of the forward and backward traveling waves. The propagation constant of the TE_{nm} mode is

$$B_{nm} = \sqrt{k^2 - \frac{{p'_{nm}}^2}{a}} \tag{3. 22}$$

While the propagation constant of the TM_{nm} mode is,

$$B_{nm} = \sqrt{k^2 - \frac{{p_{nm}}^2}{a}} \tag{3. 23}$$

Where $\boldsymbol{k = \omega\sqrt{\mu\varepsilon}}$

In order to have $.E_t = 0$ at $z=0, d$, that $A^+ = -A^-$, must be chosen, and $A^+ \sin \beta_{nm} d=0$,

Or

$$B_{nmL} = l\pi, \text{ for } l=0, 1, 2, 3, \tag{3. 24}$$

This implies that the waveguide must be an integer number of half-guide wavelengths long. Thus, the resonant frequency of the TE_{nml} mode is

$$f_{nml} = \frac{c}{2\pi\sqrt{\mu_r\varepsilon_r}}\sqrt{\left(\frac{{p'_{nm}}^2}{a}\right) + \left(\frac{l\pi^2}{d}\right)} \tag{3. 25}$$

And the resonant frequency of the TM_{nml} mode is

$$f_{nml} = \frac{c}{2\pi\sqrt{\mu_r\varepsilon_r}}\sqrt{\left(\frac{{p_{nm}}^2}{a}\right) + \left(\frac{l\pi}{d}\right)^2} \tag{3. 26}$$

Where p'_{nm} and p_{nm} are Bessel's solutions $(n, m, l) \in N$, a, d are the radius and the height of the dielectric resonator.

Free space wavenumber k_0 is:

$$k_0 = \frac{2\pi f_0}{c} \tag{3. 27}$$

Which c speed of light, for resonant frequency f_0. Re-arranging for the resonant frequency

$$f_0 = \frac{2\pi k_0}{c} \tag{3. 28}$$

And resonant frequency of isolated cylindrical DRs for $TE_{01\delta}$ mode could be

$$k_0 a_{\varepsilon_{r\gg 25}} = \frac{2.327}{\sqrt{\varepsilon_r+1}}\left(1 + 0.2123\left(\frac{a}{d}\right) - 0.00898\left(\frac{a}{d}\right)^2\right) \quad (3.\ 29a)$$

Or equivalently:

$$f_{0(TE_{01\delta})} = \frac{C\ 2.327}{2\pi a\sqrt{\varepsilon_r+1}}\left(1 + 0.2123\left(\frac{a}{d}\right) - 0.00898\left(\frac{a}{d}\right)^2\right) \quad (3.29b)$$

$TE_{011+\delta}$ Mode:

$$k_0 a_{\varepsilon_{r\gg 25}} = \frac{2.208}{\sqrt{\varepsilon_r+1}}\left(1 + 0.7013\left(\frac{a}{d}\right) - 0.002713\left(\frac{a}{d}\right)^2\right) \quad (3.\ 30a)$$

$$f_{0(TE_{011+\delta})} = \frac{c\ 2.208}{2\pi a\sqrt{\varepsilon_r+1}}\left(1 + 0.7013\left(\frac{a}{d}\right) - 0.002713\left(\frac{a}{d}\right)^2\right) \quad (3.30b)$$

$TM_{01\delta}$ Mode:

$$k_0 a = \frac{\sqrt{3.83^2 + \left(\frac{\pi a}{2d}\right)^2}}{\sqrt{\varepsilon_r + 2}}$$

$$f_{0(TM_{01\delta})} = \frac{c\sqrt{3.83^2+\left(\frac{\pi a}{2d}\right)^2}}{2\pi a\sqrt{\varepsilon_r+2}} \quad (3.\ 31)$$

The above formulas are valid in the range $0.33 \ll a/d \ll 5$.

3.2 Dielectric material

A DR is generally smaller in size, cost, and weight than an equivalent metallic cavity, and it can easily be incorporated into microwave integrated circuits and coupled to planar transmission lines.

Materials with high dielectric constants are required in order to provide miniaturization at the frequencies typically used for wireless applications. Losses must be low to provide resonators with high Q, leading to low pass-band insertion loss and maximum attenuation in the stop-bands. In addition, the dielectric constant must be stable with changes in temperature to avoid drifting of the filter pass-band over normal operating conditions.

Most materials that are commonly used in dielectric resonator filters are ceramics, such as barium tetratitanate, zinc/strontium titanate, and various titanium oxide compounds. For example, a zinc/strontium titanate ceramic material has a dielectric constant of 36, a Q of 10,000 at 4 GHz, and a dielectric constant temperature coefficient of -7 ppm/C°.

In this work a cylindrical DR screen-printable epoxy/ $BaTO_3$ with a high dielectric constant and benefit thermal stability were investigated which in next section more detail is presented.

3.2.1 Experimental and fabrication process

The dielectric constant of bulk $BaTO_3$ is affected by its grain size at room temperature. Its dielectric constant increases to the maximum with a decrease in the grain size to approximately 0.9 μm, whereas it decreases further when its grain size is below 0.9 μm. The dielectric constant of bulk $BaTO_3$ strongly depends on the crystal structure of $BaTO_3$ powder which has similar characteristics to the dielectric constant of bulk $BaTO_3$.

At room temperature, tetragonality decreases as the particle size decreases slowly to 0.3 μm. The tetragonality of $BaTO_3$ powder with a particle size less than 0.3 μm rapidly decreases, eventually disappearing when reaching approximately 0.1 μm. This implies that structural changes to the cubic or pseudo cubic structure. Therefore, it can be expected that $BaTO_3$ powder could have the maximum dielectric constant at approximately 0.9 μm, and this has been verified [11].

The most widely used dielectric material is an epoxy-$BaTiO_3$ composite while, polymers such as epoxy and polyimide can be used as the dielectric material. In some applications, epoxy has a low dielectric constant. While, ceramics such as $BaTiO_3$ have a high dielectric constant (~15,000) [12], but their processing temperature is high (~850°C) [13] and not compatible with the regular printed board manufacturing process. The advantage of using an epoxy/$BaTiO_3$ composite is that it combines the low temperature process ability of epoxy along with the high dielectric constant of $BaTiO_3$ [14].

For fabrication processes epoxy ink, thinner, and $BaTiO_3$ powder are mixed. Retarder Thinner 114-20 is used as a solvent to dissolve epoxy-$BaTiO_3$ resin and reduce the viscosity. Thinner reasonable properties are obtained on a variety of substrates by curing at temperatures ranging from 50°C to 150°C. $BaTiO_3$ powder with average size of 0.9 μm was chosen for the purposes of this study. Screen printing technology can be used to fabricate thick-film resin in conjunction with ceramic processes such as low temperature co-fired ceramic (LTCC).

3.2.2 Epoxy/$BaTiO_3$ composite

Capacitor fabrication procedure using an epoxy/BaTiO3 composite is as follows. First, the epoxy/$BaTiO_3$ blended for measurement of the dielectric constant of composite. The methodology was applied to the 7 prototypes. The amounts of all 7 composites are tabulated in Table 3.1.

Table 3.1 Particle amounts of the 7 epoxy/$BaTiO_3$ powders used in this study

sample	Epoxy(gr)	$BaTiO_3$ (gr)
1	1	0
2	0.65	0.35
3	0.30	0.70
4	0	0.99
5	0.66	0.34
6	0.47	0.53
7	0.50	0.50

These samples are printed on PCBs using a screen printing technology. Conditions for the screen printing are not easier as the viscosity of the mixed materials changed during the fabrication and they became hard and tight. To break agglomerates of the $BaTiO_3$ powder, thinner was added to the resin system.

Table 3.2 Particle amounts of the 6 epoxy/$BaTiO_3$ powders and their cure times, temperatures used in this study.

Sample	Epoxy(gr)	$BaTiO_3$ (gr)	Thinner(ml)	Temp(° C)	Cure time(min)
1	0.20	0.90	0.5	100	50
2	0.35	0.65	0.5	120	60
3	0.45	0.55	0.5	120	60
4	0.55	0.45	0.5	150	60
5	0.60	0.4	0.5	150	60
6	0.65	0.35	0.5	150	60

Different amount of epoxy and $BaTiO_3$ powder are mixed but the thinner unchanged as tabulated in table 3.2. It was observed that the maximum loading for $BaTiO_3$ particles is lower than 50% by volume, since high amount loading can cause adhesion problems. The measured dielectric constants of the epoxy/$BaTiO_3$ using S6 are higher than those using the other samples and it was able to screen-print on substrate easier. After blending process, prototypes have been put in a conventional oven at 150ºC for one hour.

For epoxy/$BaTiO_3$ composites, the dielectric constant increases with epoxy loading of up to 55-60% by volume, and then decreases due to an increase in porosity [11]. To characterize epoxy/$BaTiO_3$ reliability, solvent agent was added in various amounts to the resin system (Table 3.3).

Table 3.3 Particle amounts of the 7 epoxy/$BaTiO_3$ powders and solvent agent used in this study.

Sample	Epoxy(gr)	$BaTiO_3$(gr)	Thinner(ml)
1	0.65	0.35	0.1
2	0.65	0.35	0.2
3	0.65	0.35	0.3
4	0.65	0.35	0.4
5	0.65	0.35	0.5
6	0.65	0.35	0.05
7	0.65	0.35	0.025

It has been observed, all samples except 6, 7 were liquid fluently and they were difficult to deposit on substrate, and samples 6, 7 were hard enough to deposit and needed more thinner to diluent.

Also, it can be seen that an increase in $BaTiO_3$ loading beyond 55–65% decreases the capacitance [15] due to the presence of voids when the theoretical maximum packing density is exceeded. Typically, for reliability reasons the maximum $BaTiO_3$ loading should be lower than 50% by volume, which limits the maximum dielectric constant of this composite (epoxy/$BaTiO_3$) to about 30 in commercially available dielectrics.

In the other hand, moisture absorption in the dielectric can change the electrical parameters of capacitors. Moisture absorption is reversible; an increase in capacitance can affect the system for a period of time. However, the dissipation factor of the dielectric also found which can increase under this condition [16]. Dissipation factor is an important electrical parameter and is a measure of losses in the dielectric. An increase in loss factor and dielectric constant under the moisture uptake is a general trend in polymer materials [17]. It can be understood that the absorbed moisture changes the molecular dipoles. The polar group of water increases the polarity of the resin, resulting in an increase in the capacitance and the dielectric loss.

As shown in Fig.3.4, the dielectric constant of the composite increased up to nearly 60 as the $BaTiO_3$ powder content increased. As previously mentioned, the slow-down in the dielectric constant increment above 60 vol% occurred because the powder packing density could not reach the theoretical maximum density [10]. And according to observation, with 35% vol $BaTiO_3$ powder, dielectric constant is around 25. It can cause that the final dielectric constant of the composite is much closer to that of the low dielectric constant material, which is generally an epoxy with a value of 3 to 5. The overall dielectric constant of the composite ends up in the range of 10 to 50, even at 50% to 60% loading of $BaTiO_3$ by volume as shown in Fig 3.5.

There are various strategies to increase the effective dielectric constant of these composites. A straightforward approach to increase the effective dielectric constant, which this work is used, is utilization of high dielectric constant epoxy with dielectric constant around 45~50 instead of $BaTiO_3$ powder.

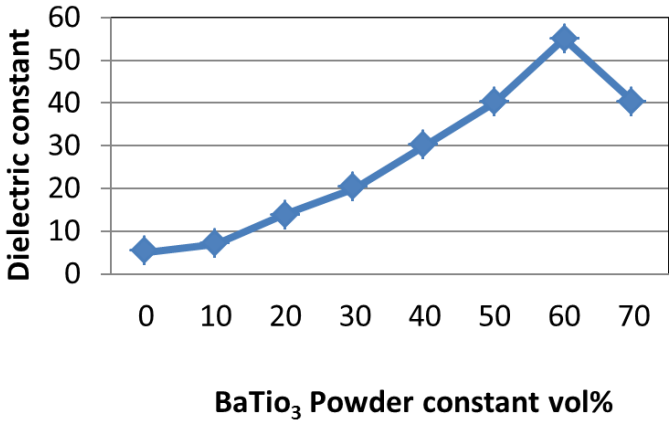

Fig. 3. 5 Dielectric constant of the composite as a function of $BaTiO_3$ powder content.

Similar results were observed when creative epoxy past is utilized as a high dielectric constant that can increase in capacitance. High dielectric constant epoxy 122-06 is used as a pad-printable ink that is formulated for a higher dielectric constant, greater adhesion and higher chemical resistance than typical high dielectric constant inks which in experiment result in this work is used. This material has gained importance with an increase in the operating frequency of electronic circuits, because it has better electrical performance and can also lead to miniaturization of electronic products.

Embedded passive technology is an interesting technology for further miniaturization and higher performance of electronic package systems. Polymer/ ceramics composites have been of great interest as embedded capacitor materials, because they did combine not only the process ability of polymers with high dielectric constant of ceramics hut also good compatibility with printed circuit boards (PCBs).

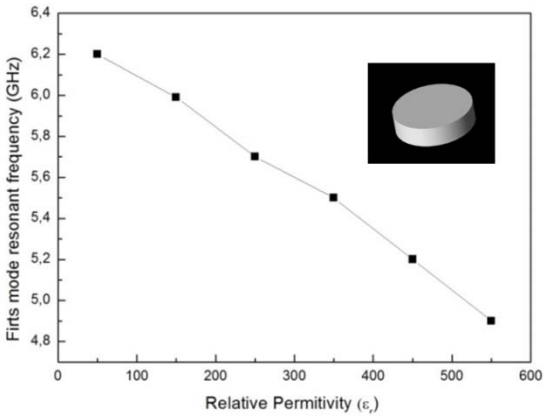

Fig. 3. 6 Relation between the first resonant mode frequency and the dielectric constant.

The increase in dielectric constant can be attributed to the fact that shifting frequency to lower frequency and aiding in product miniaturization, as shown in Fig 3.6.

3.3 Excitation of cylindrical DR

The resonance properties of dielectric cylinders is highly dependent on the electromagnetic (EM) properties of the neighboring object, the most common case be in g the grounded dielectric substrate used in micro-strip technology circuits. Indeed, the extensive use of micros-trip technology, compatible to high permittivity finite cylinder dielectric resonators, requires the development of accurate computational techniques to determine their resonance properties and especially the effects of EM structures being in their vicinity. This is due to the fact that, the very high value of the cylinders' dielectric permittivity seems to cause numerical in stability and serious convergence problems on the computational techniques to be used, which are otherwise very stable and easily convergent for low dielectric permittivity values.

DR can be easily varied by suitably choosing the dielectric constant of the resonator material and its dimensions. DR is preferred because they are easy to fabricate and offer more degree of freedom to control the resonant frequency and quality factor.

The amount of coupling depends on the distance between the tip of the strip and the center of the DR which may be defined as the overlapping distance. This is one way of tuning a DR where the resonant frequency is a function of its position on the feed.

Among the three basic shapes of DR rectangular, cylindrical, and spherical, the cylindrical shaped DR has been the most popular shape studied for practical applications. A cylindrical DR is characterized with a radius, a, height, h, and dielectric constant ε_r.

A common method for coupling to dielectric resonators in microwave circuits is by proximity coupling to micro-strip lines. Micro-strip coupling could excite the magnetic fields in the DR to produce the short horizontal magnetic dipole mode. The level of coupling can be adjusted by the lateral position of the DR with respect to the micro-strip line and on the relative permittivity of the DR. For lower permittivity values (necessary

for DRs requiring wide bandwidth), the amount of coupling is generally quite small. Thus, in order to have acceptable radiation efficiency, an array of DRs is required. Micro-strip lines can be used as a series feed for a linear array of DRs, provided that a sufficient number of elements are used. One disadvantage of this method is that the polarization of the array is dictated by the orientation of the micro-strip line.

Some examples of resonator coupling techniques are shown in Fig 3.7. In Fig 3.7e the strength of coupling is determined by the spacing, d, between the resonator and micro-strip line. Because coupling is via the magnetic field, the resonator appears as a series load on the micro-strip line, as shown in the equivalent circuit of Fig 3.7f.

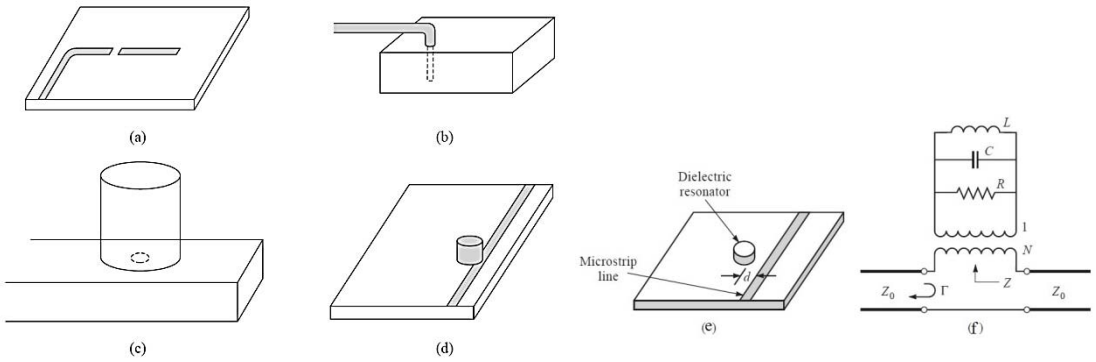

Fig. 3. 7 Coupling to microwave resonators (a) A micro-strip transmission line resonator gap coupled to a micro-strip feed-line. (b) A rectangular cavity resonator fed by a coaxial probe. (c) A circular cavity resonator aperture coupled to a rectangular waveguide. (d) A dielectric resonator coupled to a micro-strip line (e) Geometry of a dielectric resonator coupled to a micro-strip line; (f) equivalent circuit [55].

A measure of the level of coupling between a resonator and a feed is given by the coupling coefficient. To obtain maximum power transfer between a resonator and a feed line, the resonator should be matched to the line at the resonant frequency; the resonator is then said to be critically coupled to the feed. It is illustrated this concepts by considering the series resonant circuit as shown in Fig 3.8.

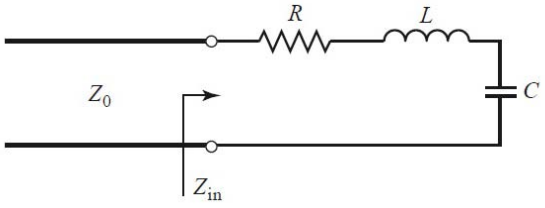

Fig. 3. 8 A series resonant circuit coupled to a feed line.

The input impedance near resonance of the series resonant circuit of Fig 3.8 is given by

$$\boldsymbol{Z_{in} = R + j2L\Delta\omega = R + j\frac{2RQ_0\Delta\omega}{\omega_0}} \quad (3.\ 32)$$

and the unloaded Q is

$$Q_0 = \frac{\omega_0 L}{R} \tag{3. 33}$$

At resonance, $\Delta\omega = 0$, so from (3.33) the input impedance is Z_{in}=R. In order to match the resonator to the line we must have R=Z_0. In this case the unloaded Q is

$$Q_0 = \frac{\omega_0 L}{Z_0} \tag{3. 34}$$

The external Q is

$$Q_0 = \frac{\omega_0 L}{Z_0} = Q_e$$

This shows that the external and unloaded Q_0 are equal under the condition of critical coupling. The loaded Q is half this value. The coupling coefficient, g, defined as

$$\mathrm{g} = \frac{Q_o}{Q_e} \tag{3. 35}$$

That can be applied to both series (g=Z_0/R) and parallel (g=R/Z_0) resonant circuits, when connected to a transmission line of characteristic impedance Z_0. Three cases can be distinguished:

1. g $<$ 1: The resonator is said to be under-coupled to the feed line.

2. g $=$ 1: The resonator is critically coupled to the feed-line.

3. g $>$ 1: The resonator is said to be over-coupled to the feed-line

3.3.1 DR mounted on micro-strip

The coupling between the line and the resonator is accomplished by orienting the magnetic moment of the resonator perpendicular to the micro-strip plane so that the magnetic lines of the resonator link with those of the micro-strip line.

The dielectric resonator placed adjacent to the micro-strip line operates like a reaction cavity which reflects the RF energy at the resonant frequency [18,19]. The equivalent circuit of the resonator coupled to the micro-strip line is shown in Fig 3.8a.

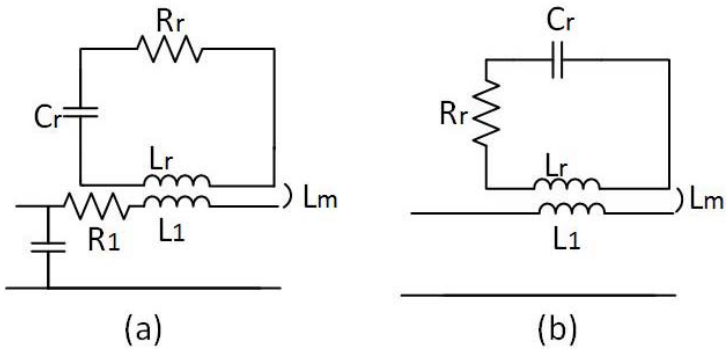

Fig. 3. 9 Equivalent circuit of the dielectric resonator coupled with a line.

In Fig 3.9, L_r, C_r and R_r are the equivalent parameters of the dielectric resonator, L_1, C_1, and R_1 those of the line. The magnetic coupling is characterized by the mutual inductance L_m.

In the coupling plane, the network of Fig3.9a can be simplified to that of Fig 3.9b (the line is assumed to be without losses). Furthermore, the equivalent circuit in Fig 3. 9b can be put in the form shown in Fig 3.10.

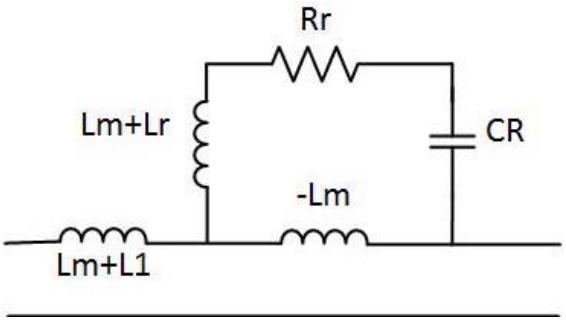

Fig. 3. 10 Simplified equivalent circuit of the dielectric resonator coupled with a line.

The transformed resonator impedance Z_t in series with the transmission line can be expressed by

$$Z_t = j\omega L_1 + \frac{\omega^2 L_m^2}{R_r + j\left[\omega L_r - \frac{1}{\omega C_r}\right]} \tag{3. 36}$$

Around the resonant frequency, ωL_1can be neglected and Z_t becomes

$$Z_t = \omega Q_0 \frac{L_m^2}{L_r} \frac{1}{1+jX} \tag{3. 37}$$

The following notation has been used:

$$X = 2Q_0 \frac{\Delta\omega}{\omega} \tag{3. 38}$$

$$Q_0 = \frac{L_r\omega_0}{R_r} \text{ and } \omega_0 = \frac{1}{\sqrt{L_rC_r}}$$

At resonant frequency X=0 and the transformed impedance become real:

$$Z_t = R = Q_0\omega_0 \frac{L_m^2}{L_r} \tag{3. 39}$$

Equation (3.39) indicates that Fig 3.10 can be represented by the simple parallel tuned circuit, such as shown in Fig 3.11. L, R, C satisfy the following equations

$$L = \frac{L_m^2}{L_r} \tag{3. 40}$$

$$C = \frac{L_r}{\omega_0^2 L_m^2} \tag{3. 41}$$

$$R = Q_0\omega_0 \frac{L_m^2}{L_r} \tag{3. 42}$$

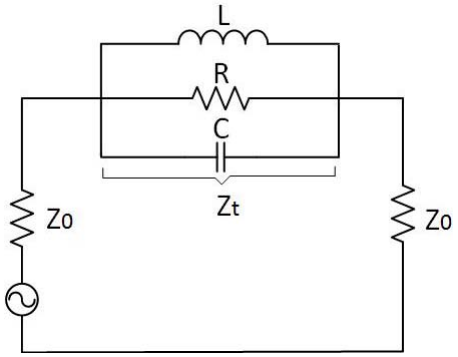

Fig. 3. 11 Final equivalent of a dielectric resonator coupled with a micro-strip line.

The coupling coefficient k is defined by

$$k = \frac{Z_t(\omega_0)}{R_{ext}} \tag{3. 43}$$

Using $R_{ext}=2Z_0$, then obtain

$$R = \frac{Q_0\omega_0}{2Z_0}\frac{L_m^2}{L_r} \tag{3. 44}$$

Let Q be the external quality factor which characterizes the coupling of the resonator with the micro-strip line, and let Z_0 be characteristic impedance of the line. Then

$$Q_e = \frac{Q_0}{k} = \frac{2Z_0L_r}{\omega_0L_m^2} \tag{3. 45}$$

To determine the coupling coefficient completely it is necessary to evaluate the Q_e factor as a function of distance d between the line and the resonators. The factor which characterizes this variation in (3.45) is $L_r/L_m{}^2$.

The dielectric resonator coupled with the micros-trip line is identical to a parallel resonant circuit placed in series with the line.

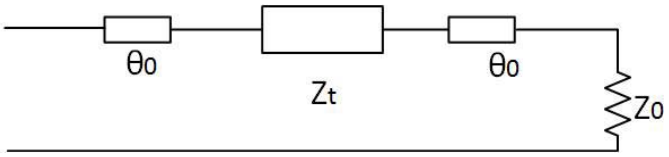

Fig. 3. 12 Distributed equivalent circuit of DR mounted on micro-strip.

Such a circuit can be conveniently described in terms of the scattering parameters. Let θ be the electrical length of the micro-strip line, as shown in Fig 3.12. Then, the parameters of the scattering matrix are

$$S_{11} = \frac{\frac{Z_t}{Z_0}}{2+\frac{Z_t}{Z_0}} e^{-2j\theta} \tag{3. 46}$$

$$S_{11} = \frac{2}{2+\frac{Z_t}{Z_0}} e^{-2j\theta} \tag{3. 47}$$

3.3.2 Mutual coupling between two DRs via a micro-strip line

For the applications of dielectric resonators in microwave filters, it is also necessary to study the coupling between two dielectric resonators [20].

The coupling coefficient k between the micro-strip-coupled resonators can be obtained by calculating the open circuit impedance parameters of the two circuits shown in Figs 3.13 and 3.14 and by identifying the corresponding elements.

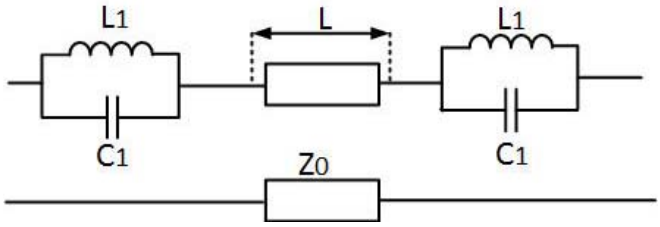

Fig. 3.13 Equivalent circuit of micro-strip-coupled dielectric resonators.

The condition for equivalence between the two circuits can be easily determined to be

$$\boldsymbol{cot\beta l = 0} \quad \boldsymbol{or} \quad \boldsymbol{L = \left[\frac{2i+1}{4}\right]\lambda_g} \; ; \qquad \boldsymbol{i = 0, 1, 2, \ldots..} \tag{3. 48}$$

That λ_g is the wavelength in the micro-strip.

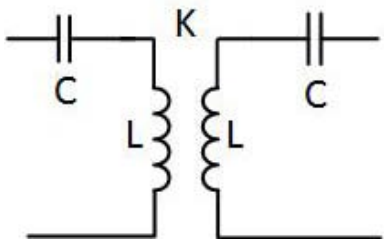

Fig. 3. 14 Lumped equivalent circuit.

For the values of L given by (3.48), the coupling between resonators is

$$k = \frac{1}{\sqrt{Q_{e1}Q_{e2}}}(-1)^i \tag{3. 49}$$

That Q_{e1} and Q_{e2} are the external Q-factors of the resonators.

Thus, for a positive coupling coefficient, the line length L must be one-quarter wavelength long, and for a negative coupling it must be three- quarters of a wavelength long. The magnitude of the coupling is controlled by the height of the resonator above the micro-strip substrate and also by the distance between the line and the resonator.

Summary

This chapter covered analysis and design of artificial dielectric resonators. Equation formulation and the method for analysis of dielectric resonators are considered that, computation and measurement of the unloaded Q factor are discussed in detail. For some practical applications, field distribution in the dielectric resonator mounted on a micro-strip and coupled to micro-strip is considered. The computation of coupling between the dielectric resonator and an external circuit is the explained. Also dielectric

resonator with a high permittivity which these properties are well-suited for miniaturization of microwave devices is explained. The more reliable property and the possibility of this material which is related to the current work are investigated in next chapter.

3.4 References

[1] R.D. Richtmyer, Dielectric Resonator, J. Appl. Phys., 10, pp 391–398, 1939.

[2] H.M. Schlicke, Quasi-degenerate Modes in High ε Dielectric Cavities, J. Appl. Phys., 24, pp 187-191, 1953.

[3] A. Okaya, L. F. Barash, "The Dielectric microwave resonator," Proc. IRE, 50, pp 2081-2092, 1962.

[4] S.B. Cohn, "Microwave Bandpass Filters Containing High Q Dielectric Resonators," IEEE Trans.
Microwave Theory & Tech., MTT-16, 218–227, 1968.

[5] T. Nishikawa, Y. Ishikawa, and H. Tamura, "Ceramic Materials for Microwave Applications", electronic Ceramics, Spring Issue, Special Issue on Ceramic Materials for Microwave Applications, Japan, 1979.

[6] G.V. Eleftheriades and K.G. Balmain "Negative refraction metamaterials," John Wiley & Sons, Inc., Hoboken, New Jersey, 2005.

[7] A. Tadjalli, A. Sebak, and T. Denidni, "Resonance frequencies and far field patterns of elliptical dielectric resonator antenna ,Analytical approach," Progress In Electromagnetics Research, Vol. 64, pp 81-98, 2006.

[8] S. Bhattacharya, R. Tummala, "Next generation integral passives: materials, processes, and integration of resistors and capacitors on PWB substrates," J. Mater. Sci. Mater. Electron. 11(3), pp 253–268, 2000.

[9] A. Petosa "Dielectric resonator antenna handbook," Artech House, Bolton, 2007.

[10] S. J. Fiedziuszko, "Dual Mode Dielectric Resonator Loaded Cavity Filters," IEEE Trans. Microwave Theory & Tech., MTT-30, pp 1311-1316, 1982.

[11] J. I. Marulanda, M. Cremona, R. Santos, M. C. R. Carvalho, and L. S. Demenicis," Characterization of SrTiO3 thin films at microwave frequencies using coplanar waveguide resonator method", Microwave and Optical Tech. Letters, vol. 53, no. 10, pp 2418-2422, 2011.

[12] S. Swartz "Electronic ceramics," IEEE Trans, Electr, Insulation 25(5), pp 935–987, 1990.

[13] M. Keimasi, M.H. Azarian, M. Pecht, "Flex cracking of multilayer ceramic capacitors assembled with Pb-free and tin-lead solders," IEEE Trans, Device Mater. Reliab. 8(1), pp 182–192, 2008.

[14] S. Bhattacharya, R. Tummala, "Next generation integral passives: materials, processes, and integration of resistors and capacitors on PWB substrates," J. Mater. Sci. Mater. Electron. 11(3), pp 253–268, 2000.

[15] K. Paik, J. Hyun, S. Lee, K. Jang, "Epoxy/BaTiO3 (SrTiO3) Composite Films and Pastes for High Dielectric Constant and Low Tolerance Embedded Capacitors in Organic Substrates," Vol 2 (Electronics Systemintegration Technology Conference, Dresden, pp 794-801, 2006.

[16] M. Alam, M. Azarian, M. Pecht "Reliability of embedded planar capacitors with epoxy $BaTiO_3$ composite dielectric during temperature humidity bias tests," IEEE Trans Device Mater Reliab, 2011.

[17] P. Myslinski, Z. Lazowski, Mater Chem Phys, 33, 139, 1993.

[18] P. Guillon and S. Mekerta "A bandstop dielectric resonatorfilter," IEEE MTT-S, Int.Microwave .Symp.Dig ,pp. 170-173, 1981.

[19] A.E. Atia and R.R. Bonetti "Generalized dielectric resonatorfilters," Comsat Technical review, vol. 11, pp. 321-343, 1981.

[20] P. Guillon, B. Byzery, and M. Chaubet "Coupling parameters between a dielectric resonator and a microstrip line," IEEE Trans microwave Theory and Tech, vol. MTT 33, pp 222-226, 1985.

CHAPTER 4

4 Multisection filters based on dielectric resonator

Recently the experimental investigation of isotropic MTMs based on resonant dielectric inclusions has been reported [1-2]. To date, MTMs have commonly been formed from resonant conducting circuits that dimensions and spacing are much less than the wavelength of operation. By engineering the dipolar response of these resonant elements, an unprecedented range of effective material responses can be realized, including artificial magnetism and large positive and negative values of the effective ε and μ. There is an alternative approach to obtain artificial magnetism that relies instead on the resonances in sub-wavelength dielectric resonators. Sub-wavelength particles with very high positive dielectric permittivity support strong resonances with a large displacement current, which may give rise to strong magnetic field induced by contra-directional displacement currents. Moreover, the large dielectric constant implies a small wavelength inside the high-permittivity region; therefore the physical size of the resonator can be many times smaller than the free-space wavelength. This situation justifies the treatment of the system as a macroscopically homogenous medium, and the use of effective constitutive parameters to describe its interaction with external waves is applicable. Section 4.1 is presented MTMs concept and their characterization.

As for methods of MTMs constructions, several geometries for the inclusions of such media have been suggested. Among those, one can mention that is split ring resonators (SRR) which is explained in section 4.1.1. Different configurations of MTMs implementation are shown in this part.

From an electromagnetic propagation viewpoint, media with periodically changing dielectric properties impose periodic boundary conditions on propagating electromagnetic modes. Electromagnetic waves which do not satisfy these boundary conditions cannot propagate. At a specific frequency band, EBG does not allow the propagation of wave in all directions that is explained in section 4.1.2.

Artificial dielectric materials are obtained with simple inclusions such as disks, spheres, ellipsoids or needles in a dielectric matrix. These inclusions have small sizes compared to the wavelength. The distance between them is also small enough with respect to λ. Such materials can be represented by an effective permittivity ε_{eff}. This effective permittivity can reach values of 4–10 within a wide frequency band. In some applications, however, one needs to obtain higher values of ε_{eff}, at least within a narrow frequency band. A solution to this problem is to prepare resonant artificial dielectrics. That section 4.1.4 is dedicated to the artificial dielectric resonators.

The aim of this chapter is the development of the scattering theory of electromagnetic waves on the DR, located in the various transmission lines, as well as an investigation of the band-pass and band-stop filters ' parameters, consisting of a number of DRs.

For the applications of DRs in microwave filters, it is necessary to study the coupling between two dielectric resonators which is mentioned in section 4.2.1. To analyze the coupling, first field analysis of single resonator based on epoxy paste commercial dielectric constant is investigated and then relation between the coupling coefficient, k, and the spacing between the two resonators are studied.

The relative dielectric constant of the materials for constructing DR in microwave filters generally was chosen from a higher value compared to the base substrate. The primary advantage in using a high dielectric constant is to miniaturize the filter size. The size of DR filter is considerably smaller than the dimension of waveguide filters operate at the same frequency.

In section 4.3 a novel stop-band filter consists of three cylindrical thick film commercial high dielectric constant epoxy paste as DRs were excited with a microstrip line is investigated. In the following a new approach of designing a band-pass filter by applying a combination of microstrip ring and embedded commercial high dielectric constant epoxy paste as DRs is presented in section 4.4.

Since, the sub-wavelength property of the SRR has been successfully applied to the miniaturization of passive microwaves devices, section 4.5 is reported the benefits of embedded high dielectric constant paste in the design of miniaturized SRR.

Another approach to reduction size of filter is to modify the traditional resonator to generate additional modes, which make the resonator to behave as a multimode resonator. Thus one physical resonator can be treated as multiple electrical resonators. Section 4.6 is devoted to a novel multimode resonator (MMR) ultra-wide band-pass (UWB) filter design using a grounded open ring resonator.

4.1 Metamaterials (MMTs)

MTMs [3-4] provide enabling technologies for several applications in the field of microwave engineering, such as antennas, filters, couplers, imaging systems and cloaking devices. Permittivity (ε) and permeability (μ) are the two major parameters used to characterize the electric and magnetic properties of materials. For certain applications in microwave engineering it is difficult to find a naturally occurring material with wanted values of ε and μ. MTMs comprise a set of artificially structured composites with tunable ε and μ that are difficult to obtain with naturally materials. Also materials with simultaneously negative values of ε and μ, known as double negative, negative refractive index, left-handed or backward wave materials. MTMs fall in one of two categories: photonic or electromagnetic crystals and effective media. The first category corresponds to structures made of periodic micro- or nano-inclusions whose period is of the same order as the signal wavelength. Therefore, their electromagnetic properties arise mainly from periodicity. Conversely, in effective media the period is much smaller than this signal wavelength. Hence, their electromagnetic properties can be obtained from a homogenization procedure. This work is mainly devoted to the second category, specifically to those MTMs that can be characterized by a negative effective ε and/or μ. MMTs are defined as effectively homogeneous electromagnetic structures which average cell size p is much smaller than the guided wavelength λ_g. Therefore, this average cell size should be at least smaller than a quarter of wavelength, $p<\lambda_g/4$. If the condition of effective-homogeneity is satisfied, the

structure behaves as a real material. The constitutive parameters are the ε and the μ, which are related to the refractive index n by

$$n = \pm\sqrt{\varepsilon_r \mu_r} \quad (4.1)$$

Where εr and μr are the relative permittivity and permeability related to the free space permittivity and permeability by $\varepsilon_0=\varepsilon/\varepsilon r=8.85.10^{-12}$ and μ0=μ/μr=4π.10^{-7}, respectively.

In (4.1), sign ± for the double-valued square root function has been a priori admitted for generality.

As illustrated in the ε-μ diagram of Fig 4.1, a medium with both ε and μ greater than zero (ε>0, μ>0) is designated a double positive (DPS) medium. Most naturally occurring media (e.g., dielectrics) fall under this designation. A medium with ε less than zero and μ greater than zero (ε<0, μ>0) is designated an epsilon-negative (ENG) medium. In certain frequency regimes many plasmas exhibit this characteristic. For example, metals (e.g., silver, gold) behave in this manner in the infrared (IR) and visible frequency domains. A medium with the ε greater than zero and μ less than zero (ε>0, μ<0) is designated a mu negative (MNG) medium. A medium with the permittivity and permeability less than zero (ε<0, μ<0) is designated a DNG medium. To date, this class of materials has only been demonstrated with artificial constructs.

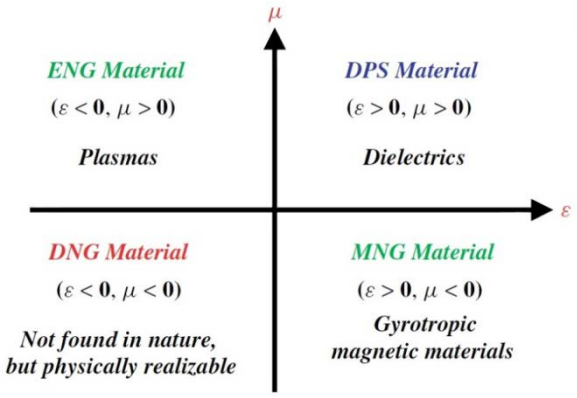

Fig. 4.1 Classification of material with permittivity-permeability (ε-μ) diagram.

One of the methods to realize MTM is using quasi-lumped elements developed on transmission lines, which usually termed composite right/left-handed transmission line (CRLH-TL) [5]. MTMs can be modeled as one-dimensional (1-D) transmission lines (TLs), which can be propagated any direction in the material. Transmission line is used to carry information and described by a series inductor (L_R) and a shunt capacitance (C_R).

Inductors and capacitors are referred to as lumped elements, and transmission lines as distributed elements. By interchanging the position of the inductor and capacitor, the resulting structure is referred to as Left Handed Transmission Line (LHTL) as shown in Fig 4.2.

Homogeneous TL has considered the restriction of incremental length $\Delta z \ll \lambda_g$ or at least $\Delta z < \lambda_g/4$ where λ_g is the guided wavelength and Δz is typically equal the average unit cell size p.

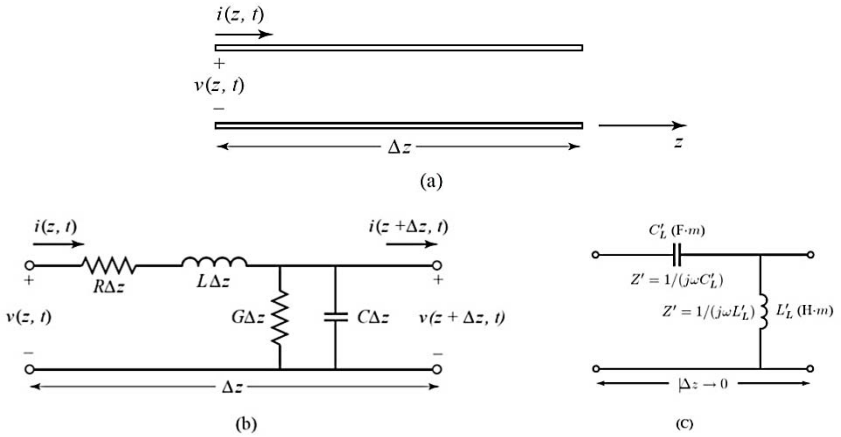

Fig. 4. 2 (a) Voltage and current definitions of transmission line b) Lumped-element equivalent circuit of right hand (RH) c) Lumped-element equivalent circuit of left hand (LH) [6].

The characteristics of a composite right/left-handed transmission line (CRLH TL) MTM can be inferred from analysis of the equivalent circuit of Fig 4.3a. At low frequencies, L_R and C_R tend to be short and open, respectively, so that the equivalent circuit is reduced to the series-C_L/shunt-L_L circuit, which is LH since it has antiparallel phase and group velocities. This LH circuit is of high pass nature; therefore, below a certain cutoff, a LH stop-band is present.

At high frequencies, C_L and L_L tend to be short and open, respectively, so that the equivalent circuit is essentially reduced to the series-L_R/shunt-C_R circuit, which is RH since it has parallel phase and group velocities. This LH circuit is of low-pass nature; therefore, above a certain cutoff, a RH stop-band is present. In general, the series resonance ω_{se} and shunt resonance ω_{sh} are different, so that a gap exists between the LH and the RH ranges [7].

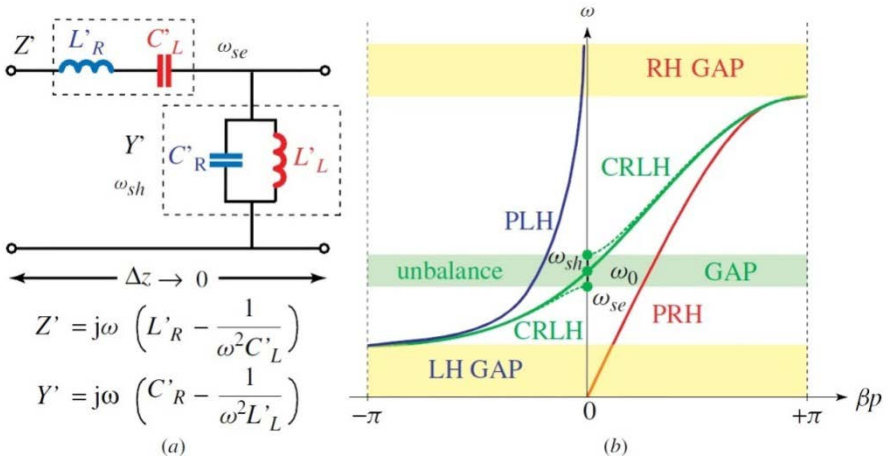

Fig. 4. 3 Fundamentals of composite right/left-handed (CRLH) MTMs. (a) Unit cell TL prototype. (b) Dispersion diagram. The curves for a purely LH (PLH) structure ($L_R = C_R = 0$) and for a purely RH (PRH) structure ($L_L = C_L = \infty$) are also shown for comparison [7].

The model reveals that a CRLH MTM is LH at lower frequencies (only L_L, C_L as $\omega \to 0$) and RH at higher frequencies (only L_R, C_R as $\omega \to \infty$), as illustrated in the dispersion diagram, which is straightforwardly obtained from the telegrapher equations as

$$\gamma = \alpha + j\beta = js(\omega)\sqrt{X'} \tag{4. 2}$$

$$X' = \omega^2 L'_R C'_R + \frac{1}{\omega^2 L'_L C'_L} - \frac{1}{L'_L C'_L}\left(\frac{1}{\omega_{se}^2} + \frac{1}{\omega_{sh}^2}\right) \tag{4. 3}$$

Where ω_{se} and ω_{sh} are the series and shunt resonances, respectively, given by

$$\omega_{se} = \frac{1}{\sqrt{L'_R C'_L}}(\text{rad/s}) \qquad \omega_{sh} = \frac{1}{\sqrt{L'_L C'_R}}(\text{rad/s}) \tag{4. 4}$$

And where $s(\omega)$ is a sign function equal to +1 if $\omega < \min(\omega_{se}, \omega_{sh})$ (LH range) and to −1 if $\omega > \max(\omega_{se}, \omega_{sh})$ (RH range). In general, a gap exists between the LH and RH ranges due to the distinct Eigen frequencies ω_{se}, ω_{sh}, where $V_g = 0$ (V_g is the slope of the dispersion curves). In principle, CRLH TLs and CRLH MTMs can be implemented in any technology. Being effectively homogeneous structures, CRLH MTMs can also be used as resonators when open or short ended. As in conventional resonators, CRLH structures resonate when their length is a multiple of half a wavelength. But because of the transfer of the phase origin from frequency zero to the transition frequency ω_0, a CRLH structure supports negative (LH band) resonances and a unique zero-order resonance at ω_0 in addition to the conventional positive resonances (RH band) [8].

$$l = |m|\frac{\lambda}{2} \qquad \text{Or} \qquad \theta_m = \beta_m l = \left(\frac{2\pi}{\lambda}\right)\left(\frac{m\lambda}{2}\right) = m\pi \tag{4. 5}$$

That $m = 0, \pm 1, \pm 2, \ldots \pm \infty$

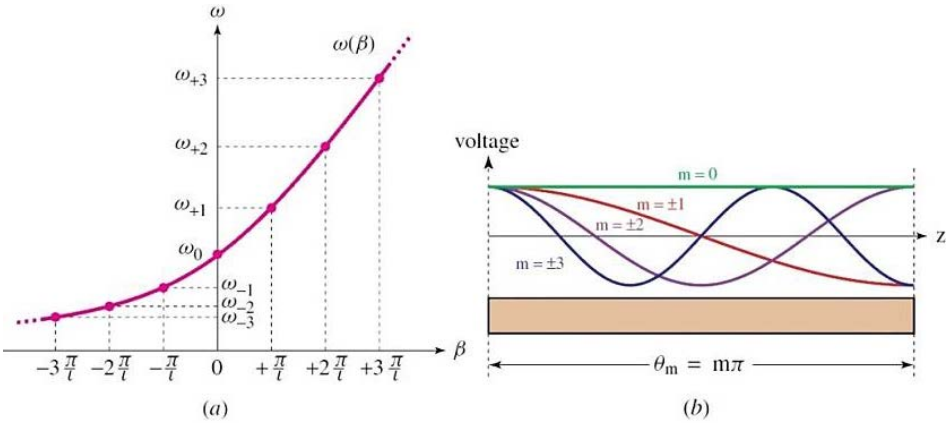

Fig. 4. 4 CRLH TL resonator: (*a*) dispersion relation and resonance frequencies ω_m of corresponding resonator based on uniform TL (*b*) typical field distributions of resonance modes (voltage/current distribution for an open/short-circuited metal/slot TL) [7].

As illustrated in Fig 4.4 an interesting feature of the dual modes ±m is their similar field and impedance characteristics due to their identical magnitude of β±.

4.1.1 Artificial Magnetics

Since MTMs can be synthesized by embedding artificially fabricated inclusions in a specified host medium or on a host surface, this provides the designer with large collections of independent parameters. Such as the properties of host materials, the size, shape, and composition of the inclusions, and the density, arrangement, and alignment of these inclusions, to work with in order to 'engineer a MTM with a specific electromagnetic response functions not found in each of the individual constituent materials. As for methods of constructions, several geometries for the inclusions of such media have been suggested. Among those, one can mention the split ring resonators (SRR) used originally by Smith, Schultz and Shelby [9], inspired by the work of Pendry [10]. A schematic of the Pendry's SRR structure is illustrated in Fig 4.5. The double ring [11], which is a special case of the SRR, was used for the fabrication of a MTM. It consists of two conductive rings placed back to back on a thin dielectric substrate with their slots oriented in opposite directions.

In SRR, a gap in each metallic ring prevents the formation of a complete circular current, and charges accumulate across the gaps. With both capacitance and inductance,

the SRR is a resonant element. Capacitance is more effectively introduced when two rings are placed concentrically with their gaps opposite of each other which are one reason why double SRRs are preferable to single SRRs in MTMs designs. Note that the pair of rings in a double SRR acts as one meta-atom. Another reason why double SRRs are preferred over single SRRs is the consideration of minimizing the electric polarizability in the system. In a single SRR, the accumulated charges around the gap induce a pronounced electric dipole moment, which may overshadow the desired magnetic dipole moment. With two SRRs placed in the manner, the fundamental electric dipole moments of the two rings tend to cancel each other, and the magnetic dipole moment dominates.

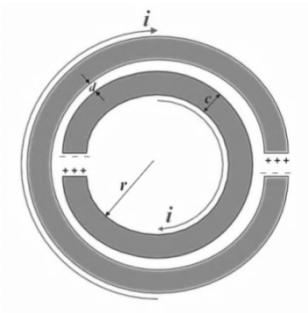

Fig. 4. 5 The double split-ring resonator with magnetic response at microwave frequencies.

Therefore, a standard double SRR structure is most often used in SRR-based MTM designs. If the gaps of the SRRs are closed, their magnetic response is switched off while their electric response remains unchanged. Generally, MTMs implemented with split ring resonators (SRRs), complementary split ring resonators (CSRRs), double slit ring split ring resonators (DS-SRRs) and double slit ring complementary split ring resonators (DS-CSRRs) are the most intensively studied structures as shown in Fig 4.6.

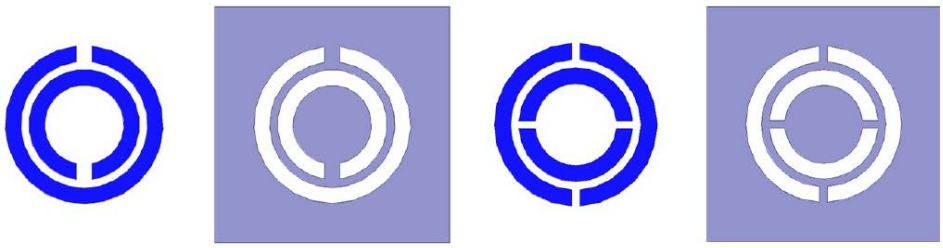

Fig. 4. 6 Schematic layout of (a) SRRs, (b) CSRRs, (c) DS-SRRs and (d) DS-CSRRs

SRRs as long as its diameter can be made much smaller than the wavelength; this particle is useful for the implementation of effective media with controllable electromagnetic properties of MTMs.

In the single ring configuration as shown in Fig 4.7, the circuit model is that of the simplest RLC resonator with resonant frequency $\omega_0 = 1/\sqrt{LC}$.

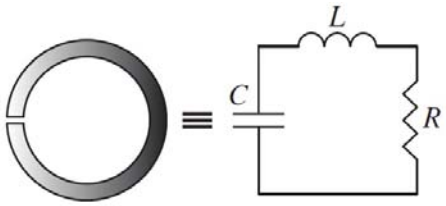

Fig. 4. 7 Single SRR configuration

In order to reduce the size of a split ring, one possible solution is to add an inner ring with the gap on the opposite side, as depicted in Fig 4.8

In Fig 4.8, capacitive coupling and inductive coupling between the larger and smaller rings are modeled by a coupling capacitance (C_m) and by a transformer (transforming ratio n), respectively.

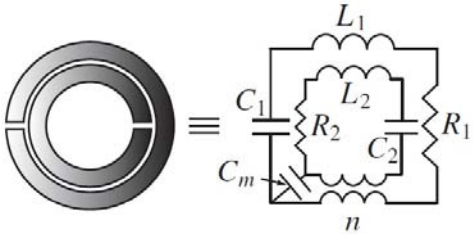

Fig. 4. 8 Double SRR configuration and equivalent circuit model of SRRs.

The double SRR is essentially equivalent to the single SRR if mutual coupling is weak, because the dimensions of the two rings are very close to each other, so that $L_1 \approx L_2 \approx L$ and $C_1 \approx C_2 \approx C$, resulting in a combined resonance frequency close to that of the single SRR with same dimensions but with a larger magnetic moment due to higher current density.

In order to calculate the radius of the ring, guided wavelength is computed using the following relation

$$\lambda_g = \frac{c}{f\sqrt{\varepsilon_{eff}}} \quad (4.\ 6)$$

Where, λ_g is guided wavelength, c is the speed of light, f is desired frequency and ε_{eff} is the effective dielectric constant which is given by

$$\varepsilon_{eff} = \frac{\varepsilon_r+1}{2} + \frac{\varepsilon_r-1}{2} \times \frac{1}{\sqrt{1+\frac{12d}{w}}} \quad (4.\ 7)$$

Where, ε_r is relative dielectric constant, w is width of the ring and d is the substrate thickness.

For a given characteristic impedance Z_0 and dielectric constant ε_r, w/d ratio can be found by using

$$\frac{w}{d} = \frac{8e^A}{e^{2A}-2} \quad \text{for } \frac{w}{d} < 2 \quad (4.\ 8)$$

$$\frac{w}{d} = \frac{2}{\pi}\left[B - 1 - \ln(2B-1) + \frac{\varepsilon_r-1}{2\varepsilon_r}\{\ln(B-1) + 0.39 - \frac{0.61}{\varepsilon_r}\}\right] \; for \; \frac{w}{d} > 2 \quad (4.\ 9)$$

Where,

$$A = \frac{Z_0}{60}\sqrt{\frac{\varepsilon_r+1}{2}} + \frac{\varepsilon_{r-1}}{\varepsilon_r+1}(0.23 + \frac{0.11}{\varepsilon_r}) \quad (4.\ 10)$$

$$B = \frac{377\pi}{2Z_0\sqrt{\varepsilon_r}} \quad (4.\ 11)$$

Feed line length and coupling gap are computed using the following relations:

Feed line length$=\frac{\lambda_g}{4}$

And, coupling gap

$$\Delta L = 0.421.d\left(\frac{\varepsilon_{eff}+0.3}{\varepsilon_{eff}-0.258}\right)\left(\frac{\frac{w}{d}+0.262}{\frac{w}{d}+0.818}\right) \quad (4.\ 12)$$

Inner and outer radius of the ring is calculated by subtraction and addition of the half of width of micro-strip to the mean radius respectively.

Inner radius:

$$R_i = R - \frac{w}{2} \quad \textbf{(4. 13)}$$

Outer radius:

$$R_o = R + \frac{w}{2} \quad \textbf{(4. 14)}$$

Examples include the creation of artificial magnetism [12–13] as well as electromagnetic band-gap (EBG) materials that are used to suppress surface-wave propagation.

In general, all dielectric resonators have a limitation in bandwidth of operation, due to their resonant nature. Several techniques can be used to increase the operational bandwidth of resonant and many of these have been successfully employed on micro-strip, which have inherently narrow bandwidth. These various approaches can be classified in to three broad categories: lowering the inherent Q-factor of the resonator; using EBG substrate; and combining multiple resonators.

One of the simplest techniques is to lower the dielectric constant of the substrate. Since the Q-factor is related to the dielectric constant, a decrease in the dielectric constant will cause a decrease in the Q-factor and thus an increase in the bandwidth. Although this is a simple solution, there are certain drawbacks. As the dielectric constant is reduced, the size of the resonator will increase, for a given frequency. This may not be desirable for many applications where a compact device is required.

The second approach to increasing the bandwidth of resonant involves the use of multiple resonator configurations. By using two or more resonators, each designed at a somewhat different frequency, the resonators can be combined to give wideband or multi-band operation. The advantage of this approach is that each resonator can be tuned more-or-less independently, allowing for a great deal of design flexibility.
The final approach to improve the bandwidth is using a thick and high permittivity substrate. But this excites surface wave propagation which EBG can be used to overcome this problem. Since, EBG does not allow the propagation of wave in all directions, it inserted between elements [14]. EBGs frequency is directly related to the geometrical parameters and material parameters of the host medium which explained in detailed next part.

4.1.2 Electromagnetic band gap (EBG) structures

Since, EBG structures are usually realized by periodic arrangement of dielectric materials that prevent/assist the propagation of electromagnetic waves in a specified band of frequency for all incident angles and all polarization states. Therefore, this chapter is devoted to brief overview on EBG structures properties

A band gap or an energy gap is an energy range in a solid, where no electron states can exist. Solids have their own characteristic energy-band structure. The term "band gap" refers to the energy difference between the top of the valence band and the bottom of the conduction band as shown in Fig 4.9. However, in order for an electron to jump from a valence band to a conduction band, it requires a specific minimum amount of energy for the transition.

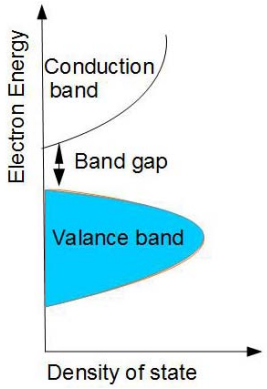

Fig. 4. 9 Semiconductor band structure

There is a distinction between "optical band-gap" and "electrical band-gap". The optical band-gap is the threshold for photons to be absorbed, while the electrical band-gap is the threshold for creating an electron–hole pair that is not bound together. In particular, characteristics such as frequency stop-bands, pass-bands, and band-gaps could be identified.

At first, the explanation of the phenomenon of band-gap structures was given by kogelnik and shank in their explanation to the dispersion characteristics of the distributed feedback lasers [15].

Much of the fundamental understanding of EBG materials can be derived from Brillouin’s work in the 1940s [16].

It is demonstrated that a periodic lattice imposes restrictions on the k vectors of waves than may propagate within it. Although Brillouin focused on mechanical waves, some of his concepts can be directly transferred to the EBG domain. From a simplistic viewpoint, media with periodically changing dielectric properties impose periodic boundary conditions on propagating electromagnetic modes. Electromagnetic waves which do not satisfy these boundary conditions cannot propagate. Brillouin´s legacy was that the concept of an energy band-gap became an integral part of solid-state physics. A parallel development took place within the field of microwave engineering, where the interaction of electromagnetic waves with periodic structures has been studied and applied for many years [7]. EBG structure is now one of the main expanding parts in the electromagnetic field which can be realized in one, two and three dimensional forms. Three dimensional EBG are more appropriate for getting a complete band-gap because they can inhibit waves for all incident angles. EBG inhibits the passage of electromagnetic wave at certain angles of incidence at some frequencies. These frequencies are called partial band-gap. At a specific frequency band, EBG does not allow the propagation of wave in all directions and this frequency region is called the complete band-gap or global band-gap [17-18]. When the two resonances coincide, the structure possesses a band-gap having maximum width. Depending on the structural characteristics and polarization of the wave, one resonance mechanism can dominate over the other.

The characteristic property of stop bands at certain frequencies enables many applications using EBG. At this stop band, all electromagnetic wave will be reflected back and the structure will act like a mirror. At other frequencies, it will act as transparent medium. This concept is illustrated in Fig 4.10.

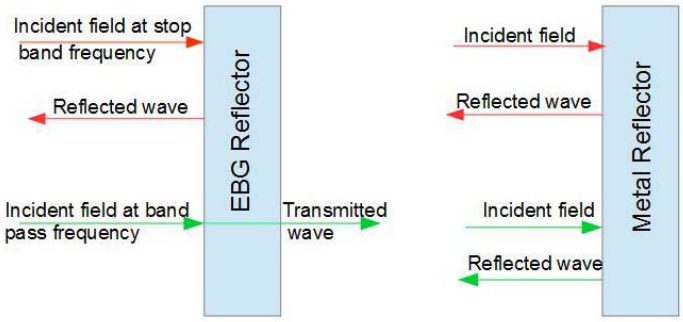

Fig. 4. 10 Diagram illustrating the application of EBG as a mirror and its comparison with a metal reflector [**18**].

Among the proposed and demonstrated EBG structure, is a periodic array of dielectric constant different from that of the host dielectric substrate (e.g., an array of holes drilled through the substrate). The holes vary in shape from simple rectangular or simple circular shape to more complicated shapes. Also the size and shape of these holes have a considerable impact on the pass-band and stop-band characteristics of the micro-strip EBG structure.

Micro-strip EBG structure is micro-strip device, incorporating with periodic structures either on the substrate or on the ground plane. In conventional micro-strip EBG structure, there is a conflict between the stop-band and pass band characteristics, that is increasing the size of the etched hole or the number of the hole produce a wider stop band width and better stop-band rejection at the expense of the pass band; reducing the size of the hole improves the return loss, but degrades the stop band characteristic.

To achieve the best performance, this trade off situation requires factors such as the number and size of the etched holes to be carefully determined.

4.1.2.1 Analysis methods for EBG structures

There are various methods to obtain the solution of the propagation of electromagnetic waves in a periodic layered medium.

- Lumped element model
- Periodic transmission line method
- Full wave numerical method

The lumped element model is the simplest one that describes the EBG structure as an LC resonant circuit. The values of the inductance L and capacitance C are determined by the EBG geometry and its resonance behavior is used to explain the band gap feature of the EBG structure. But the results are not very accurate because of the estimation of L and C as shown in Fig 4.11. At very high frequency, it may not to be correct to use lumped element model.

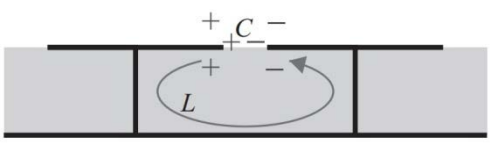

Fig. 4. 11 Lumped element model for EBG structure**.**

The periodic transmission line is another technique to analyze EBG structures. Transmission line model of EBG structures, where the impedance for each periodic element is Z_p and the coupling capacitor is X_C as depicted in Fig 4.12.

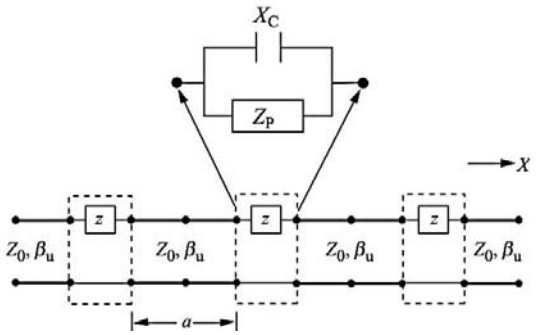

Fig. 4. 12 Periodic transmission line method for EBG analysis from [19].

After analyzing the cascaded transmission line, the dispersion curve can be obtained, which provides more information than the lumped element method (i.e. left- and right-hand regions, surface wave modes, and band gaps). Although, a difficulty in this method is accurately calculate the equivalent of Z_p and X_C values for the EBG structures.

Due to the complexity of the EBG structures, it is usually difficult to characterize them through analytical methods. Instead, full wave simulators that are based on advanced numerical methods have been used commonly in EBG analysis which is more accurate. Also it has a capability to derive different EBG characteristics, such as the dispersion curve, surface impedance, reflection phase and band gaps.

4.1.2.2 Resonant circuit models for EBG structures

As early EBG lattice periods were half-wavelength at the center band-gap frequency, practical applications of EBG structures had difficulties in accommodating their physical sizes. This problem has not been solved until the mushroom-like EBG proposed by Sievenpiper [20].

A mushroom like EBG structure consists of four parts: a ground plane, a dielectric substrate, periodic patches, and connecting vias, as shown in Fig 4.13a. This structure exhibits a distinct stop band for surface wave propagation. The operation mechanism of this EBG structure can be explained by an LC filter array: the inductance L results from the current flowing through the vias, and the capacitance C is due to the gap effect between the adjacent patches.

The parameters of the EBG structure are labeled in Fig 4.13b as patch width (W), gap width (g), substrate thickness (h), dielectric constant (ε_r) and vias radius (r). When the periodicity (W+g) is small compared to the operating wavelength, the operation mechanism of this EBG structure can be explained using an effective medium model with equivalent lumped LC elements, as shown in Fig 4.13c [2]. The capacitor results from the gap between the patches and the inductor results from the current along adjacent patches. The impedance of a parallel resonant LC circuit is given by

$$Z = \frac{j\omega L}{1-\omega^2 LC} \tag{4. 15}$$

The resonance frequency of the circuit is calculated as following:

$$\omega_0 = \frac{1}{\sqrt{LC}} \tag{4. 16}$$

At low frequencies, the impedance is inductive and supports TM surface waves. It becomes capacitive at high frequencies and TE surface waves are supported. Near the resonance frequency ω_0, high impedance is obtained and the EBG does not support any surface waves, resulting in a frequency band gap.

The high surface impedance also ensures that a plane wave will be reflected without the phase reversal that occurs on a perfect electric conductor (PEC).

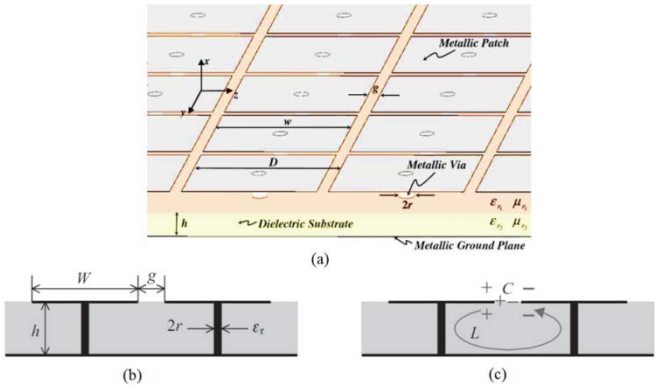

Fig. 4. 13 (a) Geometry of a mushroom-like EBG surface b) LC model for the mushroom-like EBG parameters and (c) LC model.

The mushroom-like EBG structure shows interesting behaviors with respect to surface waves and plane waves. These behaviors are frequency dependent, which is mainly determined by EBG parameters.

The reflection phases of the EBG surfaces with different patch widths are plotted in Fig 4.14a to characterize the patch width effect. It is observed that when the patch width is increased, the frequency at which the in-phase reflection occurs decreases. At the same time, the slope of the reflection-phase curve becomes steep, which implies a narrow frequency band.

The relative permittivity ε_r, also called the dielectric constant of a substrate, is another effective parameter that determines the frequency behavior of the EBG structure.

The reflection phases of the EBG surfaces with various permittivities are plotted in Fig 4.14b. It is observed that when air is used as the substrate, the in-phase reflection frequency of the EBG surface has its highest value and the corresponding largest bandwidth.

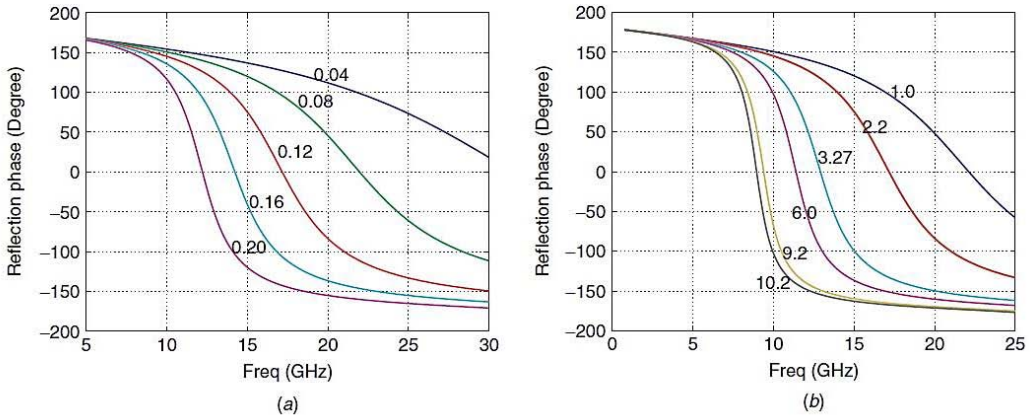

Fig. 4. 14 EBG parametric studies: effects of variations in (*a*) patch width *W* and (*b*) substrate relative permittivity εr. From [21], copy right @ 2003 by the Institute of Electrical and Electronics Engineers, Inc.

When the relative permittivity is increased, the frequency band decreases, as does the bandwidth. Therefore, when the Roger3010 substrate (εr=10.2) is used, the in-phase reflection frequency has its lowest value and the corresponding bandwidth also becomes very narrow. Therefore, the relative permittivity of the substrate of the EBG structure has an effect on its in-phase reflection behavior similar to that of the patch width but provides an additional degree of freedom to tune the EBG design. In practical applications, if one would like to design a compact EBG structure at a given frequency, increasing the permittivity is a feasible approach.

The gap width and substrate thickness also affect the operational frequency band of an EBG structure. For example, when the gap width is increased, the operational frequency will increase. In contrast, when the substrate thickness is increased, the operational frequency will decrease.

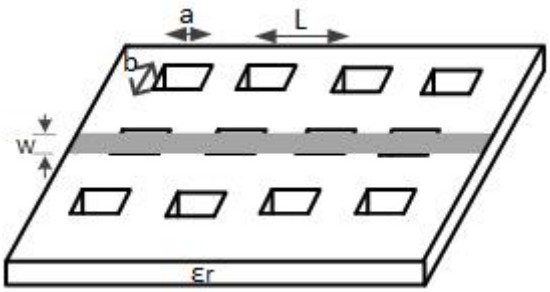

Fig. 4. 15 EBG structure from periodic dielectric substrate drilling.

Among the demonstrated EBG structure, is a periodic array of dielectric inclusions with a dielectric constant different from that of the host dielectric substrate (e.g. an array of air holes drilled through a dielectric substrate), as display in Fig 4.15 .This type of EBG structure requires the painstaking work of drilling through the substrate. In addition this EBG structure is not easy to model and analyze.

4.1.3 Artificial dielectric

From two decades especially after Second World War the realization and characterization of “artificial dielectrics,” with low-loss and lightweight structures are interested.

The term “artificial dielectrics” is used, especially in microwave technology, to describe the materials with sub-wavelength metal particles periodically distributed in a uniform background host. These materials are called “artificial dielectrics” because they serve as the macroscopic analogue of natural dielectrics except that the atoms or molecules are artificially structured–exactly what scientist are doing in today’s MTMs research.

The first recognized pioneer of artificial dielectrics was probably Winston Kock [1], an engineer working at Bell Laboratories in the 1940s. A few distinct features of Kock’s work merit his recognition as a founding pioneer of the research field of MTMs.

First, he used equivalent material parameters to characterize the response of artificial dielectrics to the impinging electromagnetic fields. Secondly, he investigated periodic metal-dielectric structures of different effective indices of refraction, both larger and smaller than unity, and he used the terms “phase delay” and “phase advance” to describe wave propagation properties [22]. Moreover, he unambiguously pointed out the analogue between artificial dielectrics and a natural crystalline dielectric material [23]. Kock also recognized that, at higher frequencies, the existence of eddy currents on the surface of the conductors prevents the penetration of magnetic field lines into the conductors, and the consequent condensation of magnetic field lines (viewed, similarly, as a change in inductance) results in a diamagnetic response.

An artificial dielectric is an infinite number of identical dielectric elements arranged on a periodic lattice in free space. And they are utilized for miniaturization of microwave resonators since their relative permittivity easily exceeds 100 [24].

4.1.3.1 Transmission-line-based artificial dielectric realizations

The familiar lumped-element model of the transmission line is determined by applying quasi-static field conditions to Maxwell's Equations and obtaining the circuit equations; hence, the analogies between permeability, inductance, permittivity, and capacitance are easily drawn. That natural media could be represented by distributed L–C circuit networks which was recognized in the 1940s by Kron, who spatially discretized Maxwell's equations to arrive at Kirchhoff's voltage and current laws for three-dimensional (3D) media, and by Whinnery and Ramo [25], who improved two-dimensional media, although it was only four years later that W. Kock [22] introduced the term "artificial dielectric".

This trend suggests that, having availed of familiarity with circuits to model the behavior of natural media, may apply the same principles to synthesize the behavior of artificial media.

The captivating elegance of the distributed L-C circuit network representation lies in the fact that the capacitive and inductive elements directly determine the constitutive parameters, the desired permittivity and permeability respectively, of the effective medium. There are some reasons which scientists are interested in artificial dielectric matter.

The main purpose of artificial-dielectrics research was often to design specific refractive indices, of which the simplest property to manipulate was the permittivity. Other purpose, the use of simple metallic inclusions could not generate any appreciable magnetic behavior beyond the typical diamagnetic response. However, one very notable suggestion to create unnaturally large artificial permeability was offered by Schelkunoff and Friis [26], it was suggested that a small inductive loop be loaded in series with a lumped capacitor. The resulting resonant response of the magnetic polarize-ability results in arbitrarily large positive permeability below the series resonance. It would be

many years later, however, before the community would reinvent these ideas and see beyond the resonance.

4.1.4 Artificial dielectric resonator

The lattices of dielectric resonators are new type of MTMs distinguished by small dissipative losses as well as convenient conjugation with external structures.

The majority of the published works [27-28-29] refer to the equivalent parameters determination, such as dielectric and magnetic effective permittivity of the medium, organized by coupled DRs.

Basically, two- and three-dimensional rectangular and cubic lattices arrangement have been explored [30]. In this case, the well-known spherical, rectangular, and cylindrical resonators in basic modes can be used as constitutive elements. The properties of DRs are usually defined by a range of parameters, such as: operation frequency, quality factor, spectrum rarefaction.

The quality factor increase problem is necessary for the DRs with no high dielectric permittivity in the millimeter and infrared wavelength range. Hence, it is interesting to investigate the new techniques of the resonance elements building with high-quality factors.

To provide this a method can be applied, coupled DRs which provide efficient coupling when are closely placed to each other. DRs interaction leads to significant spectrum rearrangement as well as changes in the quality factors.

Various modelling techniques were used to optimize the resonator dimensions to improve quality factor and spurious performance [31]. Although DR structures those are high unloaded Q_u, they are also big and bulky for most applications, especially in the cellular base station market.

Solutions to realize physically smaller resonators, while retaining the maximum Q_u are then needed. Volume reduction can be obtained by introducing surfaces of contact between the ceramic and some conductive material.

If the dielectric constant is high, the electric and magnetic fields of a given resonant mode could be confined in and near the resonator and can attenuate to negligible values at a distance small compared to free-space wavelength. Therefore, radiation loss is very small, and the unloaded Q_u of the resonance is limited mainly by losses inside the dielectric body. In materials of interest, the magnetic permeability is unity and magnetic losses are zero.

Electric field losses occur as a result of the finite loss tangent (tanδ) of the dielectric material. If all of the electric energy of the resonant mode is stored inside the dielectric resonator, and if no losses occur due to external fields, the unloaded Q_u could be given by $Q_u=l/\tan\delta$.

In the case of non in finite relative dielectric constant (ε_r), there is external loss due to radiation or dissipation in a surrounding metal shield. These losses tend to reduce Q_u while external electric stored energy tends to increase Q_u. For ε_r order of 100 or higher these effects are small, and $Q_u=1/\tan\delta$ is a benefit approximation.

Typical tanδ values for materials of interest are about 0.0001 to 0.0002. Therefore, Q_u values of about 5000 to 10000 may be expected and, in fact, values up to 12000 have been measured at room temperature with high-purity TiO_2 disks.

4.2 Filters based on dielectric resonators

The potential of DR's for microwave applications such as oscillators [32], slow wave structures [33] and band-pass and band-stop filters [34] became clear in the early 1960's.

One of their attractions was their ease of integration in microstrip circuits [35]. During this period, the research concentrated in the modelling of the DR (usually of cylindrical shape) which resulted in the characterization of the different modes of resonances and the drawing of the first mode charts.

The aim of this section is the development of the scattering theory of electromagnetic waves on the DR, located in the various positions, as well as an investigation of the band-pass and band-stop filters parameters, consisting of a number of DRs.

The first design procedures for the design of DR band-pass filters were established by Cohn [36]. The resonators were placed axially or transversally in a metallic cavity below cutoff frequency. Magnetic wall and dipole moment models were used to get approximations of the resonant frequencies and the couplings between consecutive resonators, respectively.

Band-stop filters were also designed, by locating cavities loaded with DR's $3\lambda/4$ apart and coupling either to a propagating waveguide [37] or a micro-strip line [38]. Today, $TE_{o1\delta}$ filters are widely used for narrowband and low loss applications in mobile phone base-stations.

To improve the stop-band of a DR filter, Snyder [39] proposed the use of resonant couplings. Each iris is tuned to be resonant at the center frequency of the filter and provide extra 6 dB/octave attenuation in the stop-band. However, these resonant couplings are very sensitive. The input and output couplings can also be made resonant.

The relative dielectric constant of the materials for constructing DR in microwave filters generally was chosen from a higher value compared to the base substrate. The primary advantage in using a high dielectric constant is to miniaturize the filter size.

The size of DR filter is considerably smaller than the dimension of waveguide filters operate at the same frequency. Furthermore, these DR filters are employed to replace waveguide filters in applications such as satellite communication systems where the planar filters cannot be used due to the inherent of high loss.

4.2.1 Single resonator theory and design

Recently, materials having a dielectric constant between 30 and 40 with benefit temperature stability and low dielectric losses have become available. The shape of a dielectric resonator is usually a cylinder, spherical and parallelepiped shapes.

A commonly used resonant mode in cylindrical dielectric resonators is denoted $TE_{01\delta}$. The magnetic and electric field intensity for this mode is sketched in Fig 4.16.

$TM_{01\delta}$ is resonators can have Q_u higher than $TE_{01\delta}$ resonators because of the smaller percentage of electric field concentrated in the ceramic in the case of the $TM_{01\delta}$ mode. This is of course most significant when the loss tangent of the ceramic material considered is relatively high.

Simple models were first applied to calculate resonant frequencies and couplings. The direct coupling between the fields of transversal adjacent resonators was considered in [40]. It was found to be mainly due to direct coupling between resonators [41] rather than through the evanescent fields of the cutoff waveguide, as considered [42].

As well as higher Q_u, the $TM_{01\delta}$ also offers more coupling between adjacent resonators disposed in a planar filter layout than $TE_{01\delta}$ resonators. The drawback of the $TM_{01\delta}$ filter over the $TE_{01\delta}$ filter is a significant increase of the filter dimensions. The geometrical form of a dielectric resonator is extremely simple; an exact solution of the Maxwell equations is considerably more difficult than for hollow metal cavities. This difficulty could be real for an isolated dielectric resonator such as shown in Fig 4.16, and even more so for a dielectric resonator mounted on a micro-strip, or placed within a shielding metal cavity.

For this reason, the exact resonant frequency of a certain resonant mode, such as $TE_{01\delta}$, can only be computed by rather complicated numerical procedures.

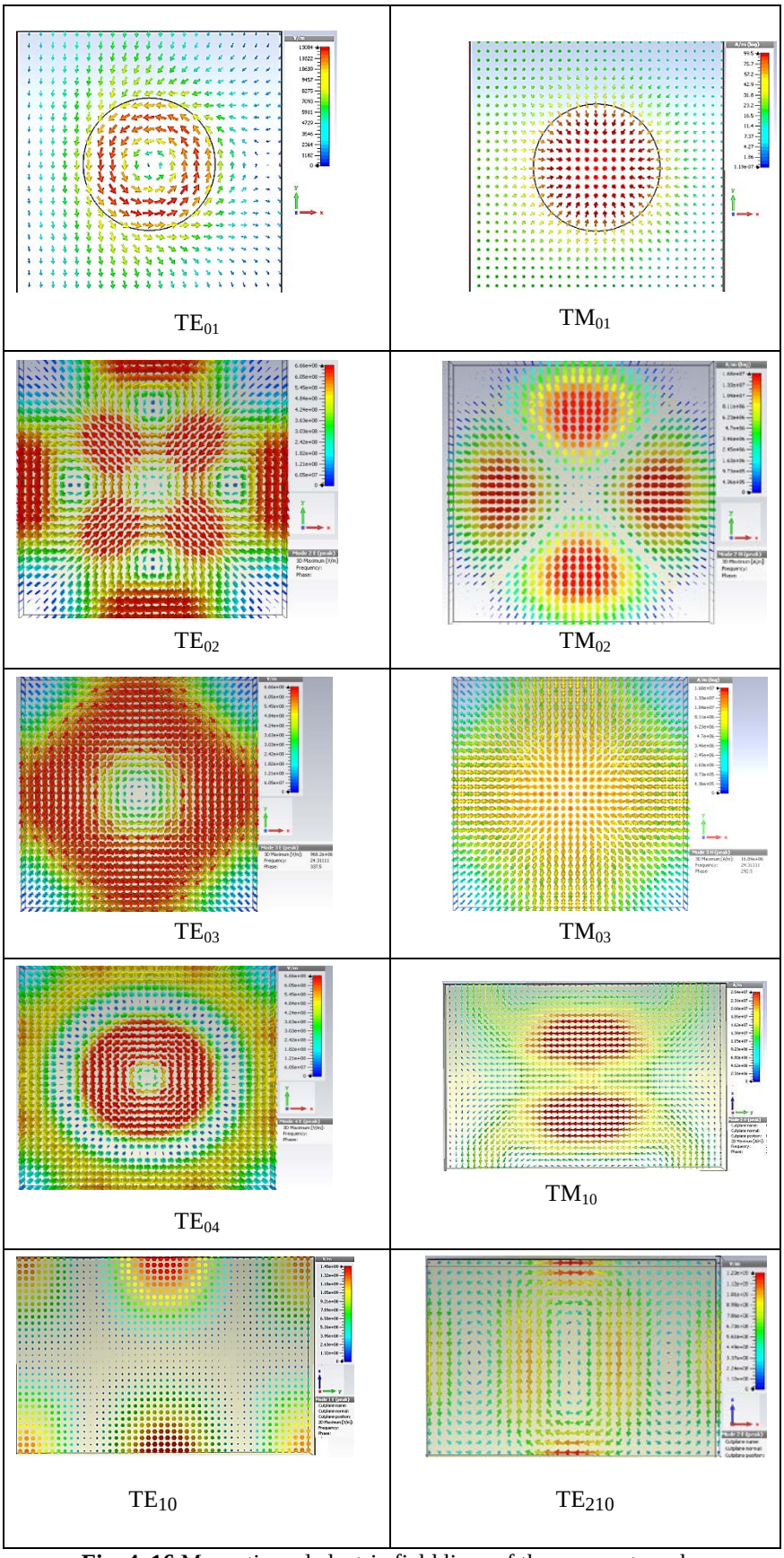

Fig. 4. 16 Magnetic and electric field lines of the resonant mode.

For an isolated short cylindrical dielectric resonator shown in Fig 4.17(a), the resonance mode with the lowest resonance frequency is the $TE_{01\delta}$ mode. According to the electric and magnetic field distribution shown in Figs. 4.17(b) and (c), the resonators behaves like a magnetic dipole in $TE_{01\delta}$ mode. Since the electric and magnetic dipole moments can be envisioned as the alphabet for making MTMs [43], the resonator is expected to be a magnetic MTM in the $TE_{01\delta}$ mode. Although the geometrical form of a dielectric resonator is extremely simple, an exact solution of the Maxwell equations is considerably more difficult than for hollow metal cavities. For this reason, the exact resonant frequency of a certain resonant mode, such as $TE_{01\delta}$ mode, can only be computed by rather complicated numerical procedures. For an approximate estimation of the resonant frequency of the isolated dielectric resonator, the resonant frequency of the TE_{nml} mode is [44].

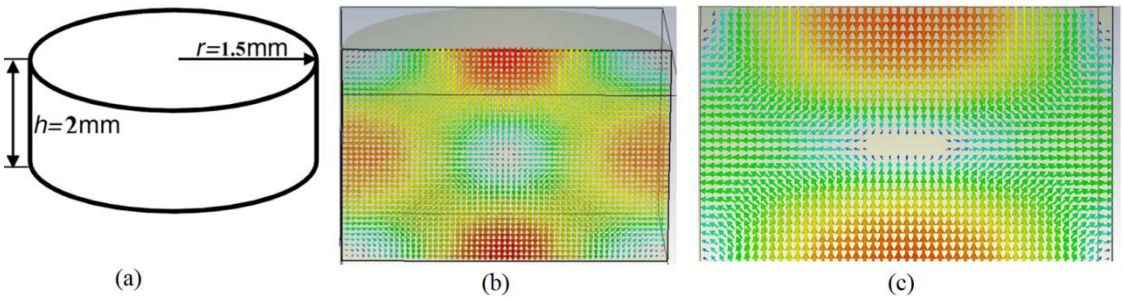

Fig. 4. 17 An isolated short cylindrical dielectric resonator and (b) Electric field distribution in equatorial plane, (c) Magnetic field distribution in meridian plane for $TE_{01\delta}$ mode.

$$f_{0(TE_{01\delta})} = \frac{C\ 2.327}{2\pi r\sqrt{\varepsilon_r+1}}\left(1 + 0.2123\left(\frac{r}{h}\right) - 0.00898\left(\frac{r}{h}\right)^2\right) = 12\ \text{GHz} \qquad (4.\ 17)$$

The radius and height of the resonator are r=1.5mm and h=2mm, respectively. DR is made of high dielectric constant epoxy paste with a relative dielectric permittivity of 45, loss angle tangent tanδ=0.008 and temperature coefficient Tf~50 ppm/±C. The quality factor Q has been found to be 125.

The software allows viewing 3D fields of each mode and having their resonant frequencies. When considering the studied example and defining perfect magnetic boundary conditions on all DR walls, except for the DR bottom where perfect electric boundary condition is considered, the software gives 12GHz for the resonant frequency value of the $TE_{01\delta}$ mode. It is also possible to see both H and E fields of this mode, they are presented Fig 4.17(b, c). This valuable information allows designer to choose the most appropriate excitation of the considered mode.

Taking into account the dielectric loading of the waveguide, the effective wavelength, λ_{eff}, is calculated from,

$$\lambda = \frac{c}{f} = \frac{3 \times 10^8}{12 \times 10^9} = 25mm \ \ and \ \ \lambda_{eff} = \frac{\lambda}{\sqrt{\varepsilon_r}} = \frac{25}{\sqrt{45}} = 3.7 \ mm$$

The principal resonance of interest is the lowest order circular-electric mode designated $TE_{01\delta}$, where the first two subscript integers denote the waveguide mode and δ is the non-integer ratio $2L/\lambda_g<1$. Note that the TE_{01} magnetic-wall waveguide mode is the dual of the TM_{01} mode in a metal-wall waveguide.

4.2.2 Calculation of coupling coefficients between cylindrical dielectric resonator

Dielectric resonators are widely used in microwave component where weight and volume savings are of two major requirements. One of the main applications of dielectric resonators is in dielectric-loaded cavity filters. In the design of certain type of these filters [45-46], the relationship between coupling coefficients and dielectric spacing should be known. To find this relationship the two dielectric resonators placed on top of substrate as shown in Fig 4.18(a).

Shown in Fig 4.18(b) is an equivalent lumped-element circuit model for magnetic coupling structure near its resonance, where L and C are the self-inductance and self-capacitance, and L_m, represents the mutual inductance. While an equivalent lumped-element circuit model for electric coupling structure is given in Fig 4.18(c), where L and C are the self-inductance and self-capacitance respectively, so that $(LC)^{-1/2}$ equals the angular resonant frequency of uncoupled resonators, and C_m, represents the mutual capacitance. Furthermore, the distance between resonators plays an important role.

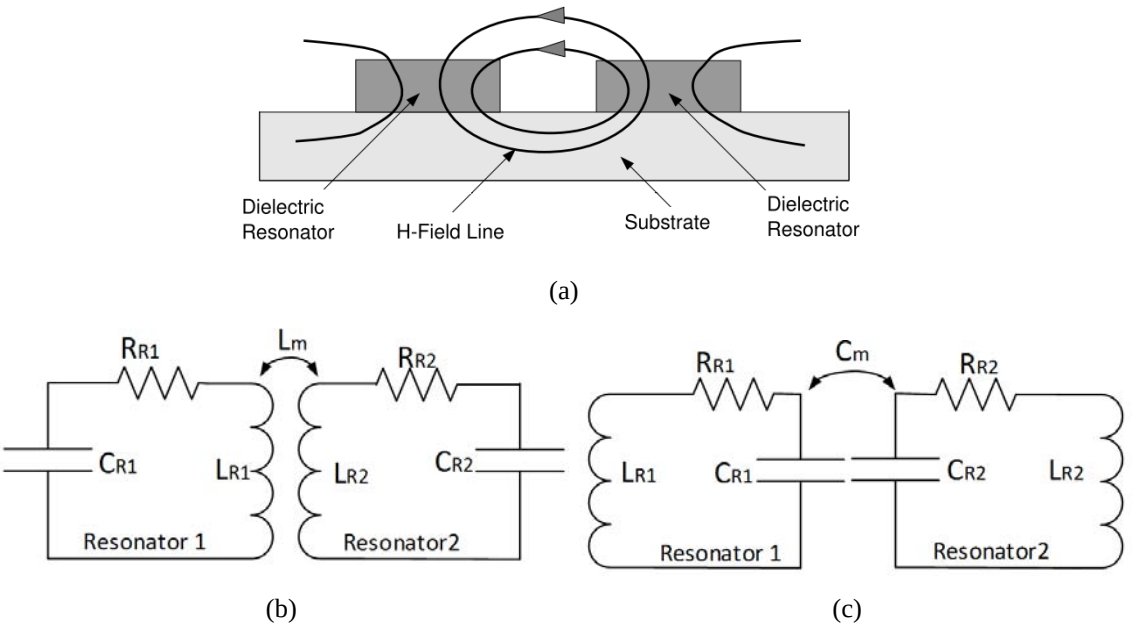

Fig. 4. 18 a) Resonator to resonator coupling by magnetic fields. b) Equivalent circuit model for resonator to resonator magnetic coupling, c) Equivalent circuit model for resonator to resonator electric coupling,

The main difference lies in the fact that the wavelength in dielectric materials is divided by the square root of the dielectric constant, ε_r in a function of $\lambda_g = \lambda_0/\sqrt{\varepsilon_r}$ where λ_0 is the free space wavelength at the resonant frequency and λ_g is the wavelength associated with the dielectric resonator which $\lambda_g = \frac{\lambda_0}{\sqrt{\varepsilon_r}} = \frac{c}{f_0\sqrt{10.2}} = 10.6\,mm$ (c is the speed of light and f_0=9 GHz is resonant frequency) when coupled to each other, require $3\lambda g/4$ spacing. According to Eq (3.48) which is

$$L = \left[\frac{2i+1}{4}\right]\lambda_g = \frac{3}{4}\cdot 10.6 = 8\,mm$$

Figure 4.19 shows typical simulated resonant frequency responses of the coupled resonator structures in Fig 4.18(a) with d=8mm, where S_{21} denotes the S parameter between the two ports that are very weakly coupled to the coupled resonator structure.

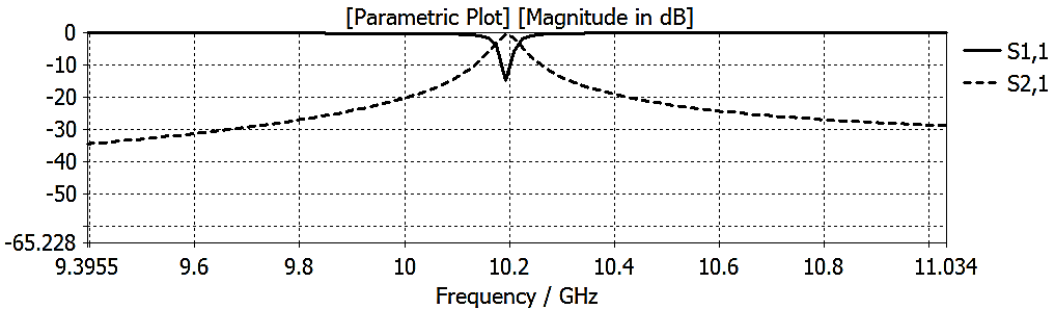

Fig. 4. 19 Simulated resonant frequency response for two coupled resonators.

When two contiguous resonators are coupled, they exhibit two split resonant peaks, as illustrated in Fig 4.20.

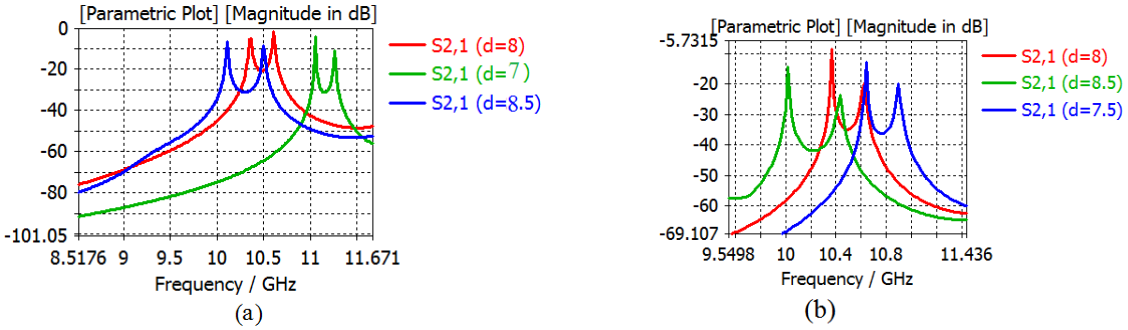

Fig. 4. 20 Typical resonant mode splitting phenomena of the a) Electrical coupled resonators b) Magnetic coupled resonators for Fig 4.19.

In both cases, the two resonant peaks that correspond to the characteristic frequencies f_{p1} and f_{p2} defined above, are clearly identified from the magnitude responses. From Figure 4.20a, for d=8 mm, it can be found f_{p1}=10.356 GHz and f_{p2}=10.604 GHz. Accordingly to the relationship which is presented in more detail in chapter 3, the coupling coefficient between two coupled resonators can be graphically estimated from the resonance curves. From the peaks values, the coupling coefficient is given by [47].

$$\boldsymbol{k} = \frac{f_2^2 - f_1^2}{f_2^2 + f_1^2} \tag{4. 18}$$

From Figure 4.20a it can be found that k=0.023.

From Figure 4.20(b) for d=8 mm it can be found that f_{p1}=10.367 GHz and f_{p2}=10.628 GHz, so that k=0.025. Hence, with the same coupling spacing d, the magnetic coupling is stronger than the electric coupling. Normally, the stronger the coupling, the wider the separation of the two resonant peaks and the deeper the trough in the middle, are obtained from the magnitude response. Since the coupled resonator structures considered are symmetrical, it can be used another approach, as suggested above, to compare the signs of the two coupling coefficients by looking for the resonant frequencies with electric and magnetic walls inserted, respectively.

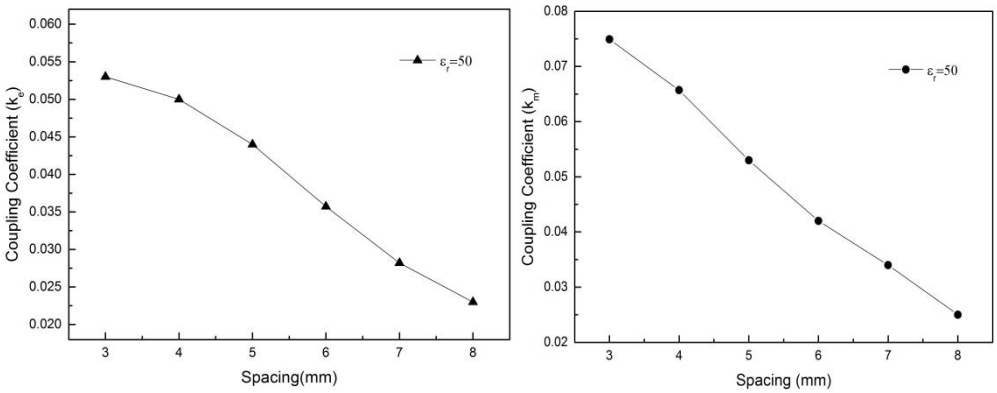

(a) (b)

Fig. 4. 21 Coupling coefficients for resonators with r = 1 mm on a substrate with a thickness h = 0.6 mm a) electric coupling b) magnetic coupling.

Drawback of the DR is that the resonant frequencies of the modes are close to each other. To make the DR practical for most applications, one of the goals of the resonator design is to separate the resonant frequency of the operating mode as far as possible from those of other modes.

Introducing a hole at the center of the DR, that is, ring resonator, can improve the separation between the TE_{01} mode (fundamental mode) and higher-order modes. This property can be used to improve the spurious performance for dielectric loaded filters.

4.2.2.1 Power density, penetration depth and temperature coefficient of DR

The rate of heating can be expressed by the power equation:

$$p_v = 2\pi f \varepsilon_0 \varepsilon'' |E|^2 \quad (4.\ 19)$$

Where p_v=energy developed per unit volume (W/m"), *f*=frequency (Hz), |E|=electric field strength inside the load (V/m).

The electric field inside the load is determined by the dielectric properties and the geometry of the load, and by the oven configuration. Therefore, this equation is generally impractical as the determination of the electric field distribution is very complex [48].

To gain a better practical understanding of the meaning values of the dielectric properties, a penetration depth can be calculated from the dielectric properties. Theoretically, the penetration depth "d_p" (or power penetration depth) is defined as the depth below a large plane surface of a substance at which the power density of a perpendicularly impinging, forward propagating plane electromagnetic wave has decayed by l/e from the surface value (l/e~37%). If tan ε is smaller than about 0.5, the following formula gives 97-100% of the correct value [49]:

$$d_p = \frac{\lambda_0 \sqrt{\varepsilon'}}{2\pi\varepsilon''} = \frac{28\times10^{-3}\sqrt{45}}{2\pi 0.36} = 0.083 \quad (4.\ 20)$$

That, λ_0 is the free space wavelength. The absorbed power density near the surface of an infinite inhomogeneous slab is, accordingly, approximately proportional to ε″ when ε′ does not vary very much.

Temperature-dependent effects that cause a change in the DRs stabilizing function within an oscillator also need to be quantified. The linear coefficient of expansion for a material is defined as the change in length of the material Δ*l*, divided by its length L such that

$$\frac{\Delta l}{L} = \alpha T \quad (4.\ 21)$$

where α (ppm/^{o}C) is the linear expansion coefficient. As a DR puck expands or contracts, its resonant frequency will vary such that

$$\frac{\Delta f}{f_0} = -\alpha \Delta T \tag{4. 22}$$

The negative sign indicates that as the DR puck becomes longer, its resonant frequency decreases. With a DR, its relative permittivity e r is also a function of temperature. This variation is expressed very approximately as

$$\frac{\Delta \varepsilon_r}{\varepsilon_r} = \tau_E \Delta T \tag{4. 23}$$

Where τ_E is the temperature coefficient of the dielectric resonator (ppm/ºC). By combining these relationships together, we obtain an approximate equation for the temperature stability of a DR:

$$\frac{\Delta f}{f} = \frac{\partial f}{\partial L}\frac{\Delta L}{f} + \frac{\partial f}{\partial \varepsilon_r}\frac{\Delta \varepsilon_r}{f} \tag{4. 24}$$

By denoting the temperature coefficient of the resonant frequency of the DR as τ_{DR}, combines three independent factors that include temperature coefficient of the dielectric, τ_e, thermal expansion of the material, α_L, and thermal expansion of the environment in which the resonator is mounted. Resonant frequency shifts due to intrinsic material parameters are related by the above temperature coefficients in the equation below

$$\tau_{Dr} = \frac{\tau_e}{2} - \alpha_L \tag{4. 25}$$

To advance the technology of these materials, the properties of the material must be measured accurately. Hakki and Coleman [50] provided a method to measure the loss tangent of the dielectric, which was later improved upon by Kobayashi and Katoh [51] with greater accuracy.

4.3 Band-Stop Filters based on thich film dielectric resonators (TFDR)

The scattering problem on DR systems in the transmission line is one of the considerable, as it allows designing various filters used today in area of radio electronic equipment [52]. The basic difficulty of filters' tuning, containing a huge number of resonators, is the complicated multi parametric dependence of their reflection and transmission characteristics on DR and waveguide parameters.

Electrodynamic modeling of DR filters [53], allows direct calculation and optimization without use of approximate low-frequency lumped element prototypes. In most cases the structure of the band-stop filter has the view as shown in Fig. 4.22, where coupling between DRs and the transmission line is marked with wavy lines and coupling between DRs on the damped and propagating waves with continuous lines. Coupling the DRs side by side enables to maintain them easily, such as on a dielectric substrate, that material is chosen to improve the temperature stability of the filter.

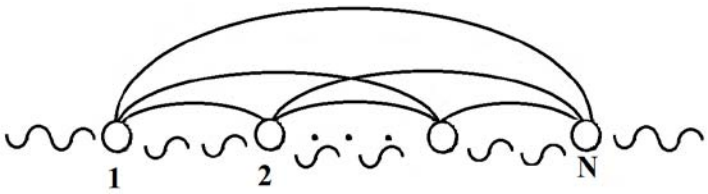

Fig. 4. 22 Structure of partial DR coupling of the band-stop filter in the propagating transmission line. The partial DRs are denoted by circles; the coupling of the DRs with transmission lines on propagating waves are marked with wavy lines; the coupling between DRs on damped and propagating waves are designated with continuous lines.

To obtain an accurate response on the symmetric modes, axial mounting and side-by-side coupling configurations can be combined.

The idea of designing this stop-band filter was due to the dielectric resonator can increase Q-factor in a circuit response and able to maximize power transfer in dielectric resonator. A dominant parameter affecting the degree of coupling is the dielectric constant of the DR. For the higher values of dielectric constant, the stronger coupling will be.

The proposed filter consists of three cylindrical dielectric resonators were excited with a micro-strip line as shown in Fig 4.23. This is the simplest way to incorporate a DR into a microwave network. In this case, the coupling is adjusted by lateral movement of the resonator from the micro-strip line. This is a typical filter consists of three DRs that are mounted on a planar configuration to obtain a suitable resonant frequency. When a dielectric resonator is situated in a propagating wave guide, it absorbs power at its resonant frequency and thus offers band-stop properties.

Fig. 4.23 shows the configuration of the proposed stop-band filter. The micro-strip transmission line is made up of a copper metal with electrical conductor, while thick film commercial high dielectric constant EPOXY paste is used as a DR with dielectric constant ε_r=45 and tangent loss of 0.008, however it would be desirable to have dielectric constants higher than 100 to obtain a better definition of the resonances and to improve the miniaturization level.

The DRs are placed above a substrate of Roger3010 with 0.635mm thickness with a permittivity ε_r=10.2 and loss tangent 0.0022. Coupling between three resonator should be considered which the coupling coefficient depending on the spacing and the shape of the gap.

The geometry of the proposed thick film DR (TFDR) consists of three cylindrical DRs which are mounted on a 25 mil Roger 3010 substrate is shown in Fig 4.23.

The radius, r, of the dielectric resonators are equal to 1 mm and height of DR is 0.6 mm, while the 50 Ω transmission line is 0.3 mm. Input and output of the circuit are connected to the end of the transmission line from both sides. The overall circuit length is 30 mm, while spacing between DRs is 6 mm.

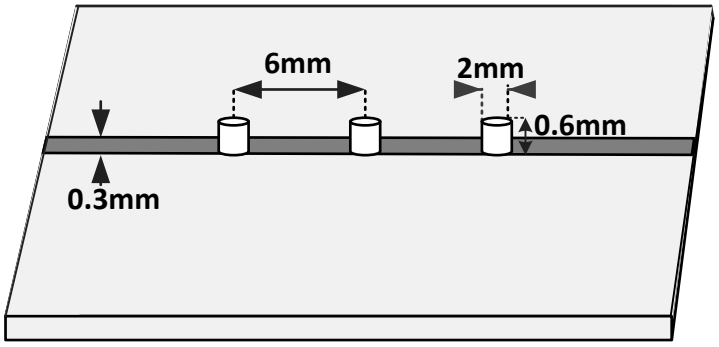

Fig. 4. 23 Configuration of the cylindrical dielectric resonator mounted.

A micro-strip feed line is etched on the top of substrate and the width of the feeding line is set to 0.4 mm. The size, location and shape of the dielectric resonators including the height and size area are influence the matching of the circuit. The size of the micro-strip line interacts between the dielectric resonators and I/O port also giving the impact to the signal response. In this project, three dielectric resonators were excited on a micro-strip transmission line in order to obtain the optimum coupling effect. The dielectric resonators offer advantages in increasing the signal transmission performance of RF and microwave devices. The match combination of dielectric resonators and microwave circuit capable to generate additional coupling effect that can be merged together to produce a wide band device as well as increasing the transmitting power and reduce the insertion loss.

The wavelength inside the DR, λ_g is also inversely proportional to the square root of the dielectric $\lambda_g = \lambda_0/\sqrt{\varepsilon_r}$ where λ_0 is the free space wavelength at the resonant frequency that $\lambda_g = \frac{\lambda_0}{\sqrt{\varepsilon_r}} = \frac{c}{f_0\sqrt{10.2}} = 12\,mm$ (c is the speed of light and f_0=7.8 GHz GHz is resonant frequency) when coupled to each other, require λg/2=6mm spacing. As shown in Fig 4.24, by increasing space between DRs, frequencies shifted to lower level.

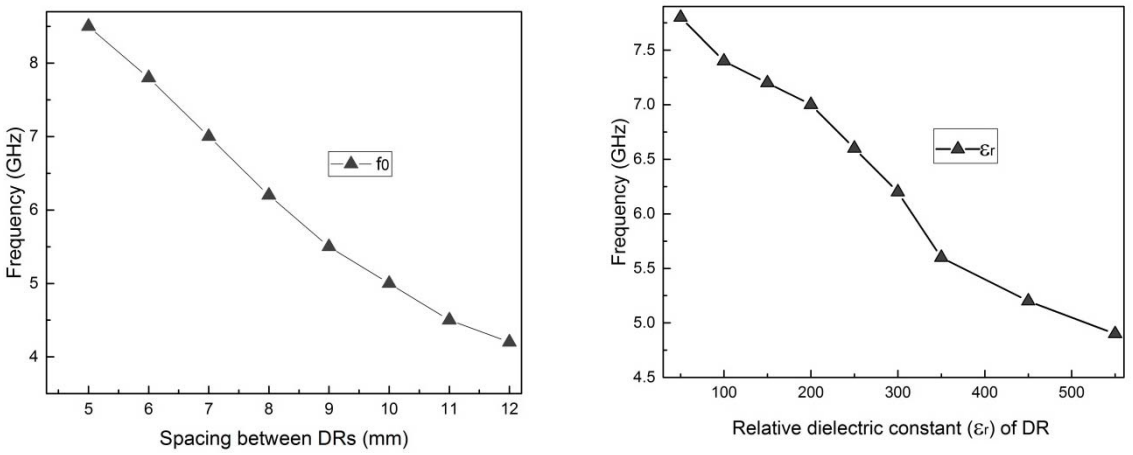

(a) (b)

Fig. 4. 24 a) Correlation of spacing between DR and frequency b) Correlation of relative dielectric constant and frequency.

Dielectric resonators interact with the microwave transmission line. At the beginning the transmission line were calculated according to characteristic impedance. All DRs are operating in a same principle. Each DR resonate for a same mode but with different frequency such that the combination response is an additional result from the single response which able to increase the overall band width.

As shown in Fig 4.25, three DRs are as coupled resonators such that the device becomes a high quality band stop filter and the transmission as a function of frequency for a pair of resonators in suitable distance placed.

The frequency response characteristics obtained from simulations mentioned above were validated by experiments. The aforementioned stop-band can be switched to a pass-band by periodically inserting metallic strips around the DRs [54].

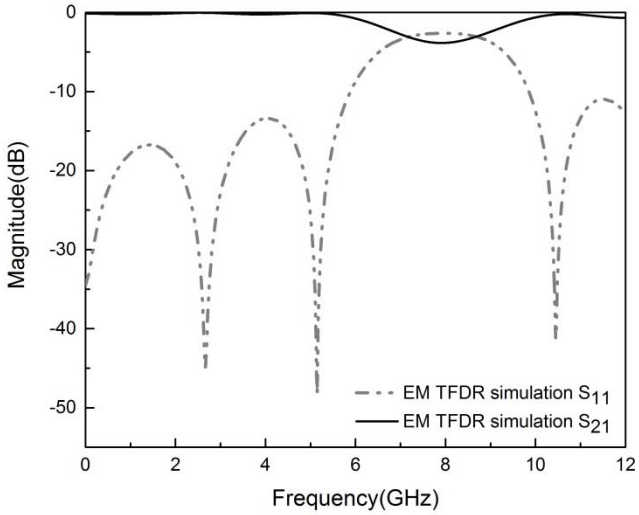

Fig. 4. 25 S-parameter response of TFDR circuit model predicts the stop-band with a reasonable accuracy.

The result is a stop-band around f_0 =7.8 GHz with a level of rejection that depends on the number of DRs mounted on substrate.

It is well known that a topology can produce, n−2 finite transmission zeros out of n resonators, where n is the degree of filter. The addition of a direct signal path between the source and the load allows the generation of n finite frequency transmission zeros instead of n−2. Furthermore, allowing the source or load to be coupled to more than one resonator brings about more diverse topologies for filter designs.

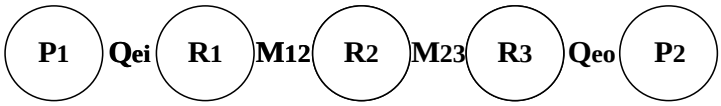

4. 26 General topology of three-coupled resonators with coupling coefficients M_{ij} and two ports with external quality factors Q_e.

Figure 4.26 illustrates a topology of 3-coupled resonators with two port couplings, where three numbered nodes represent resonators; P_1 and P_2 denote the source nodes. The coefficients M_{ij} specify the coupling between adjacent resonators i and j of the filter, Q_{ei} and Q_{eo} are the external quality factors that specify the input and output couplings, respectively M_{ij} and Q_e can be derived from the associated low-pass prototype of Fig. 4.26, which is given by

$$M_{i,j} = \frac{FBW}{\sqrt{g_i g_j}} \quad (4.\ 27)$$

$$Q_{e_i} = \frac{g_0 g_1}{FBW} \quad (4.\ 28)$$

$$Q_{eo} = \frac{g_n g_{n+1}}{FBW} \quad (4.\ 29)$$

Where g_i is element values of the low-pass prototype filter and FBW represents the fractional bandwidth of stop-band filters. When the filter is designed with third-order (N=3), Chebyshev response, and 0.01 dB ripple level, the element values of the low-pass prototype are g_0=1, g_1=g_3=0.6292, g_2=0.9703, and g_4=1. If f_0 =7.8 GHz and have a fractional bandwidth of 19% or FBW=0.19, then Q_{ei}=Q_{eo}=3.3 and the coupling coefficient is M_{12}=M_{23}=0.243.

If q_{e1} and q_{en} are the scaled external quality factors then: $q_{ei} = Q_{ei}.FBW$=0.627 and m_{ij} denotes the normalized coupling coefficient and is defined as $m_{i,j} = \frac{M_{i,j}}{FBW}$.

In many practical filter designs, it is desirable to evaluate the achievable unloaded quality factor Qu of resonators.

The important parameters which are usually associated with the losses include the conductor, dielectric substrate, and radiation. The total unloaded quality factor can be found by adding these losses together, resulting in $\frac{1}{Q_u} = \frac{1}{Q_c} + \frac{1}{Q_d}$where Qc and Qd are the conductor and dielectric quality factors, respectively.

The conductor Q of a microstrip line resonator can be evaluated by

$$Q_c = \frac{ka\eta}{2R_s} = 1970$$

While

$$k = \frac{2\pi f\sqrt{\varepsilon_r}}{c} = 1094\ m^{-1}$$

Where η=ωμ/k=$\sqrt{\mu/\varepsilon}$ is known as the intrinsic impedance of the medium. In free-space the intrinsic impedance is η_0=$\sqrt{\mu_0/\varepsilon_0}$=377Ω. The intrinsic impedance is η=377/$\sqrt{\varepsilon}$=56.2Ω. The surface resistivity of DR at 7.8GHz is $R_s = \sqrt{\frac{\omega\mu_0}{2\sigma}} = 1.56e^{-2}\ \Omega$. Where σ is the conductivity which the electrical conductivity of DRs is (σ=1×10^{14} Ω) and the other variables have the usual meaning.

The dielectric loss can be taken into account in terms of a complex permittivity of the dielectric substrate ε=ε′−jε″, with the negative imaginary part denoting energy loss. . It can be shown that

$$Q_D \geq \frac{\varepsilon'}{\varepsilon''} = \frac{1}{tan\delta} = \frac{1}{0.008} = 125$$

Where tanδ=0.008 is the dielectric loss tangent of DR.

The total unloaded quality factor can be found

$$Q_L = \frac{1}{Q_D} + \frac{1}{Q_C} = \left(\frac{1}{125} + \frac{1}{1970}\right)^{-1} = 117.5$$

4.3.1 Equivalent circuit model of TFDR stop band filter

In TFDR stop band filter, the structure is a micro-strip periodically loaded with resonators that can be characterized as LC branch. The electronic band gap has been used as an effective way to create microwave filters. The resonators are used their first resonant frequency to implement the EBG loads being enough to consider a single series LC branch to fit the filtering pattern exhibited by the experimental data, and therefore to obtain a reasonable description of the dielectric resonator in this frequency range.

The equivalent circuit model is useful in understanding the mechanics which drive the design in a familiar sense. The equivalent circuit model of TFDR stop band filter is shown in Fig 4.26. Where β is the propagation constant of the periodic structure, K_0 is the propagation constant of the microstrip host line, d is the basic cell length and the lumped elements of the equivalent circuit model of the resonators are L_R and C_R.

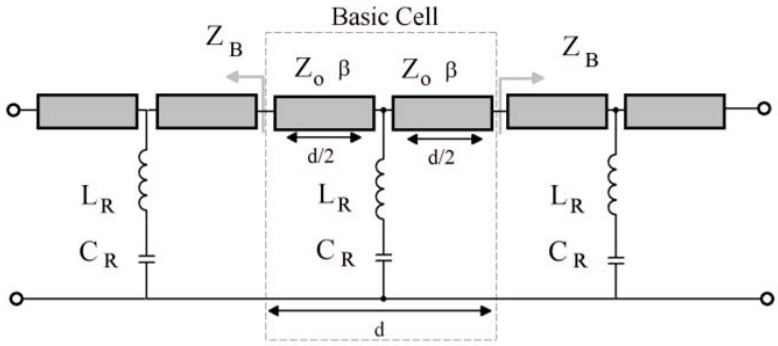

Fig. 4. 26 EGB filter structure where the grey boxes represent the microstrip host transmission line determined by the length of the basic cell d, the propagation constant β and the characteristic impedance Z_o, and the dielectric resonator is modelled by the series L_R-C_R branch.

The micro-strip host transmission line characteristic impedance Z_0 and propagation constant β can be analytically evaluated from the dimensions of the micro-strip line and the physical properties of the substrate which in this case is the 25 mil Rogers RO3010.

Maximum coupling occurs at

$$d = \frac{n\lambda_g}{4} \text{ n=0, 2, 4,…}$$

While minimum coupling occurs at

$$d = \frac{m\lambda_g}{4} \text{ m=1, 3, 5,...}$$

Waveguide for this prototype is λg=12 mm and spacing between the DRs in this design is taken as λg/2=6mm at the corresponding resonant frequency.

The dispersion relation for the circuit of Fig 4.26 can be easily obtained from standard calculus [55].

$$\cos(\beta d) = \cos(k_0 d) - \frac{\omega C_R}{2(1-\omega^2 L_R C_R)} sin(k_0 d) \quad (4.\ 30)$$

The confinement of the right hand of Eq (4.30) between -1 and 1 will determine the transmission bands. In the presented case it corresponds to a stop-band filtering structure with successive spurious bands.

For $k_0 = \frac{2\pi f}{c}$ at 7.8 GHz:

$$k_0 d = \frac{2\pi(7.8 \times 10^9)}{3 \times 10^8} 0.006 = 0.9801 = 56°$$

If L_R=1nH and C_R=0.145pF then corresponding to Eq (4.30) βd=0.988 so β=0.988/0.006=165 rad/m.

By assuming that the aspect ratio of the DR and the frequency of operation have been selected such that only a single mode is excited then an isolated DR can be represented as a series resonant circuit with equivalent-circuit components Rr, Cr, and Lr. Fig 4.27 shows DR coupled to a short section of micro-strip line, at reference plane pp′, which is represented by R, C, and L that more details mentioned in 3.3.1. It is assumed the resonator is excited in $T_{o1\delta}$ mode, and the micro-strip line has zero loss in the coupling region, R_1 can be neglected. By neglecting the micro-strip-line capacitance, the resulting simplified equivalent circuit can be expressed close to resonance as a parallel resonant circuit.

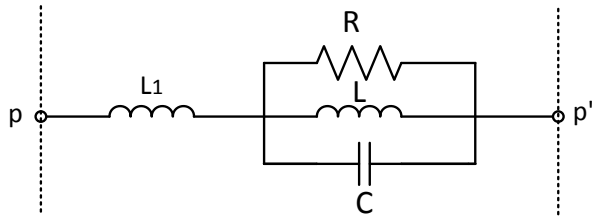

Fig. 4. 27 Simplified model of DR coupled to microstrip line.

The general expression for a parallel resonant circuit is

$$z = \frac{R}{1+j2Q_u\delta} \quad (4.31)$$

Where

$$Q_u = \omega_0 RC \quad (4.32)$$

$$\boldsymbol{\omega_0}^2 = \frac{1}{L_r C_r} = \frac{1}{LC} \quad (4.33)$$

$$\boldsymbol{\delta} = \frac{\omega - \omega_0}{\omega} \quad (4.34)$$

These results are valid close to the fundamental resonance $TE_{01\delta}$ mode of the DR where δ^2 tends to zero. Outside this frequency range other DR modes exist, which can be modeled by a Foster equivalent circuit [56] consisting of a series cascade of parallel circuits. With this approach characterization of the ith resonant circuit requires the ith resonant frequency, unloaded Q factor, and effective coupled resistance to be determined. In addition, when the resonant frequencies of several modes occur in close proximity the individual modal performances cannot be easily established because of mode interaction. It is useful to note that $TE_{01\delta}$ mode can be well separated from other modes by correct selection of DR and enclosure dimensions.

According with the Foster synthesis [55], the approximate impedance of a passive resonator can be obtained as a partial expansion of the generic impedance function displayed in [55-57].

$$Z(j\omega) = jX(\omega) = j\left[A_\infty \omega + \frac{A_0}{\omega} + \sum_{i=1}^{m} \frac{2A_i\omega}{\omega_i{}^2+\omega^2}\right] \quad (4.\ 35)$$

It can be shown that the equivalent circuit model of the passive resonator should be described with the network depicted in Fig 4.28, where $C_S=1/A_0$, $L_s=A_\infty$, $C_{pi}=1/2A_i$ and $L_{pi}=2A_i/\omega^2{}_i$.

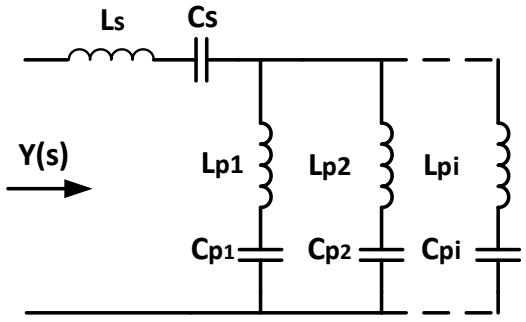

Fig. 4. 28 Foster synthesis of equivalent circuit model for any generic passive resonators.

Since the resonances of a ring resonator occur periodically, one, two (or more) resonators with different perimeters can selected so that only every peak overlaps, suppressing all resonances that lie in between.

The simulated and measured proposed design depicted in Fig 4.29(b), indicate that the desired functionality at the design frequencies is achieved and also the proposed equivalent circuit model offers an excellent fit of the measurements for L_R=1 nH and C_R=0.145 pF.

4.3.2 Measurement and discussion

The 25 mil Roger substrate used for the host micro-strip is characterized by a loss tangent δ=0.0022 and ε_r=10.2 at the operating frequencies. Several layers of the Creative 122-06 dielectric have been deposited by means of in home fabricated masks until a thickness of 0.6 mm have been achieved in the resonators. The structures have been in a conventional oven at 150ºC for one hour. Fig 4.29(a) shows the fabricated device.

In order to verify the design, the band-stop filter is fabricated and measured, as Fig 4.29b shows, and the measurement is got by Agilent 32820ET vector network analyzer, and it can be seen the measurement is similar to the simulation. The excellent agreement between the electromagnetic circuit model and the measurement are an excellent starting point to develop a robust design methodology. And also measured response of the prototype, demonstrated clearly exhibits the EBG behavior.

(a)

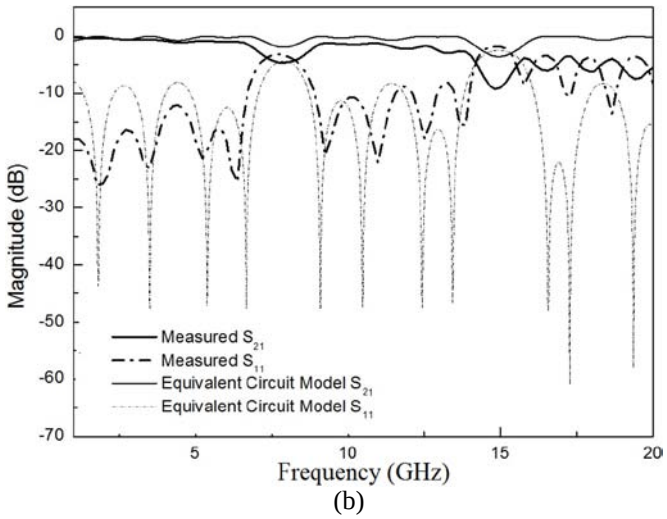

(b)

Fig. 4. 29 Photographs of the manufactured TFDR b) Measured S-parameter for a 3 stage EBG fitted with the equivalent circuit model showed in Fig 4.25.

This result shows the ability of the thick film high dielectric constant resonators to be used as passive elements for the design passive elements in the range of Ku band. The resonator physical complex behavior leads to the utilization of full 3D electromagnetic software to the design of devices based on these resonators. The proposed structure points out the possibility of using TFDR for the creation of EBGs.

To improve high rejection level one approach is use of path between input and output ports and the signals are enforced to cancel each other at the output port by proper adjustment of amplitudes and phases. In this case, by modifying the configuration of the prototype by surrounding DRs with micro-strip ring resonator, band pass could be improved which next part is development by utilization of microstrip ring resonator and embedded DRs as resonators in planar devices.

4.4 Band-pass filter by embedded high dielectric resonators (EDR)

A typical DR filter consists of a number of dielectric resonators that are mounted in a planar configuration to obtain a good resonant frequency [58]. The relative dielectric constant of the materials for constructing DR in microwave filters generally was chosen from a higher value compared to the base substrate.

The primary advantage in using a high dielectric constant is to miniaturize the filter size. The size of DR filter is considerably smaller than the dimension of waveguide filters operate at the same frequency.

The availability of dielectric resonators with small tanδ and benefit temperature stability makes them suitable for microwave filters. The band-pass filters realized with DRs are typically about one-third shorter than common waveguide filters.

In this part, a new band-pass filter consists of three dielectric resonators were excited with a micro-strip line that were used to increase the bandwidth of the design. The idea of using the three DRs is to generate few additional frequencies which can be merged together to produce a wideband devices, increase the transmitting power and reduce the

insertion loss in the pass-band. The optimum coupling effect in the filter was obtained from the matching position of the resonators on the micro-strip line.

Since cylindrical shape of dielectric resonators have a flexible radius, height, h and dielectric constant due to various sizes can be obtained from the market.

The applications of these resonators have been widely used in filters and oscillators. Such shape offers a wide degree of freedom in microwave designs since the ratio of r/h could determine the Q-factor for a given dielectric constant. Thus a height of the slender cylindrical DR can be made to resonate at the same frequency as a wide and thin DR. However, the Q-factors for these two resonators will be different. This characteristic offers a flexible degree for choosing the most suitable ratio to be the best frequency and bandwidth.

The high Q-factor and compact size make it an ideal couple especially in micros-trip technology. The proposed embedded dielectric resonators (EDR) constitute a new approach to the miniaturized resonators suitable for MTMs design without the Q degradation inherent to the coupling coefficient based sub-wavelength particles.

The geometry of the proposed structure consists in a 3 cells EBG. Each cell formed by a cylindrical DR with 2 mm diameter and 1.27 mm height, and 1.3 mm width micro-strip ring resonator with an inner radius of 2.3 mm as shown in Fig 4.30.

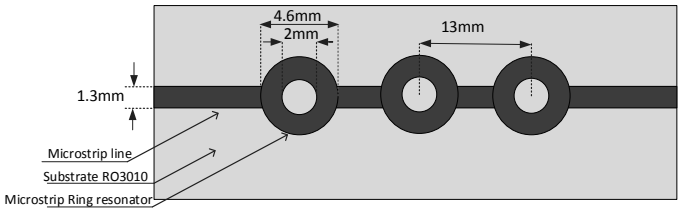

(a)

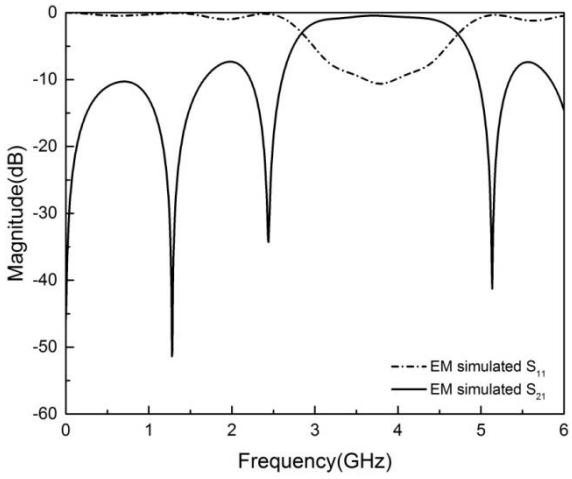

(b)

Fig. 4. 30 a) Configuration of dielectric resonator filter b) S-parameter of proposed filter before embedded epoxy.

S-parameter for proposed filter is depicted in Fig 4.30 which resonant frequency is 3.8 GHz. The basic structure of the EDR consists in the inclusion of cavities in the PCB design that will be filled with high dielectric constant (εr) pastes to generate EDR after the curing process. There are two main advantage of this technique to generate EDRs: the possibility to control the geometry of the resonator and the possibility to combine with standard structures in planar technologies such as microstrip or coplanar-waveguide. Epoxy dielectric materials with relative permittivity ε_r=45 is used as DRs. The DRs fed energy by a 50Ω micro-strip line of width =1.3 mm and length=50 mm by putting on the top of substrate. The substrate is Roger 3010 with dielectric constant of ε_r =10.2 and loss tangent 0.0022. Dielectric resonator interacts with the microwave transmission line. At the beginning the transmission line were calculated according to the 50Ω characteristic impedance. Wideband devices can be designed using two or more DRs. All DRs are operating in a same principle. Each of them is resonate for a same

mode but with different frequency such that the combination response is an additional result from the single response which able to increase the overall bandwidth.

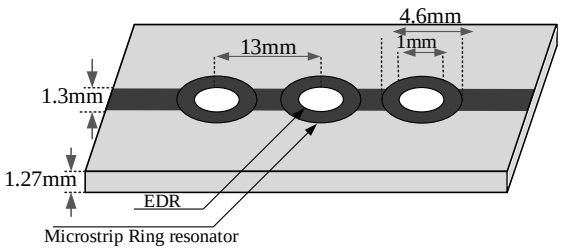

(a)

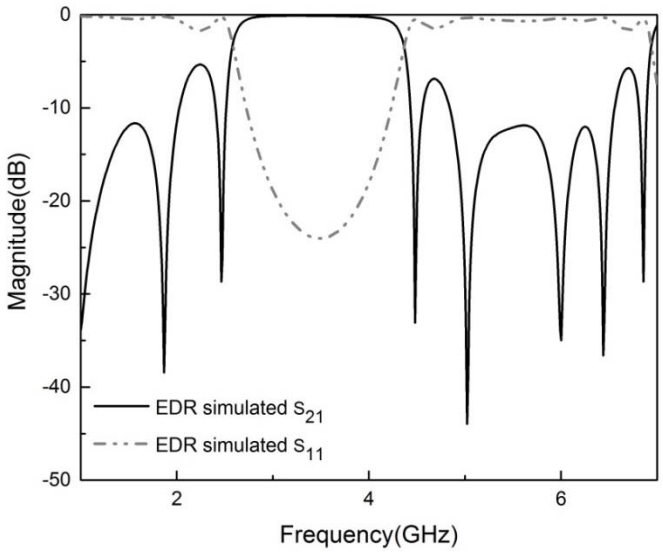

(b)

Fig. 4. 31 a) Configuration and 3D model of embedded dielectric resonator filter b) S-parameter of proposed filter.

As shown in Fig 4.31 the coefficient S_{11} that shows the reflection loss from 2.75 GHz to 4.6 GHz bands and the parameter S_{21}, the insertion loss, is less than -20dB. It also presents a flat response in the pass-band.

The wavelength inside the DR, λ_g is also inversely proportional to the square root of the dielectric $\lambda_g = \lambda_0/\sqrt{\varepsilon_r}$ where λ_0 is the free space wavelength at the resonant frequency that $\lambda_g = \frac{\lambda_0}{\sqrt{\varepsilon_r}} = \frac{c}{f_0\sqrt{10.2}} = 26mm$ (c is the speed of light and f_0=3.67GHz is resonant frequency) when coupled to each other, require $\lambda g/2$=13mm spacing between the DRs at the corresponding resonant frequency.

A coupled-cavity system shown in Fig. 4.32a consisting of three resonant cavities. In a simple cascaded configuration, there are only two coupling coefficients: k_{12} and k_{23}, but if a new coupling k_{13} is introduced between the first and the third cavities which has opposite signs compared to these of k_{12} and k_{23}, then it is possible to have a transmission zero at a finite frequency [59]. It can be accomplished that coupling by using $TE_{01\delta}$ mode of a dielectric resonator in a metallic shield.

To design a filter with band-with of 1.85 GHz at 3.67 GHz is needed a 3rd order Chebyshev filter. The design parameters are g_0=1, g_1=g_3=0.6292, g_2=0.9703 and g_4=1. If f_0=3.67 GHz and have a fractional bandwidth of 50.5% or FBW=0.505 then Q_{ei}=Q_{eo}=1.24 and the coupling coefficient is M_{12}=M_{23}=0.6463 which the coefficients M_{ij} characterize the coupling between the DRs.
Dielectric resonators (DRs) provide high unloaded quality factors. However, DRs suffer from several major drawbacks. The main drawback of DRs is their large sizes as compared to the rest of the oscillator circuit. Furthermore DRs are not amenable to integration and not suitable for mass production because of their 3-D structures.

The Q-values are supposed to be evaluated at the resonant frequency, which in this case is the center frequency of the filter. It should be mentioned that not only does the pass-band insertion loss increase and the selectivity become worse as the Q_u is decreased, but it also can be shown that for a given Q_u, the same tendencies occur as the fractional bandwidth of the filter is reduced.

The total unloaded quality factor can be found by adding these losses together, resulting in $\frac{1}{Q_u} = \frac{1}{Q_c} + \frac{1}{Q_d}$where Qc and Qd, are the conductor, and dielectric quality factors, respectively.

If the surface resistivity of DR at 3.67GHz is $R_s = \sqrt{\frac{\omega\mu_0}{2\sigma}} = 1.07e^{-2}$ Ω. Where σ is the conductivity which the electrical conductivity of DRs is (σ=1×10^{14} Ω) and the other variables have the usual meaning.

And resonant frequency is 3.67GHz, then:

$$k = \frac{2\pi f\sqrt{\varepsilon_r}}{c} = 515\ m^{-1}$$

Where $\eta=\omega\mu/k=\sqrt{\mu/\varepsilon}$ is known as the intrinsic impedance of the medium. In free-space the intrinsic impedance is $\eta_0=\sqrt{\mu_0/\varepsilon_0}=377\ \Omega$. The intrinsic impedance is $\eta=377/\sqrt{\varepsilon}=56.2\ \Omega$.

Conductor loss Q_C can be determined as:

$$Q_c = \frac{ka\eta}{2R_s} = 676$$

Where a=0.5mm.

The design of high-speed circuits requires knowledge of the dielectric constant (ε_r) and loss parameter (tanδ) of the substrate. It is desirable to develop a method allowing the design engineer to personally determine ε_r and tanδ of a substrate material. The loss in a dielectric substrate may be attributed

$\tan\delta(\text{subatrate})$

$$\frac{\mathbf{1}}{\mathbf{Q_{D(epoxy+substrate)}}} = \frac{\mathbf{1}}{\mathbf{Q_{epoxy}}} + \frac{\mathbf{1}}{\mathbf{Q_{sub}}} \tag{4. 36}$$

Since loss tangent for RO3010 is 0.0023

$$Q_{D(substrate)} = \frac{1}{\tan\delta(\text{subatrate})} = \frac{1}{0.0023} = 435$$

And loss tangent for epoxy is 0.008

$$Q_{D(epoxy)} = \frac{1}{\tan\delta(\text{epoxy})} = \frac{1}{0.008} = 125$$

Therefor $Q_D=560$

The total unloaded quality factor can be found by adding these losses together, resulting in

$$Q_u = \frac{1}{Q_D} + \frac{1}{Q_C} = \left(\frac{1}{560} + \frac{1}{676}\right)^{-1} = 307 \tag{4. 37}$$

The Q-factor is increases proportionally to the dielectric constant. This will reduce the bandwidth of the filter. By properly choosing the dielectric constant, the Q-factor can be

reduced. The volume of the DR and Q-factor can be traded off depending on the particular design application. For a low profile design, a combination of high dielectric constant and large DR area can be used to obtain a reasonable bandwidth.

4.4.1 Equivalent circuit model of EDR band pass filter

The equivalent circuit model of EDR pass band can be reproduced as an infinite of parallel LC tanks. An equivalent circuit model for proposed filter is used to describe the basic behavior of the resonator structure as depicted in Fig 4.32.

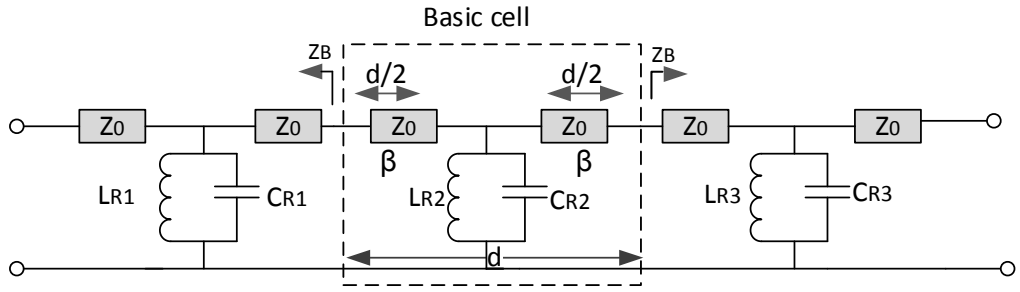

Fig. 4. 32 Equivalent circuit model of proposed filter where the grey boxes represent the micro-strip host transmission line determined by the length of the basic cell d, the propagation constant β and the characteristic impedance Z_o, and the dielectric resonator is modelled by the parallel L_R-C_R branch.

The proposed design corresponds to a non-attenuated propagating wave on the periodic structure, and defines the pass-band of the structure with $\cos\beta d = cos\theta - \frac{b}{2}sin\theta$ definition, where θ=kd, and k is the propagation constant of the unloaded line and "b" is a shunt susceptance. The microstrip host transmission line characteristic impedance Z_o and propagation constant β can be analytically evaluated from the dimensions of the micro-strip line and the physical properties of the substrate which in our case is the 50 mils Rogers RO3010. It can be shown that for a symmetrical passive structure, the dispersion equation is solved by the equation

$$\cos(\beta d) = \cos(k_0 d) - \frac{(1-\omega^2 L_R C_R)}{2\omega L_R} sin(k_0 d) \quad (4.\ 38)$$

Where β is the propagation constant of the periodic structure, k_0 is the propagation constant of the micro-strip host line, d is the basic cell length and the lumped elements of the equivalent circuit model of the resonators are L_R and C_R.

For $k_0 = \frac{2\pi f}{c}$ at 3.6 GHz:

$k_0 d = \frac{2\pi(3.6\times10^9)}{3\times10^8} 0.013 = 0.9801 = 56^o$

If L_R=1.4nH and C_R=1.3 pF then βd=0.981 so β=0.981/0.013=75.49 rad/m.

The confinement of the right hand of Eq (4.37) between -1 and 1 will determine the transmission bands. In the presented case it corresponds to a low-band filtering structure with successive spurious bands.

4.4.2 Measurement and compression

The combination of dielectric and microstrip transmission line in designing a band-pass filter with such structure is a novel. The idea of designing this band-pass filter was due to the dielectric resonator can increase Q-factor in a circuit response and able to maximize power transfer in dielectric resonators. For implementation of proposed filter the 50 mil Roger3010 substrate used as a host which is characterized by a loss tangent δ=0.0022 and εr=10.2 at the operating frequencies. The fabricated proposed filter is shown in Fig. 4.33, while Fig 4.33a corresponds to a filter with three coupled single ring and in Fig 4.33b with three EDR coupled particles.

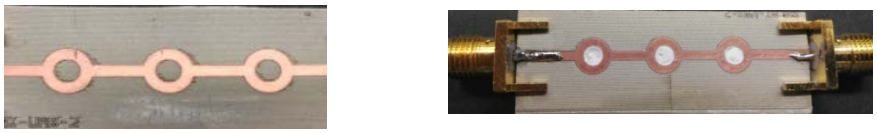

(a) (b)

Fig. 4. 33 Picture of the fabricated prototypes (a) Before embedded with DR b) After embedded with DR

By drilling an array of circle via-slot patterns in a substrate, waveguide dielectric channel can be created. Layers of the epoxy have been deposited until a thickness of the

substrate has been achieved in the resonators. The structures have been in a conventional oven at 150ºC for one hour.

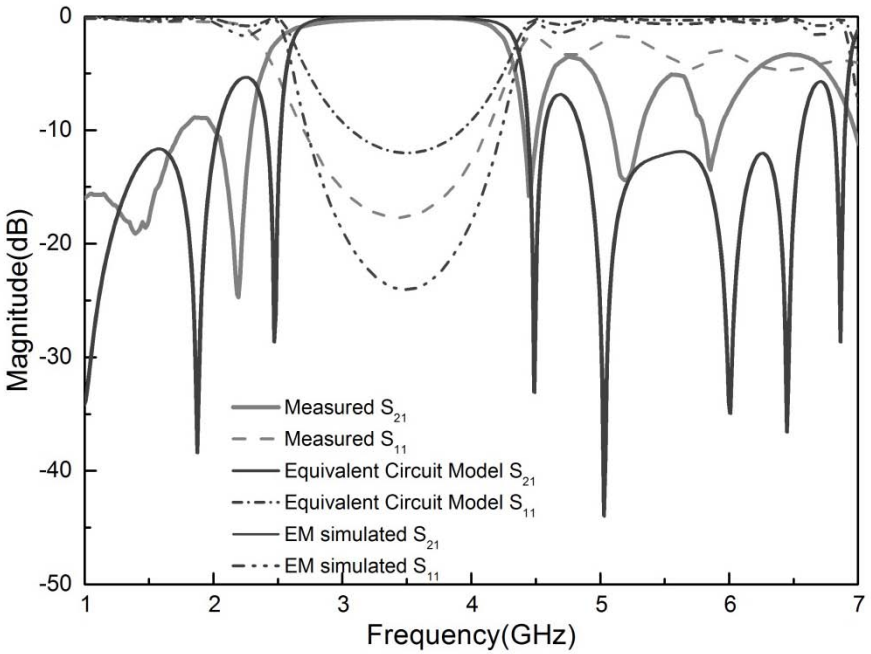

Fig. 4. 34 Measured S-parameter for a band pass EBG fitted with the equivalent circuit model showed in Fig 4.32.

As can be observed in Fig 4.34, there is an excellent agreement between simulation and measurement. In the measurement, the lower and higher cutoff frequencies of the EDR filter are equal to 2.75 GHz and 4.6 GHz, respectively as can be observed in Fig 4.34. This indicates that the relevant fractional bandwidth achieves about 50.5%.at the central frequency 3.6GHz.

One approach for miniaturization is to use very high dielectric constant materials [60]. Obviously, dielectric loading provides a size reduction factor on the order of $\sqrt{\varepsilon_r}$ for the leaky dielectric and cavity resonator type (e.g. micro-strip patch antennas), where ε_r is the relative permittivity of the dielectric material.

Although this method of miniaturization is sensitive to surface wave excitation, it might be found beneficial, especially when the electrical thickness of the substrate is small compared to the wavelength. It is worth mentioning that this type of miniaturization is not protected to the aforementioned adverse effects such as high Q, low efficiency, and complexity in the matching network.

In order to obtain a compact size of a design, a DR that contain of a high dielectric constant must be chosen. However, the range of dielectric constants that can be used is limited, since there is a tradeoff between the compact circuit and the dielectric constant due to the high percentage of power being trapped in the surface waves of the microstrip substrate. Since surface waves are not generated in DRs, the radiation efficiency is not affected by the highest dielectric constant on the top.

At the same time, the Q-factor is increases proportionally to the dielectric constant. This will reduce the bandwidth of the filter. By properly choosing the dielectric constant, the Q-factor can be reduced. The volume of the DR and Q-factor can be traded off depending on the particular design application.

To evaluate the influence of dielectric constant, different resonance circuits were manufactured using various epoxy epsilons (ε_r). Fig 4.34 shows the effect of variation of dielectric constant (ε_r) on DRs. It can be seen from the figure that as ε_r increases, the resonance frequency shifts towards the lower frequency.

Proposed filter before embedded high dielectric constant produces a resonant frequency of 3.8 GHz, and after embedded high dielectric constant with ε_r=45 frequency obtain at 3.6 GHz. This 5% of resonant frequency reduction implies an equivalent miniaturization percentage.

To further miniaturize the filter, its effectiveness as the value of ε_r increase from 45 to 100, frequency proportional to change of ε_r, shift down from 3.6 GHz to 3.2 GHz respectively, which causes 12% miniaturization filter. S-parameters of EDR in comparison between different dielectric constant are depicted in Fig 4.35.

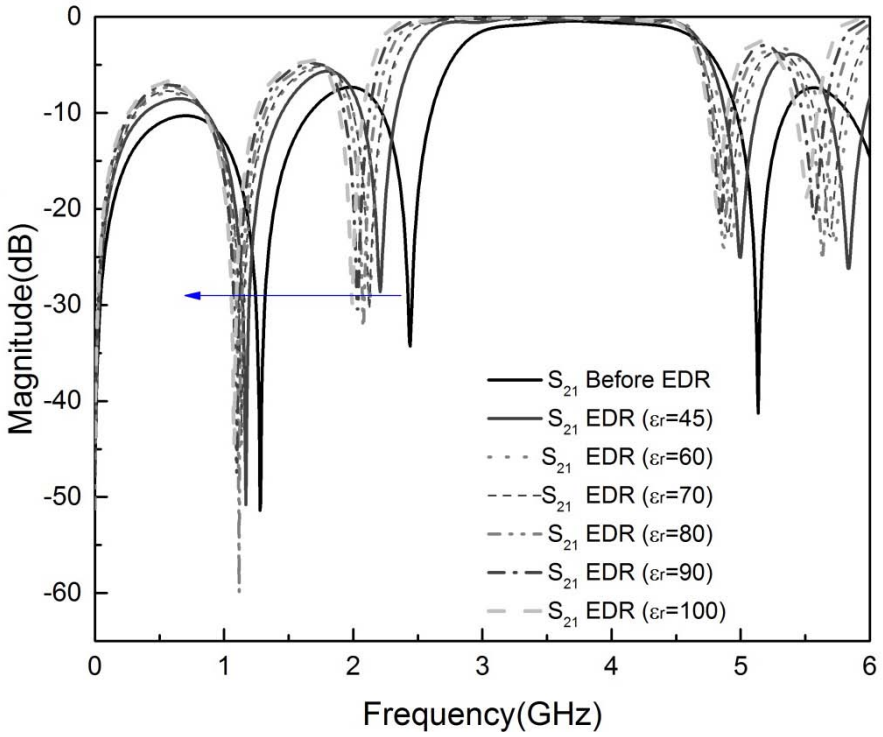

Fig. 4. 35 Simulated S_{21} response of the embedded dielectric constant to miniaturize band-pass filter with various dielectric constant from εr=45 to εr=100 and shifting frequency from 3.6 GHz to 3.2 GHz which is 400 MHz frequency shifting down.

As can be observed in Fig. 4.36, resonant frequency decreases with ε_r of EDR. An exponential relationship has been obtained between miniaturization level and EDR ε_r Fabricated EDR (εr=45) provides a resonator miniaturization level of 5%. The use of pastes with greater εr increases miniaturization factor, may reach values of 45% with εr=450.

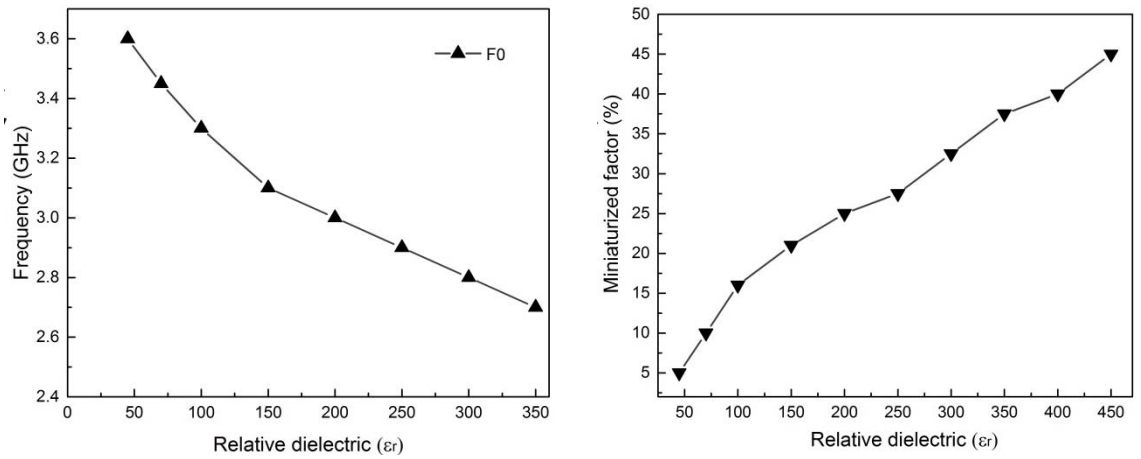

Fig. 4. 36 Relation between frequency shift to lower level by increasing of εr and miniaturized proposed design by changing εr.

As mentioned in 2.2.2 part, the effective permittivity is defined as the square of the ratio of the velocity in free space and for any propagating wave; the velocity is given by the appropriate frequency wavelength product. Which in the microstrip line, the velocity is $\upsilon_p = f\lambda_g$ and then

$$\boldsymbol{\varepsilon_{eff}} = \left(\frac{\boldsymbol{c}}{\boldsymbol{\lambda_g \cdot f_0}}\right)^{\mathbf{2}} \tag{4. 39}$$

Since the effective permittivity is frequency dependent, increasing as the frequency increases. In EDR, the presence of high ε_r material have the effect to increase the value of the ε_{eff} [61]. As shown in Table I, the increment of the ε_{eff} can be interpreted as a miniaturization, since it produces a shift toward of resonant to lower frequency. It is notable that further size reduction can be obtained once a substrate with higher permittivity is used.

4.5 Band-pass filter based on split ring resonators

The miniaturization of resonant particles has become interesting field since the introduction of Split Ring Resonator (SRR) based MTM in 1999 by Pendry [4]. The sub-wavelength property of the SRR has been successfully applied to the miniaturization of passive microwaves devices [65]. Different approaches by using coupling principle have been used to design compact resonators such as the Non-Bianisotropic SRR (NB-SRR), the Broad Side Coupling SRR (BCSRR) [62]or even more complicate shapes [4]. These resonant particles are theoretically suitable for MTMs designs, however, due to the degradation of the quality factor (Q) and the ohmic loses the practical applications exhibit a very low performance [63].

On the other hand, the presence of very close resonances in the vicinity of the sub-wavelength resonances produces spurious bands in the designs based on these resonators that complicate their even more than their practical applications [64]. The embedded dielectric resonators (EDR) presented in this paper constitutes a new approach to the miniaturized resonators suitable for MTMs design without the Q degradation inherent to the coupling coefficient based sub-wavelength particles.

Fig. 4.37 shows the layout dimensions of the proposed filter. It has been implemented in a Rogers RO3010 substrate using a Protolaser milling machine. The minimal distance between the resonators is 0.2 mm and the distance between the port line and the resonators has been fixed to 0.15 mm which is the more critical distance of the design. The ports feed the resonators though a capacitive coupling which intensity depends of the proximity to the extreme resonators (1.5 mm).

The square shape of the resonators has been chosen to maximize the capacitance of the LC resonant tank, resulting in a final thickness of 3.1 mm, and to maximize the coupling between resonators according with the previous experience with this kind of design [65]-[66]. The input and output ports are 50 Ω micro-strip lines that in this substrate correspond to 1.6 mm thick micro-strip. Extensions of the ports with a 90º angle following the square resonator profile have been included in order to maximize the coupling with the side resonators.

The fact that there are dimensions in the layout of the order of the metallic layer thickness requires the utilization of an electromagnetic simulator able to have into account this thickness. Otherwise there may be big differences between Simulation and measured response.

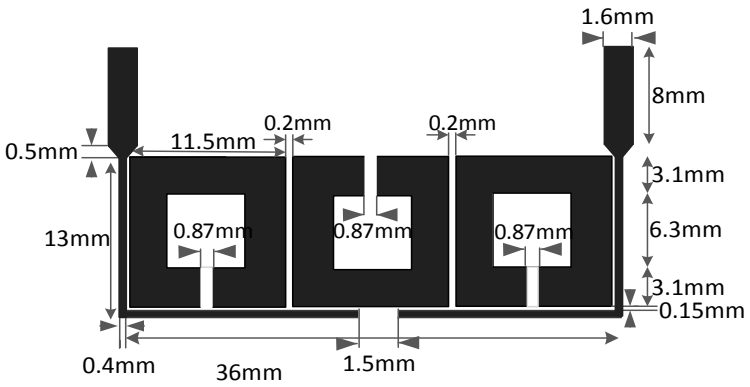

(a)

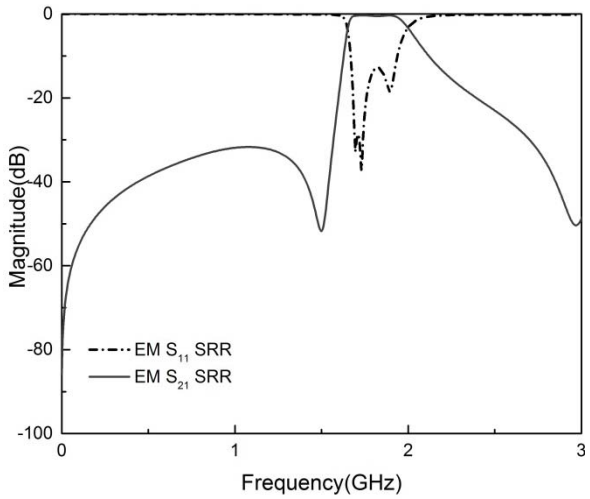

(b)

Fig. 4. 37 a) Dimensional layout of the proposed filter. b) S-parameter of proposed filter.

As can be observed from Fig 4.37b a band pass between 1.44 GHz and 1.75 GHz performing a 19.4% bandwidth. The return losses are below the -10 dB in all the band pass and the insertion losses oscillate between -1.98 dB and 0.79 dB. The outside-band transmission level stays below -30 dB. The band-pass exhibits a non-symmetrical shape being sharper for the low frequency flank.

4.5.1 Equivalent circuit model of SRR band pass filter

The equivalent circuit model of a filter helps to understand the behavior of the design. In the case in which a clear relationship between the equivalents circuit model and the layout physical dimensions can be set. Fig. 4.38 shows the equivalent circuit model of the proposed filter. Basically it is composed by three LC resonant parallel tanks that represent the three open rings, and a set of capacitive coupling networks to model the different couplings.

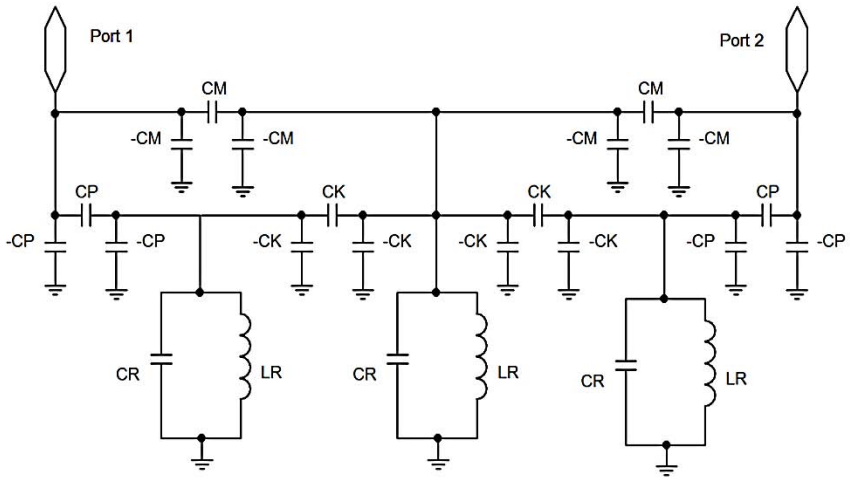

Fig. 4. 38 Equivalent circuit model of the proposed filter.

The nature of the coupling may be magnetic or electric and, in general, it uses to be a combination of both. In many cases, the geometry symmetries can force the predominance of one of the couplings [64]. In our case the orientation of the central resonator has been inverted respect to the orientation of the extremes resonators in such a way that the current distribution in the resonances guarantees the existence of a magnetic wall between adjacent particles and therefore the coupling is forced to be mainly capacitive.

As can be observed there are three different kinds of coupling, characterized by the parameters C_P, C_M and C_K. C_P is modeling the coupling between the port extensions and the extern resonators. The value of this parameter can be modified in the layout altering the horizontal distance between the port extension and the adjacent resonator. Also, there is a dependence of this parameter with the side of the adjacent resonator, being possible to modify this coupling using rectangular shape resonators. The C_K parameter

models the coupling between adjacent resonators and can be controlled directly with the distance between the resonators.

The maximum value of this capacitance is fixed by the minimal distance between metallic layers that the fabrication technology allows. This value is important because, according with the expressions that link the coupling coefficient and the standard normalized filter parameters [67], the maximum bandwidth of the filters is bounded to the maximum coupling coefficient.

Finally, C_M represents the cross coupling coefficient that represent the novelty of the proposed design. The equivalent circuit model of the capacitive coupling is a Π circuit with two negative capacitors in the parallel branches. Interpreting the negative capacitors as inductors, the structure can be thought as L-C-L matching ladder. Since the value of the C_M can be controlled with the variation of the overlap between the port extension and the central square resonator, this matching ladder can be tuned in a certain range of values.

The equivalent circuit model proposed is based on the description of the capacitive coupling coefficient as a Π model. The values of the different parameters can be initially estimated from the physical dimensions, but at the end there will be necessary to optimize them to fit the measured response

TABLE 4.2 SUMMARY OF EQUIVALEN

T CIRCUIT MODEL PARAMETERS AND GEOMETRICAL PARAMETERS

Equivalent Circuit parameter	Value	Layout dimensions	
Resonant Tank	L_R	6.5 e-5 nH	External Ring perimeter: 48.13 mm
	C_R	219000 pF	Ring : 48.13 mm
			Ring Thickness: 3.1 mm
Coupling	C_P	296 pF	Overlap length between Port extension and resonant ring: 23.63
			Distance between port extension and extreme rings: 150 μm
	C_K	36505 pF	Distance between adjacent rings: 200 μm
			Side of the rings: 13 mm
	C_M	55 pF	Overlap length between port extension and the central ring: 5 mm
			Distance between port extension and central ring: 150 μm

. Table 4.2 shows a summary of the equivalent circuit model parameters for the best fit we have been able to find, together with the value of the corresponding layout physical parameter that control that parameter.

4.5.2 Measurement and discussion

SRR band pass filter is implemented by using a Protolaser milling machine in a 50 mil Rogers RO3010 substrate which is characterized by a loss tangent δ=0.0022 and εr=10.2. The minimal distance between the resonators is 0.2 mm and the distance between the port line and the resonators has been fixed to 0.15 mm which is the more critical distance of the design.

The photograph and fabricated proposed filter is depicted in Fig. 4.39a. There is an excellent agreement in the resonant frequencies position is observed between simulation and measurement as depicted in Fig 4.39b. There is a band pass between 1.44 GHz and 1.75 GHz which is performing a 19.4% bandwidth. The return losses are below the -10 dB in all the band pass and the insertion losses oscillate between -1.98dB and 0.79dB.

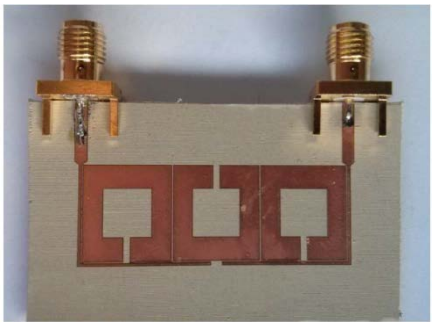

(a)

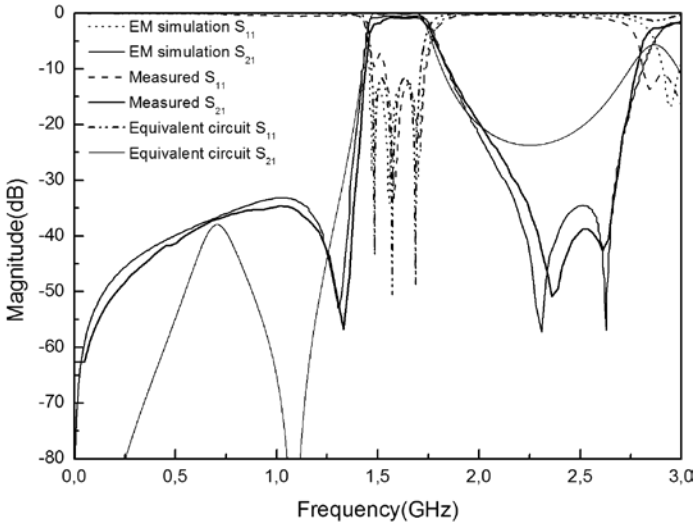

(b)

Fig. 4. 39 a) Picture of the fabricated prototype. b) Comparison between S_{11} and S_{21} measured, electromagnetically simulated and equivalent circuit response.

As can be observed in Fig. 4.39b, the equivalent circuit model is able to reproduce the main filter characteristics such as central frequency bandwidth, the band-pass shape around the transmission, and the full S_{11} response.

However, the main advantage of the equivalent circuit model is the understanding of the effects of the layout parameters variation in the filter performance.

In order to obtain a better fit between measures and the equivalent circuit response, the effects of the phase shift introduced by the input ports and the high impedance of the port extension should be considered in the equivalent circuit model.

In the case of the fit showed in the Fig. 4.40 the phase shift has been fixed to 121 degree and the impedance of the extension ports correspond to 178.25 Ω. The inclusion of the cross coupling between the port extension and the central resonator represent a small modification that introduces a considerable improvement of the filter performance.

The design methodology can be extrapolated to other designs, and, with small modifications can be extended to wideband-pass filters.

The filter showed in Fig. 4.40 include two cross coupling coefficients between the input and the central resonator which allow to introduce a second zero in the transmission function adding a notch at higher frequencies that produce a more symmetrical band-pass shape.

At the same the inclusion of an additional cross coupling coefficient has been used to match the impedance of the filter in a very wide range of frequency. The position and shape of the input ports has been modified in order to optimize the feed of the circuit and the phase introduced by the port extensions.

It is expected that a straight relation between the physical parameter an equivalent circuit model could be established in the same way it has been demonstrated for the design in Fig. 4.40.

As fig 4.40 shows, the result is a well matched wide band pass filter between 1.1 GHz and 1.79 GHz, which correspond to a FBW=50%. The measured insertion losses oscillates between -0.66 dB and -1.3 dB.

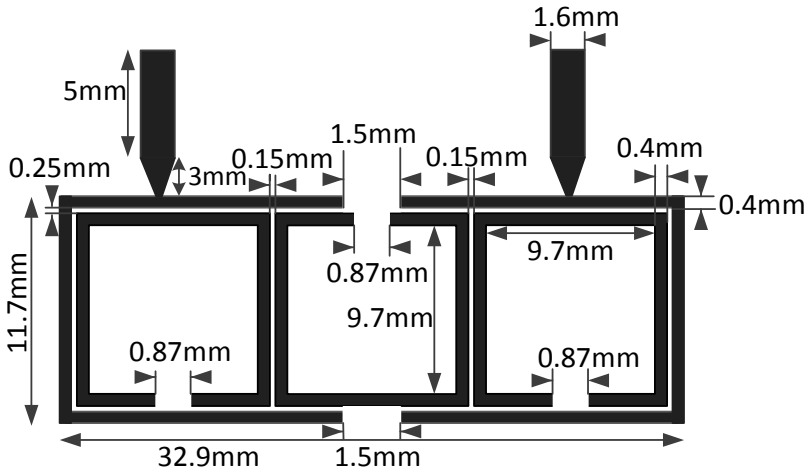

(a)

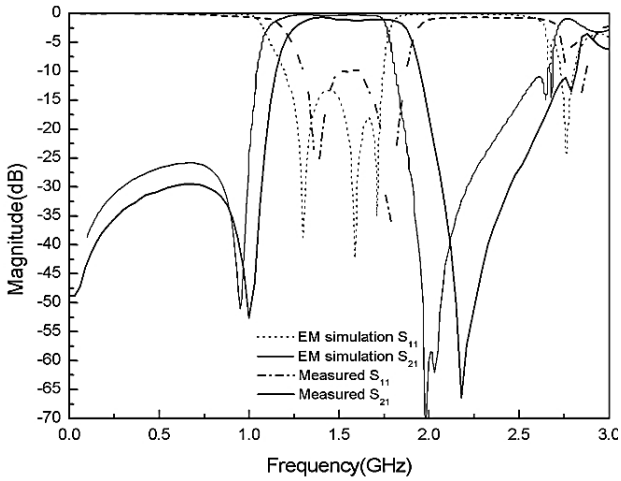

(b)

Fig. 4. 40 Layout of the wide-band prototype filter with the main dimensions b) Comparison between S_{11}, and S_{21}, measured, electromagnetically simulated and equivalent circuit response.

In the preliminary results showed in Fig. 4.40, there is a shift between measurement and electromagnetic simulations that is attributed to some tolerances in the fabrication process. The equivalent circuit model is still under development but even in this preliminary state the benefits of the new propose crossed coupling coefficients are evident in the final filter performance.

4.5.3 Miniaturization of the filter by embedded DR

One of the more interesting properties of the design is the possibility to miniaturize the structure by including high dielectric constant in the center of the SRR. The EDR is produced by depositing high dielectric constant paste in a cavity milled in the substrate. A drying process is needed to obtain the EDR however the procedure is compatible with LTCC technology. The design miniaturization level increases with the value of the dielectric constant of the EDR. CREATIVE 122-06 pad-printable high dielectric constant paste, with a value of εr=45 has been used to fabricate the resonator prototype. The host line is a microstrip line fabricated in a 50mil Rogers substrate characterized by a loss tangent δ=0.0022 and dielectric constant εr=10.2.

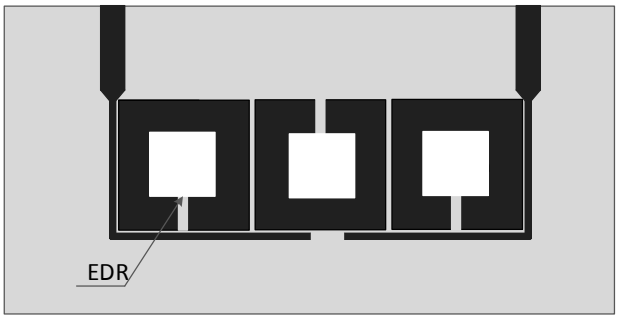

(a)

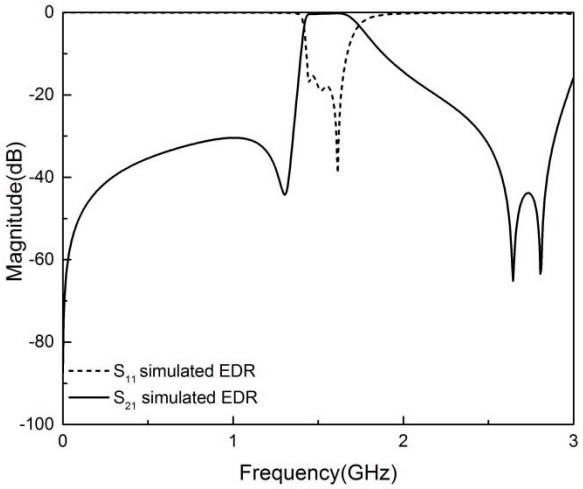

(b)

Fig. 4. 41 Layout model of the EDR proposed filter. B) S-parameter results of the proposed filter design with EDR.

The EDR cavity is milled inside the three ring space as can be observed in Fig.4.41a. Dielectric paste has been deposited into the cavity and the structure has been dried in a conventional oven at 100ºC for two hours.

S-parameters comparison between SRR and EDR SRR is depicted in Fig 4.41b. SRR particle produces a resonant frequency of 1.82GHz, and EDR (εr=50) with identical dimensions 1.56 GHz. This 14% of resonant frequency reduction implies an equivalent miniaturization percentage.

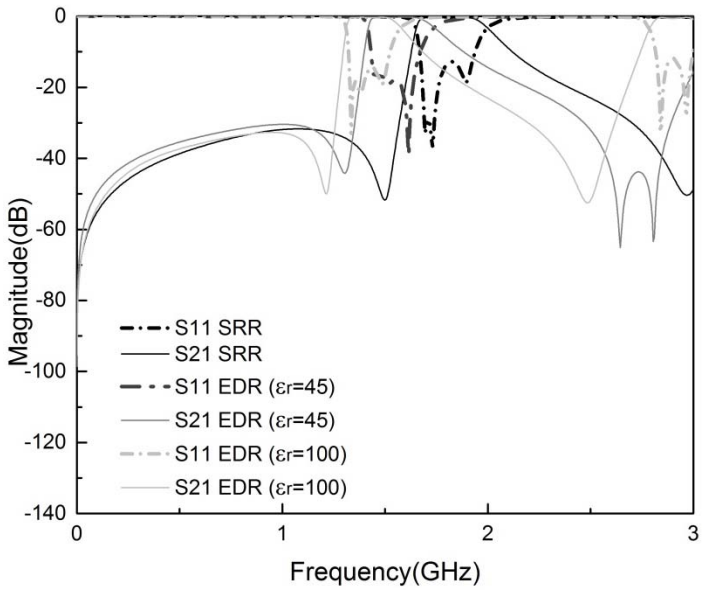

Fig. 4. 42 S-parameters comparison between SRR proposed filter and EDR SRR with dielectric constant of 45 and 100.

To further miniaturize the filter, its effectiveness as the value of ε_r increase from 50 to 100, frequency proportional to change of ε_r, shift down from 1.56 GHz to 1.43 GHz respectively. S-parameters of SRR and EDR in comparison between different dielectric constant are depicted in Fig 4.42.

4.6 Multimode resonator filters (MMR)

There are two approaches for reduction size resonator. One approach is to modify the physical structures [68]. Another approach is to modify the traditional resonator to generate additional modes, which make the resonator to behave as a multimode resonator. Thus one physical resonator can be treated as multiple electrical resonators. Although the multimode filters have advantages such as relative low insertion loss and compact size, there is a challenge to build the high order multimode filter due to the complexity of the coupling among the degenerated modes in the single multimode resonator. Because the multiple degenerate modes and their parasitic resonances or modes, operate close to the fundamental mode, it is also a challenge to build the multimode resonator filter with a wide stop-band [69]. The reported stop-band bandwidth is too narrow to reject beyond the third parasitic spurious.

In 2002, the FCC (U.S. Federal Communication Commission) released the unlicensed use of the ultra-wide band spectrum for indoor, hand-held and low power applications [70]. Ultra-wideband (UWB) components and systems have attracted in academic and industrial circles in the last few years. According to role of UWB in communication system, in this work a new approach to the modeling and optimization of UWB filters is introduced. Many efforts have been devoted to the development of the ultra-wide band pass (UWB) filter using multi-mode resonator (MMR) [71]. From the conceptual point of view, MMR is one of the simplest approaches to the design of UWB. The technique was originally proposed by Zhu and Menzel in 2005 [72], and further developed with diverse approaches can be found in literature [73]. In [66] a five-pole filter was built using a single triple-mode stepped-impedance resonator (SIR) for UWB application. In [74] two short-circuited stubs where attached to the initial MMR to form a quadruple-mode UWB band pass filter. In [75], a packaged UWB filter based on stub-loaded resonators is proposed. In [76], the triple open stubs in shunt to a SIR are used to build UWB filter.

A compact UWB using the dual-mode ring resonator is presented in [77]. In [78] a superconducting UWB band-pass filter with sharp rejection skirts by using MMR is reported. The utilization of ring resonator in the UWB design was introduced in [79].

This part reports a new multimode resonator (MMR) ultra-wide band-pass (UWB) filter design using a grounded open ring resonator. The utilization of 30 μm gaps between input ports and the central resonator achieve high coupling level. Five resonant modes are used to perform a 128% fractional bandwidth at 4.3 GHz. The fabricated prototype exhibits a band-pass with insertion losses around 0.5dB. A theoretical model based on transmission lines matrices is proposed and used to explore the limits of the design through different parametric analysis. Excellent agreement between theoretical predictions, electromagnetic simulations and measurement are found. Fig. 4.43(a) shows the physical layout of the proposed MMR-UWB. The distance between the I/O ports and the MMR is fixed to 0.03 mm. The width of the open ring resonator grounded and the extension of the I/O port have been fixed to 0.2 mm.

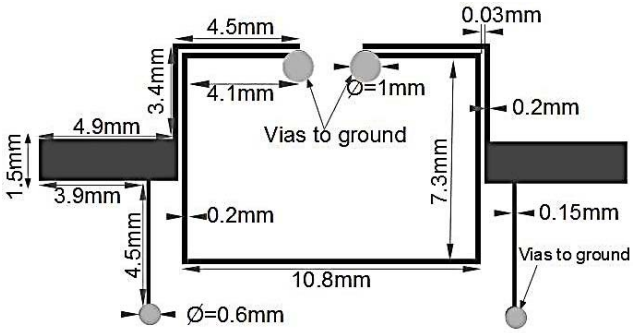

(a)

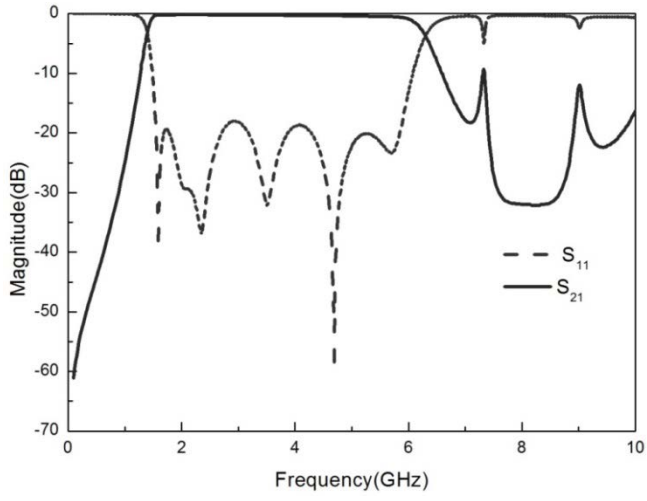

(b)

Fig. 4. 43 a) Layout of the designed MMR-UWB filter. b) S-parameter of simulated filter design.

The two 0.15 mm width, 4.5 mm long grounded stubs have been designed to match the impedance of the I/O ports. The length of these I/O ports extensions coincides with the first resonant frequency of the grounded open ring resonator. The basic idea of the design is that the length of the grounded square ring determines the position of the resonant modes, and the extension of the coupled line in the ring perimeter determines the number of modes into the band pass. On the other hand, the structure of the layout let the identification of the constituent elements of the design in terms of sections which can be theoretically described using transmission matrices representation.

4.6.1 Equivalent circuit model and analysis of MMR UWB filter

The proposed MMR-UWB equivalent circuit model based on coupled micro-strip transmission lines is depicted in Fig 4.44. The coupled transmission lines are characterized trough the even and odd characteristic impedance and electric length (Z_{oe}, θ_e, and Z_{oo}, θ_o respectively). This implies the coexistence of two different modes with different phase velocity and propagating constant corresponding to the different effective relative permittivity.

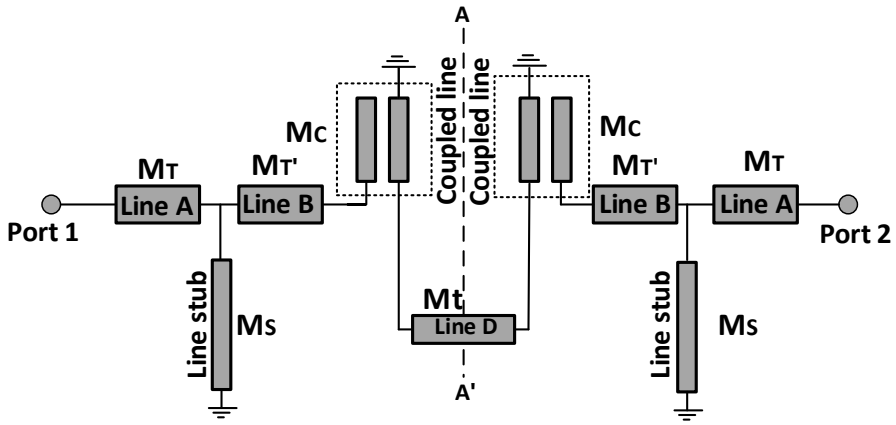

Fig. 4. 44 Schematic of proposed MMR-UWB equivalent circuit model.

The even and odd-mode characteristic impedances Z_{oe} and Z_{oo} can be obtained from the expressions:

$$Z_{oe} = \frac{1}{c\sqrt{C_e^a C_e}} \tag{4. 40}$$

$$Z_{oo} = \frac{1}{c\sqrt{C_o^a C_o}} \tag{4. 41}$$

That C_e^a and C_o^a are the even and odd mode capacitances that can be derived directly from the geometrical parameters of the design. The distributed equivalent circuit model showed in Fig.4.35 (b) can be described by a single ABCD matrix between the input and output ports. Due to the A-A' plane symmetry, the internal structure of this matrix can be described by the Eq.(4.42)

$$\begin{bmatrix} A & B \\ C & D \end{bmatrix} = M_T M_S M_{T'} M_C M_t M_C M_{T'} M_S M_T \tag{4. 42}$$

Where

$$M_T = \begin{bmatrix} cos\theta_T & jZ_T sin\theta_T \\ j\frac{1}{Z_T} sin\theta_T & cos\theta_T \end{bmatrix} \text{and } M_{T'} = \begin{bmatrix} cos\theta_{T'} & jZ_T sin\theta_{T'} \\ j\frac{1}{Z_T} sin\theta_{T'} & cos\theta_{T'} \end{bmatrix} \tag{4. 43}$$

are the ABCD matrices of the line A and B,

$$M_t = \begin{bmatrix} cos\theta_t & jZ_t sin\theta_t \\ j\frac{1}{Z_t} sin\theta_t & cos\theta_t \end{bmatrix} \tag{4. 44}$$

is the ABCD matrix associated to the center transmission line D,

$$M_S = \begin{bmatrix} 1 & 0 \\ \frac{1}{jZ_s tan\theta_s} & 1 \end{bmatrix} \tag{4. 45}$$

is the ABCD matrix associated to the grounded stub S,

$$M_C = \begin{bmatrix} \frac{-Z_{11}}{Z_{12}} & \frac{-(Z_{11}^2 - Z_{12}^2)}{Z_{12}} \\ \frac{-1}{Z_{12}} & \frac{-Z_{11}}{Z_{12}} \end{bmatrix} \tag{4. 46}$$

is the ABCD matrix associated to the coupled lines.

Being the elements of the coupled line:

$$\mathrm{Z_{11}} = \mathrm{Z_{22}} = \frac{-\mathrm{j}}{2}\mathrm{Z_{oe}} \cdot \cot(\theta_\mathrm{e}) - \frac{\mathrm{j}}{2}\mathrm{Z_{oo}} \cdot \cot(\theta_\mathrm{o}) \tag{4. 47a}$$

$$Z_{12} = Z_{21} = \frac{-j}{2} Z_{oe} \cdot csc(\theta_e) + \frac{j}{2} Z_{oo} \cdot csc(\theta_o) \tag{4.32b}$$

Analytical software was used for simplification of the analysis and equations of theory part and plotted as shown in Fig 4.45.

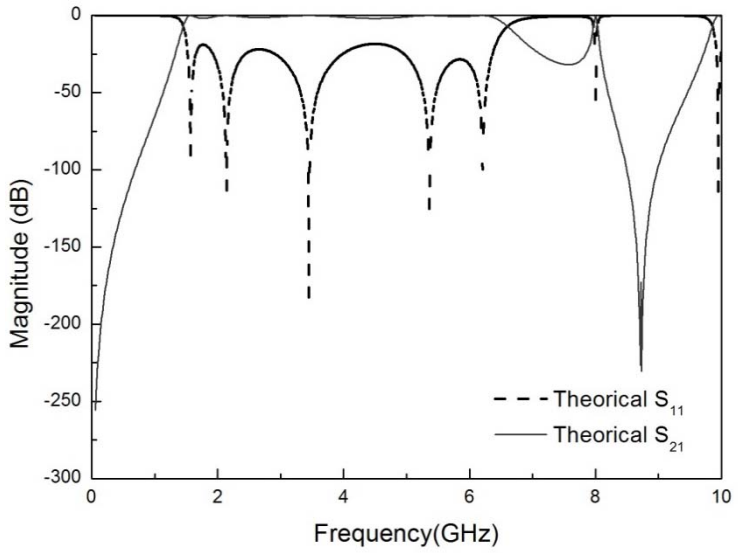

Fig. 4. 45 Theoretical results of MMR UWB filter.

The physical dimensions showed in Fig.4.43a correspond to the electrical parameters are Z_T=44.5 Ω, Z_t=66.6 Ω, Z_s=101.6 Ω, Z_{oe}=145.5 Ω, Z_{oo}=30.5 Ω and 6.5 and 5.8 effective relative dielectric constants for even and odd mode respectively.

Although expressions are complicated, the Z_{oe} and Z_{oo} impedances can be analytically evaluated from the substrate thickness (h), the strip width (W) and the separation between coupled lines (S). Fig.4.46 shows the mapping of these expressions illustrating the fact that for higher S/h relation there is a clear increment of Z_{oo} and a diminution of Z_{oe}. On the other hand, an increment in the W/h ratio implies a reduction of both Z_{oe} and Z_{oo} parameters.

According to this map, the extreme values achievable with our fabrication facilities are fixed to Z_{oe}=145.5 Ω and Z_{oo} =30.5 Ω, corresponding to W= 0.2 mm and S= 0.03 mm for a fixed h=1.27 mm.

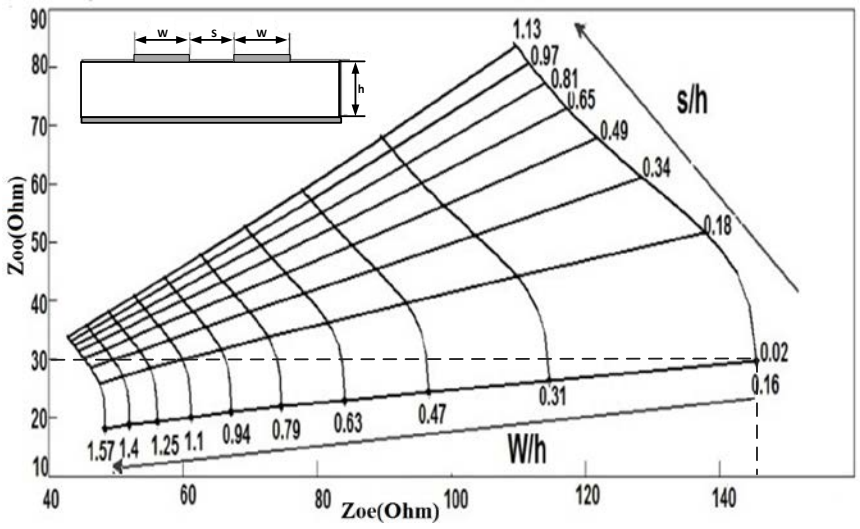

Fig. 4. 46 Even and odd mode (Z_{oe}, Z_{oo} respectively) impedance mapping as function of the S/h and W/h ratios. In all the cases substrate has a fixed valued of h=1.27mm and ε_r=10.2.

The resulting ABCD matrix can be used to evaluate the limits of the filter fractional bandwidth (FBW) following the expression

$$\text{FBW} = \frac{(f_h - f_l)}{f_c} \tag{4. 48a}$$

$$f_c = \frac{f_h + f_l}{2} \tag{4.48b}$$

Where f_c denotes the center frequency and higher and lower frequency limits of the bandwidth are represented by f_h and f_l, respectively. It is observed that the center frequency is inversely proportional to the length of coupling line, when the center frequency decreases, the length of coupling line increases. The length of the coupled line of proposed filter is 9 mm long and 0.2 mm wide, the measured high and low frequency are 5.5 GHz, 1.2GHz respectively.

Fig 4.47 shows the upper and lower limits of the MMR-filtering structure (in Fig. 4.47a) and the corresponding FBW (in Fig 4.47b) as a function of the length of the coupled line section (see Fig 4.43a).

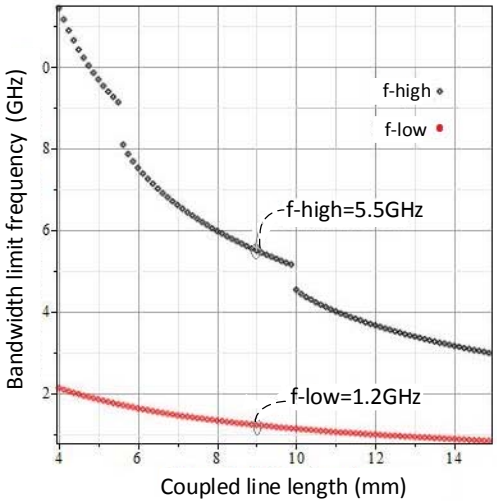

(a)

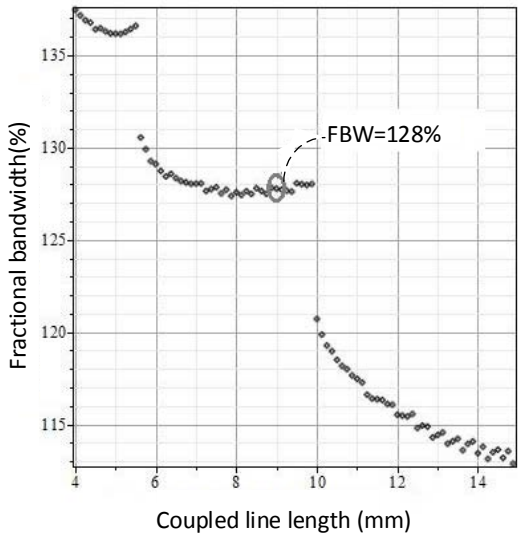

(b)

Fig. 4. 47 Show the upper and lower limits of the FBW as a function of the length of the coupled line (D).

The different number of resonant modes included in the band-pass produces the plateau like behavior observed in Fig 4.47b. For coupled line length below 5 mm there are six resonant modes into the band. In the case of coupled line length between 5 and 10 mm five resonances are included into the MMR design, and four for coupled line length between 10 and 15 mm. As the number of modes into the transmission band increases so does the FBW. However a higher number of resonant modes in the band compromise

the rejection band level and the losses in the transmission band frequencies. The proposed design maintains a rejection level below -20 dB with a 128 % FBW at the UWB standard frequencies. The design process can be complex, but due to the equivalent circuit model based on the transmission matrices of the filter sections, relations between physical parameters and filter performance can be established

As shown in Fig. 4.47a; each bandwidth, being straight proportional to the center frequency, which increasing frequencies cause contiguous bands. Except some critical frequencies (4.5 GHz to 5 GHz and 8.1 GHz to 9 GHZ) in which the resonant modes frequencies change. Also straight relationship can be established between geometrical parameters and the FBW that can be easily controlled by f_c. The variation a limit of the FBW is shown in Fig. 4.47a. The comparison of theoretical, simulation and measurement result is shown in Fig 4.47b. There are five resonant modes generated in the pass band of the MMR filter. Comparing with Fig 4.47b; it can be seen that, by decreasing lengths of coupled lines, resonant modes are changed. The theory predicts that decreasing coupled line (from 5.5 mm to 5.4 mm), increase band pass filter correlation. The theory was developed and compares well with the measurements parameter of bandwidth.

4.6.2 Measured and discussion

To verify these simulated results, proposed MMR-UWB filter is fabricated and measured by network analyzer. A photograph of the fabricated prototype is shown in Fig. 4.48a.

As shown in Fig 4.48b, there are five resonant modes generated in the pass band of the MMR filter. Comparing with Fig 4.47b; it can be seen that, by decreasing lengths of coupled lines, resonant modes are changed. The theory predicts that decreasing coupled line (from 5.5 mm to 5.4 mm), increase band pass filter correlation.

The theory was developed and compares well with the measurements parameter of bandwidth.

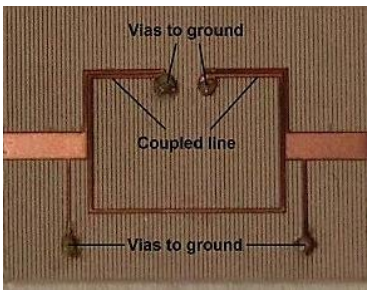

(a)

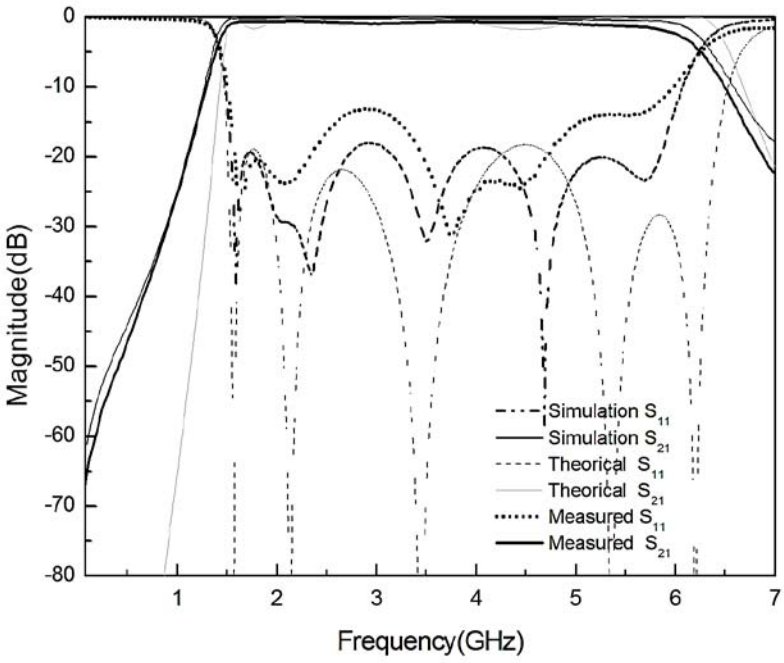

(b)

Fig. 4. 48 a) Photograph of the fabricated MMR-UWB filter b) S-parameter responses of the EM simulation, theoretical and measurement of MMR-UWB filter.

To verify these simulated results, proposed MMR-UWB filter is fabricated and measured by network analyzer. As shown in fig 4.48b, there is excellent agreement between the theoretical prediction, simulated and the measured results. In the measurement, the lower and higher cutoff frequencies of the UWB filter are equal to 1.2 GHz and 5.5 GHz, respectively as can be observed in Fig. 4.48(a). This indicates that the relevant fractional bandwidth achieves about 128%.at the central frequency 2.56 GHz.

In the last part a novel multimode resonator MMR-UWB filter design using a grounded open ring resonator is proposed. The utilization of 30 μm gaps between input ports and the central resonator achieve high coupling level. Five resonant modes are used to perform a 128% fractional bandwidth at 4.3 GHz. The fabricated prototype exhibits a band-pass with insertion losses around 0.5 dB. A theoretical model based on transmission lines matrices is proposed and used to explore the limits of the design through different parametric analysis.

4.7 References

[1] L. Liu, J. Sun, X. Fu, J. Zhou, Q. Zhao, B. Fu, J. Liao, and D. Lippens, “Artificial magnetic properties of dielectric metamaterials in terms of effective circuit model,” Progress In Electromagnetics Research, Vol. 116, pp 159-170, 2011.

[2] Q. Zhao, J. Zhou, F. Zhang, and D. Lippens, “Mie resonance-based dielectric metamaterial,” Mater, Today, Vol. 12, pp 36-45, 2009.

[3] D. R. Smith, W. J. Padilla, D. C. Vier, S. C. Nemat-Nasser, and S. Schultz, “Composite medium with simultaneously negative permeability and permittivity,” Phys. Rev. Left., vol. 84, no. 18, pp. 4184-4187, 2000.

[4] J.B. Pendry, A. J. Holden, W. J. Stewart, and I. Youngs, ”Extremely low frequency plasmons in metallic mesostructures” Physical Review Letters, Vol. 76, pp 4773-4776, 1996.

[5] M. D. Sindreu, J. Naqui, F. Paredes, J. Bonache and F. Martin “Electrically Small Resonators for Planar Metamaterial, Microwave Circuit and Antenna Design A Comparative Analysis” Appl. Sci, 2, pp 375-395; 2012.

[6] C. Caloz and T. Itoh. “Transmission Line Theory and Microwave Applications,” John Wiley and Sons, 2005.

[7] N. Engheta and R.W. Ziolkowski, “Metamaterials Physics and Engineering explorations” Canada, John Wiley and Sons, ISBN-13 978-0-471-76102-0, 2006.

[8] C. Caloz and T. Itoh, “Electromagnetic Metamaterials: Transmission Line Theory and Microwave Applications”, IEEE Press and Wiley, New York, 2005.

[9] R. A. Shelby, D. R. Smith, S. Schultz, “Experimental verification of a negative index of refraction,” Science, vol. 292, no. 5514, pp 77-79, 2001.

[10] J.B. Pendry, A.J. Holden, W.J.Stewart, I.Youngs “Extremely low frequency plasmons in metallic mesostructures”. Phys Rev Lett 76: pp 4773-4776, 1996.

[11] R. Marques, F. Medina, and R. Rafii-El-Idrissi, “Role of anisotropy in negative permeability and left-handed metamaterials,” Phys. Rev. B, vol. 65, pp 1-6, 2002.

[12] V. M. Shalaev, W. Cai, U. Chettiar, H. -K. Yuan, A. K. Sarychev, V. P. Drachev, and A. V. Kildishev, “Negative index of refraction in optical metamaterials,” Optical Letters, 30, pp 3356-3358, 2005.

[13] S. Zhang, W. Fan, N. C. Panoiu, K. J. Malloy, R. M. Osgood, and S. R. J. Brueck, “Experimental demonstration of near-infrared negative-index metamaterials,” Physical Review Letters, 95(13), 137404, 2005.

[14] S. A. Shaikh, "Electromagnetic Band Gap Structures in MSA," in International Journal of Computer Applications, p. 0975-8887, 2014.

[15] H. Kogelnik, “Coupled-wave theory of distributed feedbacklasers,” in Appl. Phys, pp. 2327-2335, 1972.
[16] L. Brillouin, “Wave Propagation in Periodic Structures: Electric Filters and Crystal Lattices,” McGraw-Hill, New York, 1946.
[17] R. Sami, “Applications of Electromagnetic Band-Gap (EBG) Structures in Microwave Antenna Designs,” in Proc. of 3rd International Conference on Microwave and Millimeter Wave Technology, pp 528-31, 2002.
[18] R. Marqués, “An Introductory overview on right-handed metamaterials,” in Proc. the 27th ESA Antenna Workshop on Innovative Periodic Antennas, pp 35-41, 2004.
[19] R. Samii, “Electromagnetic Band Gap Structures in Antenna Engineering,” in Hand book, ISBN, 978-0-521-88991, 2008.
[20] D. Sievenpiper, “High-impedance electromagnetic surfaces with a forbidden frequency band,” IEEE Trans. Microwave Theory Tech, pp 2059-2074, 1999.
[21] F. Yang and Y. R. Samii, “Reflection phase characterizations of the EBG groundplane for low profile wire antenna applications,” IEEE Trans. Antennas Propag., vol. 51, pp. 2691-2703, 2003.
[22] W.E. Kock “Metallic delay lenses” Bell Syst Tech J 27:58–82, 1948.
[23] W.E. Kock “Metal lens antennas” Proc IRE 34:828–836, 1946.
[24] I. Awai, S. Kida and O. Mizue, “Very thin and flat lens antenna made of artificial dielectrics”, Korea-Japan Microwave Conference Proceedings, pp 177-181, 2007.
[25] J. R. Whinnery and S. Ramo, “A new approach to the solution of high-frequency field problems,” Proc. IRE, vol. 32, no. 5, pp. 284288, 1944.
[26] S. A. Schelkunoff and H. T. Friis, “Antennas: Theory and Practice,” John Wiley & Sons, Inc., New York, pp. 584-585, 1952.
[27] L. Peng, L. Ran, H. Chen, H. Zhang, J.A. Kong, T.M. Grzegorczyk, “Experimental observation of left-handed behavior in an array of standard dielectric resonators,” Phys. Rev. Lett. PRL 98, 157403, pp 157403-1-157403-4, 2007.
[28] T. Ueda, N. Michishita, M. Akiyama, T. Itoh, “Dielectric-resonator-based composite right left-handed transmission lines and their application to leaky wave antenna,” IEEE Trans. MTT 56(10), pp 2259-2269, 2008.
[29] X. Cai, R. Zhu, G. Hu, Experimental study for metamaterials based on dielectric resonators and wire frame. Metamaterials 2, pp 220-226, 2008.
[30] J. Wang, S. Qu, H. Ma, J. Hu, Y. Yang, X. Wu, “A dielectric resonator-based route to left-handed metamaterials,” Prog. Electromagnet. Res. B 13, pp 133-150, 2009.
[31] K. Wakino, T. Nishikawa, S. Tamura, and Y. Ishikawa, “Microwave band pass filters containing dielectric resonators with improved temperature stability and spurious response,” IEEE Microwave Theory and Techniques Symposium Digest, vol. 1, pp. 63-66, 1975.
[32] D. Kaifez and P. Guillon, “Dielectric Resonators,” Artech House, 1986.
[33] A. Karp, H. J. Shaw, and D K. Winslow, “Circuit properties of microwave dielectric resonators” IEEE Transactions on Microwave Theory and Techniques, vol. 16, no. 10, pp. 818-828, 1968.
[34] A. Okaya and L. F. Barash, “The dielectric microwave resonator,” Proc. IRE, vol. 50, pp. 2081-2092, 1962.
[35] W. R. Day, “Dielectric resonators as micro-strip circuit elements,” IEEE Microwave Theory and Techniques Symposium Digest, vol. 1, pp 24-28, 1970.
[36] S. B. Cohn, “Microwave band-pass filters containing high-Q dielectric resonators,” IEEE Transactions on Microwave Theory and Techniques, vol. 16, no. 4, pp 218-227, 1968
[37] P. Guillon, J. P. Balabaud, and Y. Garault, “TM_{olp} tubular and cylindrical dielectric resonator mode,” IEEE Microwave Theory and Techniques Symposium Digest, vol. 1, pp. 163-166, 1981.
[38] J. K. Plourde, and D. F. Linn, “Microwave dielectric resonator filters utilizing $Ba_2Ti_9O_{20}$ ceramics,” IEEE Microwave Theory and Techniques Symposium Digest, vol. 1, pp 290-293, 1977.
[39] R. V. Snyder, “Dielectric resonator filters with wide stop-bands,” IEEE transactions on Microwave Theory and Techniques, vol. 40, no. 11, pp. 2100-2103, 1992.
[40] B. Byzery and P. Guillon, “$TM_{0\delta\gamma}$ mode of cylindrical dielectric resonators applications to microwave filters,” IEEE Microwave Theory and Techniques Symposium Digest, vol. 1, pp. 515-518, 1985.
[41] P. Skalicky “Direct coupling between two dielectric resonators,” Electronics Letters, Vol. 18, No. 8, pp 332-334, 1982.
[42] S. B. Cohn, “Microwave band-pass filters containing high-Q dielectric resonators,” IEEE transactions on Microwave Theory and Techniques, vol. 16, no. 4, pp. 218-227, 1968.

[43] A. Ahmadi, and H. Mosallaei, "Physical configuration and performance modeling of all dielectric metamaterials," Phys. Rev. B, Vol. 77, 045104, 2008.
[44] D. Kajfez and P. Guillion, "Dielectric Resonators," Artech House, Norwood, pp. 327-376, 1986.
[45] Kobayashi Y. and Minegishi K, "precise design of a band pass filter using high-Q dielectric ring resonators;" IEEE Trans. Microwave Theory Tech.; Vol. MTT-35; pp. 1156-1160, 1987.
[46] K. A. Zaki, C. Chen and A.E. Ati, "Canonical and longitudinal dual mode dielectric rsonator filters without iris;" IEEE Trans. Microwave Theory Tech., Vol. T-35; pp 1130-1135, 1987.
[47] J. Hong and M.J. Lancaster, "Coupling of microstrip square open-loopresonators for cross-coupled planar microwave filters," IEEE Trans Microwave Theory Techniques 44, pp 2099-2109, 1996.
[48] C.R. Buffler, "Microwave Cooking and Processing," Van Nostrand Reinhold, New York, 1993.
[49] P.O. Risman. "Terminology and notation of microwave power and electromagnetic energy." J Microw Power Electromagn Energy, 26, pp 243-50, 1991.
[50] B. Hakki and P. Coleman, "A dielectric resonator method of measuring inductive capacities in the millimeter range," Microwave Theory and Techniques, IRE Transactions on, vol. 8, pp 402-410, 1960.
[51] Y. Kobayashi, and M. Katoh, "Microwave measurement of dielectric properties of low-loss materials by the dielectric rod resonator method, "Microwave Theory and Techniques, IEEE Transactions on, vol. 33, pp 586-592, 1985.
[52] J. K. Plourde, and D. F. Linn "Microwave Dielectric resonator filters utilizing $Ba_2Ti_90_{20}$ Ceramic" Proceedings of the IEEE International Microwave Symposium, San diago, p. 290, 1977.
[53] A.A. Trubin, "Scattering of electromagnetic waves on the systems of coupling dielectric resonators," Radio Electron, pp 35–42, 1997.
[54] F.Martin, "A new split ring resonator based left handed coplanar waveguide," in Appl. Phys.lett, 2003, p. 4652–4654.
[55] D. M. Pozar "Microwave Engineering," John Willey, 1998.
[56] R.M. Foster "A reactance theorem," Bell System Technical Journal, pp.259-67, 1924.
[57] Ian Hunter, "Theory and design of Microwave Filters", The Institution of Electrical Engineering, IEE Electromagnetic Waves Series 48, University Press, Cambridge, 2001.
[58] X. Xiaoming, and R. Sloan, "Distributed coupling model of the dielectric resonator to microstrip line," IEEE Microwave and Guided Wave Letters, vol. 9, pp. 348-350, 1999.
[59] A. E. Atia and R.W. Newcomb, "Narrow band multiple coupled cavity synthesis," IEEE Trans. Circuits and System, vol. CAS-21, no. 5, p. 649-655, 1974.
[60] Y.-P. Zhang, T.K.-C. Lo, and Y.-M. Hwang, "A dielectric-loaded miniature antenna for micro-cellular and personal communications," in Proceedings of the IEEE AP-S Symposium, 1995, p. 1152–1155.
[61] K. Chang and L. H. Hsieh, "Measurement applications using ring resonators," in Microstrip filters for RF microwave application, John Willey & Sons, Inc., New Jersey 2004.
[62] R. Marques, J. Baena, J. Martel, F. Medina, F. Falcone, M. Sorolla, and F. Martin, "Novel small resonant electromagnetic particles for metamaterial and filter design," in Proc. ICEAA, Torino, , pp. 439-443,2003.
[63] A. S. Curnmer, B. L. Popa and T. H. Hand, "Q-based design equations and loss limits for resonant metamaterials and experimental validation," IEEE Ant. Wireless Prop. Lett., vol. 56, no. 1, pp. 127-132, Jann. 2008.
[64] J. García-García, F. Martín, J. D. Baena, R. Marqués and L. Jelinek, "On the resonances and polarizabilities of split ring resonators," J. Appl. Phys., vol. 98, p. 033103, 2005.
[65] J. García-García, J. Bonache, I. Gil, F. Martín, M.C. Velazquez-Ahumada and J. Martel. "Miniaturized microstrip and CPW filters using coupled metamaterial resonators." IEEE Transactions on Microwave Theory and Techniques.54 - 6, pp. 2628-2635, 2006.
[66] J. García-García; Martín, F.; Falcone, F.; Bonache, J.; Gil, I.; Amat, E.; Lopetegi, T.; Laso, M.A.G.; Iturmendi, J.A.M.; Sorolla, M.; Marqués, R. "Microwave Filters with Improved Stop band based on Sub-wavelength Resonators," IEEE Transactions on Microwave Theory and Techniques.53 - 6, pp 1997-2006, 2005.
[67] Jia-Sheng Hong & M.L. Lancaster, "Microstrip Filters for RF/Microwave Applications", John Willey & Sons, Inc., New York 2001.

[68] L.X. Ma, J. G. Ma, K. S. Yeo and M. A. Do "A compact size coupling controllable filter with separated electric and magnetic coupling paths," IEEE Trans. Microwave Theory Tech., Vol. 54, No. 3, pp 1113-1119, 2006.

[69] Awai, I., A. C. Kundu, and T. Yamashita, "Equivalent circuit representation and explanation of attenuation poles of a multimode dielectric-resonator bandpass filter," IEEE Trans. Microwave Theory Tech., Vol. 46, 2159-2163, 1998.

[70] Revision of Part 15 of the Commission's Rules Regarding Ultra-wideband Transmission Systems.ET-Docket 98-153, First Note and Order. Federal Communication Commission (FCC). Feb. 14 2002.

[71] Z. C. Hao and J. S. Hong, "Ultra-wideband filters technologies" IEEE Microw. Mag, Vol. 11, No. 4, pp 56-68, 2010.

[72] L. Zhu, S. Sun, and W. Menzel, 'Ultra-wideband (UWB) bandpass filter using multiple-mode resonator', IEEE Microwave Wireless Compon Lett, Vol 15, No, 11, pp 796-798, 2005

[73] S. W. Wong and L. Zhu, "Quadruple-mode UWB bandpass filter with improved out-of-band rejection", IEEE Microwave Wireless Compon. Lett, Vol, 19, No, 3, pp 152–154, 2009.

[74] S. W. Wong and L. Zhu, "Quadruple-mode UWB bandpass filter with improved out-of-band rejection," IEEE Microwave Wireless Compon. Lett, Vol, 19, No, 3, pp. 152-154, 2009.

[75] L. Han, K. Wu, and X. Zhang, "Development of packaged ultra-wide band bandpass filters", IEEE Trans. Microwave Theory Tech, Vol.58, pp 220–228, 2010.

[76] R. Li and L. Zhu, "Compact UWB band-pass filter using stub loaded multiple-mode resonator," IEEE Microwave Wireless Compon Lett., Vol.17, pp 40–42, 2007.

[77] K. Song and Y. Fan, "Compact ultra-wideband bandpass filter using dual-line coupling structure", IEEE Microwave Wireless Compon. Lett, 19, pp 30–32, 2009.

[78] Z. Shang, X. Guo, B. Cao, V. Wei, X. Zhang, Y. Heng, G. Suo, and X. Song. "Design of a Superconducting Ultra-Sideband (UWB) Bandpass Filter with Sharp Rejection Skirts and Miniaturized Size" IEEE Microwave and Wireless Comp. Lett., 23, (2), pp.72-74, 2013.

[79] H. Ishida and K. Araki, "Design and analysis of UWB bandpass filter with ring filter", in IEEE MTT-S Int. Dig., 3, pp. 1307–1310, 2004.

Chapter 5

5 Conclusions and future work

In this thesis, new strategies for miniaturization of microwave filter have been proposed. For this reason dielectric resonators as a new type of metamaterial concept have been considered which these DRs provide small dissipative losses.
The size of DR filter is considerably smaller than the dimension of waveguide filters operate at the same frequency. For a given dielectric constant, both resonant frequency and Q-factor are defined according to the dielectric resonator dimensions. That, the higher the dielectric constant, the smaller the space within which the fields are concentrated, the lower the dimension at a defined frequency.
The contents of this work have been divided into four chapters. Once the motivation and general objectives were pointed out in chapter 1, the specific objectives and achieved goals of each chapter are listed below

In chapter 2, a brief theory of microwave filters based on passive components has been presented, with special emphasis on transmission lines and resonators. Since, these theoretical concepts are used in the thesis.

In chapter 3 the dielectric resonators descriptions and different ways to deal with these elements in the design process has been studied. Since, higher the dielectric constant cased the lower dimension at a defined frequency, by given dielectric constant, both resonant frequency and Q-factor are defined according to the dielectric resonator dimensions. The experimental and fabrication process for epoxy/$BaTiO_3$ composite is investigated in this chapter.

In chapter 4 the basic MTMs concepts have also been introduced, providing all the theory and tools that were required in the following sections, including the planar transmission line, electromagnetic band gap and the split ring resonator concept. Development of the scattering theory of electro-magnetic waves on the DRs, located in the various positions of transmission lines carried out in this chapter.

Different applications have been investigated by designing, fabricating and characterizing different prototypes, which are reported as follow:

- A novel stop-band filter consists of three cylindrical dielectric resonators were excited with a microstrip line has been investigated. The proposed design shows the ability of the thick film high dielectric constant resonators to be used as passive elements for the design passive elements in the range of Ku band. The resonator physical complex behavior leads to the utilization of full 3D electromagnetic software to the design of devices based on these resonators. The proposed structure points out the possibility of using TFDR for the creation of EBGs.
- A novel design combining standard microstrip resonators with high dielectric constant resonators, for design of band-pass filtering electromagnetic band gaps (EBG) structures, operating in the range from 1 to 20 GHz has been investigated. The basic cell of the EBG is composed by a standard microstrip ring and a DR embedded (EDR) in the PCB, in such a way that the microstrip ring act as a feed structure for some of the dielectric resonator resonant modes. The DR is generated depositing commercial high dielectric constant Epoxy paste (CREATIVE 122-06 pad-printable high dielectric constant epoxy paste, with a value of ε_r=45). The technological process is compatible with Low Temperature Cofired Ceramics (LTCC) technology. The proposed structure points out the possibility of using DR for the creation of EBGs.
- A new SRR band-pass filter based on EDR high dielectric resonator has been reported which applied to the miniaturization of passive microwaves devices. Measured of a 19.4% band pas filter at 1.6 GHz is compared with EM simulation and equivalent circuit model has been showed an excellent agreement.

- A novel multimode resonator (MMR) ultra-wide band-pass (UWB) filter design using a grounded open ring resonator has been presented. Five resonant modes are used to perform a 128% fractional bandwidth at 4.3 GHz. The fabricated prototype exhibits a band-pass with insertion losses around 0.5 dB. A theoretical model based on transmission lines matrices has been proposed and used to explore the limits of the design through different parametric analysis. Excellent agreement between theoretical predictions, electromagnetic simulations and measurement are found.

The study undertaken in this thesis revealed that some further developments may be of interest in future research lines. Some general suggestions are outlined below:

- TFDR and EDR as high dielectric resonator could be implemented for miniaturization of MTMs and various microwave components. Further work is under development to improve the utilization of EDR in planar devices.

- Another interesting topic to be investigated relates to increase the number of resonators in the filters which leads to improvement of the S-matrix parameters. Although, by increasing the number of resonators, costs, dimensions, computation difficulties, could be problems of practical tuning.
  The design of stop-band TFDRs filter with high dielectric constant based on more than 3 numbers of cylindrical DRs which are mounted in a planar substrate could be studied to obtain a good resonant frequency. Example of stop-band pass filter with 20 cylindrical DRs lattices in the propagating rectangular metal waveguide is shown in Fig 4.49 [1], it was fabricated from dielectric material: $\varepsilon r=36$, $Q_D=2500$, situated on the axis of symmetry of the propagating rectangular metal waveguide of section $a\times b=58\times25$ mm^2. The distance between adjacent DR centers are equal to a quarter of guided wavelength $\lambda_0/4$ on the central frequency ω_0.

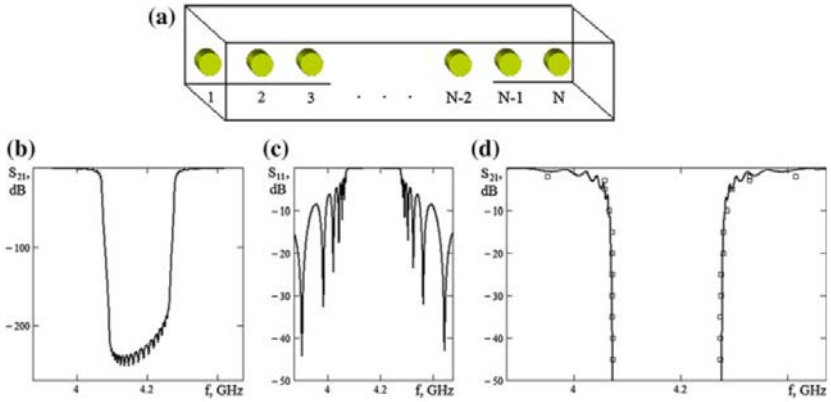

Fig. 4. 49 N Cylindrical DR system on the symmetry axis of propagating rectangular metal waveguide (a) S-parameters of the band-stop filter on 20 cylindrical DRs (b, c) Comparison of theoretical calculations and measured results (d) of the 20 DR band-stop filter. Relative dielectric permittivity of the DRs is $\varepsilon_r = 36$ and the relative dimensions is $\Delta = L/2\ r_0 = 0.44$. Here r_0 is the radius and L is the height of each cylindrical DRs [1].

- Further investigation in order to design a wideband ban-pass DRs filter, could be implemented with number of resonators more than 3. The design of pass-band DRs filter with high dielectric resonator based on more than 3 numbers of DRs which are embedded on PCB could be investigated to obtain wideband width and miniaturized device. Example of pass band filter with 20 cylindrical DRs lattices in the propagating rectangular metal waveguide is shown in Fig 4.50 [80]. It was fabricated from dielectric material: $\varepsilon r=80$, $Q_D=2000$, situated on the axis of symmetry of the propagating rectangular metal waveguide of section $a \times b = 58 \times 25\ mm^2$. It is supposed that all resonators excited on basic magnetic mode. The distance between adjacent DR centers are equal to a quarter of guided wavelength $\lambda 0/4$ on the central frequency $\omega 0$.

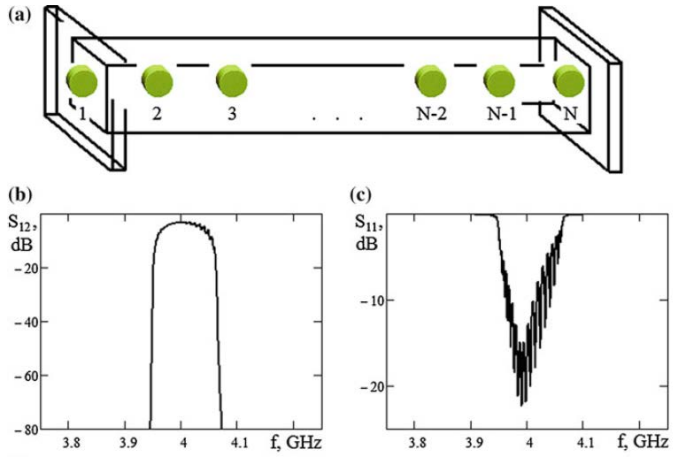

Fig. 4. 50 Frequency responses (b, c) of the 20 cylindrical DRs inserted in the segment of evanescent rectangular waveguide (a) Every DR excited on basic magnetic mode Relative dielectric permittivity of the DRs is ε_r= 80, Q_D=2000 and the relative dimensions is Δ=L/2 r_0 =0.2. Here r_0 is the radius and L is the height of each cylindrical DRs [1].

Another topic can be considered in the further work is a multi-mode resonator by using proposed MMR-UWB filter. This can be done by changing lengths of coupled lines, which resonant modes could be changed. From theoretical point of view, that is predicted, the band-pass can be increase by decreasing coupled line lengths.

Additional research lines based on MTMs concepts and miniaturization of microwave device are being studied in the research group GAEMI to which the author belongs.

[1] A. Trubin “Lattices of Dielectric Resonators,” Springer International Publishing Switzerland. Vol, 53. ISSN 1437-0387, 2016.

Appendix A

Abbreviations and acronyms

RF	Radio frequency
DR	Dielectric resonator
TEDR	Thick-film embedded dielectric resonator
EDR	Embedded dielectric resonator
Q	Quality factor
TE	Transverse electric
TEM	Transverse electromagnetic
TM	Transverse magnetic
SRR	Split ring resonator
RH	Right-handed
RL	Return losses
LH	Left-handed
LTTC	Low-temperature co-fired ceramic
MTM	Metamaterial
MIC	Microwave integrated circuits
NB-SRR	Non-bianisotropic split ring resonator
OCSRR	Open complementary split

	ring resonator
OSRR	Open split ring resonator
BST	Barium-strontium-titanate
IL	Insertion losses
LCP	Liquid crystal polymer
CRLH	Composite right-/left-handed
D-CRLH	Dual- composite right-/left-handed
EBG	Electromagnetic band gap
EM	Electromagnetic
CPW	Coplanar waveguide
CSR	Complementary spiral resonator
CSRR	Complementary split ring resonator

List of Principal Symbols

Note: In the text of the thesis, some symbols is followed by one or several subscripts, defining for example the region of the resonator or the mode to which the symbol applies.

B, B'	Susceptance value
c	Speed of light in vacuum
C	Capacitor value
D	Diameter of cylindrical dielectric resonator
$d\omega$	Angular bandwidth of filter
E	Electric field
E_x	Electric field component in the x direction
H	Magnetic field
H_x	Magnetic field component in the x direction
In	Modified Bessel function of order n
Ji-1,i ,	Admittance of inverter between nodes i-1 and i
Jn	Bessel function of the first kind of order n
k	Wave number
k_o	Wave number in free space
k_{yn}	Wave number of a mode in waveguide n in the y direction
Q_C	Quality factor due to conductor losses
Q_d	Quality factor due to dielectric losses
Q_u	Unloaded Q factor
$\tan\delta$	Loss tangent of material

Z(p)	Input impedance
Ze, Zo.	Even and odd mode impedance of network
ε	Permittivity of the medium $\varepsilon = \varepsilon' - j\varepsilon''$
ε_0	Vacuum permittivity
ε_r	Relative permittivity of the medium
λ	Wavelength
λ_0	Wavelength in free space
μ_0	Vacuum permeability
σ	Conductivity of the material
ω	Angular frequency
ω_0	Angular resonant frequency
ω_c	Cut-off angular frequency

Appendix B

Author list of publications

International Journals and International Conferences

1- Bahareh. Moradi, Ursula Martinez, Oriol Ymbern, Cynthia Martinez, Julian Alonso, and Joan. Garcia-Garcia, “New approach to electronic band gap filtering structures combining microstrip and dielectric resonators”, 2013 Asia-Pacific Microw. Conf. Proc. (APMC), pp 417-419, 2013.

2- Bahareh Moradi, Ursula martinez, and Joan Garcia Garcia. “Additional cross coupling coefficient used as matching ladder network in coupled based band pass Filters.” Progress in Electromagnetics Research Symposium Proceedings, 1, Cambridge, MA: [Electromagnetics Academy], 01/08/2014. ISSN 1559-9450 Type of production: Article Type of platform: Journal.

3- Úrsula Martínez Iranzo, Bahare Moradi and Joan Garcia Garcia, “Compact Chipless RFID Tag based on Open Riong resonator spectrum” International Microwave Symposium, Conference, Poster, Phoenix, United States of America, 2015.

4- Bahareh moradi, Ursula Martinez, and Joan Garcia Garcia. “Electronic Band Gap filtering structures combining Microstrip and Dilectric Resonators” Progress in Electromagnetics Research Symposium, Stockholm, Sweden, 2013.

5- Ursula Martinez-Iranzo, Bahareh Moradi and Joan Garcia-Garcia “Design of passive filters using dual-mode embedded dielectric resonator” 10th Conference on Ph.D. Research in Microelectronics, Grenoble, France, 2014.

6- Ursula Martinez-Iranzo, Bahareh Moradi, and Joan Garcia-Garcia “Ultra-wide-band band-pass filter based on coupled electromagnetic band gap structure” Microwave and Optical technology letters, Vo.57, No. 12, 2015.

7- Bahareh moradi, Ursula Martinez, Joan Garcia Garcia. “Multimode Ultra-Wideband filters by using a Grounded Open Ring Resonator,” Microwave and Optical technology letters, submitted. 2016
8- Úrsula Martínez Iranzo, Bahareh Moradi, and Joan Garcia Garcia “Left-Handed Transmission Lines Equivalent Circuit Model Based on ABCD Matrices” Progress In Electromagnetics Research Symposium, conference Prague, Czech Republic, 2015.

EBG filtering structure using Thick film high dielectric constant resonators

B. Moradi, O. Ymbern, C. Martinez, J. Alonso and J. Garcia-Garcia

This paper reports the design lines of a Low-pass filtering EBG structure operating in the Ku band using thick film high dielectric constant resonators. The design is based on a microstrip line periodically loaded with a new kind of dielectric resonator fabricated with a commercial high dielectric constant EPOXY paste compatible with serigraphy and screen printing technology. The geometry of the ressonator has been chosen in such a way that the filtering structure appear below the first resonator resonant frequency. An equivalent circuit model of the proposed structure is discussed and compared with electromagnetic simulations and measurements.

Introduction: Periodically loaded waveguide constitutes a well new by known method to synthesize band pass and low-pass filters in the microwave theory [1, 2]. In this paper, we propose thick film dielectric resonators (TFDR) to implement loads on a microstrip line, compatible with screen printing, serigraphy and LTCC technologies [3]. Moreover, dielectric resonators have been widely studied and applied to the design of the microwave communication systems from the beginning of the activity in the field [3]. Although, an equivalent circuit model can be used to describe the basic behavior of the resonator structure, the complexity of the physical behavior (with multiple resonator modes) overwhelms the description by any equivalent circuital model, being necessary a full 3D numerical analysis to optimize the final design. The first resonant frequency of the TFDR used in the proposed design is determined by the cylindrical geometry as well as the value of the dielectric permittivity of the resonator material. CREATIVE 122-06 pad-printable high dielectric constant epoxy paste, characterized by a value of εr=45 has been used to point out the possibility of using commercial dielectric pastes.

The dielectric resonator: The utilization of high dielectric constant films allows the miniaturization of both active and passive components reducing the losses [4]. The existence of surface modes in high dielectric constant thick layers has been reported by some of the authors in previous works [5]. TFDR resonant frequencies depend on of both geometrical and dielectric constant values, however, the more important parameter for the resonance frequency is the relative permittivity. Fig. 1 shows the simulated first mode resonant frequency as a function of the relative permittivity. The geometry of the proposed TFDR consists of a flat cylinder with 0.6 mm height and 1 mm radius. The resonant frequency plotted in Fig. 1, have been estimated using the Agilent-Empro full 3D EM simulator. The dielectric paste used in the proposed structure εr=45 is in the extreme of the Fig. 1 graph highlighting the miniaturization possibilities as far as the dielectric constant increases. Higher values of dielectric constant can be found in the literature for noncommercial ink and pastes, especially for those containing BaTiO3 [6, 7], however, commercial solutions for both ink and paste rarely have dielectric constants above 50. It can be shown that the approximate impedance of a passive resonator can be obtained as a partial expansion of the generic impedance function displayed in (1) [8, 9].

$$z(j\omega) = jX(\omega) = j\left[A_\infty \omega - \frac{A_0}{\omega} + \sum_{i=1}^{m} \frac{2 \cdot A_i \cdot \omega}{\omega_i^2 - \omega^2}\right] \quad (1)$$

According with the Foster synthesis [8], the equivalent circuit model of the passive resonator should be described with the network depicted in Fig. 2 , where $CS=1/A_o$, $Ls=\underline{A}_\infty$, $C_{pi}=1/2\ A_i$, $Lpi= 2\ A_i/\ \omega^2 i$.

In our case, the resonators are used below their first resonant frequency to implement the EBG loads being enough to consider a single series LC branch to fit the filtering pattern exhibited by the experimental data, and therefore to obtain a reasonable description of the dielectric resonator in this frequency range as it will be showed in the following

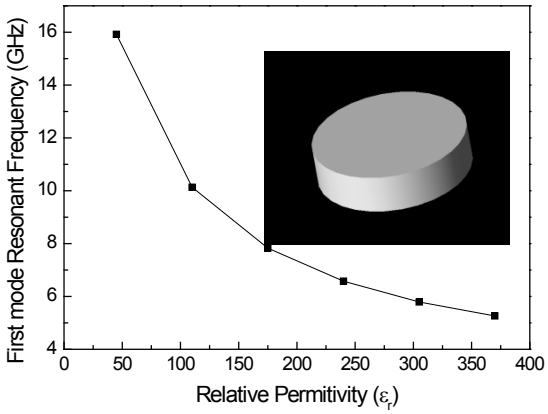

Fig. 1 *Simulated relation between the first resonant mode frequency and the dielectric constant. The simulated values have been obtained by using Agilent-Empro 2012.09 software. The cylindrical resonator is 0.6 mm thick with a radius of 1 mm.*

The utilization of higher dielectric constant inks will result in the reduction of the operating frequency as well as a relaxation of the minimum thickness needed to hold resonances and therefore a miniaturization of the resonator. In the case of εr=45 a minimum value of 0.6 mm has been fixed according to 3D EM simulation results. Notice that the resonant frequency is ruled basically by the dielectric constant value and not for the geometry. In our design the geometrical dimensions are applied to obtain a single resonator mode.

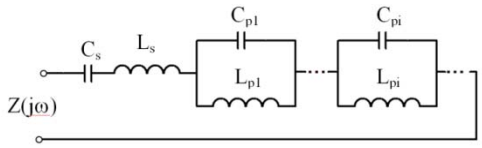

Fig. 2 *Foster synthesis of equivalent circuit model for any generic passive resonators [8].*

The filtering structure: The electronic band gap has been used as an effective way to create microwave filters. In our case the structure is a microstrip periodically loaded with resonators that can be characterized as series LC branch (showed in Fig. 3).

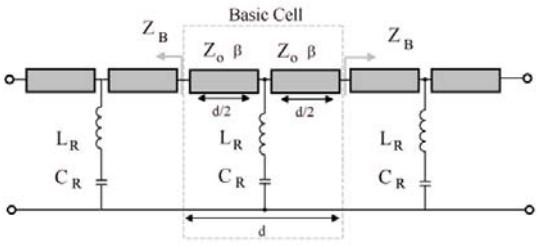

Fig. 3 *EGB filter structure where the grey boxes represent the microstrip host transmission line determined by the length of the basic cell d, the propagation constant β and the characteristic impedance Zo, and the dielectric resonator is modelled by the series LR-CR branch.*

The microstrip host transmission line characteristic impedance Zo and propagation constant β can be analytically evaluated from the dimensions of the microstrip line and the physical properties of the substrate which in our case is the 25 mils Rogers RO3010.

It can be shown that for a symmetrical passive structure, the dispersion equation is ruled by the equation (2) [1]

$$\cos(\beta d) = \cos\left(\frac{k_0 d}{2}\right) - \frac{\omega^2 L_R C_R - 1}{\omega C_R} sin\left(\frac{k_0 d}{2}\right) \qquad (2)$$

Where β is the propagation constant of the periodic structure, k0 is the propagation constant of the microstrip host line, d is the basic cell length and the lumped elements of the equivalent circuit model ok the resonators are LR and CR. The confinement of the right hand of (2) between -1 and 1 will determine the transmission bands. In the presented case it corresponds to a low-band filtering structure with successive spurious bands.

Fabrication process: The used substrate for the host line is a 25 mil thickness Rogers RO3010 with a εr=10.2 and a loss tangent δ=0.0022 at the operating frequencies. Several layers of the Creative 122-06 dielectric have been deposited by means of in home fabricated masks until a thickness of 0.6 mm have been achieved in the resonators. The structure has been in a conventional oven at 150ºC for one hour. Fig. 4 shows the fabricated device.

Fig. 4 *Picture of the fabricated prototype.*

Measurements and discussion: The measurements of the fabricated prototype has been done using a Vectorial Analyzer and the results has been used to generate the two-port touchstone file format which has been used in ADS software to compare with equivalent circuit model of the structure. As can be observed in figure 5 the proposed equivalent circuit model offers an excellent fit of the measurements for LR=0.25 nH and CR= 0.07 pF.

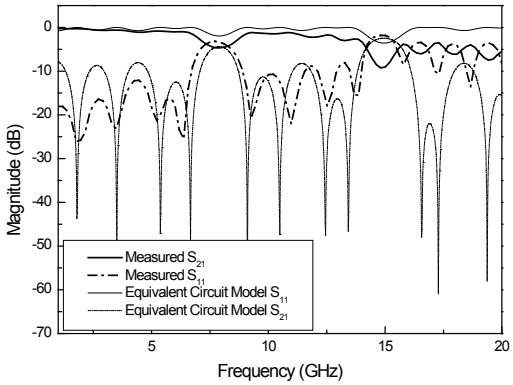

Fig. 5 *Measured S-parameter for a 3 stage EBG fitted with the equivalent circuit model showed in Fig. 3.*

Fig. 5 illustrates the measured response of the prototype which clearly exhibits the EBG behaviour.Conclusion: This paper shows the ability of the thick film high dielectric constant resonators to be used as passive elements for the design passive elements in the range of Ku band. The resonator physical complex behaviour leads to the utilization of full 3D electromagnetic software to the design of devices based on these resonators. The proposed structure points out the possibility of using TFDR for the creation of EBGs. Further work is under development to improve the utilization of TFDR as resonators in planar devices.

Acknowledgments: This work has been supported by Ministerio de Ciencia y Educación of the Spanish government under the project TEC2010-16060.

Information on Author affiliations:B. Moradi, and J. Garcia-Garcia (Grupo de Aplicaciones Electromagnéticas Industriales-GAEMI, Departament d'Enginyeria Electrònica de la Universitat Autònoma de Barcelona, Campus de Bellaterra, 08208 Cerdanyola del Vallés, Barcelona, Spain). corresponding author E-mail: Bahareh.moradi@uab.es.

O. Ymbern, C. Martinez, J. Alonso (Grupo de Sensores y Biosensores, Departamento de Química Analítica de la Universitat Autònoma de Barcelona, Campus de Bellaterra, 08208 Cerdanyola del Vallés, Barcelona, Spain)

References

[1] David M. Pozar, “Microwave Engineering”, John Willey & Sons, Inc. New Cork 1998.
[2] Jia-Sheng Hong & M.L. Lancaster, “Microstrip Filters for RF/Microwave Applications”, John Willey & Sons, Inc., New York 2001.
[3] S. Jerry Fiedziuszko, Ian C. Hunter, Tatsuo Itoh, Fellow, Yoshio Kobayashi, Toshio Nishikawa, Steven N. Stitzer, and Kikuo Wakino, , "Dielectric Materials, Devices, and Circuits", IEEE Trans. Microwave Theory & Tech., vol. 50, no. 3, pp. 706-720, March 2002.
[4] J. I. Marulanda, M. Cremona, R. Santos, M. C. R. Carvalho, and L. S. Demenicis, " Characterization of SrTiO3 thin films at microwave frequencies using coplanar waveguide resonator method", Microwave and Optical Tech. Letters, vol. 53, no. 10, pp. 2418-2422, 2011.
[5] J.; Ocampo, J.; Martinez, C.; Alonso, J. Garcia-Garcia, "Thick film high dielectric constant resonators", Microwaves, Communications, Antennas and Electronics Systems (COMCAS), 2011 IEEE eInternational Conference on, Tel Aviv Israel, Page(s): 1 - 3
[6] M. T. Sebastian, and H. Jantunen, "Low losss dielectric materials for LTCC applications: a revview", International Materials Reviews, vol. 53, nº 2, pp: 57-90, 2008.
[7] X. Lu, Y. Lee, S. Yang, Y. Hao, R. Ubic, J.R.C. Evans, and C. G. Parini, "Fabrication of Millimeter-Wave Electromagnetic Bandgap Crystals using Dielectric Powders" J. Am. Ceram. Soc, vol 2, pp. 371-378, 2009.
[8] Foster R.M. “A reactance theorem”, Bell System Technical Journal, (3), pp.259-67, 1924.
[9] Ian Hunter, “Theory and design of Microwave Filters”, The Institution of Electrical Engineering, IEE Electromagnetic Waves Series 48, University Press, Cambridge 2001.

New approach to Electronic Band Gap filtering structures combining Microstrip and Dielectric Resonators

Bahareh.Moradi[1], Ursula.Martinez-Iranzo[1], Oriol. Ymbern[2], Cynthia. Martinez[3], Julian Alonso[2] and Joan Garcia-Garcia[1]
[1]Departament of Electronic Engineering, [2]Department of Analytical Chemistry, [3]Institute of Integrative Nanosciences , [1,2]Autonomous University of Barcelona, Campus of Bellaterra, 08208 Cerdanyola del Vallés, Barcelona, Spain, [3]Helmholtzstrasse 20, 01069 Dresden, Germany
Corresponding author E-mail: bahareh.moradi@e-campus.uab.cat

***Abstract* — A novel design combining standard microstriptechnology with single ring resonator and high dielectric constant resonator for design of low and band pass filtering electromagnetic band gap(EBG) structures, operating in the range from 1 to 20 GHz is presented in this paper. The design is based on a high dielectric constant resonator embedded in a microstrip structure substrate. The dielectric resonator is fabricated by using commercial high dielectric constant EPOXY paste in a process compatible with serigraphy and screen printing technology.**
Index Terms —resonators, passive microwave circuits, microstrip, dielectric resonators

I. INTRODUCTION

Filters have a wide range of applications such as wireless systems, radio frequency (RF), television and satellite broadcast, mobile communications, broadband microwave, millimeter-wave communication systems, radars and many other systems related to the information telecommunication, which makes them so interesting to develop novel technologies. Since micro-strip has a compact size, light weight, planar structure and is easy to integrate with other component, being much less expensive than traditional waveguide technology it is a very attractive technology to design of filters. On the other hand, periodically loaded waveguide constitutes a well-known method to synthesize band pass and low-pass filters in the microwave theory [1]-[2]. In this paper, it is proposed, a novel design combining standard micro-strip resonators with high dielectric constant resonators, for design of low-pass and band-pass filtering electromagnetic band gaps (EBG) structures, operating in the range from 1 to 20 GHz.
The basic cell of the EBG is composed by a standard microstrip ring resonator and a Dielectric Resonator (DR) embedded in the microstrip PCB, in such a way that the micro-strip ring act as a feed structure for some of the DR resonant modes. Moreover, dielectric resonators have been widely studied and applied to the design of the microwave communication systems from the beginning of the activity in the field [3]. Although, an equivalent circuit model can be used to describe the basic behavior of the resonator structure, the complexity of the physical behavior (with multiple resonator modes) overwhelms the description supplied by any equivalent circuital model, being necessary a full 3D numerical analysis to optimize the final design. The first resonant frequency of the DR used in the proposed design is determined by the cylindrical geometry as well as the value of the dielectric permittivity of the resonator material. CREATIVE 122-06 pad-printable high dielectric constant epoxy paste, characterized by a value of ε_r=45 has been used in the design pointing out the possibility of using commercial dielectric pastes.
The fabrication process of such structure is compatible with screen printing, serigraphy and LTCC technologies [3].
The first resonant frequency of the DR used in the proposed design is determined by the cylindrical geometry as well as the value of the dielectric permittivity of the resonator material. The utilization of high dielectric constant films allows the miniaturization of both active and passive components reducing the losses [4]. The existence of surface modes in high dielectric constant thick layers has been reported by some of the authors in previous works [5]. DR resonant frequencies depend on of both geometrical and dielectric constant values; however, the more important parameter for the resonance frequency is the relative permittivity. The geometry of the proposed structure, consists in a 3 cells EBG each one formed by a cylindrical DR with 2 mm diameter and 1.27 mm height, and 1.3 mm width microstrip ring resonator with an inner radius of 2.3 mm. It can be shown that the impedance of a passive resonator can be obtained as a partial expansion of the generic impedance function displayed in (1) [6, 7].

$$z(j\omega) = jX(\omega) = j\left[A_\infty \omega - \frac{A_0}{\omega} + \sum_{i=1}^{m} \frac{2 \cdot A_i \cdot \omega}{\omega_i^2 - \omega^2}\right]$$

According with the Foster synthesis [6], the equivalent circuit model (1) can be reproduced as an infinite series of LC parallel tanks with a series LC resonator. The parameter values can be obtained by fitting measures obtaining a reasonable agreement between both.

II. THE FILTERING STRUCTURE

The electronic band gap has been used as an effective way to create microwave filters. In our case the structure is a microstrip periodically loaded with resonators that can be characterized as series LC branch. (Showed in Fig. 1)

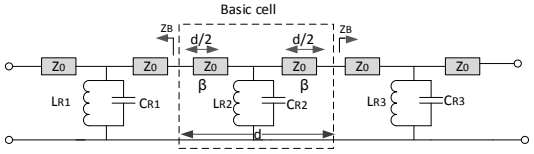

Fig. 1. EGB filter structure where the grey boxes represent the micro-strip host transmission line determined by the length of the basic cell d, the propagation constant β and the characteristic impedance Zo, and the dielectric resonator is modeled by the series LR-CR branch.

The microstrip host transmission line characteristic impedance Z_o and propagation constant β can be analytically evaluated from the dimensions of the microstrip line and the physical properties of the substrate which in our case is the 50 mil Rogers RO3010.
It can be shown that for a symmetrical passive structure, the dispersion equation is ruled by the equation (2) [1]

$$\cos(\beta d) = \cos(k_0 d) - \frac{(1-\omega^2 L_R C_R)}{2\omega L_R} sin(k_0 d) \qquad (2)$$

where β is the propagation constant of the periodic structure, k_0 is the propagation constant of the microstrip host line, d is the basic cell length and the lumped elements of the equivalent circuit model of the resonators are L_R and C_R. The confinement of the right hand of (2) between -1 and 1 will determine the transmission bands. In the presented case it corresponds to a low-band filtering structure with successive spurious bands.

III. FABRICATED PROCESS

The 50 mil Roger substrate used for the host micro-strip is characterized by a loss tangent δ=0.0022 and ε_r=10.2 at the operating frequencies.
Layers of the Creative 122-06 dielectric have been deposited until a thickness of the substrate has been achieved in the resonators. The structures have been in a conventional oven at 150ºC for one hour.
The dielectric paste used in the proposed structure and PCB embedded with DR is in the extreme of the Fig. 2, an illustrative example of a band pass filter that is embedded with DR and the response of the frequency is around 2.1 GHz.

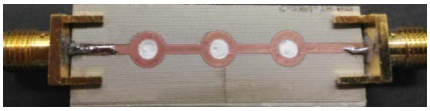

Fig. 2. Picture of the fabricated prototypes that was embedded with DR

IV. MEASUREMENTS AND DISCUSSION

The measurements of the fabricated prototype embedded with DR has been done using a Vectorial Analyzer and the results has been used to generate the two-port touchstone file format which has been used in ADS software to compare with equivalent circuit model of the structure. As you can see in Fig .3 the measured response of the prototype clearly exhibits the EBG behavior.

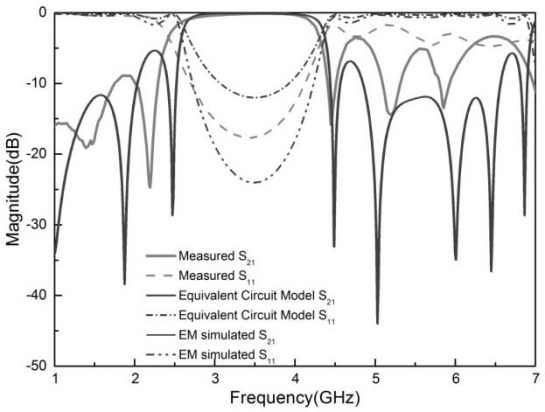

Fig. 3. Measured S-parameter for a band pass EBG fitted with the equivalent circuit model showed in Fig. 1.

The frequency responses are verified by simulation and measurement with good agreement. The simulation is achieved with the aid of Agilent-Empro 2012.09 software.

V. CONCLUSION

This paper shows the ability of the high dielectric constant resonators to be used as elements for the design passive elements in the range between 1 to 10 GHz bands. The resonator physical complex behavior requires the utilization of full 3D electromagnetic software in the design of devices based on these resonators. The proposed structure points out the possibility of using DR for the creation of EBGs. Further work is under development to improve the utilization of embedded DR as resonators in planar devices.

ACKNOWLEDGEMENT

This work has been supported by Ministerio de Ciencia y Educación of the Spanish government under the project TEC2010-16060.

REFERENCES

[1] David M. Pozar, “Microwave Engineering”, John Willey & Sons, Inc. New Cork 1998.
[2] Jia-Sheng Hong & M.L. Lancaster, “Microstrip Filters for RF/Microwave Applications”, John Willey & Sons, Inc., New York 2001.
[3] S. Jerry Fiedziuszko, Ian C. Hunter, Tatsuo Itoh, Fellow, Yoshio Kobayashi, Toshio Nishikawa, Steven N. Stitzer, and Kikuo Wakino, , "Dielectric Materials, Devices, and Circuits", IEEE Trans. Microwave Theory & Tech., vol. 50, no. 3, pp. 706-720, March 2002.
[4] J. I. Marulanda, M. Cremona, R. Santos, M. C. R. Carvalho, and L. S. Demenicis," Characterization of SrTiO3 thin films at microwave frequencies using coplanar waveguide resonator method", Microwave and Optical Tech. Letters, vol. 53, no. 10, pp. 2418-2422, October 2011
[5] J.; Ocampo, J.; Martinez, C.; Alonso, J. Garcia-Garcia, "Thick film high dielectric constant resonators", Microwaves, Communications, Antennas and Electronics Systems (COMCAS), IEEE eInternational Conference on, Tel Aviv Israel, Page(s): 1 – 3, 2011.

[6] Foster R.M. “A reactance theorem”, Bell System Technical Journal, (3), pp.259-67, 1924.
[7] Ian Hunter, “Theory and design of Microwave Filters”, The Institution of Electrical Engineering, IEE Electromagnetic Waves Series 48, University Press, Cambridge 2001.

Additional cross couppling coefficient used as matching ladder network in coupled based band pass filters.

Bahareh Moradi[1], Ursula Martinez[1], Eva Arasa[2], Julian Alonso[2] and Juan Jose García-García[1]
Electronic Engineering Department GAEMI Universitat Autònoma de Barcelona Cerdanyola del Vallés, Spain[2]
GSB Universitat Autònoma de Barcelona Cerdanyola del Vallés, Spain[2]

***Abstract*—A three coupling coefficient filter based on coupling coefficient is presented in this paper. The novelty of the proposed design is the introduction of a cross coupling interactions that allows to match the impedance achieving excellent performance in the transmission and reflection response. Equivalent circuit model is discussed, establishing a clear relation between each component and physical parameter of the proposed design. Measured of a 19.4% band pas filter at 1.6 GHz is compared with EM simulation and equivalent circuit model showing an excellent agreement.**

Index Terms—Microstrip filter, couppling coefficient, matched impedance.

I. Introduction

Coupling coefficients based design filter is an easy way to synthetize standard filter response [1]. In the design process of this kind of filters it is necessary to use electromagnetic simulators to optimize the filter performance in order fit the specifications. The designs based on the coupling coefficient exhibit an inherent limitation fixed by the minimal distance allowed by the technology between adjacent resonators. The interaction between resonators and, specially, the interaction between the input-output ports introduces loads in the resonators that affects to the fundamental resonant frequencies as well as to the matching impedance. Therefore, to obtain a good performance it is necessary to go through some optimization process in which the design physical dimensions are modified to balance the resonators resonant frequencies and to achieve the best impedance matching. However, even after this optimization process there is a big gap between the perfect impedance match and the optimized structure. In this paper we propose a small modification of the layout that introduce a cross coupled that can be interpreted as an additional matching ladder network. The proposed equivalent circuit model fits the measured and EM simulated response. Since it is possible to set up direct relation between the equivalent circuit model parameters and the physical layout parameters, the equivalent circuit model becomes a very useful tool in the optimization stage of the filter design.

II. Layout of the Proposed Design

Fig. 1 shows the layout dimensions of the proposed filter. It has been implemented in a Rogers RO3010 substrate using a Protolaser milling machine. The minimal distance between the resonators is 0.2 mm and the distance between the port line and the resonators has been fixed to 0.15 mm which is the more critical distance of the design.

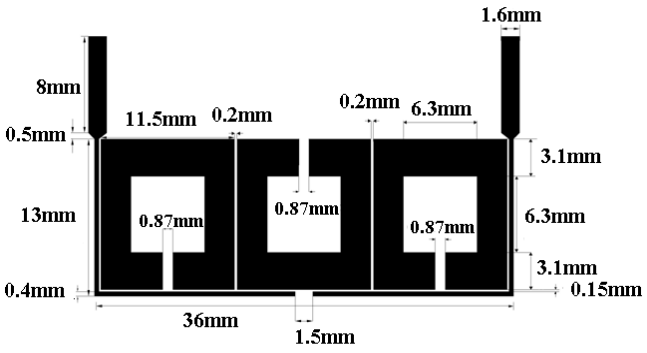

Fig. 1. Layout of the proposed coupling coefficient based Chebyshev filter implementation

The ports feed the resonators though a capacitive coupling which intensity depends of the proximity to the extreme resonators (1.5 mm). The square shape of the resonators has been chosen to maximize the capacitance of the LC resonant tank, resulting in a final thickness of 3.1 mm, and to maximize the coupling between resonators according with the previous experience with this kind of design [3]-[5]. The input and output ports are 50 Ω microstrip lines that in this substrate correspond to 1.6 mm thick microstrip. Extensions of the ports with a 90º angle following the square resonator profile have been included in order to maximize the coupling with the side resonators. The fact that there are dimensions in the layout of the order of the metallic layer thickness requires the utilization of an electromagnetic simulator able to have into account this thickness. Otherwise there may be big differences between Simulation and measured response.

III. Equivalent Circuit Model

The equivalent circuit model of a filter helps to understand the behavior of the design. In the case in which a clear relationship between the equivalents circuit model and the layout physical dimensions can be set. Fig. 2 shows the equivalent circuit model of the proposed filter. Basically it is composed by three LC resonant parallel tanks that represent the three open rings, and a set of capacitive coupling networks to model the different couplings.

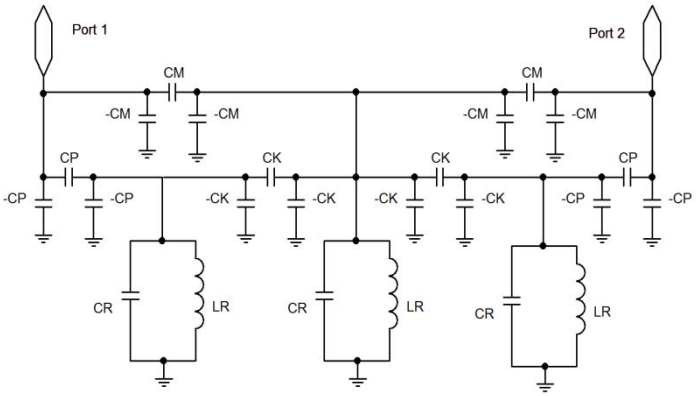

Fig. 2. Equivalent circuit model of the proposed filter.

The nature of the coupling may be magnetic or electric and, in general, it uses to be a combination of both. In many cases, the geometry symmetries can force the predominance of one of the couplings [5]. In our case the orientation of the central resonator has been inverted respect to the orientation of the extremes resonators in such a way that the current distribution in the resonances guarantees the existence of a magnetic wall between adjacent particles and therefore the coupling is forced to be mainly capacitive. As can be observed there are three different kinds of coupling, characterized by the parameters CP, CM and CK. CP is modeling the coupling between the port extensions and the extern resonators. The value of this parameter can be modified in the layout altering the horizontal distance between the port extension and the adjacent resonator. Also, there is a dependence of this parameter with the side of the adjacent resonator, being possible to modify this coupling using rectangular shape resonators. The CK parameter models the coupling between adjacent resonators and can be controlled directly with the distance between the resonators. The maximum value of this capacitance is fixed by the minimal distance between metallic layers that the fabrication technology allows. This value is important because, according with the expressions that link the coupling coefficient and the standard normalized filter parameters [1], the maximum bandwidth of the filters is bounded to the maximum coupling coefficient. Finally, CM represents the cross coupling coefficient that represent the novelty of the proposed design. The equivalent circuit model of the capacitive coupling is a Π circuit with two negative capacitors in the parallel branches. Interpreting the negative capacitors as inductors, the structure can be thought as L-C-L matching ladder. Since the value of the CM can be controlled with the variation of the overlap between the port extension and the central square resonator, this matching ladder can be tuned in a certain range of values. The equivalent circuit model proposed is based on the description of the capacitive coupling coefficient as a Π model. The values of the different parameters can be initially estimated from the physical dimensions, but at the end there will be necessary to optimize them to fit the measured response. Table I shows a summary of the equivalent circuit model parameters for the best fit we have been able to find, together with the value of the corresponding layout physical parameter that control that parameter. Work is in progress to improve this fit and to extend these relations to functions that can link the filter specifications with physical parameters in a useful range for the design process.

TABLE I. SUMMARY OF EQUIVALENT CIRCUIT MODEL PARAMETERS AND GEOMETRICAL PARAMETERS

Equivalent Circuit parameter	Value	Layout dimensions	
Resonant Tank	LR	6.5 e-5 nH	External Ring perimeter: 48.13 mm
	CR	219000 pF	Ring : 48.13 mm
			Ring Thickness: 3.1 mm
Coupling	CP	296 pF	Overlap length between Port extension and resonant ring: 23.63
			Distance between port extension and extreme rings: 150 μm
	CK	36505 pF	Distance between adjacent rings: 200 μm
			Side of the rings: 13 mm
	CM	55 pF	Overlap length between port extension and the central ring: 5 mm
			Distance between port extension and central ring: 150 μm

IV. Results Analisis

Measures of the fabricated prototype depicted in Fig. 3 shows a band pass between 1.44 GHz and 1.75 GHz performing a 19.4% bandwidth. The return losses are below the -10 dB in all the band pass and the insertion losses oscillate between -1.98 dB and 0.79 dB. The outside-band transmission level stays below -30 dB. The band-pass exhibits a non-symmetrical shape being sharper for the low frequency flank. This asymmetry may be caused by the extreme geometry of the used resonators and will be improved in future works.

The excellent agreement between the electromagnetic simulation and the measurement are an excellent starting point to develop a robust design methodology. As can be observed in Fig. 4, the equivalent circuit model is able to reproduce the main filter characteristics such as central frequency bandwidth, the band-pass shape around the transmission, and the full S_{11} response. However, the main advantage of the equivalent circuit model is the understanding of the effects of the layout parameters variation in the filter performance. On this regard, the more interesting

In order to obtain a better fit between measures and the equivalent circuit response, the effects of the phase shift introduced by the input ports and the high impedance of the port extension should be considered in the equivalent circuit model.

In the case of the fit showed in the Fig. 4 the phase shift has been fixed to 121 degree and the impedance of the extension ports correspond to 178.25 Ω. The inclusion of the cross coupling between the port extension and the central resonator represent a small modification that introduces a considerable improvement of the filter performance.

The design methodology can be extrapolated to other designs, and, with small modifications can be extended to wideband-pass filters. In this sense, work is in progress, and the very promising preliminary results are depicted in Fig. 3 has been obtained.

The filter showed in Fig. 4 include two cross coupling coefficients between the input and the central resonator which allow to introduce a second zero in the transmission function adding a notch at higher frequencies that produce a more symmetrical band-pass shape.

At the same the inclusion of an additional cross coupling coefficient has been used to match the impedance of the filter in a very wide range of frequency. The position and shape of the input ports has been modified in order to optimize the feed of the circuit and the phase introduced by the port extensions.

It is expected that a straight relation between the physical parameter an equivalent circuit model could be established in the same way it has been demonstrated for the design in Fig. 1. The result is a well matched wide band pass filter between 1.1 GHz and 1.79 GHz, which correspond to a FBW=50%. The measured insertion losses oscillates between -0.66 dB and -1.3 dB. In the preliminary results showed in Fig. 4, there is a shift between measurement and electromagnetic simulations that is attributed to some tolerances in the fabrication process. The equivalent circuit model is still under development but even in this preliminary state the benefits of the new propose crossed coupling coefficients are evident in the final filter performance.

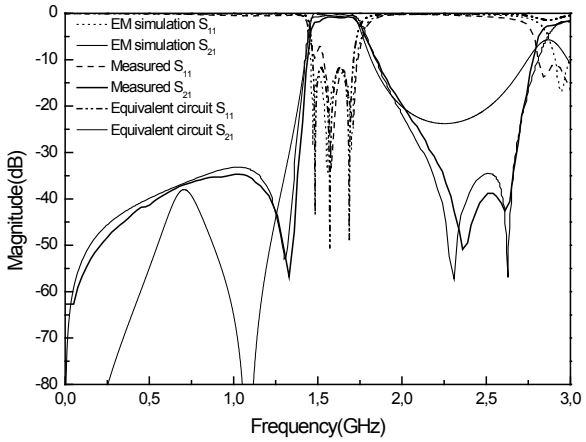

Fig. 3. Comparison between S_{11} and S_{21}measuremed, electromagneticcaly simulated and equivalent circuit response.

V. Conclusions

The inclusion of the cross coupling in the standard Chebyshev filter supplies an additional matching ladder allowing to match the impedance of the design. The proposed equivalent circuit model based on the capacitance coupling transmission line lets to establishing a clear relation between the equivalent circuit model and the layout physical dimensions and, therefore establishing a link between the filter specifications and the layout physical dimensions. The designed filter using this cross coupling coefficient has been fabricated and tested. The measured shows and excellent agreement with the electromagnetic simulations and the equivalent circuit response. Work is in progress to extend the technique to match wide band filters through ladder networks produced with coupling interaction to other filters.

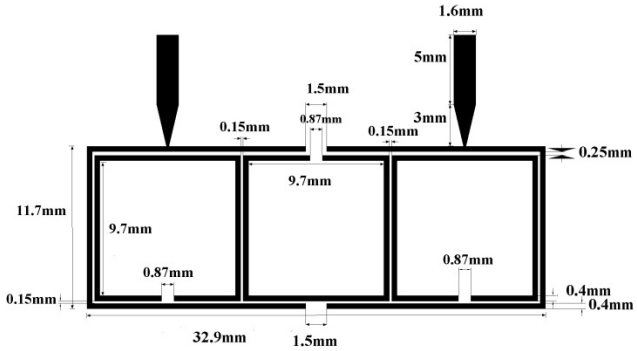

(a)

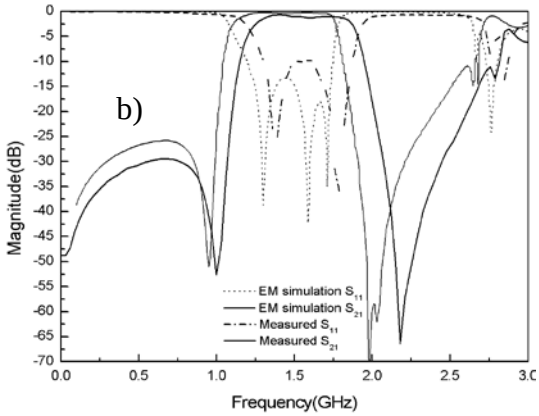

(b)

Fig. 4. a) Layout of the wide-band prototype filter with the main dimensions b) Comparison between S_{11}, and S_{21}, measuremed, electromagneticcaly simulated and equivalent circuit response.

Acknowledgment

This work has been supported by Ministerio de Ciencia y Educación of the Spanish government under the project TEC2010-16060.

References

[1] Jia-Sheng Hong & M.L. Lancaster, "Microstrip Filters for RF/Microwave Applications", John Willey & Sons, Inc., New York 2001.

[2] David M. Pozar, "Microwave Engineering", John Willey & Sons, Inc. New Cork 1998.

[3] J. García-García, J. Bonache, I. Gil, F. Martín, M.C. Velazquez-Ahumada and J. Martel. "Miniaturized microstrip and CPW filters using coupled metamaterial resonators." IEEE Transactions on Microwave Theory and Techniques.54 - 6,pp. 2628 – 2635, 2006

[4] Comparison of electromagnetic band gap and split-rings resonators microstrip lines as stop band structures."Comparison of electromagnetic band gap and split-rings resonators microstrip lines as stop band structures." Microwave and Optical Technology Letters.44 - 4,pp. 376 – 379, 2005

[5] García-García, J.; Martín, F.; Falcone, F.; Bonache, J.; Gil, I.; Amat, E.; Lopetegi, T.; Laso, M.A.G.; Iturmendi, J.A.M.; Sorolla, M.; Marqués, R." Microwave Filters with Improved Stopband based on Sub-wavelength Resonators.IEEE Transactions on Microwave Theory and Techniques.53 - 6,pp., 2005.

Multimode Ultra-Wideband filters by using a Grounded Open Ring Resonator

B. Moradi, U. Martínez and J.J. García-García, *Member, IEEE*

***Abstract*—This paper reports a novel multimode resonator (MMR) ultra-wide band-pass (UWB) filter design using a grounded open ring resonator. The utilization of 30 μm gaps between input ports and the central resonator achieve high coupling level. Five resonant modes are used to perform a 128% fractional bandwidth at 4.3 GHz. The fabricated prototype exhibits a band-pass with insertion losses around 0.5 dB. A theoretical model based on transmission lines matrices is proposed and used to explore the limits of the design through different parametric analysis. Excellent agreement between theoretical predictions, electromagnetic simulations and measurement are found.**

***Index Terms*: Multi-mode resonator, parallel-coupled microstrip line, ultra-wideband band-pass filters**.

I INTRODUCTION

Many efforts have been devoted to the development of the ultra-wide band pass (UWB) filter using multi-mode resonator (MMR) [1]. From the conceptual point of view, MMR is one of the simplest approaches to the design of UWB. The technique was originally proposed by Zhu and Menzel in 2005 [2], and further developed with diverse approaches can be found in literature [3-7]. In [2] a five-pole filter was built using a single triple-mode stepped-impedance resonator (SIR) for UWB application. In [3] two short-circuited stubs where attached to the initial MMR to form a quadruple-mode UWB band pass filter. In [4], a packaged UWB filter based on stub-loaded resonators is proposed. In [5], the triple open stubs in shunt to a SIR are used to build UWB filter. A compact UWB using the dual-mode ring resonator is presented in [6]. In [7] a superconducting UWB band-pass filter with sharp rejection skirts by using MMR is reported. The utilization of ring resonator in the UWB design was introduced in [8].

A compact UWB band-pass filter using grounded open ring resonator as a MMR is proposed in this paper. The approach allows using five resonances to produce a 128% fractional bandwidth into the ultra-wide band bandwidth standard frequencies. A general theoretic framework has been established using transmission matrix description of the filter constituent components. As illustrative example, a 128% FBW filter between 1.2 GHz and 5.5 GHz has been designed and fabricated. The prototype has been fabricated in a 1.27 mm thick Rogers 3010 substrate with a relative dielectric constant of 10.2. The dimensions of the filter are 21.5mm×10mm ($\cong 0.66\lambda_g \times 0.30\lambda_g$), where λ_g is the central frequency wavelength.

This work has been supported by Ministerio de Ciencia y Educación of the Spanish government under the project TEC2010-16060". B. Moradi, U. Martinez-Iranzo and J.J. Garcia-Garcia are with the Electronic Engineering Department of Universidad Autónoma de Barcelona, Cerdanyola del Vallès, 08193 Spain (corresponding author e-mail: Bahareh.moradi@uab.cat).

II PROPOSED DESIGN DESCRIPTION

Fig. 1(a) shows the physical layout of the proposed MMR-UWB. The distance between the I/O ports and the MMR is fixed to 0.03 mm. The width of the open ring resonator grounded and the extension of the I/O port have been fixed to 0.2 mm.

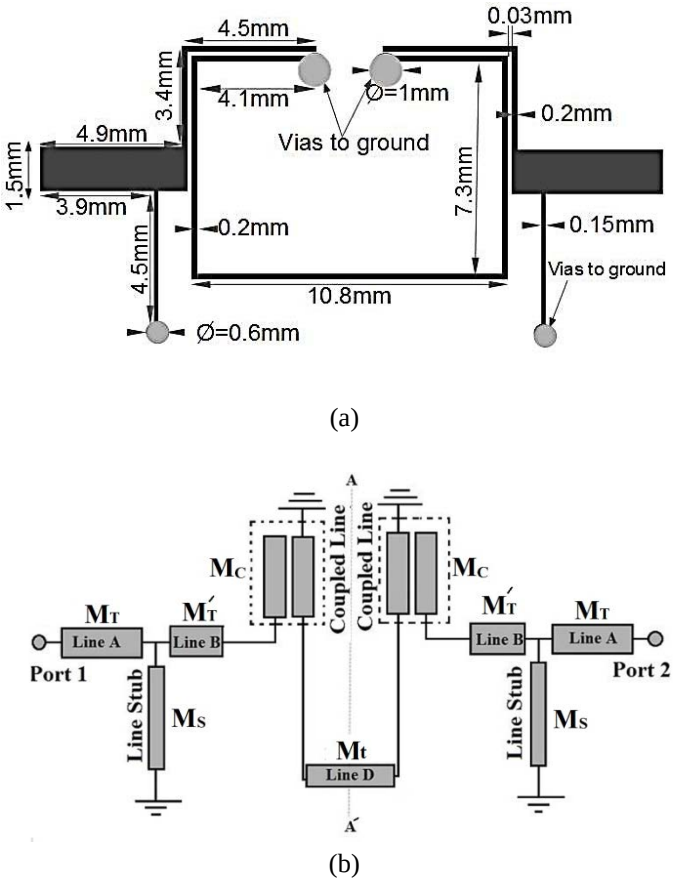

Fig. 1. a) Layout of the designed MMR-UWB filter. (b) Schematic of proposed MMR-UWB equivalent circuit model.

The layout and corresponding equivalent circuit model for the proposed filter are shown in Figs. 1(a) and 1(b), espectively. The two 0.15 mm width, 4.5 mm long grounded stubs have been designed to match the impedance of the I/O ports. The length of these I/O ports extensions coincides with the first resonant frequency of the grounded open ring resonator. The basic idea of the design is that the length of the grounded square ring determines the position of the

resonant modes, and the extension of the coupled line in the ring perimeter determines the number of modes into the band pass. On the other hand, the structure of the layout let the identification of the constituent elements of the design in terms of sections which can be theoretically described using transmission matrices representation.

III CIRCUIT ANALYSIS

Fig. 1(a) shows the proposed MMR-UWB filter layout and Fig. 1(b) the proposed equivalent circuit model based on coupled microstrip transmission lines. The coupled transmission lines are characterized trough the even and odd characteristic impedance and electric length (Zoe, θe, and Zoo, θo respectively). This implies the coexistence of two different modes with different phase velocity and propagating constant corresponding to the different effective relative permittivity.

The even and odd-mode characteristic impedances Zoe and Zoo can be obtained from the expressions:

$$Z_{oe} = \frac{1}{c\sqrt{C_e^a C_e}} \quad (1)$$

$$Z_{oo} = \frac{1}{c\sqrt{C_o^a C_o}}) \quad (2)$$

where Ceα and Coα are the even and odd mode capacitances that can be derived directly from the geometrical parameters of the design [9].

The distributed equivalent circuit model showed in Fig.1 (b) can be described by a single ABCD matrix between the input and output ports. Due to the A-A' plane symmetry, the internal structure of this matrix can be described by the Eq.(3)

$$\begin{bmatrix} A & B \\ C & D \end{bmatrix} = M_T M_S M_{T'} M_C M_t M_C M_{T'} M_S M_T \quad (3)$$

Where

$$M_T = \begin{bmatrix} cos\theta_T & jZ_T sin\theta_T \\ j\frac{1}{Z_T} sin\theta_T & cos\theta_T \end{bmatrix} \text{and} M_{T'} = \begin{bmatrix} cos\theta_{T'} & jZ_T sin\theta_{T'} \\ j\frac{1}{Z_T} sin\theta_{T'} & cos\theta_{T'} \end{bmatrix}$$

(4)

are the ABCD matrices of the line A and B,

$$M_t = \begin{bmatrix} cos\theta_t & jZ_t sin\theta_t \\ j\frac{1}{Z_t} sin\theta_t & cos\theta_t \end{bmatrix} \quad (5)$$

is the ABCD matrix associated to the center transmission line D,

$$M_S = \begin{bmatrix} 1 & 0 \\ \frac{1}{jZ_s tan\theta_s} & 1 \end{bmatrix} \quad (6)$$

is the ABCD matrix associated to the grounded stub S,

$$M_C = \begin{bmatrix} \frac{-Z_{11}}{Z_{12}} & \frac{-(Z_{11}^2 - Z_{12}^2)}{Z_{12}} \\ \frac{-1}{Z_{12}} & \frac{-Z_{11}}{Z_{12}} \end{bmatrix} \quad (7)$$

is the ABCD matrix associated to the coupled lines.

Being the elements of the coupled line:

$$Z_{11} = Z_{22} = \frac{-j}{2} Z_{oe} \cdot cot(\theta_e) - \frac{j}{2} Z_{oo} \cdot cot(\theta_o) \quad (8)$$

$$Z_{12} = Z_{21} = \frac{-j}{2} Z_{oe} \cdot csc(\theta_e) + \frac{j}{2} Z_{oo} \cdot csc(\theta_o) \quad (9)$$

The physical dimensions showed in Fig.1 (a) correspond to the electrical parameters are Z_T=44.5 Ω, Zt=66.6 Ω, Zs=101.6 Ω, Zoe=145.5 Ω, Zoo=30.5 Ω and 6.5 and 5.8 effective relative dielectric constants for even and odd mode respectively.

Although expressions are complicated [9], the Zoe and Zoo impedances can be analytically evaluated from the substrate thickness (h), the strip width (W) and the separation between coupled lines (S). Fig.2 shows the mapping of these expressions illustrating the fact that for higher S/h relation there is a clear increment of Zoo and a diminution of Zoe. On the other hand, an increment in the W/h ratio implies a reduction of both Zoe and Zoo parameters. According to this map, the extreme values achievable with our fabrication facilities are fixed to Zoe=145.5 Ω and Zoo =30.5 Ω, corresponding to W= 0.2 mm and S= 0.03 mm for a fixed h=1.27 mm.

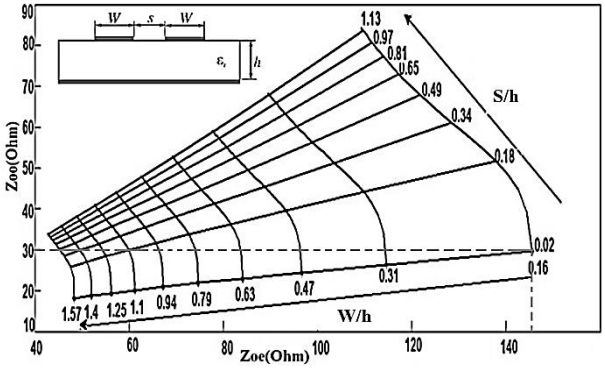

Fig. 2. Even and odd mode (Zoe, Zoo respectively) impedance mapping as function of the S/h and W/h ratios. In all the cases substrate has a fixed valued of h=1.27mm and εr=10.2.

The resulting ABCD matrix can be used to evaluate the limits of the filter fractional bandwidth (FBW) following the expression.

$$\text{FBW} = \frac{(f_h - f_l)}{f_c} \quad (10)$$

$$f_c = \frac{f_h + f_l}{2} \quad (11)$$

Where fc denotes the center frequency and higher and lower frequency limits of the bandwidth are represented by fh and fl, respectively. It is observed that the center frequency is

inversely proportional to the length of coupling line, when the center frequency decreases, the length of coupling line increases. The length of the coupled line of proposed filter is 9 mm long and 0.2 mm wide, the measured high and low frequency are 5.5 GHz, 1.2GHz respectively.

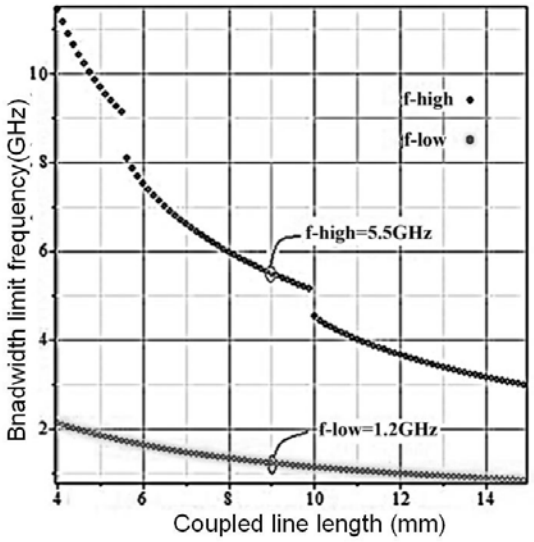

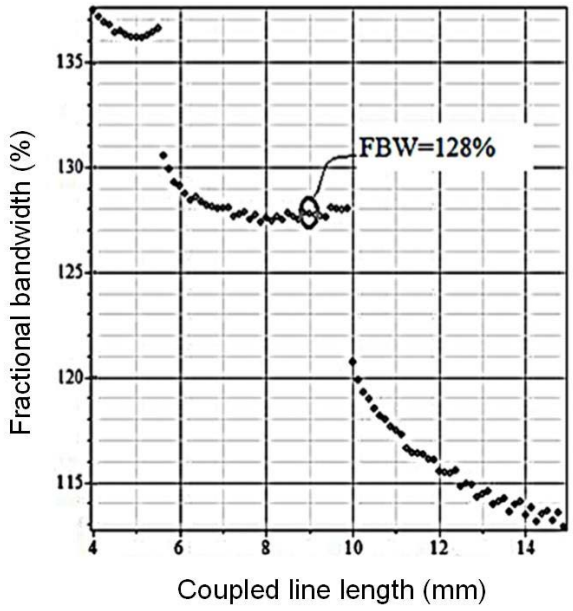

Fig. 3. Show the upper and lower limits of the FBW as a function of the length of the coupled line (D).

Fig.3 shows the upper and lower limits of the MMR-filtering structure (in Fig. 3.a) and the corresponding FBW (in Fig. 3.b) as a function of the length of the coupled line section (see Fig. 1.a). The different number of resonant modes included in the band-pass produces the plateau like behavior observed in Fig. 3.b. For coupled line length below 5 mm there are six resonant modes into the band. In the case of coupled line length between 5 and 10 mm five resonances are included into the MMR design, and four for coupled line length between 10 and 15 mm. As the number of modes into the transmission band increases so does the FBW. However a higher number of resonant modes in the band compromise the rejection band level and the losses in the transmission band frequencies. The proposed design maintains a rejection level below -20 dB with a 128 % FBW at the UWB standard frequencies. The design process can be complex, but due to the equivalent circuit

model based on the transmission matrices of the filter sections, relations between physical parameters and filter performance can be established.

Comparison of fractional bandwidth of this work with other references is given in Table I.

TABLE I
Comparison with other proposed UWB Filters.

Ref.	FBW
[2]	113٪@2dB
[3]	119٪@3dB
[5]	114٪@3dB
[7]	111٪@3dB
Proposed filter	128٪@3dB

IV MEASURED RESULT AND DISCUTION

As shown in Fig 5, there are five resonant modes generated in the pass band of the MMR filter. Comparing with Fig 3b; it can be seen that, by decreasing lengths of coupled lines, resonant modes are changed. The theory predicts that decreasing coupled line (from 5.5 mm to 5.4 mm), increase band pass filter correlation. The theory was developed and compares well with the measurements parameter of bandwidth. To verify these simulated results, proposed MMR-UWB filter is fabricated and measured by network analyzer. A photograph of the fabricated prototype is shown in Fig. 4.

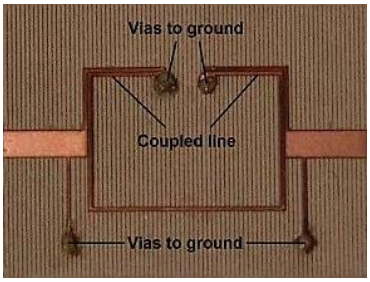

Fig. 4. Photograph of the new compact designed MMR-UWB filter.

The comparison of theoretical, simulation and measurement result shows in Fig .5.

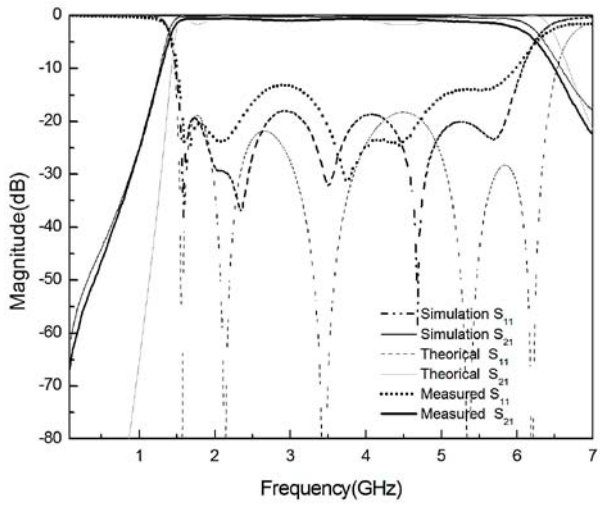

Fig. 5. S-parameter responses of the EM simulation, theoretical and measurement of MMR-UWB filter.

There is good agreement between the theoretical prediction, simulated and the measured results.

In the measurement, the lower and higher cutoff frequencies of the UWB filter are equal to 1.2 GHz and 5.5 GHz, respectively as can be observed in Fig. 3(a). This indicates that the relevant fractional bandwidth achieves about 128%.at the central frequency 2.56 GHz.

V CONCLUSION

The paper presents a MMR-UWB filter approach with controllable characteristics. Relations between physical parameters and filter performance characteristics such as the central frequency, FBW, or the number of resonant modes into the band-pass have been studied using a distributed transmission matrices model.

References

[1] Z. C. Hao and J. S. Hong, 'Ultra-wideband filters technologies' IEEE Microw. Mag, Vol. 11, No. 4, pp. 56-68, 2010

[2] L. Zhu, S. Sun, and W. Menzel, 'Ultra-wideband (UWB) bandpass filter using multiple-mode resonator', IEEE Microwave Wireless Compon Lett, Vol 15, No, 11, pp. 796-798,2005.

[3] S. W. Wong and L. Zhu, 'Quadruple-mode UWB bandpass filter with improved out-of-band rejection', IEEE Microwave Wireless Compon. Lett, Vol, 19, No, 3, pp. 152–154, 2009.

[4] L. Han, K. Wu, and X. Zhang, 'Development of packaged ultra-wide band bandpass filters', IEEE Trans. Microwave Theory Tech, Vol.58, pp. 220–228, 2010.

[5] R. Li and L. Zhu, 'Compact UWB bandpass filter using stub-loaded multiple-mode resonator,' IEEE Microwave Wireless Compon Lett., Vol.17, pp. 40–42, 2007.

[6] K. Song and Y. Fan, 'Compact ultra-wideband bandpass filter using dual-line coupling structure', IEEE Microwave Wireless Compon. Lett, 19, pp. 30–32, 2009.

[7] Z. Shang, X. Guo, B. Cao, V. Wei, X. Zhang, Y. Heng, G. Suo, and X. Song. 'Design of a Superconducting Ultra-Sideband (UWB) Bandpass Filter with Sharp Rejection Skirts and Miniaturized Size' IEEE Microwave and Wireless Comp. Lett., 23, (2), pp.72-74, 2013.

[8] H. Ishida and K. Araki, 'Design and analysis of UWB bandpass filter with ring filter', in IEEE MTT-S Int. Dig., 3, pp. 1307–1310, 2004.

[9] M. J. Lancaster, Jia-Sheng Hong, 'Microstrip Filters for RF/Microwave Applications' John Wiley & Sons, ISBNs: 0-471-38877-7 (Hardback); 0-471-22161-9, 2001.

Appendix C

Maple codes

```
restart :
ε_0 := 8.85·1e−12 :
j := I :
mypi := 3.14159265359 :
ε_r := 10.2 :
c := 3e8 :
ω := 2·f·1e9·Pi :
W := 0.0002 :
h := 1.27e−3 :
s := 0.03e−3 :
l := 0.009 :
```

Coupled line

$$Z0 := 65 :$$

$$\varepsilon_{rec} := \frac{\varepsilon_r + 1}{2} + \frac{\varepsilon_r - 1}{2}\left(\left(1 + \frac{12 \cdot h}{W}\right)^{-0.5} + 0.04 \cdot \left(1 - \frac{W}{h}\right)^2\right) :$$

$$Zc\_c := \frac{60}{\sqrt{\varepsilon_{rec}}} \ln\left(\frac{8 \cdot h}{W} + \frac{0.25\, W}{h}\right) :$$

$$Cp := \frac{\varepsilon_0 \cdot \varepsilon_r \cdot W}{h} :$$

$$Cf := \frac{\sqrt{\varepsilon_{rec}}}{2 \cdot c \cdot Zc\_c} - \frac{Cp}{2} :$$

$$G := e^{\left(-0.1 \cdot e^{\left(2.23 - \frac{2.53 \cdot W}{h}\right)}\right)} :$$

$$C\_fprime := \frac{Cf}{1 + G \cdot \left(\frac{h}{s}\right) \cdot \tanh\left(\frac{8 \cdot s}{h}\right)} :$$

$$Cgd := \frac{\varepsilon_0 \cdot \varepsilon_r}{mypi} \cdot \ln\left(\coth\left(\frac{mypi}{4} \cdot \frac{s}{h}\right)\right) + 0.65 \cdot Cf \cdot \left(\frac{0.02 \cdot \sqrt{\varepsilon_{rec}}}{\frac{s}{h}} + 1 - \frac{1}{\varepsilon_r^{\,2}}\right) :$$

$$K := \frac{\frac{s}{h}}{\frac{s}{h} + \frac{2 \cdot W}{h}} :$$

$$K\_prime := \sqrt{1 - K^2} :$$

$$Cga := \varepsilon_0 \cdot \frac{1}{mypi} \cdot \ln\left(2 \cdot \frac{1 + \sqrt{K\_prime}}{1 - \sqrt{K\_prime}}\right) :$$

$$Ce := Cp + Cf + C\_fprime :$$

$$Co := Cp + Cf + Cgd + Cga :$$

$$\varepsilon_{ra} := 1 :$$

$$\varepsilon_{reca} := \frac{\varepsilon_{ra} + 1}{2} + \frac{\varepsilon_{ra} - 1}{2}\left(\left(1 + \frac{12 \cdot h}{W}\right)^{-0.5} + 0.04 \cdot \left(1 - \frac{W}{h}\right)^{2}\right) :$$

$$Zc\_ca := \frac{60}{\sqrt{\varepsilon_{reca}}} \ln\left(\frac{8 \cdot h}{W} + \frac{0.25\, W}{h}\right) :$$

$$Cpa := \frac{\varepsilon_0 \cdot \varepsilon_{ra} \cdot W}{h} :$$

$$Cfa := \frac{\sqrt{\varepsilon_{reca}}}{2 \cdot c \cdot Zc\_ca} - \frac{Cpa}{2} :$$

$$G := e^{\left(-0.1 \cdot e^{\left(2.23 - \frac{2.53 \cdot W}{h}\right)}\right)} :$$

$$C\_fprimea := \frac{Cfa}{1 + G \cdot \left(\frac{h}{s}\right) \cdot \tanh\left(\frac{8 \cdot s}{h}\right)} :$$

$$Cgda := \frac{\varepsilon_0 \cdot \varepsilon_{ra}}{mypi} \cdot \ln\left(\coth\left(\frac{mypi}{4} \cdot \frac{s}{h}\right)\right) + 0.65 \cdot Cfa \cdot \left(\frac{0.02 \cdot \sqrt{\varepsilon_{ra}}}{\frac{s}{h}} + 1 - \frac{1}{\varepsilon_{ra}^{2}}\right) :$$

$$K := \frac{\frac{s}{h}}{\frac{s}{h} + \frac{2 \cdot W}{h}} :$$

$$K\_prime := \sqrt{1 - K^2} :$$

$$Cgaa := \varepsilon_0 \cdot \frac{1}{mypi} \cdot \ln\left(2 \cdot \frac{1 + \sqrt{K\_prime}}{1 - \sqrt{K\_prime}}\right) :$$

$$Cea := Cpa + Cfa + C\_fprimea :$$

$$Coa := Cpa + Cfa + Cgda + Cgaa :$$

$$Zoe := \frac{1}{c \cdot \sqrt{Cea \cdot Ce}} :$$

$$Zoo := \frac{1}{c \cdot \sqrt{Coa \cdot Co}} :$$

$$\varepsilon_{e\_eff} := \frac{Ce}{Cea} :$$

$$\varepsilon_{o\_eff} := \frac{Co}{Coa} :$$

$$Vp\_e := \frac{c}{\sqrt{\varepsilon_{e\_eff}}} :$$

$$Vp\_o := \frac{c}{\sqrt{\varepsilon_{o\_eff}}} :$$

$$\theta e := \frac{\omega \cdot l}{Vp\_e} :$$

$$\theta o := \frac{\omega \cdot l}{Vp\_o} :$$

$$\theta := 60.7 :$$

$$Z11 := -\frac{j}{2} \cdot Zoe \cdot \cot(\theta e) - \frac{j}{2} \cdot (Zoo \cdot \cot(\theta o)) :$$

$$Z21 := -\frac{j}{2} \cdot Zoe \cdot \csc(\theta e) + \frac{j}{2} \cdot (Zoo \cdot \csc(\theta o)) :$$

$$Z12 := -\frac{j}{2} \cdot Zoe \cdot \csc(\theta e) + \frac{j}{2} \cdot (Zoo \cdot \csc(\theta o)) :$$

$$Z22 := -\frac{j}{2} \cdot (Zoe \cdot \cot(\theta e)) - \frac{j}{2} \cdot (Zoo \cdot \cot(\theta o)) :$$

$$A := -\frac{Z11}{Z12} :$$

$$B := -\frac{Z11^2 - Z12^2}{Z12} :$$

$$C := -\frac{1}{Z12} :$$

$$\mathrm{d} := -\frac{Z11}{Z12} :$$

$$T\_c := \begin{bmatrix} A & B \\ C & d \end{bmatrix} :$$

$$Zi := \sqrt{\frac{B}{C}} :$$

A B C D matrix parameter for line between two port

$$W_l := 0.0002 :$$

$$\varepsilon_{rl} := \frac{\varepsilon_r + 1}{2} + \frac{\varepsilon_r - 1}{2} \cdot \left(\frac{1}{\mathrm{sqrt}\left(1 + \frac{12 \cdot h}{W_l}\right)} + 0.04\left(1 - \frac{W_l}{h}\right)^2 \right) :$$

$$Zc\_l := \frac{Zoe - Zoo}{2} :$$

$$l_l := 0.0165 :$$

$$vp\_l := \frac{c}{\mathrm{sqrt}(\varepsilon_{rl})} :$$

$$theta\_l := evalf\left(\frac{\omega \cdot l_l}{vp\_l}\right) :$$

$$T\_l := \begin{bmatrix} \cos(theta\_l) & j \cdot Zc\_l \cdot \sin(theta\_l) \\ \frac{j}{Zc\_l} \cdot \sin(theta\_l) & \cos(theta\_l) \end{bmatrix} :$$

A B C D matrix Parameter for port line_1

$$W\_p := 0.0015 :$$

$$e\_re\_p := \frac{\varepsilon_r + 1}{2} + \frac{\varepsilon_r - 1}{2} \cdot \left(\frac{1}{\mathrm{sqrt}\left(1 + \frac{12 \cdot h}{W\_p}\right)} + 0.04\left(1 - \frac{W\_p}{h}\right)^2\right) :$$

$$Zc\_p := evalf\left(\frac{120\ mypi}{2\ mypi \cdot \mathrm{sqrt}(e\_re\_p)} \cdot \ln\left(\frac{8 \cdot h}{W\_p} + \frac{0.25 \cdot W\_p}{h}\right)\right) :$$

$$l\_p := 0.0039 :$$

$$\lambda gp := \frac{300}{f \cdot \mathrm{sqrt}(e\_re\_p)} :$$

$$\beta\_p := evalf\left(\frac{2 \cdot mypi}{\lambda gp}\right) :$$

$$vp\_p := \frac{c}{\mathrm{sqrt}(e\_re\_p)} :$$

$$theta\_p := evalf\left(\frac{\omega \cdot l\_p}{vp\_p}\right) :$$

$$T\_p := \begin{bmatrix} \cos(theta\_p) & j \cdot Zc\_p \cdot \sin(theta\_p) \\ \frac{j}{Zc\_p} \cdot \sin(theta\_p) & \cos(theta\_p) \end{bmatrix} :$$

A B C D matrix parameter for stub line

$$W\_s := 0.00015 :$$

$$e\_re\_s := \frac{\varepsilon_r + 1}{2} + \frac{\varepsilon_r - 1}{2} \cdot \left(\frac{1}{\mathrm{sqrt}\left(1 + \frac{12 \cdot h}{W\_s}\right)} + 0.04\left(1 - \frac{W\_s}{h}\right)^2 \right) :$$

$$Zc\_s := \frac{120\, mypi}{2\, mypi \cdot \mathrm{sqrt}(e\_re\_s)} \cdot \ln\left(\frac{8 \cdot h}{W\_s} + \frac{0.25 \cdot W\_s}{h} \right) :$$

$$\lambda gs := \mathrm{evalf}\left(\frac{300}{f \cdot \mathrm{sqrt}(e\_re\_s)} \right) :$$

$$l\_s := 0.00455 :$$

$$\beta\_s := evalf\left(\frac{2 \cdot mypi}{\lambda gs} \right) :$$

$$vp\_s := \frac{c}{\mathrm{sqrt}(e\_re\_s)} :$$

$$theta\_s := evalf\left(\frac{\omega \cdot l\_s}{vp\_s} \right) :$$

$$Zi\_s := evalf(j \cdot Zc\_s \cdot \tan(theta\_s)) :$$

$$L := \frac{Zc\_s \cdot l\_s}{vp\_s} :$$

$$T\_s := \begin{bmatrix} 1 & 0 \\ \frac{1}{Zi\_s} & 1 \end{bmatrix} :$$

A B C D matrix Parameter for port line_2

$$W\_p2 := 0.0015 :$$

$$e\_re\_p2 := \frac{\varepsilon_r + 1}{2} + \frac{\varepsilon_r - 1}{2} \cdot \left(\frac{1}{\mathrm{sqrt}\left(1 + \frac{12 \cdot h}{W\_p2}\right)} + 0.04\left(1 - \frac{W\_p2}{h}\right)^2 \right) :$$

$$Zc\_p2 := \frac{120\, mypi}{2\, mypi \cdot \mathrm{sqrt}(e\_re\_p2)} \cdot \ln\left(\frac{8 \cdot h}{W\_p2} + \frac{0.25 \cdot W\_p2}{h} \right) :$$

$$l\_p2 := 0.001 :$$

$$vp\_p2 := \frac{c}{\mathrm{sqrt}(e\_re\_p2)} :$$

$$theta\_p2 := evalf\left(\frac{\omega \cdot l\_p2}{vp\_p2} \right) :$$

$$T\_p2 := \begin{bmatrix} \cos(theta\_p2) & j \cdot Zc\_p2 \cdot \sin(theta\_p2) \\ \frac{j}{Zc\_p2} \cdot \sin\left(theta\_p2\right) & \cos(theta\_p2) \end{bmatrix} :$$

$M := T\_p.T\_s.T\_p2.T\_c.T\_l.T\_c.T\_p2.T\_s.T\_p :$
$a\_1 := M[1,1] :$
$b\_1 := M[1,2] :$
$c\_1 := M[2,1] :$
$d\_1 := M[2,2] :$

$Z\_0 := 50 :$

$$S11 := f \rightarrow \left(\frac{\left(a\_1 + \frac{b\_1}{Z\_0} - (c\_1 \cdot Z\_0) - d\_1 \right)}{a\_1 + \frac{b\_1}{Z\_0} + (c\_1 \cdot Z\_0) + d\_1} \right) :$$

$$S12 := f \rightarrow \left(\frac{2 \cdot (a\_1 \cdot d\_1 - b\_1 \cdot c\_1)}{a\_1 + \frac{b\_1}{Z\_0} + (c\_1 \cdot Z\_0) + d\_1} \right) :$$

$$S21 := f \rightarrow \left(\frac{2}{a\_1 + \frac{b\_1}{Z\_0} + (c\_1 \cdot Z\_0) + d\_1} \right) :$$

$$S22 := f \rightarrow \left(\frac{\left(-a\_1 + \frac{b\_1}{Z\_0} - (c\_1 \cdot Z\_0) + d\_1 \right)}{a\_1 + \frac{b\_1}{Z\_0} + (c\_1 \cdot Z\_0) + d\_1} \right) :$$

$with(plots) :$

$plot([\, 20 \cdot \log(\, abs(S11(f)\,)\,), 20 \cdot \log(\, abs(S21(f)\,)\,)\,], f = 0..10, legend = [typeset("S11"), typeset("S21")], axes = boxed, gridlines = true);$

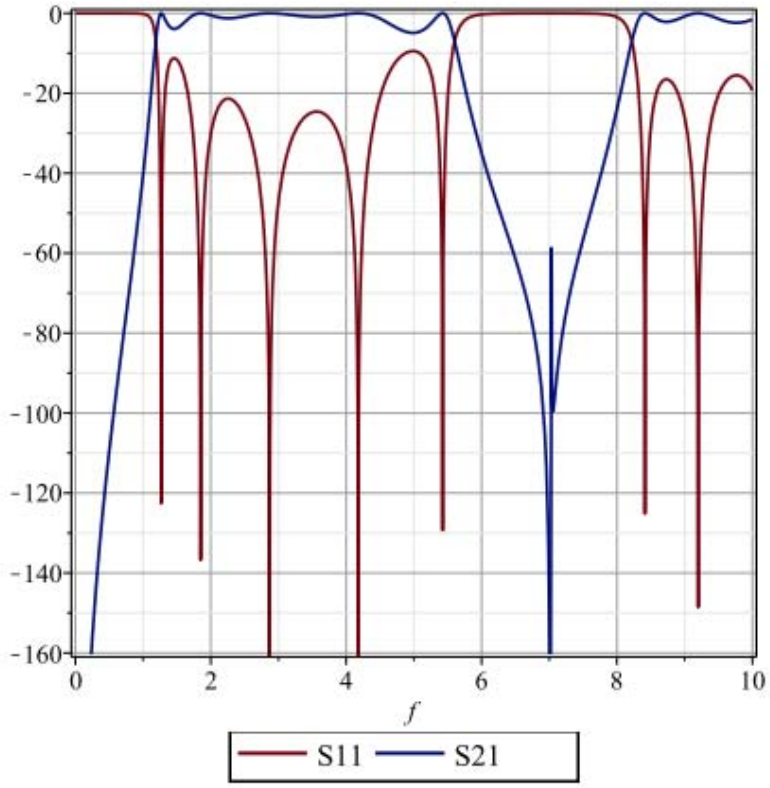


```
> for i from 1 by 1 to 1000 do f := evalf( i/100 ); res(i, 1) := f; res(i, 2) := evalf(20
      ·log( abs(S11(f) ) ) ); res(i, 3) := evalf(20·log( abs(S12(f) ) ) );end do:
```